

Aus dem Bereich Biophysik
Theoretische Medizin und Biowissenschaften
der Medizinischen Fakultät
der Universität des Saarlandes, Homburg/Saar

**Response of mammalian eye lenses to space radiation
qualities *in vitro* and in organ culture**

Dissertation

zur Erlangung des Grades eines Doktors der Naturwissenschaften
der Medizinischen Fakultät
der UNIVERSITÄT DES SAARLANDES

2019

vorgelegt von: Bikash Konda
geb. am: 14.02.1986 in Bhaktapur, Nepal

Tag der Promotion: 20.12.2019
Dekan: Prof. Dr. M.D. Menger
Berichterstatter: Prof. Dr. J. Engel
PD Dr. Y. Dzierma

Content

| | | |
|----------|--|-----------|
| 1 | Introduction | 1 |
| 1.1 | Basic terms in radiation biology | 2 |
| 1.2 | Space radiation..... | 4 |
| 1.3 | Biological consequences of ionizing radiation exposure..... | 6 |
| 1.4 | Cellular effects of radiation | 8 |
| 1.4.1 | DNA damage and repair pathways..... | 10 |
| 1.4.2 | Cell cycle arrest..... | 11 |
| 1.5 | The crystalline lens..... | 14 |
| 1.5.1 | The lens capsule | 14 |
| 1.5.2 | Lens epithelium | 15 |
| 1.5.3 | Lens fibers..... | 15 |
| 1.6 | Cataract and its types..... | 15 |
| 1.7 | Radiation cataractogenesis | 17 |
| 1.8 | Mechanisms leading to radiation-induced cataract..... | 17 |
| 1.9 | Osteogenic differentiation as an alternative mechanism behind lens turbidity..... | 19 |
| 1.10 | Porcine lens and porcine lens epithelial cells (pLEC)..... | 21 |
| 1.11 | Aims of the study..... | 22 |
| 2 | Materials and methods..... | 23 |
| 2.1 | Materials..... | 23 |
| 2.1.1 | Equipment | 23 |
| 2.1.2 | Consumables..... | 24 |
| 2.1.3 | Reagents and Kits | 24 |
| 2.1.4 | Culture medium | 26 |
| 2.1.5 | Buffers and solutions | 26 |
| 2.1.6 | Antibodies and diluents | 27 |

| | | |
|----------|--|----|
| 2.1.7 | Software | 27 |
| 2.2 | Methods..... | 28 |
| 2.2.1 | Preparation and culture of the whole lens | 28 |
| 2.2.2 | Isolation and routine culture of pLEC monolayer | 29 |
| 2.2.3 | Giemsa staining for cytogenetics..... | 30 |
| 2.2.4 | Microtomy..... | 31 |
| 2.2.4.1 | Sample fixation | 31 |
| 2.2.4.2 | Paraffin infiltration..... | 31 |
| 2.2.4.3 | Embedding the lens in paraffin block..... | 32 |
| 2.2.4.4 | Sectioning of the lens | 32 |
| 2.2.5 | Radiation exposure..... | 33 |
| 2.2.5.1 | X-ray exposure | 33 |
| 2.2.5.2 | Heavy ion exposure..... | 34 |
| 2.2.6 | Microscopic investigation..... | 35 |
| 2.2.7 | Analysis of cell growth | 35 |
| 2.2.8 | Radiobiological characterization | 35 |
| 2.2.8.1 | Plating efficiency..... | 35 |
| 2.2.8.2 | Colony forming ability test..... | 36 |
| 2.2.8.3 | Calculating Dose Effect Relations | 36 |
| 2.2.9 | Analysis of cell cycle progression by flow cytometry | 38 |
| 2.2.10 | Immunofluorescence staining of γ H2AX | 39 |
| 2.2.11 | Staining of microtome sections..... | 40 |
| 2.2.12 | Oxidative stress determination in pLECs | 41 |
| 2.2.13 | Detection of replicative S-phase cells..... | 41 |
| 2.2.14 | Osteogenic induction of pLECs | 42 |
| 2.2.15 | Quantitative real-time PCR for gene expression analysis of pLEC..... | 43 |
| 2.2.15.1 | RNA extraction and isolation | 43 |

| | | |
|----------|---|-----------|
| 2.2.15.2 | RNA integrity and quantity determination | 44 |
| 2.2.15.3 | cDNA synthesis | 45 |
| 2.2.15.4 | Primer design | 45 |
| 2.2.15.5 | Quantitative real-time polymerase chain reaction (qPCR)..... | 46 |
| 2.2.15.6 | Relative quantification of gene expression levels | 48 |
| 2.2.16 | Statistics | 49 |
| 3 | Results | 50 |
| 3.1 | Growth properties of porcine lens epithelial cells (pLEC) in monolayer and in whole lens organ culture | 51 |
| 3.1.1 | pLEC characteristics, morphology and growth pattern | 51 |
| 3.1.2 | Whole lens organ culture | 54 |
| 3.2 | Determination of DNA synthesis during S-phase..... | 56 |
| 3.2.1 | Replication and synthesis in the monolayer culture..... | 56 |
| 3.2.2 | Replication and synthesis in whole organ culture | 58 |
| 3.3 | Oxidative stress in pLEC monolayer culture | 58 |
| 3.4 | Radiobiological characterization | 61 |
| 3.4.1 | Plating efficiency of pLECs | 61 |
| 3.4.2 | Cellular survival after X-ray exposure | 61 |
| 3.5 | Cell cycle progression after X-ray exposure | 63 |
| 3.5.1 | The effect of passage number on cell cycle progression | 64 |
| 3.5.2 | The effect of PIKK related kinases on cell cycle progression | 68 |
| 3.6 | DNA damage induction and repair..... | 69 |
| 3.6.1 | DNA damage induction and repair analysis after X-ray exposure | 71 |
| 3.6.2 | γ H2AX formation in pLECs after exposure to low doses of X-rays | 71 |
| 3.6.3 | The effect of PIK-related kinases on DNA double strand break repair | 75 |
| 3.6.4 | DNA damage induction and repair after heavy ion exposure..... | 77 |
| 3.7 | DNA damage response after X-ray exposure in whole organ culture | 79 |

| | | |
|----------|---|------------|
| 3.8 | Gene expression after exposure of pLECs to different radiation qualities | 82 |
| 3.8.1 | Gene expression after X-ray exposure | 82 |
| 3.8.2 | Gene expression after heavy ion exposure | 87 |
| 3.9 | Osteogenic differentiation of lens epithelial cells | 92 |
| 3.9.1 | Calcium deposition during osteogenic differentiation..... | 93 |
| 3.9.2 | Gene expression during differentiation | 94 |
| 3.9.3 | Influence of X-irradiation on differentiation-related gene expression | 98 |
| 4 | Discussion | 100 |
| 4.1 | Growth properties of porcine lens epithelial cells (pLECs) and whole lens organ culture | 100 |
| 4.2 | Oxidative stress determination in pLEC monolayer culture | 103 |
| 4.3 | pLEC survival after X-ray exposure | 103 |
| 4.4 | Cell cycle progression after X-ray exposure | 105 |
| 4.5 | DNA damage induction and repair after exposure to X-rays..... | 108 |
| 4.5.1 | Comparison to foci formation in other cell types | 109 |
| 4.5.2 | Comparison to foci formation in lens epithelial cells from other species... | 109 |
| 4.5.3 | Obstacles in foci quantification | 110 |
| 4.5.4 | Relevance for the threshold dose of radiation-induced cataractogenesis. | 111 |
| 4.5.5 | DNA damage and repair in the porcine eye lens | 111 |
| 4.5.6 | Involvement of kinases in γ H2AX phosphorylation | 112 |
| 4.5.7 | Relevance for space missions | 113 |
| 4.6 | Gene expression after exposure of pLECs to different radiation quantities and qualities | 114 |
| 4.7 | Role of epithelial to mesenchymal transition in cataractogenesis..... | 118 |
| 4.7.1 | Osteogenic differentiation of lens epithelial cells | 119 |
| 4.7.2 | Gene expression during differentiation | 119 |
| 4.8 | Conclusion and Outlook | 123 |

| | | |
|-----------|------------------------------|------------|
| 5 | Abstract..... | 125 |
| 6 | Zusammenfassung..... | 127 |
| 7 | References..... | 129 |
| 8 | Appendix..... | 152 |
| 8.1 | Supplementary results..... | 152 |
| 8.2 | Abbreviations..... | 155 |
| 8.3 | List of figures..... | 159 |
| 8.4 | List of tables..... | 163 |
| 9 | Acknowledgments..... | 164 |
| 10 | Curriculum Vitae..... | 165 |

1 INTRODUCTION

Human necessity and curiosity are not only the reasons for new inventions but they also motivate adventures that increase the horizon of our knowledge. Two of the best examples for this activity are the continuous human presence on the International Space Station (ISS) (Figure 1) and the preparation of long-term missions to Moon and Mars. In such missions, astronauts inevitably encounter physical and psychological hindrances due to microgravity, the confined situation and the complex space radiation environment. These extreme environmental conditions differing from that on Earth are root causes for health problems during missions. Although, psychological conditions and degenerative diseases like bone loss, muscle atrophy, cardiovascular diseases, etc. are mainly due to weightlessness and closed environment, ionizing radiation adds up to increase their severity by affecting respective cells and organs.

Furthermore, it is also known that exposure to high doses of ionizing radiation can cause acute effects starting with nausea and vomiting and even death within hours or days, depending on dose. On the other hand, late effects of radiation impose a lifelong risk for cancer, cataract, birth defects and sterility.

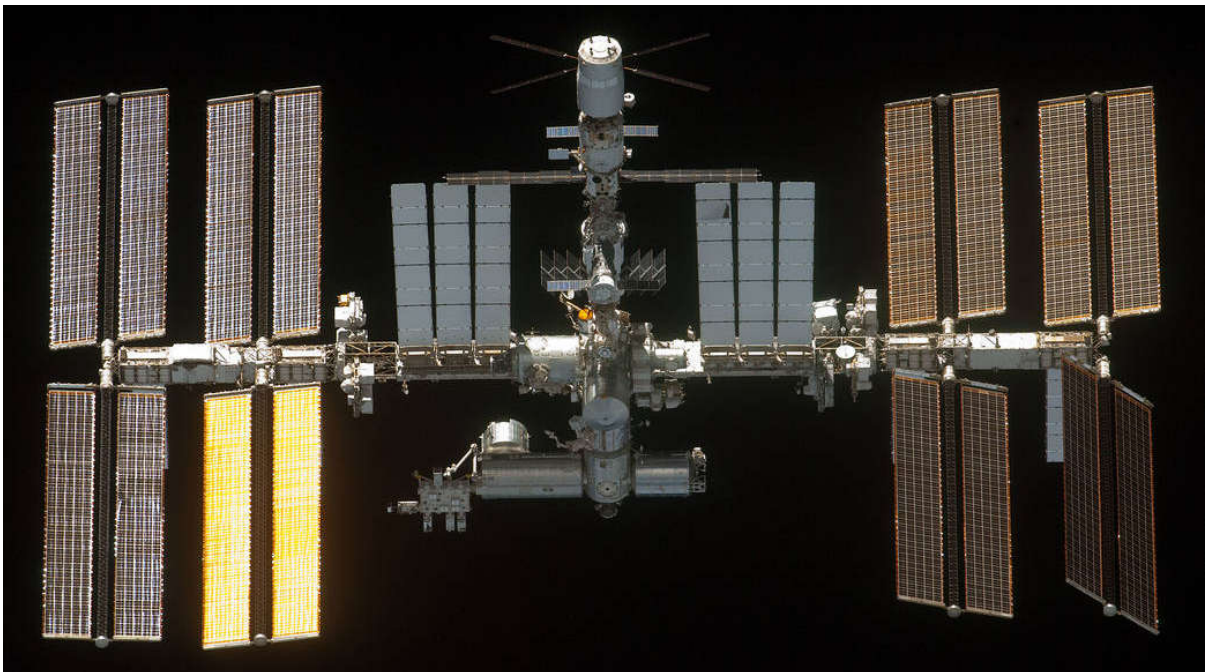


Figure 1: International Space Station (ISS). For more than 10 years so far, the ISS has been providing a permanent facility for research in space. It is located at an altitude of ~415 km in the low Earth orbit (LEO). Photo credit: National Aeronautics and Space Administration (NASA) Space Station Gallery at <https://www.nasa.gov/image-feature/international-space-station-33>, picture S134-E-011548 (29 May 2011).

Despite the excellent availability of surgical cataract treatment on Earth, formation of radiation-induced cataract during a long-term space mission would immerse as a critical threat to the mission due to the lack of treatment during such missions. For both, radiation-induced cataract and lens turbidity caused by other conditions, the exact mechanism of formation is yet unclear. This fact bears the need to elucidate the underlying mechanisms of cataractogenesis and subsequently to the search for appropriate countermeasures.

1.1 Basic terms in radiation biology

Radiation biology can be simply defined as the study of action of ionizing radiation on living systems. If the radiation has sufficient energy, which is capable of ejecting one or more electrons from orbitals of the atom or the molecule, it is defined as **ionizing radiation**.

Ionizing radiation can be of electromagnetic nature, as it is the case for X-rays, γ -radiation and vacuum ultraviolet light, or of particulate matter, e.g. protons, α -particles (helium nuclei), β -particles (electrons) and heavy ions (ions exceeding ^4He). α -, β - and γ -radiation is emitted from decaying radioisotopes; naturally occurring radioisotopes are e.g. uranium, thorium and radon (Hall 2012). To enable a better understanding of radiation effects, relevant dose-quantities are defined (Hall 2012). Different radiation units are used to describe the radiation quantity. The absorbed dose (D) is the energy deposited per mass unit. The corresponding unit is Gray (Gy, Equation 1 and Equation 2).

$$D = \frac{dE}{dm} = \frac{\text{mean energy}}{\text{mass}} = \text{absorbed dose} \quad \text{Equation 1}$$

$$1 \text{ Gy} = \frac{1 \text{ J}}{1 \text{ kg}} \quad \text{Equation 2}$$

The equivalent dose (H_T , Equation 3) is the energy dose weighted by the biological effectiveness of a certain radiation quality (W_R). W_R is a dimensionless weighting factor. The corresponding unit of H_T is Sievert (Sv, Equation 4) and is also measured in J kg^{-1} . It has to be differentiated from the strictly physical definition of dose. The linear energy transfer (LET, Equation 5) is especially important for densely ionizing radiation and

describes the energy transfer along a distance (ΔL) in the respective matter. The unit is $\text{keV } \mu\text{m}^{-1}$.

$$H_T = W_R \times D = \text{radiation weighting factor} \times \text{absorbed dose} \quad \text{Equation 3}$$

$$1 \text{ Sv} = \frac{1 \text{ J}}{1 \text{ kg}} \quad \text{Equation 4}$$

$$LET = \frac{\Delta E}{\Delta L} = \frac{\text{energy deposited along path}}{\text{path length}} \quad [LET] = \frac{\text{keV}}{\mu\text{m}} \quad \text{Equation 5}$$

The relative biological efficiency (RBE, Equation 6) is a measure for the effect size of a certain radiation quality in biological systems. The absorbed dose (D) of a test radiation (D_{Test}) is compared to a reference radiation dose (D_{Ref}) which is assumed to cause the same biological effect. The RBE depends on parameters like dose, dose rate, tissue or cell type, or biological endpoints of interest, like mutagenesis, survival, chromosomal aberration, or cancer induction.

$$RBE = \frac{D_{\text{Ref}}}{D_{\text{Test}}} = \frac{\text{absorbed dose of reference radiation}}{\text{absorbed dose of test radiation}} \quad \text{Equation 6}$$

With increasing LET also the RBE increases slowly in the beginning with regard to a cell system. Beyond 10 $\text{keV}/\mu\text{m}$ up to 100 $\text{keV}/\mu\text{m}$, the RBE increases rapidly with augmenting LET. For most of mammals cells the peak RBE value is reached around 100 $\text{keV}/\mu\text{m}$ and beyond the RBE drops to lower values Figure 2.(Hall 2012)

The optimal LET value (around 100 $\text{keV}/\mu\text{m}$) to achieve efficient RBE is of particular interest for both, radiation protection and radiotherapy of cancer. At this ionizing density, the average distance between ionizing events approximately coincides with the diameter of the DNA double helix and thus the passage of a single charged particle has the highest probability of causing a double-strand break (DSB). DSBs are known to be major players in most biological effects. In case of sparsely ionizing X-rays (LET ~ 3 $\text{keV}/\mu\text{m}$) the probability for a single track creating a DSB is lower, resulting in a low RBE for X-rays. On the other hand, densely ionizing radiation (e.g. LET of 200 $\text{keV}/\mu\text{m}$) produces enough DSBs but most energy is wasted as ionizing events are too close to each other.

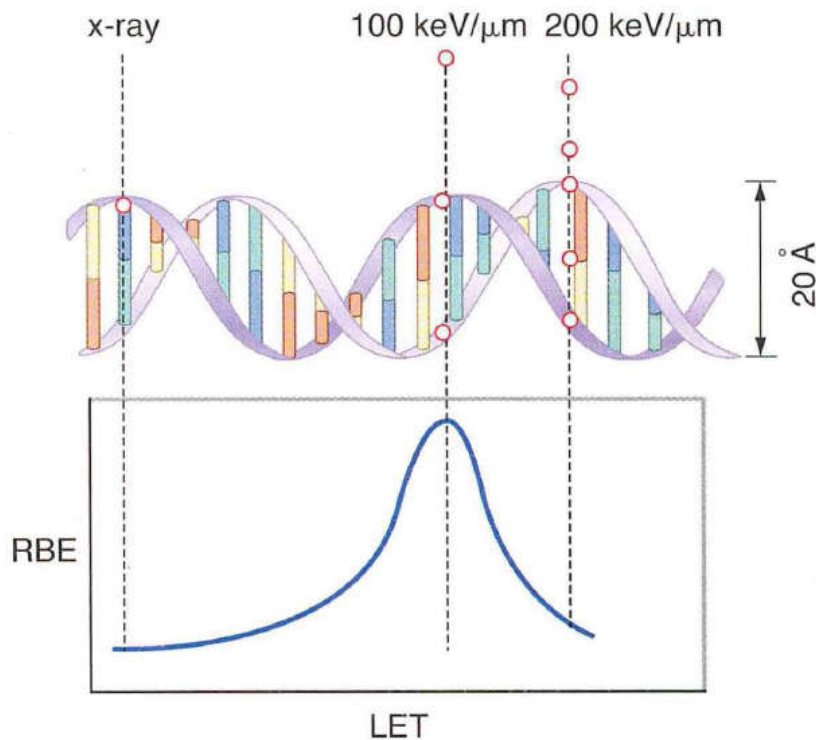


Figure 2: RBE and LET relationship. The biological effects like cell killing, mutagenesis and carcinogenesis are highest after exposure to ionizing radiation with an LET of about 100 keV/μm. For such radiation, the distance between two ionizing events coincides with the diameter of the DNA double helix (20 Å or 2 nm) (Hall 2012).

Since the RBE is the ratio of doses which produce the same extent of a biological effect, for low LET radiation RBE augments slowly with increasing LET whereas for high LET radiation RBE increases sharply to a maximum then follows a drop which is due to the overkill effect (such high energy can kill more cells than actually available, or for an individual cell, more dose is deposited than would be required for inducing cell death).

1.2 Space radiation

The radiation environment in space is quite distinct from the Earth's. Within the low Earth orbit (LEO), the Earth's magnetic field contributes to a partial protection, however, in future interplanetary and planetary missions beyond LEO, astronauts will be exposed to higher dose rates of galactic cosmic radiation (GCR), solar cosmic radiation (SCR) as well as radiation in the van Allan Belts (Figure 3). Additionally, the South Atlantic Anomaly (SAA) (Kurnosova et al. 1962), the area where Earth's inner van Allen Belt (1000 to 6000 km above Earth (Ganushkina et al. 2011)) dips down to an altitude of about 200 km (ECSS 2008) due to the weakened geomagnetic field center, poses a threat to all astronauts, space crafts or satellites due to increased flux of energetic particles.

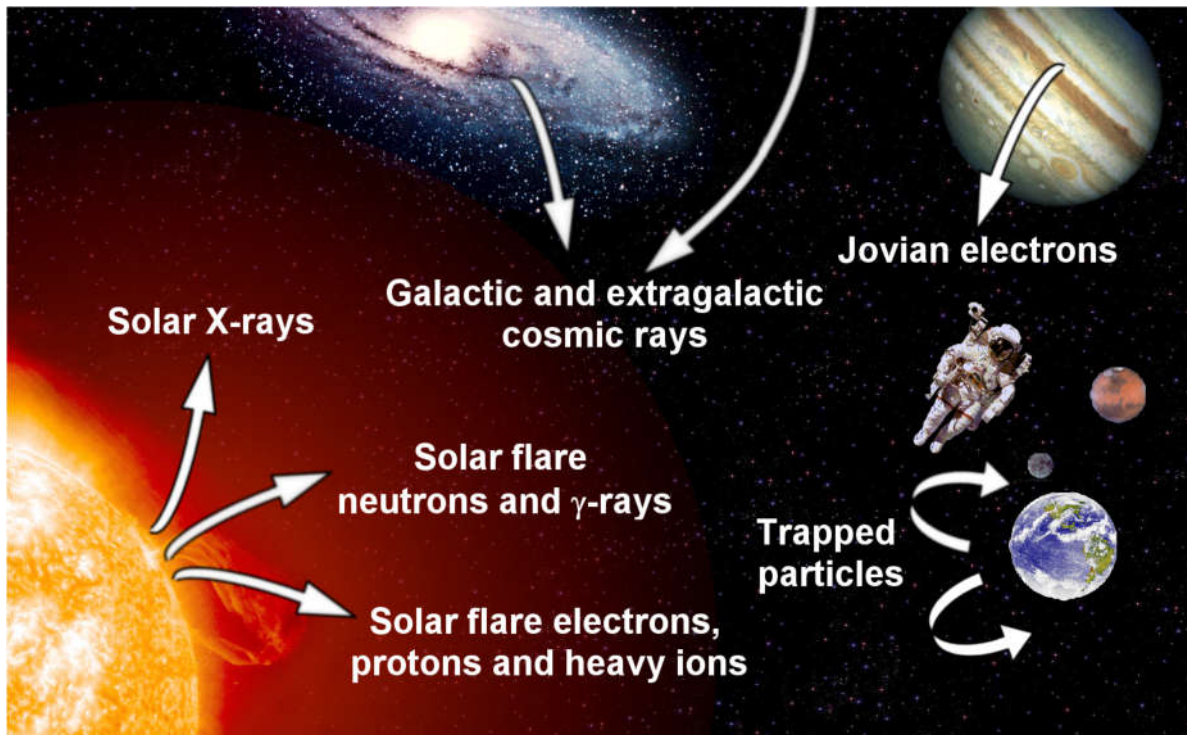


Figure 3: Space radiation. The components of space radiation are either of solar origin (predominantly protons but also neutrons, X-rays, γ -rays, electrons and heavy ions, which are especially recognized after solar flares) and of galactic origin (energetic protons, α -particles and heavy ions). Charged particles (protons and electrons) are trapped in the van Allen Belts surrounding the Earth (modified from (Hellweg and Baumstark-Khan 2007)).

GCR (Badhwar and O'Neill 1994, Baranov et al. 2002, Bazilevskaya et al. 1994, Pissarenko 1994, Shea and Smart 1998, Wilson et al. 1999) originates from outside our solar system. It is composed of ~87% protons (hydrogen nuclei), ~12% α -particles (helium nuclei), and ~1% of heavy ions with an energy range of less than 1 MeV to more than 10^{12} MeV. The flux of GCR fluctuates with the solar cycle (Badhwar 1997, Wilson et al. 1989, Hellweg and Baumstark-Khan 2007). The GCR flux of increases at minimum solar activity and decreases at maximum solar activity.

SCR is mainly composed of protons, about 10% of helium ions and about 1% of heavy ions and electrons. SCR originates from the Sun's surface and constantly travels to the Earth via the solar wind. During solar particle events (SPE), highly energetic charged particles are ejected from magnetically disturbed regions of the sun (Wilson et al. 1999, Smart and Shea 2003).

Van Allen Belts consists of highly energetic particles from GCR and SCR, mainly electrons and protons, which are trapped in two belts due to Earth's geomagnetic field. The biological evidence of presence of such energetic particles have been experienced

as visualization of light flashes by astronauts during Apollo, Skylab, MIR and ISS missions (Sannita et al. 2006, Zaconté et al. 2006, Avdeev et al. 2002, Casolino 2006, Bidoli et al. 2002, Fuglesang 2007). Light flashes are different shapes (strike, spot, line, etc.) of light perceived due to interaction of cosmic radiation with the human eye. Measurements of the radiation environment and particle abundance in MIR and ISS have shown that, at SAA, the flux of protons as well as heavy ions, with an energy at the MeV range, is increased (Sannita et al. 2006, Bidoli et al. 2002). Due to higher prevalence of radiation in the SAA, the ISS needs additional shielding, astronauts avoid extravehicular activities and also the astronomical data are being disturbed (Heitzler 2002).

On the ISS, a radiation dose rate of 0.5 mSv per day (Beaujean et al. 2002, Reitz et al. 2005) was measured which increased by three times during extravehicular activities (Reitz and Berger 2006). Similarly, in an interplanetary Mars mission, which might last around three years (Grigoriev et al. 1998), a GCR dose of up to 1.0 Sv can accumulate at blood-forming organs which might cause late radiation effects in the astronauts (Horneck et al. 2006). On the other hand in such a mission, during the solar flares the dose can reach up to 4.2 Gy within a few hours to days which can trigger acute radiation effects (Horneck et al. 2006). However, since the solar flare dose depends on the solar cycle and shielding, it can be avoided to some extent by proper alerts and shelters but at the cost of valuable time and a much higher launch weight.

Despite the low frequency of heavy ions (HZE) in space radiation, their high charge (Z) and high energy (E) and their secondary radiation make them more dangerous for the cells compared to protons or X-rays. For this reason, it is important to know the RBE of space radiation quality. In view of the higher biological effectiveness of space radiation (compared to most environmental radiation on Earth) 1 Gy of heavy ions may result in an equivalent dose of up to 20 Sv (Cucinotta and Durante 2006).

1.3 Biological consequences of ionizing radiation exposure

The biological consequences of ionizing radiation exposure are preceded by very short-lived physico-chemical chain of events. The formation of primary radicals by ejection of an electron takes 10^{-10} seconds. The hydroxyl radical (OH^{*}) has a lifetime of 10^{-9} seconds in a cell. The DNA radicals formed have a lifetime of about 10^{-5} seconds. Eventually, the time between the breakage of chemical bonds and a biological effect

may vary from hours, days, months, years and even to generations depending on the nature of damage involved.

The damaging effects of ionizing radiation depend on dose, frequency and quality of the radiation. A brief overview of biological consequences due to acute and chronic exposure of ionizing radiation is presented in Table 1.

Acute radiation effects appear within a short period of time (minutes to days) usually after exposure to a high radiation dose, whereas, chronic radiation effects are the result of long-term exposure exceeding a permissible occupational dose (Hellweg and Baumstark-Khan 2007). Likewise, delayed radiation effects, like cancer, occur when the combined dose and dose rate are not high enough to generate acute cytotoxicity effects but rather generate genotoxicity.

Table 1: Radiation effects in humans after whole body irradiation (adapted from (Hellweg and Baumstark-Khan 2007)).

| Chronic dose | Risk | |
|-------------------|--|--|
| ~0.4 Sv | First evidence of increased cancer risk as late effect from protracted radiation | |
| 2-4 Sv/year | Chronic radiation syndrome with complex clinical symptoms | |
| Acute single dose | Effect | Outcome |
| <0.25 Sv | No obvious direct clinical effects | |
| >0.5 Sv | Nausea, vomiting | No early death anticipated |
| (>0.7) 3–5 Sv | Bone marrow syndrome: Symptoms include internal bleeding, fatigue, bacterial infections, and fever. | Death rate for this syndrome peaks at 30 days, but continues out to 60 days. |
| 5–12 Sv | Gastrointestinal tract syndrome: Symptoms include nausea, vomiting, diarrhea, dehydration, electrolytic imbalance, loss of digestion ability, bleeding ulcers | Deaths from this syndrome occur between 3 and 10 days post exposure. |
| >20 Sv | Central nervous system syndrome: Symptoms include loss of coordination, confusion, coma, convulsions, shock, and the symptoms of the blood forming organ and gastrointestinal tract syndromes | No survivors expected |

Deterministic and stochastic effects are two well-known terminologies in understanding radiation effects. The deterministic effect has a threshold value, above which the severity of the effect increases with radiation dose. Deterministic effects are predictable effects depending on radiation dose. The probability of occurrence of such an effect increases with radiation dose (e.g., acute radiation syndrome, side effects of radiotherapy). Stochastic effect does not have a threshold value and the severity of effect is independent of radiation dose. The occurrence of stochastic effects is not predictable whereby even damage to a single cell could be its cause. Nevertheless, the probability of occurrence of stochastic effects also increases with radiation dose like the deterministic effect (e.g., cancer) (Hall and Giaccia, 2012). The induction of tumors has been discussed as one very important long-term secondary disorders (Pierce et al. 1996, Zaider 2001, Brooks 2003, Cancer 1994) for less than 1 Sv/year exposure (Hellweg and Baumstark-Khan 2007).

In ICRP 2012, it was pointed out that the classically defined radiation effects depend upon the target cell whereby severity, latency and manifestation of injuries are dependent on killing and the characteristics of the target cells (radiation sensitivity, repair capacity, proliferation rate, etc.) as well as on tissue organization. Now, it is clear that cell killing alone is not sufficient to explain radiation effects of the exposed tissues. In addition to direct cell killing, alterations of biomolecules, signaling pathways, reactive oxygen and nitrogen species, genetic damage, etc. could impart radiation effects which eventually lead to alterations of cell function as well as delayed cell death (Clement 2012, Denham 2001, Brush et al. 2007, Bentzen 2006).

1.4 Cellular effects of radiation

The mode of action of ionizing radiation at the cellular level can be of direct or indirect nature. If the radiation energy is directly absorbed by macromolecules (like DNA or proteins) that are responsible for the biological effects, then it is called direct effect. The effect is called indirect if the ionizing radiation first interacts with a water molecule to produce $\text{OH}\bullet$ radicals or other reactive oxygen species (ROS), which then affect important biomolecules (Figure 4).

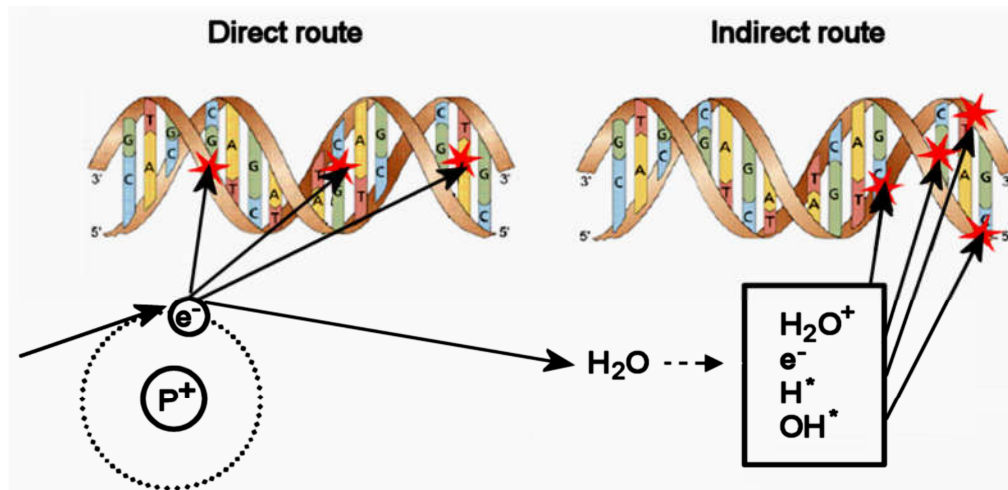


Figure 4: Direct and indirect radiation damage. Damage to DNA can be induced either directly or indirectly via free radicals evolved from the irradiated water molecules (courtesy of C. Baumstark-Khan, DLR, Germany)

One of the most critical biomolecules within the cell is DNA that carries genetic information required for the correct functioning of the cell. The radiation-induced DNA damage in the cells triggers the activation of cellular defense systems as DNA repair pathways, cell-cycle check points or even apoptosis and senescence. Successful repair of damages results in cellular survival. In case of faulty repair, consequences may include genetic damage and possibly also the induction of carcinogenesis. Finally, if the damage is not repaired cell death or senescence can be induced (Figure 5).

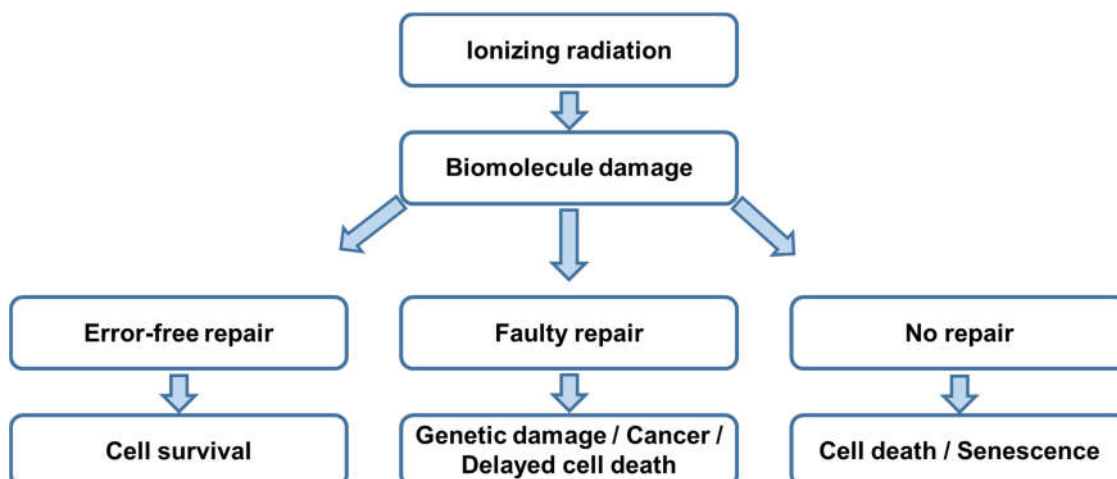


Figure 5: Consequences of ionizing radiation exposure of a biological system. Cells damaged due to ionizing radiation can further survive healthily if the damages are repaired without any error. The cellular fate also could be death or senescence if damage could not be repaired. The faulty repair resulting in mutation could lead to carcinogenesis, bring about hereditary changes or delayed cell death.

1.4.1 DNA damage and repair pathways

It is well known that the main target for the biological effects of ionizing radiation is the DNA in terms of cell killing, carcinogenesis and mutations. The type and amount of damage is governed by the type and dose of radiation (Baumstark-Khan 1993, Hada and Sutherland 2006). Radiation exposure can produce various types of DNA damage encompassing base damages, single strand breaks (SSBs), double strand breaks (DSBs), sugar damages as well as DNA-DNA and DNA-protein crosslinks. The energy deposition of sparsely ionizing low-LET radiation (X-rays and γ -rays) is diffusely distributed and produces four times more non-DSB damages than direct DSB (Eccles et al. 2011). Densely ionizing high-LET radiation (heavy-ions) generates clustered DNA damage with a high percentage of DSB (Ward 1994). The lesions caused by high-LET radiation are difficult to repair accurately and thus are assumed to be one cause for the high RBE of this radiation quality (Kozubek and Krasavin 1984, Fakir et al. 2006).

In order to overcome DNA strand breaks cells have evolved very specialized DNA repair pathways. SSBs are less effective in killing of cells because they are easily repaired by using the opposite strand as the template. The main pathway that cells have selected for SSB repair is the single-strand break repair (SSBR) involving amongst others poly(ADP-ribose) polymerase 1 (PARP1), Poly(ADP-ribose) glycohydrolase (PARG), AP endonuclease I (APE1), XRCC1, polynucleotide kinase 3'-phosphatase (PNKP), aprataxin (APTX), flap endonuclease 1 (FEN1), PCNA, polymerase β or δ/ϵ and DNA ligase 1 or 3 (Caldecott 2008). Indirect SSBs and some base damages can be repaired by the base excision repair pathway (BER) where molecules like PARP1, XRCC1 and ligase 3 play a very crucial role. DNA-DSBs, on the other hand, are known to cause fatal damage either by genetic damage or by cell killing when not repaired (Dalinka and Mazzeo 1985). In repairing DSBs, mammalian cells make use of two main basic processes known as homologous recombination (HR) and non-homologous end joining (NHEJ). The amount of repetitive DNA and the phase of the cell cycle of the damaged cell govern the choice of repair pathway for DSBs. HR occurs at the late S and G2 phase of the cell cycle in which it uses the undamaged sister chromatid as the template. The use of an undamaged template makes HR an error-free repair pathway. NHEJ on the other hand is an error prone pathway where the damaged sites are directly ligated in absence of sister chromatids. This pathway is known to produce mutagenic lesions. NHEJ occurs at the G1 phase of the cell cycle.

DSBs generation due to ionizing radiation activates many sensor molecules, which play a key role in damage detection and initiation of DNA repair. Protein kinases belonging to the phosphatidylinositol-3-kinase-related kinase (PIKK) family: ataxia telangiectasia mutant (ATM), ataxia telangiectasia and rad3-related protein (ATR) and DNA-dependent protein kinase (DNA-PK), are activated in response to ionizing radiation (Cimprich and Cortez 2008, Shrivastav et al. 2008, Tichý et al. 2010). ATM is a key player, whose activation leads to phosphorylation of many proteins including p53 and Checkpoint kinase 2 (Chk2) resulting in activation of DNA damage checkpoints, cell cycle arrest, damage repair or apoptosis (Warmerdam and Kanaar 2010). The detection of DSBs starts with phosphorylation of histone H2AX to γ H2AX by ATM at serine 139. ATM also promotes the activity of the Mre11-Rad50-Nbs1 (MRN) complex which results in resection of DNA ends (Zhao et al. 2000, Wu et al. 2000). 53BP1 proteins (at this step) are in part capable of inhibiting HR by binding to histones and blocking phosphorylation by ATM (Bunting et al. 2010).

HR takes place after lesion recognition and processing of the broken DNA double strand into a 3' DNA single strand by the MRN protein complex. Some of other key proteins that are involved in HR are RPA, RAD52, RAD51 and BRCA1/2. **NHEJ** is initiated by binding of the Ku70/Ku80 heterodimer at the DSB region. The Ku complex then recruits and activates DNA-PK and in the following, DNA-PK recruits other molecules required for ligation including XRCC4 and DNA ligase 4 (**Figure 6**).

1.4.2 Cell cycle arrest

For the continuity of life, it is necessary to produce copies of cells from a parent cell in a continuous process called the cell cycle. In mammalian cells, the mitotic cell cycle consists of four phases i.e. M-phase representing mitosis, S-phase which stands for DNA synthesis phase, G1-phase being the first gap between M- and S-phase and G2-phase being the second gap between S- and M-phase.

The regulation of the cell cycle (**Figure 7**) is governed by the protein complexes of cyclins and their respective cyclin-dependent kinases (Cdks) (Cude et al. 2007, Wilson 2004). Similarly, different checkpoints (G1/S checkpoint, S-phase checkpoint and G2/M checkpoint) provide cells with possibility to either have time to repair the damage before entering the subsequent phase or stay at halt if the damage cannot be repaired. It is widely accepted that a lack of the ability to respond to those signals is a main reason for carcinogenesis (Ford et al. 1998, Hartwell 1992, Deng 2006).

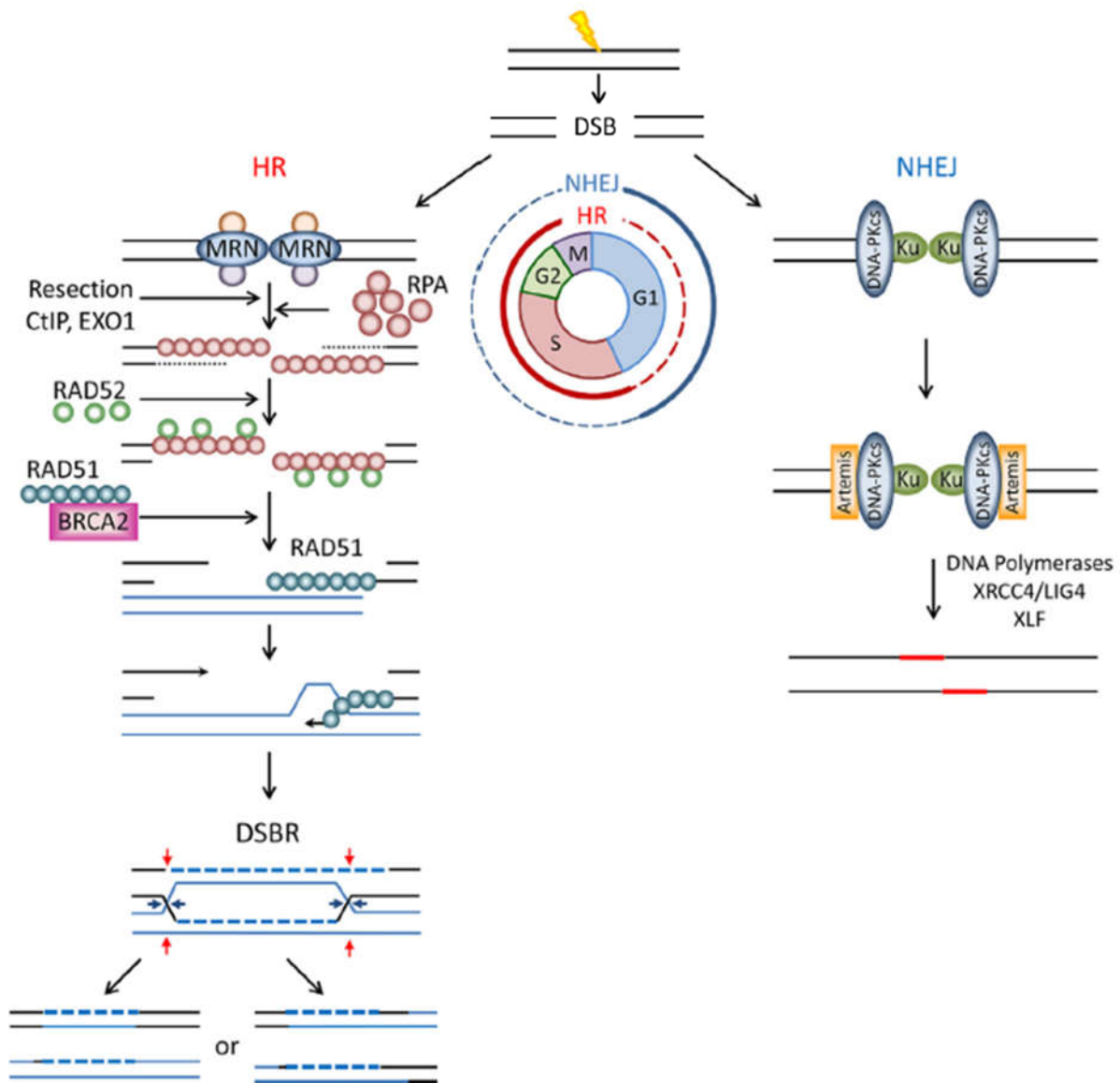


Figure 6: DNA double strand break repair pathways. HR takes place in dividing cells during S- and G2-phase of the cell cycle. HR starts by binding of MRN complex (MRE11-RAD50-NBS1) to the break. 5'→3' resection takes place by help of C-terminal binding protein 1 (CtBP1) interacting protein 1 (CtIP) to form a 3' ssDNA overhang. Further resectioning is performed by exonuclease EXO1. The ssDNA thus formed is stabilized by binding of RPA, and RAD52 is recruited to RPA. Then RAD51-BRCA2 complex replaces RAD52-RPA to form RAD51 nucleoprotein filament which catalyzes the interaction with the sister chromatid. Strand invasion in the sister chromatid results in formation of a Holliday junction which is followed by synthesis and religation and finally disintegration of strands. NHEJ occurs in both dividing and non-dividing cells independent of cell cycle phase. It starts by recognition of DSB ends by the Ku-heterodimer (Ku70/Ku80) to prevent degradation. DNA-dependent protein kinase catalytic subunit (DNA-PKcs) is recruited and activates Artemis protein that generates 3'/5' overhangs. Finally, DNA synthesis is carried out to fill-in the gaps and end joining is done by XRCC4-LIG4 with cooperation with XLF. (Adapted from (Iyama and Wilson 2013))

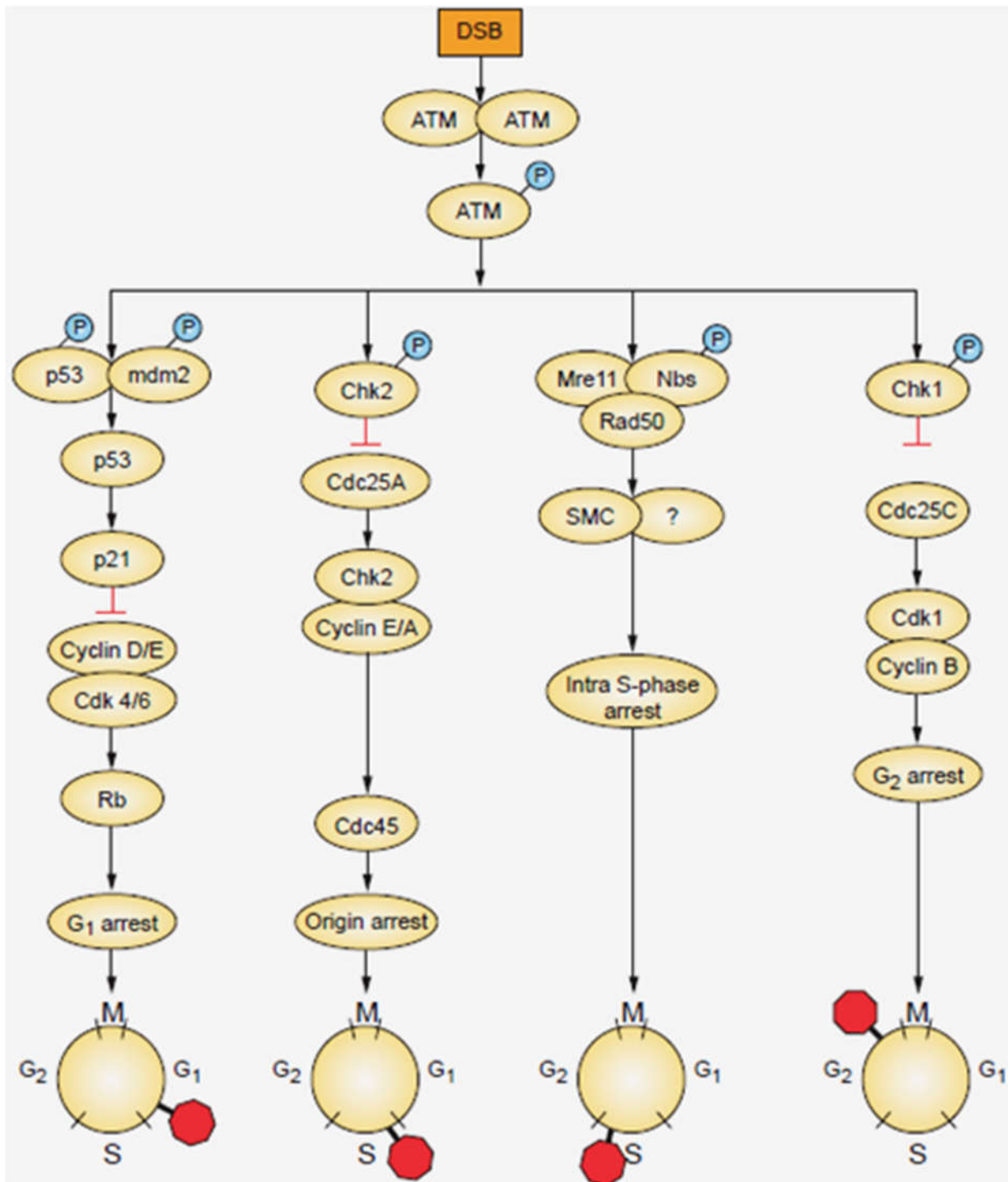


Figure 7: Role of ATM and its downstream effectors in the regulation of the cell cycle. With induction of DNA damage, ATM is activated by autophosphorylation at Ser(367), Ser(1893), Ser(1981) and Ser(2996) and acetylation on Lys(3016). This activated ATM then phosphorylates different target molecules at different cell cycle phases. In G₁-phase, ATM phosphorylates p53 and mdm2, resulting in increase of p21, which inhibits Cyclin D/E-Cdk4/6. In late G₁- or in early S-phase, ATM phosphorylates Chk2 that in turn phosphorylates Cdc25A, a phosphatase that inhibits Cyclin E/A-Cdk2 activity. In S-phase, ATM phosphorylates NBS and SMC proteins, which transiently inhibit DNA synthesis. In G₂-phase, ATM phosphorylates Chk1 that in turn phosphorylates Cdc25C, a phosphatase that inhibits Cyclin B-Cdk1 activity. (Hall 2012)

A lot of investigations have been carried out to analyze the interplay of DNA damage induction by radiation and regulation of cell cycle control mechanisms. Of all, the G2/M checkpoint is found to be most important for radiation-induced DNA damage (Cucinotta et al. 2001, Gogineni et al. 2011, Xu and Kastan 2004, Hu et al. 2014). Regardless of the checkpoint, ATM has been found to be the key player in cell cycle regulation after DNA damage. Figure 7 shows the role of ATM as the primary effector molecule for different checkpoints.

1.5 The crystalline lens

The eye lens is a transparent biconvex structure with a steeper curve at the posterior surface, whose primary function is refraction and focusing of the light on the retina. The lens is located just behind the iris, anterior to the vitreous chamber, suspended from the ciliary body by zonular fibers. The absence of blood vessels, fewer cellular organelles, orderly arranged fibers and the short distance between components of different refractive indices are the basis for lens transparency (Trokel 1962).

1.5.1 The lens capsule

The lens capsule envelops the whole lens and shapes it. It is considered to protect the lens from bacteria and viruses as it sequesters the lens epithelium and fibers. It accumulates molecules and growth factors that are required for proliferation, migration and differentiation of lens cells (Danysh and Duncan 2009). Similarly, it also allows the only passive exchange of metabolic substrates and waste, and it filters molecules depending on their size and charge (Danysh and Duncan 2009).

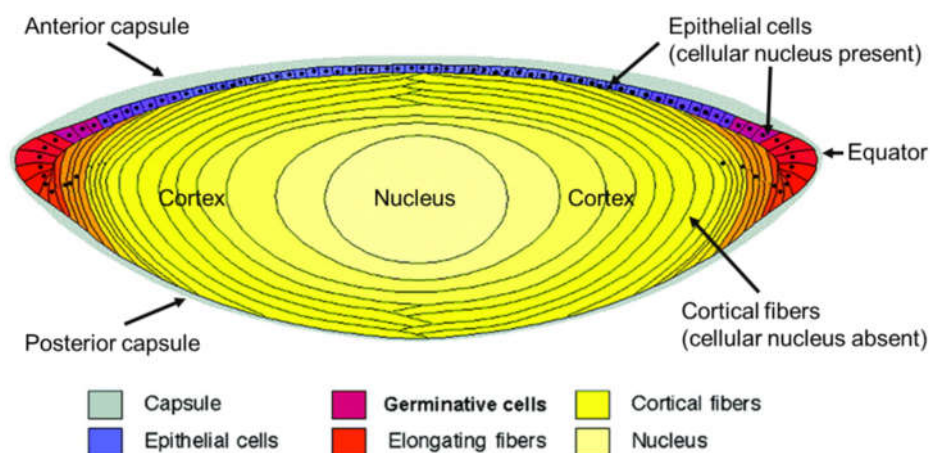


Figure 8: A cross-section diagram of the human eye lens. (Adapted from (Maidment et al. 2004))

1.5.2 Lens epithelium

Lens epithelial cells are cuboidal. Their basal surface is connected to the capsule and their apical part orients itself toward the center of the lens. Lens epithelial cells secrete the capsular material throughout life and are also the site of metabolic transport mechanisms. These lens epithelial cells are connected with each other by desmosomes and gap junctions. The cells at the anterior pole are in a mitotically resting state while the cells in the germinal zone (just anterior to the equator) are mitotically active. Cell division occurs throughout the life whereby divided cells move towards the equator, withdraw from the cell cycle and differentiate into the lens fiber cells. After the division, the cells elongate; they degrade their nucleus and other cell organelles and become secondary lens fibers or cortical fibers (Remington and Goodwin 2011, Kuwabara 1975).

1.5.3 Lens fibers

Lens fibers are the continuously produced concentric layer of secondary lens fiber cells and they are arranged like layers in an onion. The lens fiber cells contain about 30 % to 35 % proteins of which 90 % are water-soluble crystallins and 10 % are insoluble proteins (microtubules and filaments) that form the cell membrane and the cytoskeleton. Lens crystallins are categorized in the alpha family and the beta/gamma superfamily. Alpha-crystallins act as molecular chaperons to stabilize beta- and gamma-crystallins that prevent the formation of protein aggregates and thus provide lens transparency (Takemoto and Sorensen 2008).

1.6 Cataract and its types

The eye lens is one of the most radiosensitive tissues in the human body and lens cataractogenesis is the leading cause of blindness worldwide (Roodhooft 2002). Cataract is defined as opacification of a transparent lens, which would lead from a simple obstruction to the complete loss of vision. The etiology of cataract formation is complex and not fully understood and cataract development is the outcome of multiple co-acting factors. Besides aging as a major contributor, diseases, metabolic deficiencies, trauma, congenital factors and environmental stress (e.g., radiation) comprise major risk factors for cataractogenesis (Remington and Goodwin 2011). Based on the location of the opacification, the cataract can be categorized into three main types; nuclear cataract, cortical cataract and posterior sub-capsular cataract.

The **Nuclear cataract** is mainly age-related and occurs at the center of the lens. It is due to oxidative damage leading to modifications of the crystallins which gives a characteristic yellow or brown color to the cataract (Truscott 2005). In the lens capsule, glutathione is the main molecule that maintains the reducing environment and protects from oxidative stress. A reduction of the glutathione concentration is correlated with the development of cataract (Reddy 1990, Sweeney and Truscott 1998, Truscott 2000). The amount of glutathione in the lens nucleus decreases with age, which can be due to either an increase in thickness of the cortex or to continuous growth of lens epithelial cells or to modification of gap junctions (Sweeney and Truscott 1998, Moffat et al. 1999) and aquaporin (Korlimbinis et al. 2009).

Similar to the nuclear cataract the **Cortical cataract** also occurs mainly because of aging. The affected cells are comparatively younger fiber cells, which overlie the nucleus. Such cataracts are mainly associated with disturbances in fluid regulation. The dysfunction of Na^+/K^+ ATPase pump is an example where the influx of water is increased in fiber cells due to an increase in the Na^+ concentration in the cytoplasm (Delamere and Tamiya 2008). Similarly, an increase of the cytoplasmic Ca^{++} concentration (Delamere and Tamiya 2009) is also associated with the increased fluid influx in the fiber cells. Such swelling results in fiber cell disruption and contributes to the scattering of light.

Posterior sub-capsular cataract (PSC) is the opacification of the lens at the posterior capsule. It is well known that ionizing radiation causes PSC although the exact mechanism for cataract formation is yet unclear. Nonetheless, the lens opacification is hypothesized to initiate from post irradiative activity of genetically damaged lens epithelial cells with conflicts in cell cycle control, apoptosis, abnormal differentiation, and cellular disorganization, or other pathways leading to abnormal lens protein fibers (Worgul and Merriam 1979, Worgul and Merriam Jr 1980, Worgul and Merriam Jr 1981, Rothstein et al. 1982). PSC is also known to be caused by long-term use of high doses of steroids (Weatherall et al. 2009, Hodge et al. 1995). Posterior capsular opacification has been reported to occur after cataract removal surgeries as well. Those incidences ranges from as high as 50% to as low as <5% (Schmidbauer et al. 2002, Dholakia and Vasavada 2004, Thompson et al. 2004, Raj et al. 2007) on the newly implanted intra-ocular lens (IOL). Such secondary cataract arises due to growth of residual lens epithelial cells that move towards to the posterior capsule of the lens.

1.7 Radiation cataractogenesis

Not only astronauts in space and jet crew members who are confronted with a different quantity and quality of radiation than on Earth (Hellweg and Baumstark-Khan 2007), have an increased risk for larger PSC lens opacities from exposure to even relatively low radiation doses (Chylack Jr et al. 2009, Cucinotta et al. 2001, Jones et al. 2007, Peterson et al. 1993, Rastegar et al. 2002) but also radiotherapy patients, atomic bomb survivors, individuals experiencing nuclear accidents, occupational exposure (Ainsbury et al. 2009, Dynlacht 2013) have been reported to develop PSC. Cataracts can also be induced in animal experiments.

Previously, the International Commission on Radiological Protection (ICRP) categorized cataracts as a deterministic effect with a threshold of 2 Gy for acute radiation exposure, 4 Gy for fractionated exposure and higher doses of protracted exposures (Valentin 2007). However, recent studies showed that the threshold dose for radiation-induced cataract is very low or even zero leading to the hypothesis that cataractogenesis is a stochastic late effect. Consequently, the ICRP (2011) set 0.5 Gy as the threshold in absorbed dose for radiation-induced cataract and recommended to reduce the occupational exposure limit to 20 mSv/yr, averaged over defined periods of 5 years, with no single year exceeding 50 mSv (Cousins et al. 2011).

1.8 Mechanisms leading to radiation-induced cataract

The mechanism of age related cataract is mostly attributed to oxidative damage, the lack of glutathione (the reducing agent) and the dysfunction of gap junctions and ion pumps, which actually lead to redox state dis-balance (Sweeney and Truscott 1998, Korlimbinis et al. 2009). On the other hand, mechanistic studies of radiation induced cataract (PSC) are mainly based on DNA damage and repair incapability of lens epithelial cells, which differentiate to fiber cells and in some extent also due to structural protein damage after radiation exposure. Studies have shown that ultraviolet (UV) radiation exposure led to changes in crystallins which disturbed the arranged folded structure of crystallins leading to opacification (Xia et al. 2013, Schafheimer and King 2013). Also a recent study by Abdelkawi showed a link of cataract formation between the induction of crystallin's cross-linking and the aggregation by single (4.0 Gy) and fractionated (8 weeks, 0.5 Gy/week) doses of γ -radiation (from Cesium-137) in Wistar albino rats (Abdelkawi 2012).

With regard to cataract, which is attributed to a genetic damage in lens epithelial cells, it is important to inspect the genes or the proteins that are key players in cellular growth and survival. Owing to this fact, one of the key molecules that has been extensively studied for cataractogenesis is the ATM gene. On the one hand, ATM is involved in regulating multiple cell cycle checkpoints by phosphorylating different target molecules (Abraham 2001, Jazayeri et al. 2006, Goodarzi et al. 2003). On the other hand, ATM is important for the phosphorylation of γ H2AX which is a vital step in DNA repair (Morrison et al. 2000, Stiff et al. 2004, Burma et al. 2001, Riballo et al. 2004, Celeste et al. 2003). It has been shown in ATM-deficient mice, that homozygotes developed opacification earlier compared to heterozygotes and that cataract formation after X-ray exposure was dose-dependent and appeared earlier in heterozygotes compared to the wild-type mice (Worgul et al. 2002). Along with ATM, RAD9 and BRCA1 are involved in radiation cataractogenesis (Kleiman et al. 2007, Hall 2008). To study the role of ATM in heavy ions-induced cataract formation, mice were exposed to ^{56}Fe ions. It could be depicted that ATM heterozygous mice were more sensitive to heavy ion-irradiation compared to wildtype mice (Worgul et al. 2005, Ainsbury et al. 2009). Similarly, in vitro data from the lens epithelial cells for the function of different key proteins in the DNA damage response from DNA damage repair proteins to transcription factors like Nuclear Factor κ B (NF- κ B) also assume a strong correlation for damage in the epithelial cell layer and opacifications in the fiber cells (Carper et al. 1999, Sivak et al. 2004, Imai et al. 2010, Shirai et al. 2001, Wu et al. 2009, Zhang et al. 2010).

Other extensive research to uncover the mechanism of radiation-induced cataracts was carried out at the Life Science Division in Lawrence Berkeley National Laboratory, California. For their studies, primary human lens epithelial (HLE) cells were isolated from 18-weeks prenatal lenses (Blakely et al. 2000). The alteration of gene and protein expression profiles of selected key molecules like CDKN1A (Chang et al. 2005), MMP (Chang et al. 2007) and FGF2 (Chang et al. 2000) after the exposure to different radiation qualities was correlated with the possibility of changes in the lens fiber cells' differentiation process which could be the reason for lens opacification. On the other hand, CDKN1A, which has a key role in the regulation of cell cycle, DNA synthesis and stress responses, was found to be up-regulated as a function of the LET (Chang et al. 2005).

Both studies with non-human and with human cells contribute to exploring the mechanism of cataract formation and also indicate the threat of exposure of lens epithelial cells to space related high-LET radiation which crave for much more detailed understanding and possibilities for its prevention and cure.

1.9 Osteogenic differentiation as an alternative mechanism behind lens turbidity

Currently, many studies with regard to the formation of cataracts focus on oxidative environment imbalance, dysfunction of Na^+/K^+ pump, gap junction malfunction and injury to lens epithelial cells. In similar ways, also the involvement of calcium in cataract formation has been an interesting and reasonable assumption.

Already in 1937, Burge et al. who were working with pig lenses proclaimed the accumulation of calcium salts that resulted in loss of elasticity and transparency of the crystalline lens (Burge et al. 1937). In this study, the group summarized that calcification of the crystalline lens could have taken place (similar to calcification of other soft tissues e.g. vascular calcification) due to the production of negatively charged phosphate ions that interact with positively charged calcium ions resulting in the precipitation of insoluble calcium phosphate. In their experiments, the production of negatively charged phosphate ions was induced by exposure to 302 nm ultra-violet rays. Seeing the importance of the increased calcium in lens for loss of transparency and decrease in dry weight (Boutros et al. 1984), Marcantonio and colleagues worked with bovine lenses to study the role of calcium in cataract formation and protein leakage (Marcantonio et al. 1986). They found out that the loss of transparency and protein was seen only in the lenses in which calcium was increased, mainly at the outer cortical fiber region. In addition to that, the proteins mainly β_L -crystallins, were lost and the increased calcium level caused the susceptibility of crystallins to form aggregates.

In a recent study (Balogh et al. 2016), the authors showed the capability of human lens epithelial cells to undergo osteogenic differentiation in the presence of differentiation medium and proposed that such misdifferentiation might play a role in lens calcification. This study was based on the fact that vascular calcification and lens calcification share a similar mechanism. As mentioned earlier, calcification starts with the generation of negatively charged phosphate ions which combine with positively charged calcium ions. But since recently, it is well accepted that vascular calcification is an active and highly

regulated cellular process where osteo-/chondrogenic differentiation of vascular smooth muscle cells (VSMCs) takes place similar to mineralization of bone (Liu and Shanahan 2011, Steitz et al. 2001, Giachelli 2001, Balogh et al. 2016). Till today many osteogenic triggers for VSMCs have been documented and studied including for example an increased amount of phosphate (Kendrick and Chonchol 2011, Giachelli et al. 2005, Jono et al. 2000), an increased amount of calcium (Mizobuchi et al. 2009, Yang et al. 2004, Reynolds et al. 2004), chronic inflammation, oxidative stress and aging (Doherty et al. 2003, Mizobuchi et al. 2009, Scatena et al. 2007, Johnson et al. 2006). On one hand an increased level of phosphate (Pi) could elevate the VSMCs mineralisation in a concentration-dependent manner (Giachelli 2003, Giachelli et al. 2001), on the other hand Pi also could induce osteogenic differentiation markers in VSMCs like Osteocalcin (OCN), Osteopontin (OPN) and Runt-related transcription factor 2 (RUNX2) (Beck and Knecht 2003, Beck Jr et al. 2003, Sage et al. 2011, Beck Jr 2003, Fujita et al. 2001). Regarding the osteogenic differentiation process, one of the extensively studied molecules is Bone morphogenetic protein 2 (BMP2) due to its involvement in bone and cartilage development (Hruska et al. 2005, Shao et al. 2006, Ryoo et al. 2006, Thomas et al. 2001, Li et al. 2008b).

It is clear that lens epithelial cells undergo epithelial to mesenchymal transformation to form fiber cells. Injuries and aberrations during such transitions are hypothesized to cause opacification. Space travel for longer duration directly corresponds to longer physical inactivity of astronauts' musculoskeletal system. There is clear evidence that astronauts face muscle atrophy and bone loss (LeBlanc et al. 2000, Sibonga et al. 2007, Heer et al. 1999). 4-6 months of stay in space costs about 0.9 - 1.6% of bone mass per month (Heer et al. 1999). Despite the observed bone loss in astronauts, the serum calcium and ionized calcium actually did not show consistent measurable changes during the flight (Smith et al. 2012). Contrarily, in some of bed-rest studies simulating the unloading in microgravity, the serum calcium levels were shown to increase within normal limits (Smith et al. 2003, Smith et al. 2008). Interestingly, in a recent study performed by Deokar and colleagues, the serum levels of calcium and phosphate in cataract patients were significantly higher than that of controls (Deokar et al. 2018). In their study, they hypothesized that the higher intercellular calcium concentrations, decreased Ca^{2+} -ATPase activity and increased membrane permeability probably lead to higher intracellular calcium which then results in cataracts.

For the study of osteogenic differentiation of various cell types, specific chemicals are supplemented to the cell culture medium. Most of such differentiation studies used L-ascorbic acid (50 $\mu\text{mol/l}$), β -glycerophosphate (10 mmol/l) and dexamethasone (100 nmol/l) in cell culture medium (Kern et al. 2006, Scutt and Bertram 1999, Covas et al. 2003, Hu et al. 2012). With the fact that studies of the senile cataractous lenses reported high concentrations of calcium and phosphorus (Chen et al. 2005, Lin et al. 2010, Chiang et al. 2004, Fagerholm et al. 1986), Balogh and colleagues could induce human lens epithelial cells to move towards osteogenic differentiation by only using different concentrations of inorganic phosphate (Pi) ($\text{NaH}_2\text{PO}_4\text{-Na}_2\text{HPO}_4$, pH 7.4) and CaCl_2 without using above mentioned chemicals (Balogh et al. 2016). Interestingly, osteoblastic differentiation of VSMCs could be induced by supplementation of 4 mmol/l Pi alone to the growth medium (Zarjou et al. 2009).

With such a probability of lens epithelial cells to behave as cells of the osteogenic lineage in presence of calcium and phosphate, the loss of calcium and phosphate from astronauts' bones during space flight could be a triggering mechanism for osteogenic differentiation of lens epithelial cells that would lead to lens turbidity.

1.10 Porcine lens and porcine lens epithelial cells (pLEC)

To better understand the mechanism of radiation-induced cataractogenesis, it is essential to study the reaction of lens epithelial cells to ionizing radiation exposure. In other studies, either human transformed epithelial cell lines (which most likely have altered characteristics compared to primary cell lines) or lens epithelial cells (samples are rare) from donor patients have been used. Similarly, many animal experiments which include rats (Merriam Jr and Szechter 1973, Dynlacht et al. 2010), mice (Worgul et al. 2002, Zhang et al. 2012), rabbits (Lett et al. 1985, Cogan and Donaldson 1951), monkeys (Sonneveld et al. 1979) and bovine lenses (Baumstark-Khan et al. 1998) have been used to uncover the underlying mechanism of radiation-induced cataractogenesis due to different quality ionizing radiations. Porcine lenses have a diameter of ~ 10 mm and stay viable in culture for many days, which provide time for systematic inspection of DNA damage response in lens epithelial and lens fiber cells. In this study, porcine lens and lens epithelial cell are used mainly because of following reasons:

- They are non-transformed primary cells
- Porcine lenses are similar to human lenses in shape, size and crystallin content (Sanchez et al. 2011, Keenan et al. 2008)
- They can be easily isolated from the porcine eye which is a waste product in slaughter houses

1.11 Aims of the study

The aim of this study was to establish porcine lens and lens epithelial cells as a new model cell system to elucidate the mechanism of radiation-induced cataracts by analyzing the cellular characteristics after exposure to space-relevant radiation quantities. The following investigations were performed:

- Proliferation, cell cycle progression and cellular survival analysis of the lens epithelial cells after exposure to different radiation qualities
- Analysis of radiation-induced DNA damage and repair in the lens epithelial cells in vitro and in organ culture
- Quantification of gene expression related to DNA repair and differentiation of epithelial cells to lens fibers after radiation exposure
- Determination whether porcine lenses in organ culture and porcine lens epithelial cells (pLEC) in vitro display similar radiation-induced damage and repair capacities after exposure to space-relevant radiation qualities
- Correlation of biological radiation effects in cell culture and in whole organs
- Investigate if osteogenic induction of lens epithelial cells leads to their differentiation towards the osteogenic lineage

2 MATERIALS AND METHODS

2.1 Materials

2.1.1 Equipment

The equipment used in this study is listed in the following Table 2.

Table 2: Equipment

| Appliance | Supplier |
|--|---|
| Autoclave | Systec 2540-EL, Systec GmbH, Wettenberg, Germany |
| Centrifuge | Multifuge 3 S-R, Thermo Scientific, Schwerte, Germany |
| Dosimeter | UNIDOSwebline, PTW, Freiburg, Germany |
| Flow cytometer | FACScan, BD Biosciences, Heidelberg, Germany |
| Fluorescence microscope | Axiovision 135, Carl Zeiss AG, Oberkochen, Germany |
| Fluorescence microscope | Zeiss Axio Imager M2, Göttingen, Germany |
| Fuchs-Rosenthal haemocytometer | W. Schreck, Hofheim, Germany |
| Incubator | Heraeus Jubilee Edition, Heraeus Instruments, Hanau, Germany |
| Laminar flow hood | HeraSafe, Thermo Scientific, Schwerte, Germany |
| Light microscope | Axiovision 35, Carl Zeiss AG, Oberkochen, Germany |
| Microelectrophoresis unit | Agilent 2100 Bioanalyzer, Agilent Technologies, Santa Clara CA, USA |
| Mini-scissors, Tweezer, Scissors and Forceps | Geuder AG, Germany |
| pH-meter | Sartorius, Göttingen, Germany |
| Pipetting aid | Hirschmann Laborgeräte, Eberstadt, Germany |
| Real-time thermocycler | DNA Engine Opticon2 System, Biorad Ltd., Munich, Germany |
| Refrigerator | Bosch, Hamburg, Germany |
| Scale | Sartorius, Göttingen, Germany |
| Spectrophotometer | Nano Drop 2000c, Thermo Scientific, Schwerte, Germany |
| Stereomicroscope | LYNX Stereomikroskop, Vision Engineering Ltd., Surrey, United Kingdom |
| Thermocycler | peqSTAR 96X Universal Thermocycler, VWR, Darmstadt, Germany |
| Vortexer | Heidolph, Schwabach, Germany |
| Water Bath | Aqualine AL 12, Lauda, Königshofen, Germany |
| X-ray tube | Gulmay RS225, X-strahl, Surrey, United Kingdom |

2.1.2 Consumables

The list of consumable materials is given in Table 3.

Table 3: Consumables.

| Appliance | Supplier |
|---|---|
| 96-well plate for qPCR | 4titude Ltd, Berlin, Germany |
| Cell scraper | TPP, Trasadingen, Switzerland |
| Entellan® (mounting medium) | Merck, Darmstadt, Germany |
| Falcon tubes 15 ml | Nunc, Wiesbaden, Germany |
| Falcon tubes 50 ml | Nunc, Wiesbaden, Germany |
| High Precision Microscope Cover Glasses 24x60 mm | Thermo Fisher Scientific, Schwerte, Germany |
| Microscope Slides, 76x26 mm | Thermo Fisher Scientific, Schwerte, Germany |
| Pasteur pipettes | Brand, Wertheim, Germany |
| Petri dishes Ø 30 mm and 60 mm | Nunc, Wiesbaden, Germany |
| Pipet tips (10, 100, 1000 µl) | Eppendorf Ltd, Hamburg, Germany |
| qPCR adhesive seal sheets | 4titude Ltd, Berlin, Germany |
| Side flasks | Nunc, Wiesbaden, Germany |
| Syringe, sterile, 10 ml | Terumo Syringe (Leuven, Belgium) |
| Tissue Culture flasks 25 cm ² and 80 cm ² | Nunc, Wiesbaden, Germany |

2.1.3 Reagents and Kits

All the reagents and kits and assays used for the study are listed in Table 4.

Table 4: Reagents and Kits

| Item | Supplier |
|--|------------------------------------|
| α-MEM | PAN Biotech, Aidenbach, Germany |
| β-Mercaptoethanol | Sigma Aldrich, Steinheim, Germany |
| 4',6-Diamidino-2-phenylindole (DAPI) | Sigma Aldrich, Steinheim, Germany |
| Acetic acid | Merck, Darmstadt, Germany |
| Alizarin Red S | Sigma Aldrich, Steinheim, Germany |
| Ammonium Chloride | Merck, Darmstadt, Germany |
| Amphotericin B (250 µg ml ⁻¹) | PAN Biotech, Aidenbach, Germany |
| Betaisodona | Mundipharma GmbH, Limburg, Germany |
| Bisbenzimidazole (C ₂₇ H ₂₈ N ₆ O • 3HCl • 3H ₂ O) | Sigma Aldrich, Steinheim, Germany |
| Bovine Serum Albumin (BSA) | Sigma Aldrich, Steinheim, Germany |
| CellROX® Green | Thermo Fisher Scientific, Germany |
| Click-iT® Cell Reaction Buffer Kit | Thermo Fisher Scientific, Germany |
| Colcemid | Merck, Darmstadt, Germany |
| Crystal violet | Merck, Darmstadt, Germany |
| Disodium phosphate | Merck, Darmstadt, Germany |

| Item | Supplier |
|---|---|
| Eosin | Sigma Aldrich, Steinheim, Germany |
| Ethanol | Merck, Darmstadt, Germany |
| Fetal Bovine Serum (FBS) | Biochrom AG, Berlin, Germany |
| Formaldehyde 37 % | Merck, Darmstadt, Germany |
| Giemsa stain | Merck, Darmstadt, Germany |
| Glycine | Merck, Darmstadt, Germany |
| HCl | Merck, Darmstadt, Germany |
| iScript™ cDNA synthesis kit | Bio-Rad, Munich, Germany |
| Isopropanol | VWR, Darmstadt, Germany |
| KU55933 (ATM inhibitor) | Merck, Darmstadt, Germany |
| L-Glutamine (200 mmol/L) | PAN Biotech, Aidenbach, Germany |
| L-Lysine | Merck, Darmstadt, Germany |
| Mayers Haemalaun | Sigma Aldrich, Steinheim, Germany |
| Menadione | Sigma Aldrich, Steinheim, Germany |
| Methanol | Merck, Darmstadt, Germany |
| Mounting medium | Invitrogen, California, USA |
| NU7441 (DNA-PK inhibitor) | Bio-Techne GmbH, Wiesbaden-Nordenstadt Germany |
| One-Step RT-PCR Kit | Invitrogen, Carlsbad, USA |
| Penicillin/ Streptomycin | PAN Biotech, Aidenbach, Germany |
| Platinum® SYBR®Green qPCR SuperMix-UDG kit | Invitrogen, Carlsbad, USA |
| Potassium chloride | Merck, Darmstadt, Germany |
| Prolong gold antifade reagent | Thermo Scientific, Langenselbold, Germany |
| Propidium iodide (PI) | Invitrogen, Carlsbad, USA |
| QIAprep Miniprep | QIAGEN, Hilden, Germany |
| RNA 6000 Nano Assay | Agilent Technologies, Böblingen, Germany |
| RNase A | Calbiochem, La Jolla, USA |
| RNase-Free Dnase Set | QIAGEN, Hilden, Germany |
| RNeasy Plus Mini Kit | QIAGEN, Hilden, Germany |
| RT2 First strand kit | SABiosciences, Frederick, MD, USA |
| Sodium chloride | Merck, Darmstadt, Germany |
| Sodium dihydrogen phosphate | Merck, Darmstadt, Germany |
| Tris | Sigma Aldrich, Steinheim, Germany |
| Triton X-100 | Sigma Aldrich, Steinheim, Germany |
| Trypsin/EDTA | PAN Biotech, Aidenbach, Germany |
| Tween-20 | Sigma Aldrich, Steinheim, Germany |
| VE821 (ATR inhibitor) | Haoyuan Chemexpress, Shanghai, China |
| Xylol | Merck, Darmstadt, Germany |

2.1.4 Culture medium

The composition of media used in cell culture as well as lens organ culture is given in following Table 5

Table 5 : Medium for cell culture

| Medium | Composition |
|----------------------|--|
| Culture medium | 500 ml α -MEM 10 % (v/v) FBS 10,000 IU / 10,000 μ g/ml Penicillin / Streptomycin 2 mmol/l L-Glutamine 250 μ g/ml Amphotericin B |
| Calcification medium | 4 mmol/l inorganic phosphate ($\text{Na}_2\text{HPO}_4 \cdot 2\text{H}_2\text{O}$ and $\text{Na}_2\text{H}_2\text{PO}_4 \cdot \text{H}_2\text{O}$) in culture medium |

2.1.5 Buffers and solutions

Buffers and different staining solutions used in the experiments were prepared according to Table 6. Phosphate buffer is diluted to 1x before use.

Table 6: Buffers and solutions

| Solutions | Composition |
|--|--|
| Alizarin red S Solution | 2 g Alizarin red S in aqua dest. pH 4.2, adjusted by 1 mol/l HCl |
| Bisbenzimidazole (Hoechst 33342) 10 μ mol/l | 12.5 μ l Bisbenzimidazole (8 mmol/l) in 10 ml PBS |
| Blocking solution | 0.27% (w/v) NH_4Cl , 0.75% (w/v) Glycine and 1.64% (w/v) L-Lysine in TBST |
| Carnoy's fixative | 1:3 of acetic acid and methanol |
| Crystal Violet staining solution | 0.5 g Crystal Violet 50 ml 37% Formaldehyde in 500 ml tap water |
| DAPI staining solution | 0.1 μ g ml^{-1} DAPI in PBS |
| Giemsa stain | 5 % giemsa in 15 ml PBS |
| Hypotonic solution | 0.075 mol/l i.e. 0.56 g Potassium chloride in 100 ml dist. water |
| PBS 5x | 80 g NaCl 2 g KCl 14.4 g Na_2HPO_4 2 g KH_2PO_4 in 1000 ml dist. water pH 7.2 |
| PI-staining solution | 50 μ g ml^{-1} RNase A 0.1% (v/v) Triton X-100 |

| Solutions | Composition |
|-----------|---|
| | 20 $\mu\text{g ml}^{-1}$ PI in PBS |
| TBST | 150 mmol/l NaCl, 50 mmol/l Tris, 0.05% Tween 20 and pH 7.5 |

2.1.6 Antibodies and diluents

The primary and secondary antibodies and its diluent used in γH2AX assay are listed in Table 7.

Table 7: Antibodies and antibody diluent

| Antibodies | Type | Supplier |
|-------------------------------|--|---|
| AF2288 (Primary antibody) | Phospo-Histone H2AX (S139) affinity purified polyclonal antibody, rabbit IgG | R&D systems, Bio-Techne GmbH, Wiesbaden- Nordenstadt Germany |
| NL004 (Secondary antibody) | Donkey anti-rabbit IgG purified polyclonal antibody | R&D systems, Bio-Techne GmbH, Wiesbaden- Nordenstadt Germany |
| Antibody diluent | | Zytomed Systems, Berlin, Germany |

2.1.7 Software

The software that was used to edit and evaluate data obtained from the study is shown in Table 8.

Table 8: Software

| Software | Supplier |
|---|---|
| 2100 Expert Software for Bioanalyzer | Agilent Technologies, Karlsbrunn, Germany |
| AxioVision LE | Carl Zeiss (Oberkochen, Deutschland) |
| Basic Local Aligment Search Tool (BLAST) | http://www.ncbi.nlm.nih.gov/tools/primer-blast |
| CellQuest Pro™ | BD Biosciences |
| DEK_PLEC_Master, CFA- AllData_pLEC_BK & qPCR ANALYSIS V2.01 | Microsoft Excel worksheets developed by C. Baumstark- Khan, DLR, Germany |
| Flowing Software 2.5 | Perttu Terho, Cell Imaging Core, Turku Centre for Biotechnology, Turku, Finland |
| Image Pocessing and | Free online |

| Software | Supplier |
|---------------------------|---|
| Analysis in Java (ImageJ) | software, http://rsbweb.nih.gov/ij/download.html |
| Opticon 2 | Bio-Rad, Munich, Germany |
| SigmaPlot 12 and 13 | Systat Software GmbH, Erkrath, Germany |

2.2 Methods

2.2.1 Preparation and culture of the whole lens

The porcine eyes for all the experiments were bought at the local slaughterhouse “Metzgerei Arno Schmitz Inh. Frank Schmitz e.K.” (Landskroner Straße 88-90, 53474 Bad Neuenahr-Ahrweiler, Germany).

Eyes were transported cooled in ice in a styrofoam box from the slaughter house. Preparation of lenses was done immediately after reaching lab, which was within 2 hours of arrival.

Firstly, the muscles around the porcine eyeball were removed using scissors (**Figure 9A**). The eye was washed once with PBS before it was disinfected with Betaisodona. The eyeball was once again thoroughly washed with PBS for the dissection process. The eyeball was cut carefully at the coronal plane using scalpel and scissors to divide the eyeball to anterior and posterior parts (**Figure 9B**). The lens being at the anterior part is attached to the ciliary body by means of zonular fibers. The zonular fibers were separated under the stereo-microscope using mini-scissors and a tweezer to isolate the uninjured and intact lens (**Figure 9C and 9D**).

Isolated whole lenses were cultured in 6-well culture plates containing about 9 mL of culture medium, with the anterior surface facing upward, at 37 °C and 5 % CO₂ in humidified atmosphere. Culture medium was changed twice a week.

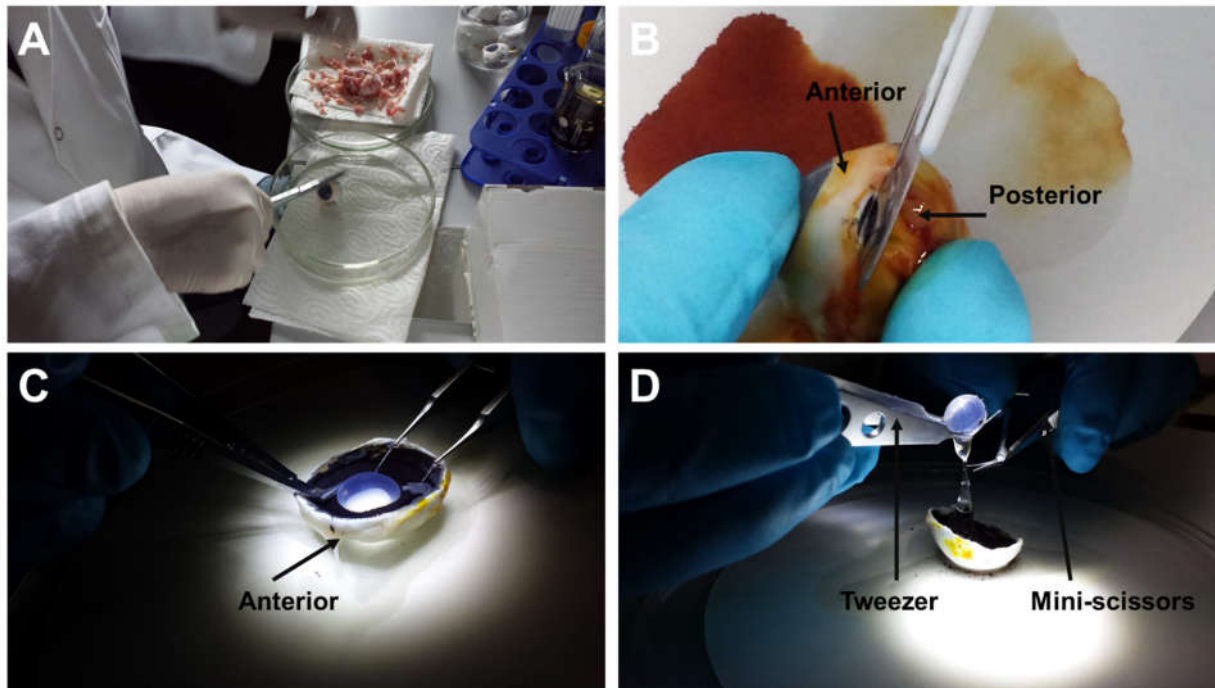


Figure 9 : Isolation of lens from the porcine eye. (A) Removal of muscles from the eyeball. (B) Cutting eye through coronal plane. (C) Separating zonular fibers with help of mini-scissors and tweezers. (D) Isolated crystalline lens.

2.2.2 Isolation and routine culture of pLEC monolayer

For the isolation of pLEC, the whole lens was shortly dried on a sterile filter paper through rolling and then it was placed in the Petri dishes (\varnothing 3 cm, PS3) with the posterior (more curved) surface facing upwards (Figure 10A). Then a very small incision was made at the middle of the posterior surface (Figure 10B). With the help of mini-scissors the posterior surface was cut open to four sides and the outer layer was attached to the surface of Petri dishes (\varnothing 6 cm, PS6) using the forceps (Figure 10C). The middle capsule and cortex was removed so that only the epithelial layer was remaining (Figure 10D and 10E). The cutting and separation of cortex from the epithelial layer was done under the highly magnifying stereomicroscope. Culture medium was carefully pipetted over the epithelial layer to avoid that the layer would float along with the medium (Figure 10F). The layer was incubated at 37 °C and 5 % CO₂ in humidified atmosphere and the culture medium was changed twice a week. After a week of incubation, the pLECs were obtained by incubating in trypsin-EDTA solution for about 5 min at 37 °C.

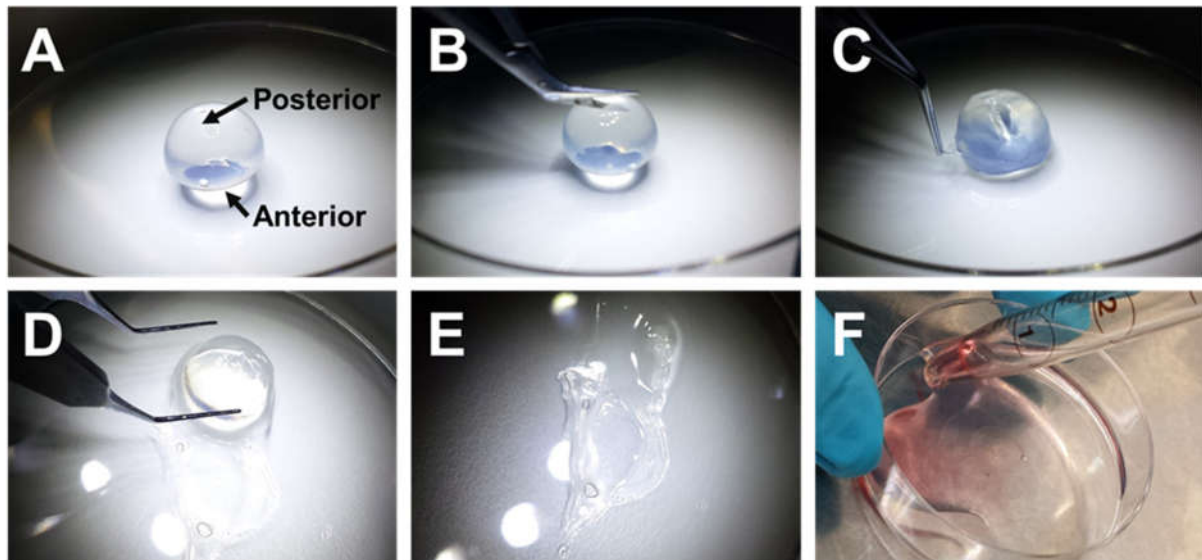


Figure 10: Isolation of lens epithelial layer from the porcine lens for lens epithelial cells. The images show the steps for lens epithelial cells isolation in alphabetical order.

2.2.3 Giemsa staining for cytogenetics

Cytogenetic analysis was performed by analysis of metaphase spreads of pLECs. Colcemid at 0.1 $\mu\text{g/ml}$ working concentration is known to block cells at the metaphase of the mitosis during the cell cycle.

The pLECs were seeded at the density of 5×10^3 cells per cm^2 in PS6. During the exponential growth phase (4 days after seeding), 0.1 $\mu\text{g/ml}$ of Colcemid were added to the cells for 5 h. Then the cells were harvested by trypsinization in a falcon tube and PBS was added to stop further action of trypsin. The cells were then centrifuged at 1200 rpm for 7 min at 4 °C. The supernatant was removed and the hypotonic solution (section 2.1.5) was added drop wise up to 10 ml. The cell pellet was broken by flipping the falcon against an uneven surface and was incubated for 10 min at RT. Once again centrifuged as mentioned above, hypotonic solution was removed leaving few drops still remaining where the pellet was resuspended by flipping the falcon. After that, the Carnoy's fixative was added drop wise till 10 ml and the sample was left overnight at 4 °C. On the next day, the sample was centrifuged as mention above, the fixative was removed and the pellet was resuspended by flipping. It was washed two times with fresh fixative and the pellet was obtained by centrifugation.

To stain the cells, the pellet was diluted with few drop of fixative and suspended by shaking. A thin layer of water was made on a clean glass slide by a sheet of paper

soaked in distilled water. 15 µl of cell suspension was spread over the prepared glass slide. The slide was then allowed to dry for 5 to 6 h. Next, the cells were stained with 5 % Giemsa in phosphate buffer for 15 min in a staining chamber. The slides were slowly rinsed with cold tap water and let dry for 2 to 3 h at RT. Finally the slide was mounted with Entellan[®].

2.2.4 Microtomy

In order to study radiation effects on whole lenses in organ culture, the X-ray exposed lenses (see section 2.2.5.1) were taken to the “Universitäts-Augenklinik Bonn (Ernst-Abbe-Straße 2, 53127 Bonn)” for preparation of microtome sections of the lenses. All the material used in this microtomy section was kindly provided by “Universitäts-Augenklinik Bonn”. The steps for microtomy are described below.

2.2.4.1 Sample fixation

Both X-ray exposed and unexposed samples were fixed with 3.5 % formaldehyde in PBS for 15 min at different harvesting time points and then formaldehyde was replaced with PBS and lenses were stored at 4 °C. The stored lenses were then transferred to 70 % ethanol and transported to “Augenklinik Bonn” for further procedure. 70 % ethanol can also be used for long-term storage at 4 °C.

2.2.4.2 Paraffin infiltration

For the infiltration of paraffin in the whole lens, the lenses were wrapped with a filter paper and were placed inside a plastic cassette (Figure 11). The infiltration process includes a gradual dehydration of the lens (whole cassette) in stepwise increasing concentration of ethanol, cleaning by xylol and finally infiltration of paraffin. It started from 70 %, 80 % and two times 96 % ethanol, each step being 30 min. Dehydration is continued with absolute ethanol for 3 more steps, with the first two steps lasting for 60 min and the last one was 90 min. The next step was washing twice with xylol for 60 min each. Finally, the lens was placed into paraffin (~60 °C) for 60 min for three times. All these steps were performed with an automated processor.

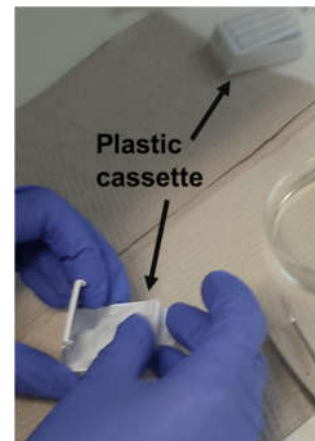


Figure 11: Packing of lenses into the plastic cassette for paraffin infiltration

2.2.4.3 Embedding the lens in paraffin block

In a next step, a tissue-paraffin block of the paraffin-infiltrated lens was made on the surface of plastic cassette using a steel mold (Figure 12).

First of all, the extra wax present in the lens and cassette was melted away by placing it on a heating block (~60 °C) for 15 min. Then the lens was obtained by discarding the cassette lid and filter paper. A small amount of molten paraffin was put in the steel mold from the paraffin reservoir. The lens was gently transferred into the mold with paraffin. The mold was then transferred to the cold plate where paraffin slowly started solidifying. During this step the lens was placed in the desired position (vertical position) as the solidifying paraffin holded the lens. Then the mold with the properly oriented lens was returned to the dispenser to fill the mold with paraffin. A second plastic cassette was then placed over the mold and its face was covered with molten paraffin, too. The next step was solidifying of the paraffin on the cooling plate (about 30 min). When the wax was hardened, a smooth paraffin block with the sample was obtained. Then the sample was easily removed from the mold because the solid wax covering the sample was firmly attached to the second cassette.

2.2.4.4 Sectioning of the lens

The sectioning of the lens was done using a microtome. Firstly, the water bath filled with distilled water was set to 37 °C. The paraffin block was vertically inserted into the cassette holder facing the blade. At the beginning, the dial was set to 10 µm to start cutting. Once the lens started to get visible after removal of the wax layer, the sectioning

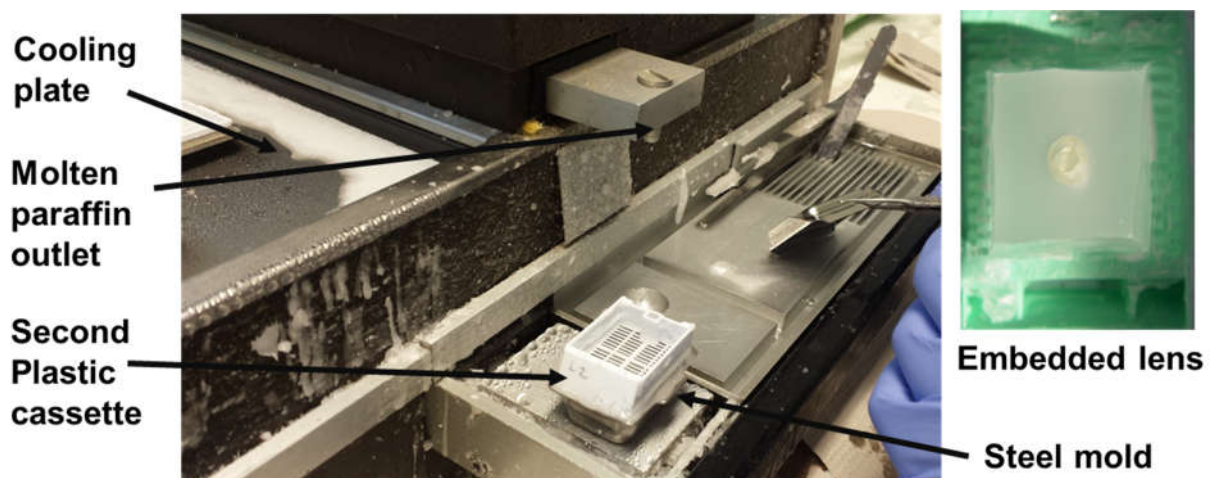


Figure 12: Paraffin dispenser and embedded lens

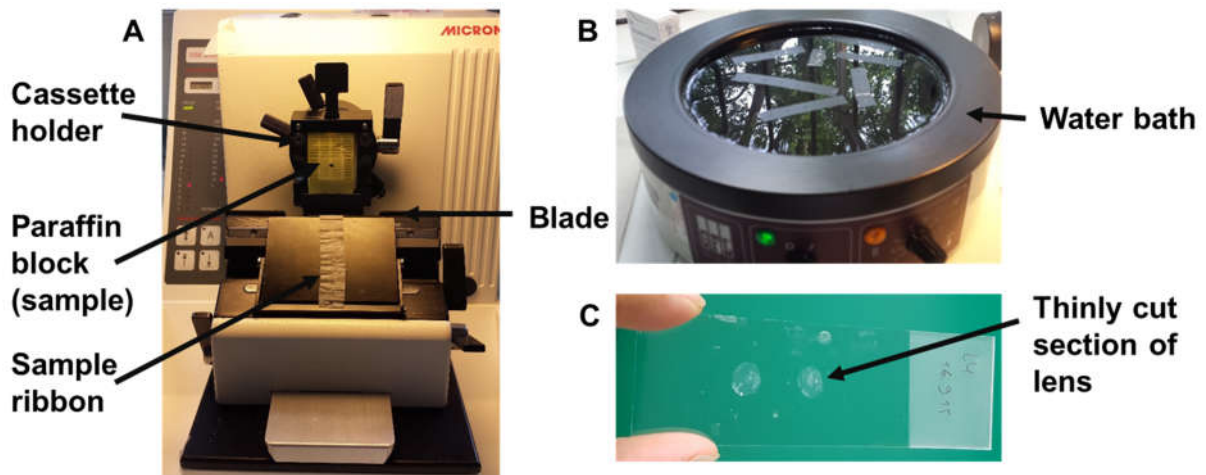


Figure 13: Sectioning of the lens. The lens embedded in a paraffin block was sectioned using a microtome (A). (B) Cut ribbon section in the water bath. The lens sections after the wax had been melted away (C).

was done at 5 μm thickness. The cutting of the block resulted in ribbons of sample and wax. A paint brush was used to gently transfer this cut ribbon sections in the water bath. The warm water helps to stretch the sample smoothly. A clean glass slide was taken to float the ribbons onto its surface. The slides with the samples were then kept at 65 $^{\circ}\text{C}$ for an hour so that wax melted and helped the tissue to attach to the glass.

2.2.5 Radiation exposure

2.2.5.1 X-ray exposure

X-ray irradiation (0.3-3 keV/ μm) was performed at DLR by using the X-ray tube operated at a voltage of 200 kV and a current of 15 mA. Dose and dose rate were measured with the UNIDOS^{Webline} dosimeter. For all experiments, X-rays were filtered through a copper filter. Lenses and pLECs were irradiated at a dose rate of 1 Gy min^{-1} (focus object distance of 444 mm, 21.1 $^{\circ}\text{C}$).

Cells were irradiated at the exponential growth phase (at day 4) either in flasks or in plates, where the cell surface was perpendicular to the X-rays. The whole lenses were irradiated directly in the cell culture plates with the anterior surface of the lens facing upward. After X-irradiation, cells and lenses were further incubated at standard conditions and harvested for analyses at various time points after irradiation.

2.2.5.2 Heavy ion exposure

Irradiation with Ar-36 and C-12 ions was performed at the “Grand Accélérateur National d’Ions Lourds” (GANIL) in Caen, France. The beam energy was 95 MeV/n (where ‘n’ stands for nucleon). For Ar-36, the energy on target was 84.7 MeV/n with a resulting LET of 269.4 keV/μm. For C-12, the beam energy was reduced to 35 MeV/n using a polymethylmethacrylate (PMMA, thickness 16.9 mm) and the energy on target was 28.6 MeV/n with resulting LET of 71 keV/μm.

Cells were seeded in slide flasks (growth area 9 cm²) at a density of 1×10⁴ cells/cm² 3 days prior to the irradiation. Before subjecting cells to the beam, the side flasks were completely filled with serum free α-MEM in order to prevent desiccation of the cells during the irradiation time. The samples were exposed to heavy ions in upright position placed at the sample mover/holder in front of the beam exit window (Figure 14). After irradiation, the serum-free α-MEM was discarded and 5 mL of culture medium was added.

The dosimetry was carried out by the staff at the accelerator (Durantel et al. 2016). A dose rate of 1 Gy/min was used to irradiate the samples. The fluence (F) for heavy ions was converted to the absorbed dose by following Equation 7 (Wulf et al. 1985). Fluence is defined as the number of particles (P) per unit area (cm²).

$$Dose (Gy) = 1.6 \times 10^{-9} \times LET \left(\frac{keV}{\mu m} \right) \times F \left(\frac{P}{cm^2} \right) \quad \text{Equation 7}$$

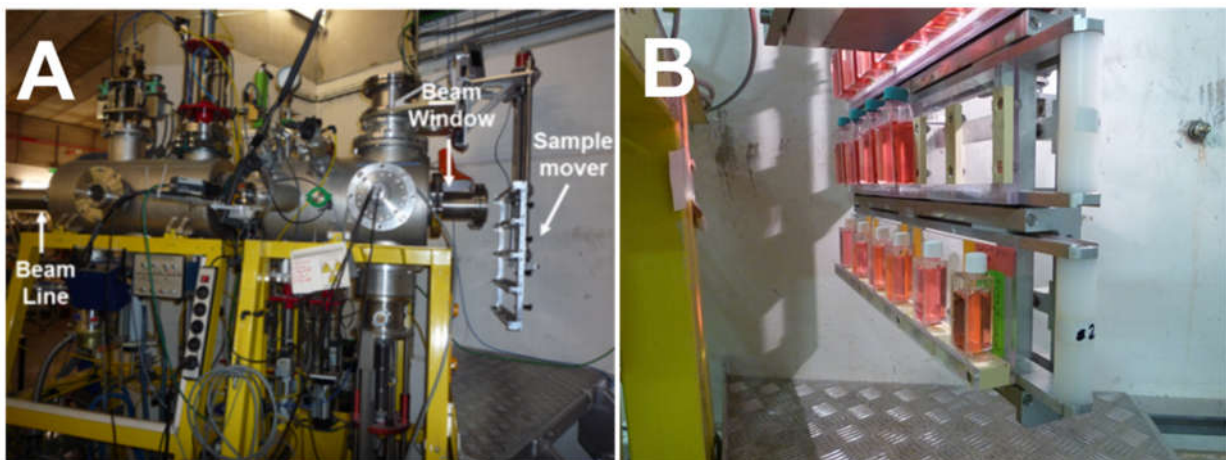


Figure 14: Heavy ion irradiation at the GANIL accelerator. Beam line (A) and setup of samples in cell culture flask placed on the specially designed sample mover/holder (B).

2.2.6 Microscopic investigation

For microscopic investigations, formaldehyde-fixed cells were used. The phase contrast microscope Axiovert 25 was used with the appropriate objective (5x, 10x, 20x, 40x) in order to visualize cells for routine cell culture. For microphotography the fluorescence microscope Axiovert 125 linked to the color camera MRc5 was applied. Axiovision 4.4 software was used to operate microphotography.

2.2.7 Analysis of cell growth

Cells were seeded in Petri dishes (PS3) at a density of either 2.5×10^3 or 5×10^3 cells cm^{-2} and incubated at 37°C in a CO_2 -incubator (95 % air, 5% CO_2). For the period of twelve days two plates were trypsinized each day and the cell number was determined by counting with a hemocytometer.

Doubling time (T_d) was determined by the slope calculated for the exponential part (log-phase) of the growth curves according to Equation 8:

$$T_d = (t_2 - t_1) \times \frac{\log(2)}{\log\left(\frac{C_2}{C_1}\right)} \quad \text{Equation 8}$$

Where, t_1 = time point 1 [day after seeding] C_1 = count at t_1
 t_2 = time point 2 [day after seeding] C_2 = count at t_2

2.2.8 Radiobiological characterization

To determine the radiobiological parameters, first of all the plating efficiency of cells seeding at low density was determined. After that the radiobiological parameters from the dose-effect relation can be computed from the colony forming assay or the cellular survival assay.

2.2.8.1 Plating efficiency

The plating efficiency (PE) describes the ability of a given cell line or primary cell to adhere to its growth substrate and to multiply thereby giving rise to colonies formed from one seeded cell. pLEC (passage 2) were seeded on Petri dishes \varnothing 6 cm with defined numbers of cells (from 100 to 1000 cells per plate). After 3 weeks, the grown colonies were fixed and stained with crystal violet staining solution. Colonies with at

least 50 cells were counted by eye and the PE was calculated according to Equation 9. Statistics was calculated from 6 replicates for each condition of seeded cells.

$$PE = \frac{\textit{number of counted colonies}}{\textit{number of seeded cells}} \quad \text{Equation 9}$$

2.2.8.2 Colony forming ability test

In radiobiology the cell is considered to be a survivor when it retains or regains its ability to divide and to form macroscopic colonies (of at least 50 cells). Accordingly, the colony forming ability (CFA) test was developed for mammalian cells (Puck and Marcus 1956). In order to estimate the colony forming ability, trypsinized cells were irradiated with X-rays in 25 cm² flasks and seeded in six Petri dishes (Ø 6 cm) per dose. The amount of cells to be seeded per dose per PS6 was determined using a Microsoft Excel worksheet (developed by C. Baumstark-Khan, DLR, Germany) which predicts the fraction of remaining clonogenic cells for a certain dose of ionizing radiation from the plating efficiency for the cell line and putative survival levels. In anticipation of effects from higher radiation doses the seeding density increased with dose.

After radiation exposure cells were allowed to grow for at least 30 days without any medium change. Regular microscopic inspection was done once a week in order to identify the time point when the colonies consisted of about 50 single cells. At this time point the medium was removed and the plates were carefully washed with 1x PBS. Thereafter, the plates were stained by using 0.1% crystal violet staining solution for 2 h at RT and washed with tap water. After drying overnight, the colonies were inspected and counted by eye. The PE for every dose (PE_{dose=0}, PE_{dose}) were calculated as already described (see equation 8).

2.2.8.3 Calculating Dose Effect Relations

The relative survival (S) is the proportion of the PE of the irradiated samples (PE_{dose}) to the PE of non-irradiated samples (PE_{dose=0}) (Equation 10).

$$S_{dose} = \frac{PE_{dose}}{PE_{dose=0}} \quad \text{Equation 10}$$

From this definition, it results that $S_0=1$. Assuming that clonogenicity is decreasing or is unaffected after irradiation, S_{dose} will have values ≤ 1 . The dose-effect curve was created by plotting the relative survival as a function of dose on a semi-logarithmic scale (Figure 15). Typical dose-effect curves of cells with repair capabilities present two segments in a semi-logarithmic scale: a shoulder in the lower dose range and a linear part in the higher dose range.

Dose-effect curves are characterized and compared via three parameters: D_0 , D_q and n . The point where the extrapolation of the linear part of the curve intersects with the y-axis defines the extrapolation number (n). The intersection of this extrapolation and the function $y=1$ is called quasi-threshold dose (D_q). From both values conclusions can be drawn on the width of the shoulder (shoulder is present if $n>1$), which represents the recovery potential of the cells after irradiation. If the cells lack a repair capability, no shoulder can be seen (Figure 15). The linear part of the curve is described by D_0 , which is the negative reciprocal of the slope. D_0 , which is also known as D_{37} , is the dose of radiation that reduce the population of surviving fraction to 37 %. From the D_0 -value conclusions can be drawn on the radiation sensitivity after exhaustion of intracellular recovery processes.

The decrease in survival can be described by a regression curve which is derived from the single-hit multi-target model (Kiefer 1971) according to Equation 11. The linear part of the regression curve can be simplified to Equation 12. In a cell survival curve such linear exponential part is due to higher killing of cells due to high dose. The three characteristic parameters of a dose-effect curve are related according to Equation 13.

$$S = 1 - (1 - e^{-\frac{D}{D_0}})^n \quad \text{Equation 11}$$

$$\ln(S) = \frac{-D}{D_0} + \ln(n) \quad \text{Equation 12}$$

$$D_q = D_0 + \ln(n) \quad \text{Equation 13}$$

Finally, the obtained data were analysed in “DEK_PLEC_Master” for calculation of plating efficiency and survival for individual experiments. Then the data from individual

experiments were transferred into “CFA-AllData_pLEC_BK” (a second Microsoft Excel™ worksheet developed by C. Baumstark-Khan, DLR, Germany) for combination of data from individual repeat experiments to generate regression curve from mean data. F-test was used to test the linearity of the regression and t-test was done to compare the slopes of regression.

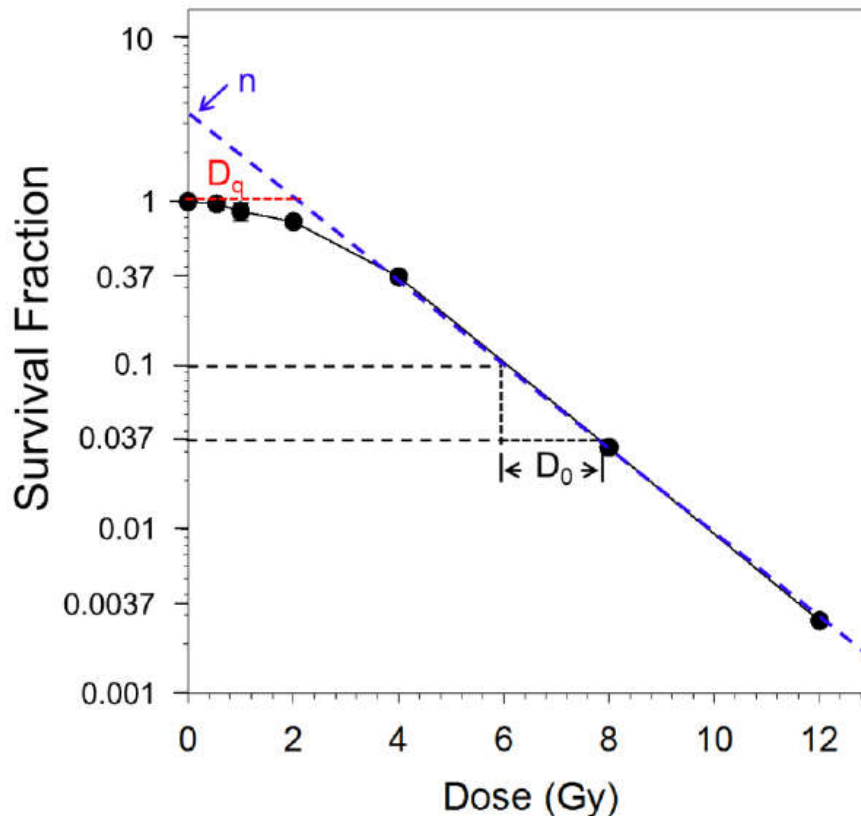


Figure 15: Parameters of dose-effect curves. The descriptive parameters D_0 , D_q and n are shown for typical dose-effect curves. The surviving fraction is plotted on a logarithmic scale against dose on a linear scale. D_0 is the reciprocal of the curve slope (k) in the exponential part of the curve ($D_0=1/k$). D_0 is the dose required to reduce the surviving fraction to 37% of the previous value. n is the value that is intercepted at y-axis after extrapolation of the exponential part of the curve. The intersection of this extrapolated curve with the 100% survival line is the quasi-threshold dose D_q . This dose is required to inactivate all but last target and can be defined by: $-\ln(n) = D_q/D_0$. (Adapted from (Hu 2014).

2.2.9 Analysis of cell cycle progression by flow cytometry

Cells were harvested at various time intervals after X-ray exposure by trypsinization. 1.5 ml of trypsinized cells were fixed with 4.5 ml ice-cold 100 % ethanol and stored at -20 °C for at least 24 h. For staining, the ethanol was diluted by adding PBS to a final volume of 14 ml and cells were collected by centrifugation (5 min, $500 \times g$). After resuspension in 1 ml PI-staining solution cells were incubated at 37 °C for 1 h, and analysed by flow cytometry on the same day.

For each sample 10,000 events were counted at the flow rate of 200-500 cells s^{-1} . CellQuest Pro™ Software was used to collect data from the flow cytometer, FACScan.

Flowing Software Version 2.5 was used to transform CellQuest Pro™ data files into PC-readable files. With the flowing software, a dot plot of FSC and SSC was created with a live gate set (Figure 16A). Another dot plot was created to plot the cells with the fluorescence signals of the area (FL2- Area) versus the width (FL2- Width) (Figure 16B). Cells of lower FL2-W were gated as apoptotic cells. After that, with the defined single cells, a histogram was created using fluorescence signal of the height (PI fluorescence or FL2- Height) (Figure 16C).

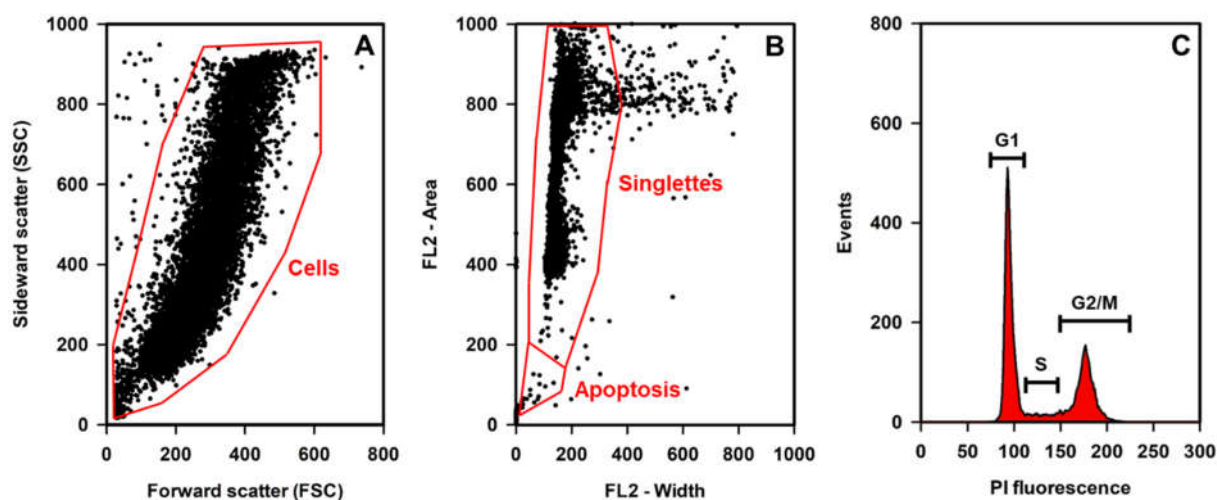


Figure 16: Analysis of cell cycle distribution by flow cytometry of PI-stained cells. (A) Dot plot showing single cells that are sorted with respect to their morphology; granularity (side scatter) and size (forward scatter). (B) Dot plot with respect to fluorescence. (C) Histogram of PI fluorescence (FL2-H).

From the histogram, a semi-automated “Cell Cycle Control” module of the Flowing Software was used to analyze cell cycle where G1-phase marker, G2-peak multiplier and peak width multiplier was manually defined. The software finds G2- and S-phase markers and finally the number of events from each G1-, S- and G2-phases in the form of exportable table. Statistics was done with the in Sigma Plot™ software package used at DLR.

2.2.10 Immunofluorescence staining of γ H2AX

PLECs cultivated in cell culture slide flasks were exposed to ionizing radiation at the confluency of 50 % - 70 % and harvested at different time points by fixing the cells with 3.5 % formaldehyde in TBST for 10 min at 4 °C. In order to visualize the DNA DSBs,

staining was started with three TBST washing steps where the last step included incubation on a shaker for 5 min. In the next step, cells were permeabilized on ice using the solution containing 0.5 % (v/v) Triton-X and 1 % (w/v) BSA in TBST. Once again the three TBST washing steps followed, with the last step 5 min on a shaker. Blocking solution was used for blocking the unspecific background for 10 min on a shaker at room temperature (RT). After washing with TBST as mentioned above, the cells were covered with a 1:500 dilution of primary antibody (polyclonal anti- γ H2AX antibody) in antibody diluting solution for 45 min at RT or overnight at 4 °C. Then again the washing steps followed before covering the cells with 1:500 dilution of secondary antibody in antibody diluting solution for 45 min in the dark at RT. Once again the washing steps performed as mentioned before, and the cell nuclei were stained with 0.1 μ g/ml DAPI staining solution for 15 min. Finally, the samples were stored at 4 °C to let the mounting medium dry overnight. On the next day, the samples were analysed with a fluorescence microscope.

In case of whole lens organ culture, lenses were fixed with 3.5 % formaldehyde in PBS for 10 min at harvesting time points and stored in TBST at 4 °C until all the samples were collected. Then the outermost epithelial layer at the anterior part of the lens was separated. The remaining staining procedure was followed as it was done for pLEC.

2.2.11 Staining of microtome sections

Microtome sections obtained after sectioning of lens were stained to visualize the structure of lens and γ H2AX as marker of DNA damage induction and repair.

Hematoxylin-Eosin staining of lens

For hematoxylin-eosin staining of microtome-sectioned lens, the glass slide with the lens was washed two times inside xylol for 5 minutes each. After that the glass slide was dipped in descending concentrations of isopropanol (2x in 100 %, 2x in 96 %, 80 % and 70 %) for 3 min each. Then it was washed with tap water for 3 min and 1 min with distilled water. Next, it was dipped in Mayers Haemalaun for 4 min, which was followed by 30 sec wash with HCl-alcohol. After washing with 5 min with tap water and 1 min with distilled water, it was stained with 1 % Eosin for 5 min. Once again sections were washed with different concentrations of isopropanol (80 %, 96 % and 2x 100 % respectively) for 3 min each. Finally, the slide was washed twice with xylol for 5 min each before mounting the coverslip.

Immunofluorescence staining of γ H2AX in lens epithelial cells in lens sections

In order to study the DNA damage induction and repair in whole lens, microtome sections of irradiated and non-irradiated lens were stained for γ H2AX. First of all, the glass slides with the lens sections were washed twice with xylol for 5 min each to remove excess paraffin from the slide. After that, gradual rehydration of the sample was done by washing the slides with decreasing concentration of isopropanol (2x in 100 %, 2x in 96 %, 80 % and 70 %) for 3 min each. Next, the sample was washed with tap water for 3 min and with distilled water for 1 min. The remaining steps for γ H2AX staining were performed as described in section 2.2.10 for pLECs in side flasks.

2.2.12 Oxidative stress determination in pLECs

It is well known that reactive oxygen species (ROS) within cells play a crucial role in cellular damage. In order to establish a positive control of oxidative stress and to quantify the ROS, different concentrations of menadione (25, 50 and 100 μ mol/l) were added to the cell culture medium for 1 h at 37 °C, 5 % CO₂. Menadione, which is known to generate ROS, is insoluble in water, hence was dissolved in chloroform in order to prepare stock solution (50 mmol/l). The working concentrations were prepared by diluting the stock solution with cell culture medium.

The fluorescent dye CellROX[®] Green was used to measure the intracellular ROS according to the manufacturer's instructions. Medium from pLEC, treated or untreated with menadione, was aspirated and 5 μ mol/l CellROX[®] Green reagent (diluted in normal cell culture medium) was applied to cells for 30 min at 37 °C, 5 % CO₂. Cells were then washed 3 times with PBS and fixed with 3.5 % formaldehyde in PBS for 15 min. For the X-ray exposed cells, CellROX[®] Green was applied 30 min after irradiation. Finally, the images were taken using fluorescence microscope within 24 h at the excitation and emission of wavelengths of 485 nm and 520 nm, respectively.

2.2.13 Detection of replicative S-phase cells

Detection of replicative S-phase cells was done using the Click-iT EdU Assay. EdU is an analogue of thymidine that is incorporated during DNA synthesis, which is easily detected by a fluorescent marker. The assay was performed for pLEC monolayer culture, epithelial layer and lens organ culture. These cells, layer and lens were supplied 10 μ mol/l EdU for different time intervals. The samples were then harvested and fixed

either with 3.5 % formaldehyde in PBS for microscopy or with 70 % ethanol for flow cytometry.

For staining of EdU incorporated in DNA, firstly the fixed samples were washed twice with PBS. For staining of the whole lens, pieces of epithelial layer were cut from the already fixed lens. The samples were permeabilized using 0.5 % Triton-X 100 in PBS at RT for 20 min. Then they were washed twice with 1.5% BSA in PBS in a shaker for 2 min. After that, freshly prepared Click-iT reaction mix was added to the samples and incubated in the dark at RT for 30 min. All remaining procedures were performed in the dark. Once again the samples were washed twice with 1.5 % BSA in PBS in the shaker. Nuclei were stained with 200 ng/ml DAPI for 20 min. Finally, after washing twice with PBS, the slides were dried and prepared for fluorescence microscopy with mounting medium and coverslips.

Table 9: Click-iT reaction mixture.

| | Stock conc. | Working conc. | Volume |
|---|----------------|---------------|-------------|
| 1x Click-iT Reaction Buffer | 10x | 1x | 423 μ l |
| Alexa Fluor® 488 | 30 μ mol/l | 1 μ mol/l | 17 μ l |
| CuSO ₄ | N/S | - | 5 μ l |
| Cu protectant mix | N/S | - | 5 μ l |
| 1x Click-iT Buffer Additive (Diluted immediately before usage) | 10x | 1x | 50 μ l |
| | | Total: | 500 μ l |

Note: N/S means not specified by the company

For flow cytometric analysis of Click-iT EdU Assay, the ethanol-fixed pLECs were collected by centrifuging at 500xg for 3 min. The staining procedure was the same as described above except for the collection of cells after each washing, permeabilization and incubation by centrifugation as pellet. After counter staining the nucleus with DAPI, the cells were re-suspended in 1 ml PBS for flow cytometry. After that, fluorescence counting of 10,000 events from FL-1 channel at a flow rate of 200-500 cells s⁻¹ was done for each sample. The Apple-based CellQuest Pro™ Software collected the data from the flow cytometer, FACScan.

2.2.14 Osteogenic induction of pLECs

For osteogenic induction of pLECs, the cells were first seeded at a density of 5×10³ cells/cm² in 6 cm petri-dishes with culture medium. After day 7, the culture medium was

changed with either osteogenic induction medium (also called calcification medium, CM) or culture medium (also called normal medium, NM). pLECs were fixed at different time intervals after medium change with 70 % ethanol and stored at -20 °C until all samples were harvested. Since calcium co-precipitates with phosphate ions under *in vitro* culture conditions, detection of such mineralized matrix can be shown by chelating action of calcium and Alizarin Red S (Wang et al. 2006). For Alizarin Red S staining, the fixed cells were rinsed twice with distilled water, then incubated with Alizarin Red S solution for 20 min at RT and finally rinsed twice with distilled water before taking photographs.

The procedure to analyze the gene expression of target genes during differentiation by quantitative real-time polymerase chain reaction was performed as described in section 2.2.15 for samples collected after radiation exposure. Day 0 sample in osteogenic induction experiment means that cells were harvested within few min (4-5 min) after changing the medium with CM (i.e. pLECs were kept in CM for only 4-5 min).

2.2.15 Quantitative real-time PCR for gene expression analysis of pLEC

Reverse Transcriptase quantitative real-time polymerase chain reaction (RT-qPCR) was used to evaluate gene expression after radiation exposure and osteogenic induction. The basis of this method is production of 2^n copies of target DNA fragments after n PCR cycles if no reagents are limited. Following steps are being followed for analysis gene expression.

2.2.15.1 RNA extraction and isolation

Firstly, RNA samples were collected at various time points after exposure to X-rays and heavy ions. In order to reduce RNA degradation by heat shock or RNases, only the pre-cooled (-20 °C) syringes, cell scrapers and micro-centrifuge were used. To isolate RNA, the cell culture medium was completely sucked off and 600 µl RLT-lysis buffer (from the RNeasy Plus Mini Kit with 10 µl/ml of 14.3 mol/l β-mercaptoethanol) was added to the cells to lyse them. A cell scraper was used to gather the lysed cells. After that, with 2 ml syringe the lysed cells were homogenized by moving lysate through the needle for 5 times and eventually transferred them into RNase-free micro-centrifuge tubes. Finally, the samples were promptly stored at -80 °C for future processing.

The remaining isolation steps were done according to the manufacturer's instructions (using the RNeasy Plus Mini Kit). At the end of isolation, RNA was eluted with 50 µl of

RNase-free water and its concentration was determined by spectrophotometry (Nanodrop).

2.2.15.2 RNA integrity and quantity determination

RNA 6000 Nano Assay was used to determine the integrity and the quantity of the isolated RNA samples by micro-electrophoresis technique in the Bioanalyzer. This electrophoretic analysis is based on capillary gel electrophoresis where fluorescent dye bound RNA give information about RNA integrity and concentration. Micro-electrophoresis was carried out according to the manufacturer's protocol for eukaryotic RNA analysis.

The RNA was quantified and assigned a RNA integrity number (RIN) between 0 and 10 by the 2100 Expert Software for Bioanalyzer. The software quantifies RNA using the RNA ladder, which contains 6 different sizes of RNA fragments (0.2, 0.5, 1.0, 2.0, 4.0 and 6.0 kb) at a known concentration of 150 ng/ μ l, to construct a standard electropherogram that can be compared to the samples (Figure 17). The RIN is calculated by the software by considering ratio between the area under the curve of 18 S and 28 S rRNA, the height of the 28S rRNA peak, the area between the 18S and 5S rRNA peaks and the marker peak height (Figure 17) (Schroeder et al. 2006). For X-irradiation and osteogenic induction experiments, a RIN of 8 and above was accepted. On the other hand, even the RIN of at least 6.4 was accepted for carbon ion-irradiated samples due to the rarity of the samples to obtain. The concentration and RIN number for all isolated RNA is listed in supplementary results (Table 18, Table 19, and Table 20).

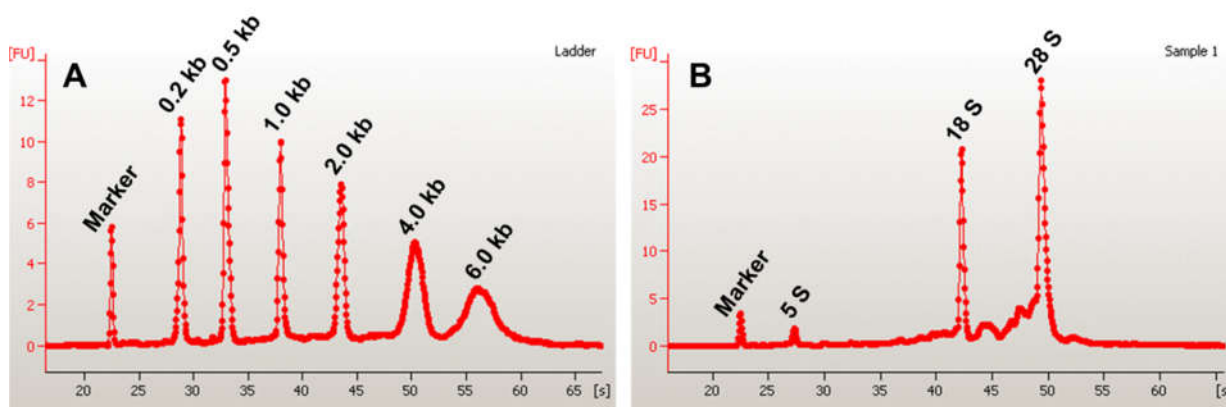


Figure 17: Electropherogram of separated RNA. RNA ladder (A) and RNA sample (B). Abbreviations: FU, fluorescence units; kb, kilobases; s, seconds.

2.2.15.3 cDNA synthesis

The iScript cDNA Synthesis Kit, which contained a recombinant RNase H⁺ MMLV reverse transcriptase and RNase inhibitor mix, was used to reverse transcribe the RNA into first-strand cDNA. RNA concentrations were determined according to section 2.2.15.2, which were diluted to 200 ng/μl. Reaction mixture for cDNA synthesis was prepared as shown in Table 10 with 1 μg of RNA sample (5 μl of 200 ng/μl) along with other kit components. Along with the samples, 2 negative controls, one containing no RNA template and another containing no iScript reverse transcriptase (RT minus) were prepared. Incubation of reaction mixture in the thermocycler was performed according to the iScript protocol: warm-up step (heating of lid to 110 °C), annealing step (5 min at 25 °C), elongation step (30 min at 42 °C) and deactivation step (5 min at 85 °C). The cDNA hence produced was regarded to be 50 ng/μl and was stored at -20 °C until the qPCR analysis

Table 10: The cDNA synthesis reaction mixture

| Reagents | Volume |
|-------------------------------|--------|
| Nuclease-free water | 10 μl |
| 5x iScript reaction mix | 4 μl |
| RNA sample (1 μg total RNA) | 5 μl |
| iScript reverse transcriptase | 1 μl |
| Total | μl |

2.2.15.4 Primer design

During designing of primer, the length of primer was maintained between 14-24 base pairs with 40-60 % of guanine and cytosine (GC) content. The product size of the primer was set to 100-250 base pairs. The melting temperature (T_m) of the primer was set to around 60 °C which should be approximately the same for both forward and reverse primers. It was also kept in mind that the primers do not form any internal secondary structures. The Blast tool from NCBI website was used to retrieve and test the primer sequence and corresponding gene. Finally, the primer pairs were ordered from Invitrogen.

The primers (Table 11) were reconstituted to 100 μmol/l stock solutions using DNase-free H₂O as per the supplier's protocol. The concentration of working solution for primer was 10 μmol/l. The final concentration of primer in qPCR reaction mixture was 0.2

$\mu\text{mol/l}$. Use of 0.5 μl primer working solution in total of 25 μl reaction mix gave the required final concentration. Both stock and working solutions were stored at $-20\text{ }^{\circ}\text{C}$.

Table 11: Primers used for gene expression analysis with their gene name, product size and NCBI database codes.

| Gene name | Primer sequence 5' → 3' | Optimized T_m | Length (bp) | NCBI |
|---------------------------|--|-----------------|-------------|----------------------|
| Housekeeping genes | | | | |
| ACTB | Fwd: TCCCCTTCTCCTTCCAGATC Rev: GCAACTAACAGTCCGCCTAG | 59 | 177 | NC_010445 .3 |
| B2M | Fwd: GCAGAGAAGAATCCCATGGG Rev: AGTGCTGTGGGTAAATGCTG | 59 | 160 | NC_010443 .4 |
| HPRT | Fwd: TGACACTGGCAAACAATGCA Rev: GGTCCTTTTCACCAGCAAGCT | 62 | 120 | NM_000194 |
| Target genes | | | | |
| CDKN1A | Fwd: TCGAGCGGTTTTGTTTTCGT Rev: CACACACACACACTCACACA | 59 | 178 | NC_010449 .4 |
| CRYAB | Fwd: GAGCAAGAAGAAGCAGCCTT Rev: CTTTCTGCTCGGGTAGTTGG | 59 | 240 | NC_010451 .3 |
| DNASE2 | Fwd: GCTAATCCACAGCGTTCCAA Rev: ATGGGGTAGGTGTAGGTCAG | 59 | 249 | NC_010444 .3 |
| GADD45G | Fwd: TGTGTGAGTATAGACGCGGT Rev: GTGAAGTGAATTTGCAGCGC | 59 | 214 | NC_010456 .4 |
| PAX6 | Fwd: CGTCCATCTTTGCTTGGGAA Rev: CAGAGAAAGACACAGGCAGG | 59 | 186 | NC_010444 .3 |
| RELA | Fwd: GTCTGAGAAGGTGTGGTTGG Rev: TCTCGTGGTCTCATCGTTCA | 59 | 104 | NC_010444 .3 |
| SOD3 | Fwd: CCAAAGTGACGGAGATCTGG Rev: TTCAGGTGGAAGAAGGCCT | 59 | 193 | NC_010450 .3 |
| BMP2 | Fwd: TTTGGAAGAAGTCCAGAAATGA Rev: TTAATTCGGTGATGGAAACTGCT | 59 | 165 | NM_001195 399.1 |
| COL1A2 | Fwd: TCTACTTGCTTAAATTGTGGGCA Rev: TGGTGCAAATGTTTCATGGTTT | 59 | 214 | NM_001243 655.1 |
| OPN | Fwd: TTCACCAAATACCCACATGACA Rev: ATGCATTTCAAGGGCGATTTT | 59 | 190 | GenBank: M84121.1 |
| RUNX2 | Fwd: TCCAAACACCCAGCAAATATGAA Rev: TGTTTTGTGCCTCCTCCTTTTAT | 59 | 174 | XM_013977 989.1 |

2.2.15.5 Quantitative real-time polymerase chain reaction (qPCR)

Platinum[®] SYBR[®] Green qPCR SuperMix-UDG kit and its protocol was used to carry out qPCR in the DNA Engine Opticon 2 System. In order to prevent the evaporation and

condensation of the reaction mixture, all the procedures from thawing to preparing of the sample plates were carried out on ice.

To make the standard curve of cDNA concentration, 2 μl of cDNA was pooled from each treatment conditions. As mentioned earlier the expected yield of cDNA for each sample condition was 50 ng/ μl . From the collected cDNA pool a dilution series from 25 ng/ μl to 0.04 ng/ μl was prepared. Furthermore, cDNA for each sample condition were also dilute to 5 ng/ μl with nuclease-free water. The composition of qRT-PCR reaction mixture was prepared according to the Platinum[®] SYBR[®] Green qPCR SuperMix-UDG protocol (Table 12).

Table 12: Reaction mix for qPCR per well

| Reagents | Volume |
|---|--------------------|
| SYBR Green Mix | 12.5 μl |
| Forward Primer (final conc. 0.2 $\mu\text{mol/l}$) | 0.5 μl |
| Reverse Primer (final conc. 0.2 $\mu\text{mol/l}$) | 0.5 μl |
| cDNA (5 ng/ μl) sample solution | 2.0 μl |
| Nuclease-Free Water | 9.5 μl |
| Total Volume | 25.0 μl |

The reaction mixture was carefully pipetted at the bottom of the 96-well plates (25 μl /well) where cDNA was either sample or standard dilutions from the pool. All samples, controls, standards and blanks were loaded either in triplicates or duplicates. Then the plates were inserted into the real time thermocycler after it was properly sealed with an adhesive film. Finally, following amplification protocol was used for qPCR (Table 13).

Table 13: qPCR amplification protocol

| No. | Step | Incubation time | Temperature |
|-----|------------------------|-----------------|--------------|
| 1 | Pre-heating | 2 min | 50 °C |
| 2 | Pre-denaturation | 2 min | 95 °C |
| 3 | Denaturation | 15 sec | 95 °C |
| 4 | Annealing | 30 sec | 59 °C |
| 5 | Elongation | 30 sec | 72 °C |
| 6 | Plate read | | |
| 7 | Final extension | 20 sec | 78 °C |
| 8 | Reading fluorescence | | |
| 9 | Repeat (3-8) 44 times | | |
| 10 | Melting curve analysis | | 60-95 °C |
| 11 | Plate read | hold 3 sec | every 0.2 °C |
| 12 | Heat block cool down | 1 min | 29 °C |

2.2.15.6 Relative quantification of gene expression levels

For the analysis of gene expression levels, first of all the threshold cycle (C_t) values were calculated using the Opticon2 software (Figure 18A). The reliability of the PCR products was verified using melting curve analysis (Figure 18B).

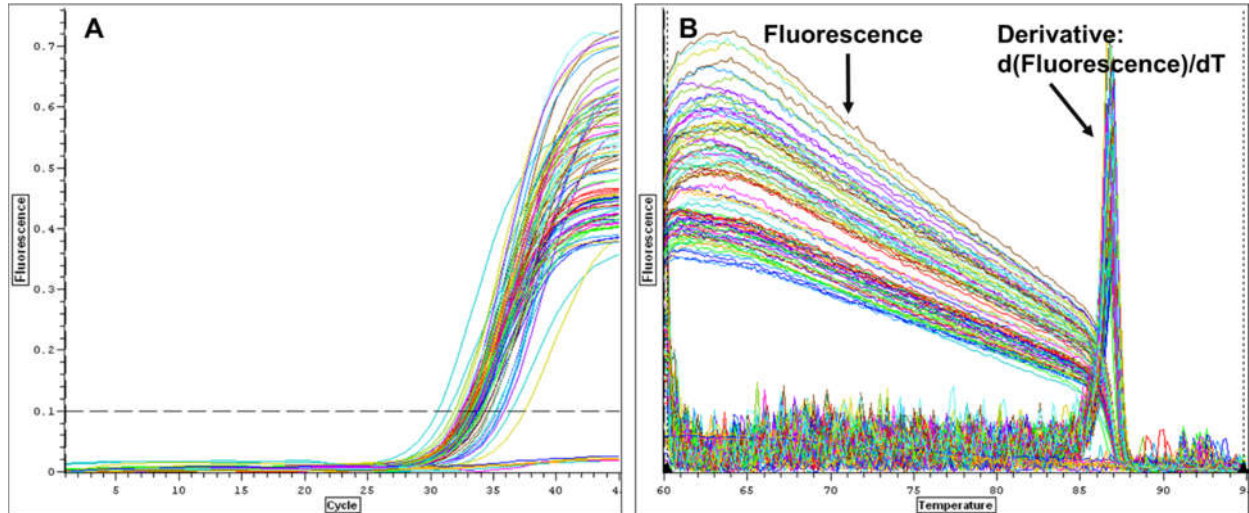


Figure 18: Amplification curves and melting curves from qPCR of B2M gene. (A) The C_t is the cycle number at which the fluorescence value is above the threshold line (dotted-line). The threshold was set manually at the exponential phase of DNA amplification. (B) A single and sharp peak represented by the first derivative fluorescence curve indicates generation of one specific PCR product.

The C_t values thus obtained were used for calculating the relative gene expression of the target gene compared to the reference or the housekeeping genes. All the calculations were done using “qPCR ANALYSIS V2.01” (Microsoft Excel™ worksheet developed by C. Baumstark-Khan, DLR, Germany). The worksheet first calculates the efficiency (E) of the PCR from the standard curve using Equation 14. It also calculates the quantity of sample DNA by comparing the standard curve using Equation 15. Then it calculates the relative quantity by dividing each sample quantity by the mean quantity of all housekeeping genes with the same treatment and time point. Then the relative quantity of each sample was divided by the mean relative quantity of the 0 Gy untreated control for the same time point, which gave the measure of regulation. The regulation (R) was then converted to the fold change (FC) values by following Equation 16.

$$Efficiency = -1 + 10^{\left(-\frac{1}{slope}\right)} \quad \text{Equation 14}$$

$$Quantity = 10^{\left(\frac{Ct - intercepts}{slope}\right)} \quad \text{Equation 15}$$

$$If R > 1 then FC = R \quad \text{and} \quad If R < 1 then FC = -1/R \quad \text{Equation 16}$$

2.2.16 Statistics

If not otherwise mentioned, means and standard deviations or standard errors were calculated using the statistics functions of the software packages Microsoft Excel™, Sigma Plot™, and Flowing Software Version 2.5. Regression curves were calculated likewise. Two-tailed Student's test was applied to determine the statistical significance between different samples. Only the data sets which passed Normality Test as well as Equal Variance Test were subjected to t-test. Mann-Whitney Rank Sum Test was used for the data sets that failed Equal Variance Test. Significant differences between two conditions were represented by the probability, p, assuming the truthfulness of null hypothesis (*, p < 0.05; **, p < 0.01 and ***, p < 0.001). The null hypothesis is that the two conditions are same (i.e. they are not different from each other). Small p-value (typically < 0.05) signals strong evidence against null hypothesis, which means one can reject null hypothesis.

3 RESULTS

The main intention of this study was to establish a novel and reliable cell and organ model that can be used for investigations to uncover the underlying mechanism of radiation-induced cataractogenesis.

First of all, the growth properties and morphology of pLECs were determined. Investigating the transparency of whole lens in culture medium was equally important for whole lens organ culture. The proliferation of pLECs in monolayer and within the lens organ culture was determined by inspecting DNA synthesis with the EdU-assay. Similarly, the proliferation behavior of different passages pLECs was analysed so that only the healthily proliferating pLECs could be selected for following experiments.

In order to assess the response to ionizing radiation exposure, the cellular survival of pLECs was determined using the colony forming ability assays after X-irradiation. It is well known that ionizing radiation induces genetic damage (e.g. DNA-DSBs). To maintain genomic stability as well as to survive, different cell-cycle checkpoints are activated in the cells. Therefore, analysis of cell-cycle distribution after X-irradiation was performed to examine the nature of checkpoints involved in pLECs. In addition, the radiation-induced cell-cycle distribution of pLECs was determined, after inhibiting molecules like ATM, ATR and DNA-PK. These molecules are known to play a key role in DNA repair and checkpoint activation.

There is a hypothesis that radiation-induced cataracts emerge due to post-irradiative activity of genetically damaged lens epithelial cells. Based on this hypothesis, the dose and quality of radiation-induced damage and repair activity of cells would play a big role in cataractogenesis. For this reason, DNA damage induction and repair in pLECs was studied using the γ H2AX assay after X-irradiation as well as heavy ions exposure. Likewise, the influence of ATM, ATR and DNA-PK was subject of the study. Furthermore, the γ H2AX assay on whole lens organ culture was performed to investigate if lens epithelial cells exhibit a similar response *in vitro* and in organ culture. γ H2AX analysis in organ culture also gave the possibility to inspect if the lens epithelial cells in different regions (anterior and equatorial region) of the epithelial layer react differently to ionizing radiation.

In a next step, the expression of genes that are involved in DNA repair, cell-cycle progression, cataractogenesis, oxidative stress, growth and survival were analysed for pLECs after exposure to X-rays and Carbon-12 ions.

Last but not the least, the osteogenic induction of pLECs was verified by Alizarin Red S staining and gene expression of osteogenic marker genes were investigated using RT-qPCR.

3.1 Growth properties of porcine lens epithelial cells (pLEC) in monolayer and in whole lens organ culture

For establishing a whole organ culture of the eye lens and culturing pLEC, the growth properties had to be determined. The number of chromosomes was verified and growth properties in the *ex vivo* environment of supplied medium were assessed. To investigate cellular viability and cell division under these culture conditions, DNA replication and synthesis were examined.

3.1.1 pLEC characteristics, morphology and growth pattern

For chromosome counting, metaphase spreads from pLEC were prepared and stained with Giemsa. The count revealed the healthy number of chromosome pairs. There were in total 38 chromosomes - 18 pairs of autosomal chromosomes and a pair of allosome (sex) chromosomes. Figure 19 shows the chromosome preparation of a female pig since two X chromosomes are shown at the bottom right of the karyogram.



Figure 19: Chromosome preparation. Colcemid induced metaphase spreads of pLEC were prepared and Giemsa staining was performed to visualize the condensed chromosomes.

The epithelial cells, which are located just beneath the anterior lens capsule, are tightly packed and have an epithelial cuboidal shape. The region marked with a red oval in Figure 20A shows the arrangement of the cells on the epithelial layer beneath the anterior part of the lens capsule. The unmagnified image of epithelial layer is shown in Figure 10E and F. When the pLECs within the epithelial layer are incubated for a week in culture medium, the cells start proliferating and begin covering the empty space in the petri-dish as well. Trypsinization of such cells and sub-culturing in a new petri-dish is the first passage (Figure 20B). At a lower density these first passage cells demonstrate a flattened and wider morphology. The cells also show high transparency.

In order to determine the growth characteristics of pLEC cells, the cells were seeded at passage 2 and 3 in 3 cm petri dishes and counted at different time points with a Fuchs-Rosenthal haemocytometer. Images were also taken before counting which are shown in Figure 21. During further sub-culturing from passage 1 to passage 2 and 3, cells get much wider and flatter. In the growth curve shown in **Fehler! Verweisquelle konnte nicht gefunden werden.**, the lag phase lasts around one day, which is followed by an exponential growth phase until about day 10 and then comes to the stationary phase where the culture surface is already completely covered with the cells. The exponential phase is not that steep, representing the slow dividing nature of pLECs.

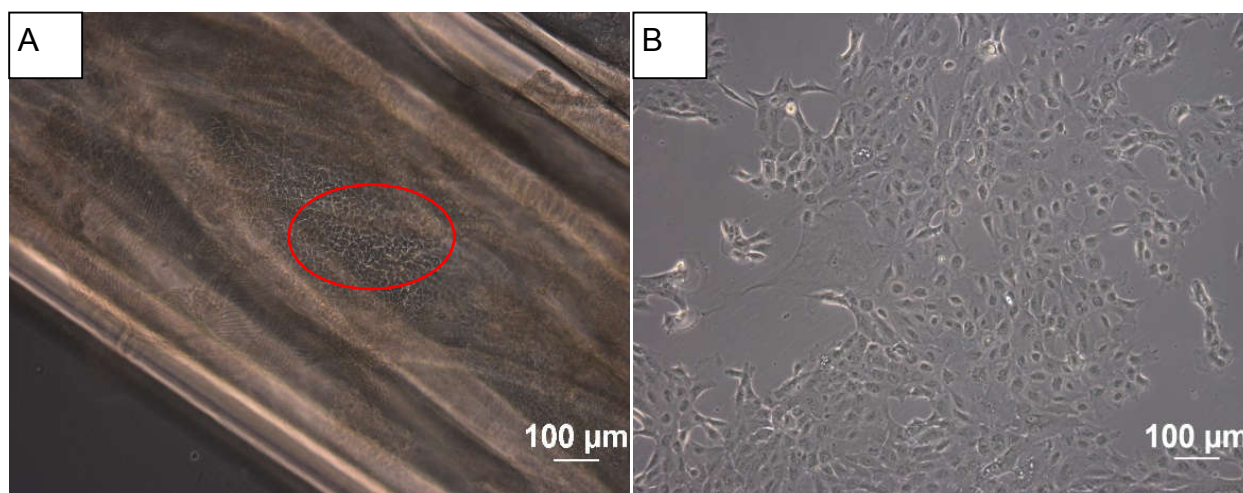


Figure 20: Cultivation of porcine lens epithelial cells (pLEC). Figure A shows the epithelial layer as a monolayer of tightly arranged pLEC attached to the lens capsule at the anterior part of the lens. Figure B shows the pLECs sub-cultured from the epithelial layer (A) at the 8th day of the culture (passage 1). Photos were taken with the phase contrast optics and the scale bar represents 100 µm.

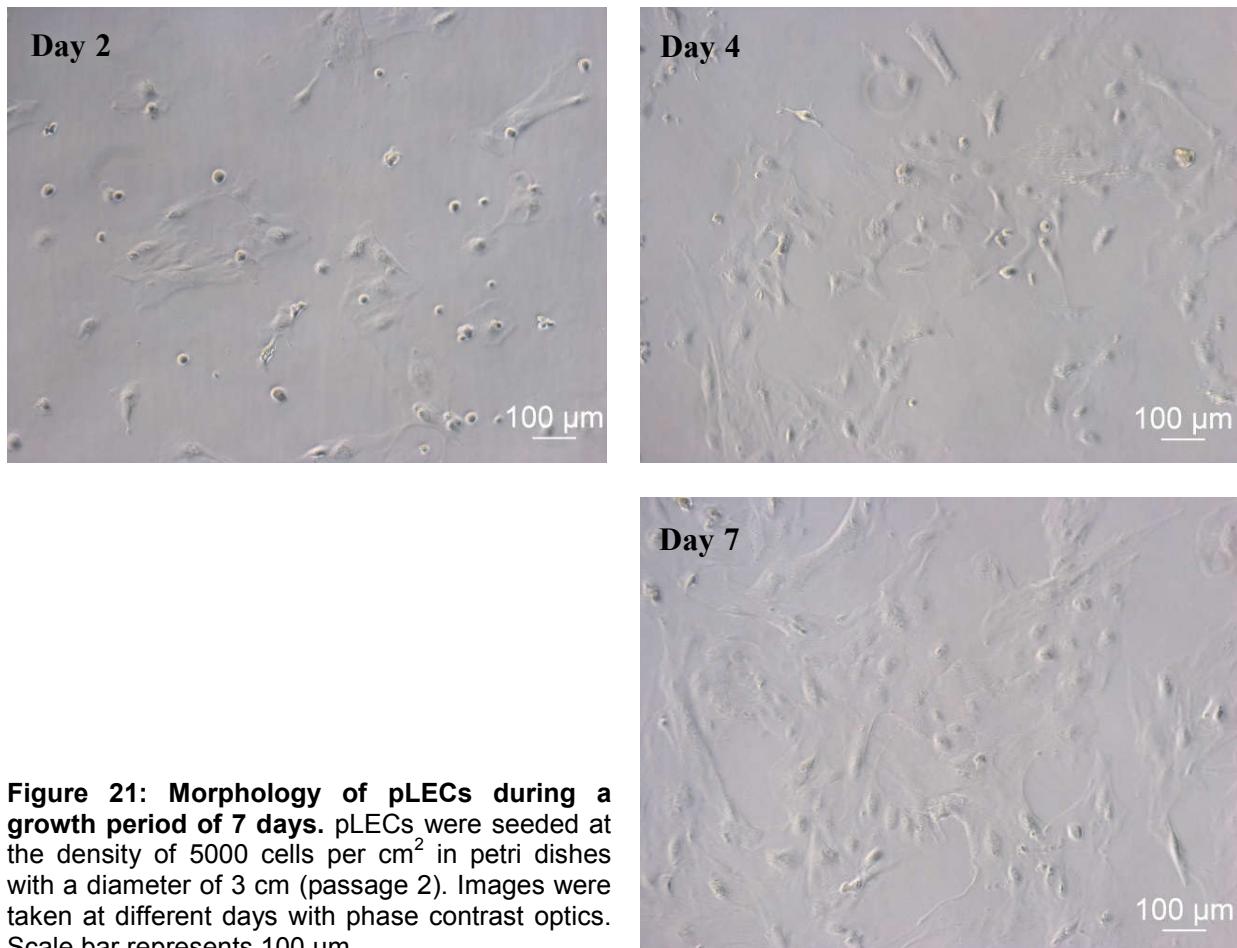


Figure 21: Morphology of pLECs during a growth period of 7 days. pLECs were seeded at the density of 5000 cells per cm^2 in petri dishes with a diameter of 3 cm (passage 2). Images were taken at different days with phase contrast optics. Scale bar represents 100 μm .

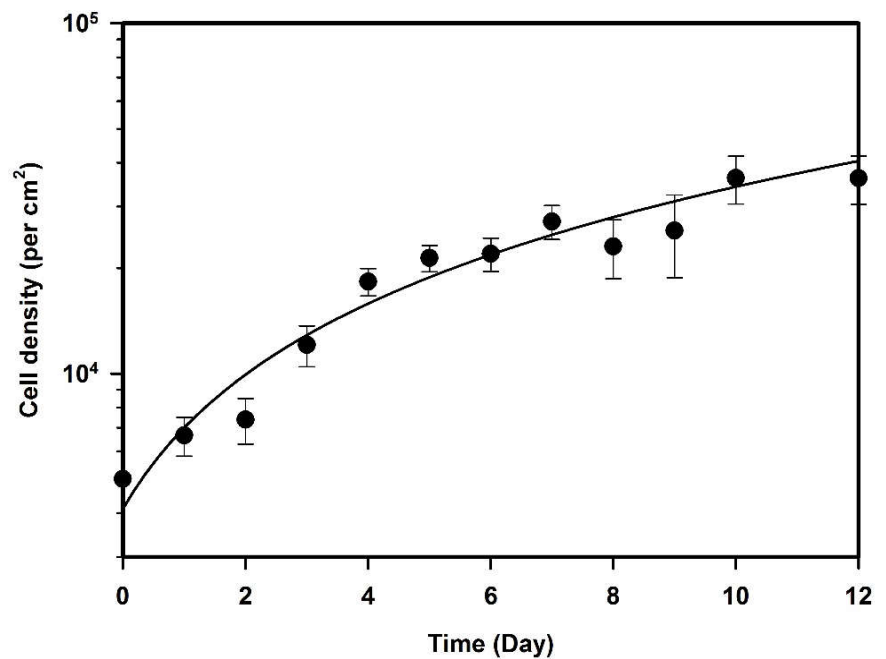


Figure 22: Growth behavior of pLECs. Cells were seeded at a density of 5000 cells cm^{-2} in petri dishes (\varnothing 3 cm). At each time point at least two dishes were trypsinized and cells were counted using a haemocytometer. Error bars indicate \pm SE from at least 4 samples (from at least 2 independent experiments with 2 replicates each).

3.1.2 Whole lens organ culture

The whole lenses isolated from the porcine eyes were supplemented with culture medium to observe their viability under cell culture conditions. In a healthy lens, its transparency is still maintained. In Figure 23, the clarity of the lens can be distinctively seen in the culture medium even after 7 days of isolation. Slight decrease in lens transparency is noticeable at day 14 where, through the same lens, the small squares of the background graph paper are blurred compared to day 7. Furthermore, the whole lens was stained for live imaging of the nuclei of the lens epithelial cells. The image was taken for the anterior part of the lens near to the equatorial region. The blurriness at the top and bottom of the Figure 24 is due to the curvature in this part of the lens.

Moreover, the whole lenses were also prepared for microtomy (see section 2.2.4) for further investigation of whole eye lenses. In Figure 25, the hematoxylin and eosin staining of a microtome-cut section is shown where the different parts of a porcine eye and also the whole lens capsule can be distinguished. The epithelial cells in the anterior as well as the equatorial region of the lens capsule were the subjects of interest in this thesis. This is because the single layered lens epithelial cell continues only up the equatorial region and there they start to differentiate into fiber cells with a longitudinal cellular morphology. Both epithelial cells and longitudinal fiber cells are clearly visible in the zoomed section of Figure 25.

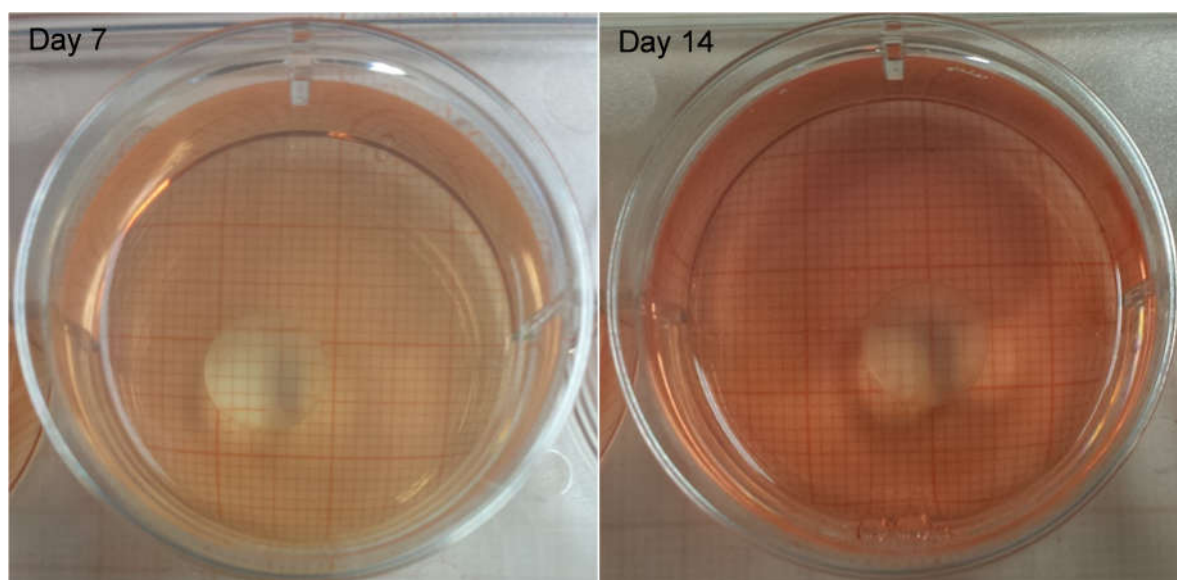


Figure 23: Lens organ culture. Photographs of a lens where taken after 7 and 14 days incubation at 37°C and 5% CO₂ in humidified atmosphere.

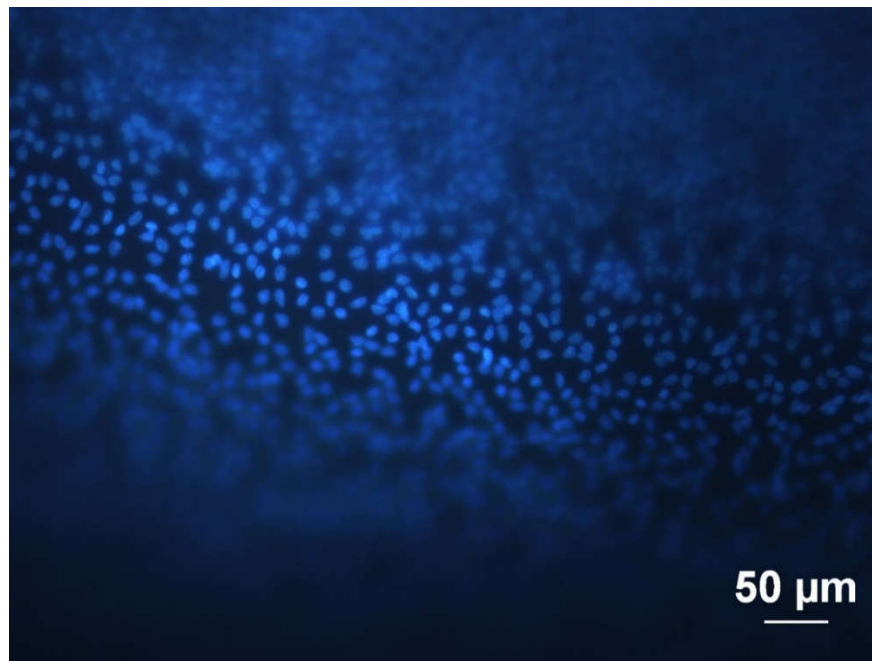


Figure 24: Live staining of lens epithelial cells in lens organ culture. The whole lens was stained with 30 $\mu\text{mol/l}$ Hoechst 33342 solution for staining the nuclei and fluorescence microscopy was performed with the whole lens suspended in PBS.

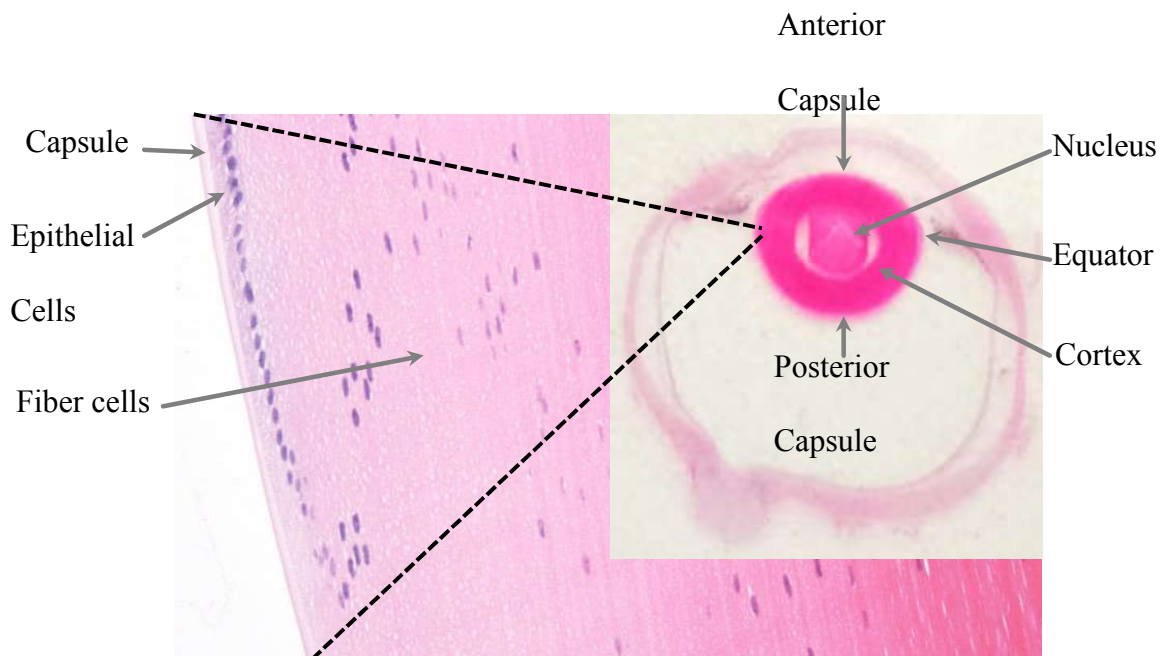


Figure 25: Hematoxylin-Eosin staining of lens. Paraffin-embedded porcine eye and lens were cut to 5 μm thin slices and were stained with Mayer's Haemalaun and 1 % Eosin. Hematoxylin stains the nucleic acids resulting in blue color for nuclei and Eosin non-specifically stains proteins resulting in a varying pink color.

3.2 Determination of DNA synthesis during S-phase

To investigate the replication of DNA during S-phase, the Click-iT EdU Assay was used in a next set of experiments. EdU (5-ethynyl-2'-deoxyuridine), a nucleoside analogue of thymidine, gets incorporated into the DNA during DNA synthesis and can be detected by a “click” reaction comprising a covalent reaction between an azide from a AlexaFluor dye and an alkyne from EdU catalysed by copper. This assay can be used to confirm whether the cells are proliferating (accompanied by DNA synthesis) or not.

3.2.1 Replication and synthesis in the monolayer culture

The supplementation of EdU to the epithelial layer of the lens led to its incorporation in the DNA of lens epithelial cells, which is visualised by green fluorescence in the middle and the right images in Figure 26. In the negative control without EdU, no green fluorescent nuclei were detected. The number of green fluorescent nuclei in the sample that was directly fixed after an EdU pulse of 2 h was lower compared with the number of labelled nuclei in the sample that was fixed 24 h after the 2 h EdU pulse.

Similarly, when the same experiment was performed with pLECs grown as a monolayer culture, the results showed the same trend of higher numbers of nuclei with EdU in the 24 h sample as compared to the sample that was directly fixed after a 2 h EdU pulse (Figure 27). The comparison of the 24 h samples clearly revealed a higher ratio of green to blue nuclei in the epithelial layer than in the monolayer culture.

Next, EdU incorporation was measured with a flow cytometer. Figure 28 shows the flow cytometric analysis of EdU incorporation in pLECs demonstrating the synthesis of DNA in the monolayer culture.

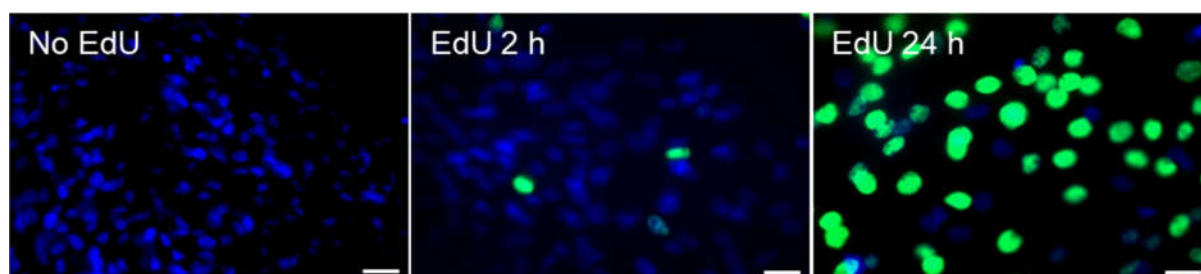


Figure 26: DNA synthesis in the epithelial layer. The epithelial layer cut off from the lens was supplied with 10 $\mu\text{mol/l}$ EdU for 2 h and fixed with 3.5 % formaldehyde in PBS immediately after the 2 h pulse or 24 h later. Nuclei (blue) were stained with DAPI (200 ng/ml) and EdU (green) was stained with AlexaFluor 488 (1 $\mu\text{mol/l}$). Scale bar represents 20 μm .

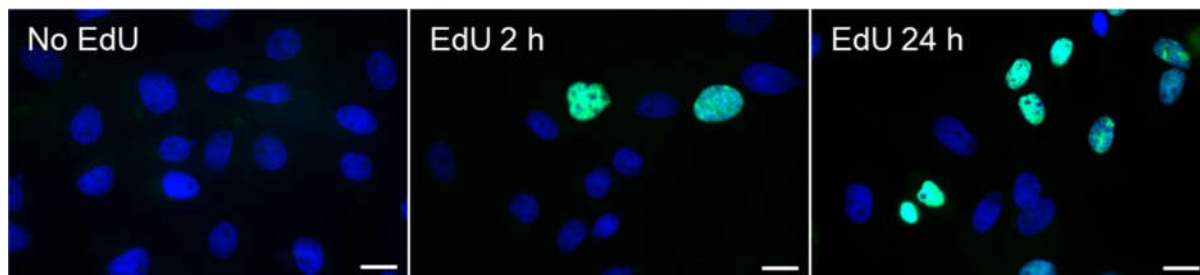


Figure 27: DNA synthesis in epithelial cell monolayer culture. The pLECs were supplied with 10 $\mu\text{mol/l}$ EdU for 2 h and fixed with 3.5 % formaldehyde in PBS immediately after the 2 h pulse or after 24 h. Nuclei (blue) were stained with DAPI (200 ng/ml) and EdU (green) was stained with AlexaFluor 488 (1 $\mu\text{mol/l}$). Scale bar represents 20 μm .

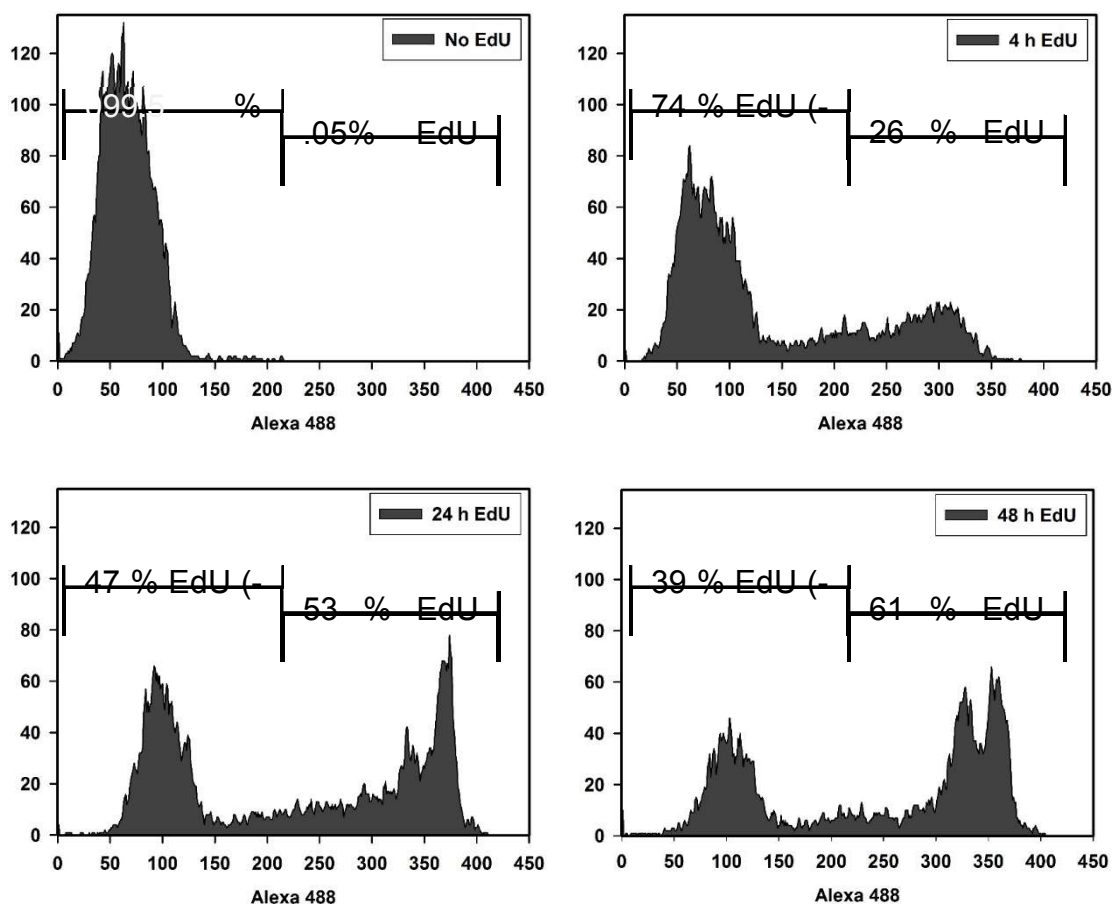


Figure 28: Flow-cytometric analysis of DNA synthesis, determined by EdU incorporation into the DNA of pLECs. The pLECs were supplied with 10 $\mu\text{mol/l}$ EdU for different time intervals. Samples were then harvested and fixed in 70 % ethanol. Alexa 488 was used to stain the EdU-positive cells. Flow cytometry was performed to separate EdU positive (+) and negative (-) cells which are shown in above histograms.

4 h of EdU supplementation resulted in 26 % cells with EdU incorporation. The percentage of EdU positive cells increased to 53 % and 61 % when EdU was provided for 24 h and 48 h, respectively. This result indicates a slower population doubling time of the porcine lens epithelial cells on the petri dishes as only 61 % of cells were EdU-positive even after 48 h of its supplementation.

3.2.2 Replication and synthesis in whole organ culture

After successful demonstration of DNA synthesis in lens epithelial layers and pLECs in monolayer culture, the experiment was performed with whole lenses grown in organ culture. This experiment was of particular interest in order to know if epithelial cells within the whole lens would reveal a similar EdU incorporation profile.

The results shows that there was not much difference in the number of cells with EdU incorporation for the sample which was directly fixed after 2 h EdU supplementation compared to the 24 h sample (Figure 29). On the other hand, when the 24 h sample images from epithelial layer (Figure 26) and monolayer culture (Figure 27) are compared with the whole lens (Figure 29), the number of EdU incorporating cells is obviously lower in the latter.

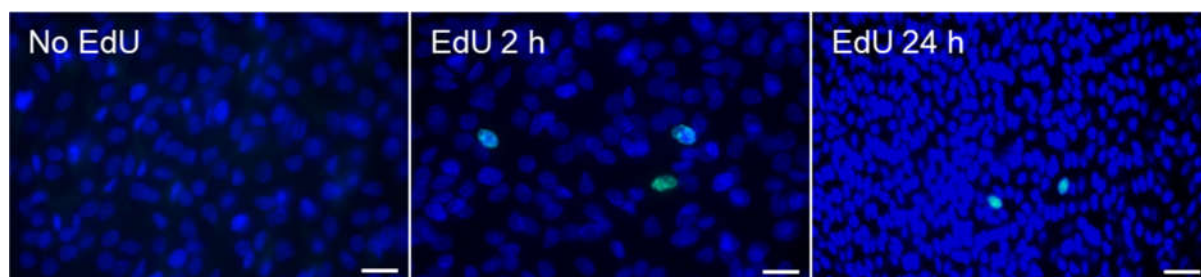


Figure 29: DNA synthesis in the whole lens. The whole lenses were supplied with 10 $\mu\text{mol/l}$ EdU for 2 h and fixed with 3.5 % formaldehyde in PBS directly or 24 h later. From the fixed lenses, the epithelial layer was cut off for staining. For microscopy the nucleus (blue) was stained with DAPI (200 ng/ml) and EdU (green) was stained with AlexaFluor 488 (1 $\mu\text{mol/l}$). Scale bar represents 20 μm .

3.3 Oxidative stress in pLEC monolayer culture

Oxidative stress within the cell can cause genetic damages, senescence and even cell death. Despite the significance of this player in cellular fate, oxidative stress determination is difficult mainly due to the short-lived nature of the reactive oxygen species (ROS). To measure oxidative stress via ROS, the CellROX[®] Green dye was used, which in reduced form can oxidize to a fluorescent form that binds to DNA. Its fluorescence is excited at 485 nm and emission was measured at a wavelength of 520 nm.

A potent agent to generate ROS in cells is menadione. Different concentrations of menadione were added to pLECs in order to induce oxidative stress, and the effects were compared to pLECs exposed to X-rays.

The bar diagram presented in **Figure 30** shows an increasing amount of ROS formation with increasing concentration of menadione. The quantity of ROS represented as “mean grey value” (arbitrary units from the monochromatic image of green fluorescence) of the cell was 1.06 ± 0.19 , 4.78 ± 0.42 and 23.56 ± 4.54 for 25, 50 and 100 $\mu\text{mol/l}$ of menadione, respectively. In the negative control, without menadione and irradiation treatment, the value was 0.31 ± 0.10 . For the sample exposed to 6 Gy (with 30 min incubation time after irradiation) of X-rays, the value amounted to 0.60 ± 0.09 . Another aspect of this experiment was to create a standard for generation of ROS, which could be compared to ROS production after X-rays exposure.

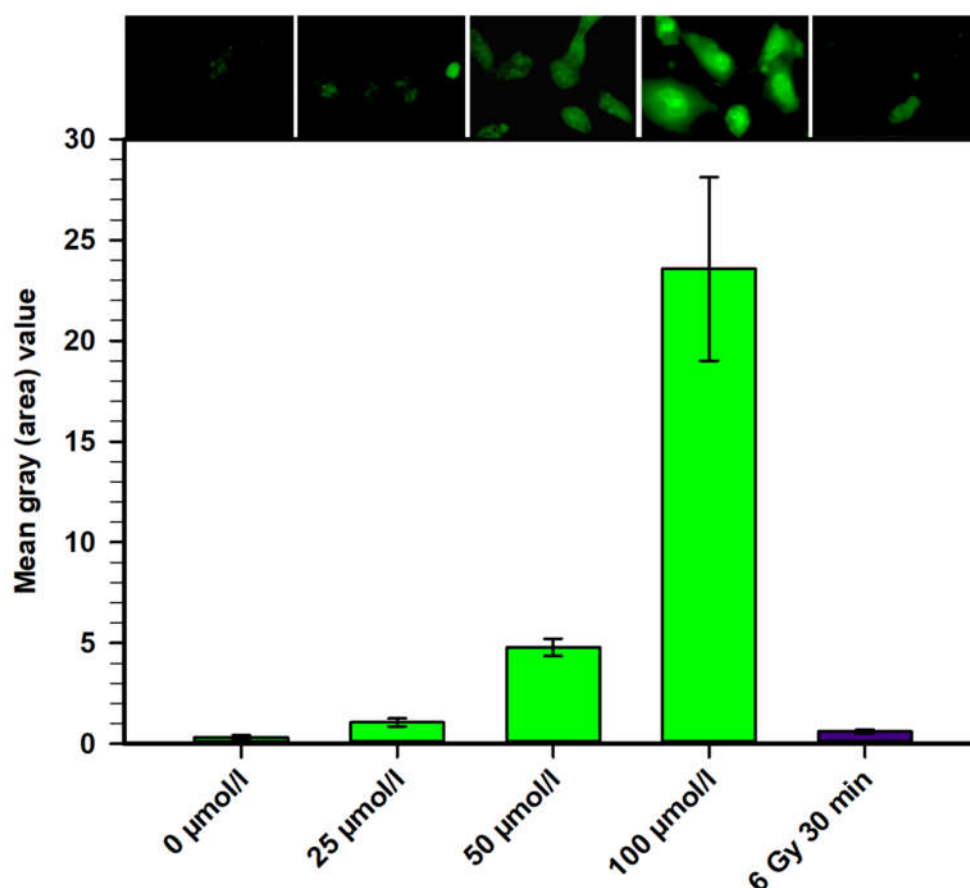


Figure 30: Oxidative Stress measurement by CellIROX® Green. pLECs treated and untreated with menadione for an hour and X-ray exposed (30 min after exposure) samples were stained with 5 $\mu\text{mol/l}$ CellIROX® Green for 30 min at 37 °C. Images were taken with the AxioCam attached to a fluorescence microscope. The bar graph represents the mean of the mean grey value in the monochrome image of green fluorescence from at least 12 images \pm SEM.

After quantifying the ROS generated by menadione, the kinetics of ROS production after X-ray exposure were determined. The results for this experiment is plotted in **Figure 31**, where the value for the negative control (no menadione, no X-rays) and the positive control (1 h 100 $\mu\text{mol/l}$ menadione, no X-rays) was found to be 0.69 ± 0.16 and 18.08 ± 2.00 , respectively. pLECs exposed to 6 Gy of X-rays had mean a grey values of 1.76 ± 0.65 , 1.58 ± 0.41 , 1.11 ± 0.19 , 0.95 ± 0.27 , 0.90 ± 0.28 and 1.27 ± 0.27 after incubation of 0 min, 15 min, 30 min, 1 h, 4 h and 24 h of irradiation. Although for 0 min incubation sample, it took at least a min before putting CellROX[®] Green due to time required for opening the door of the X-ray exposure chamber.

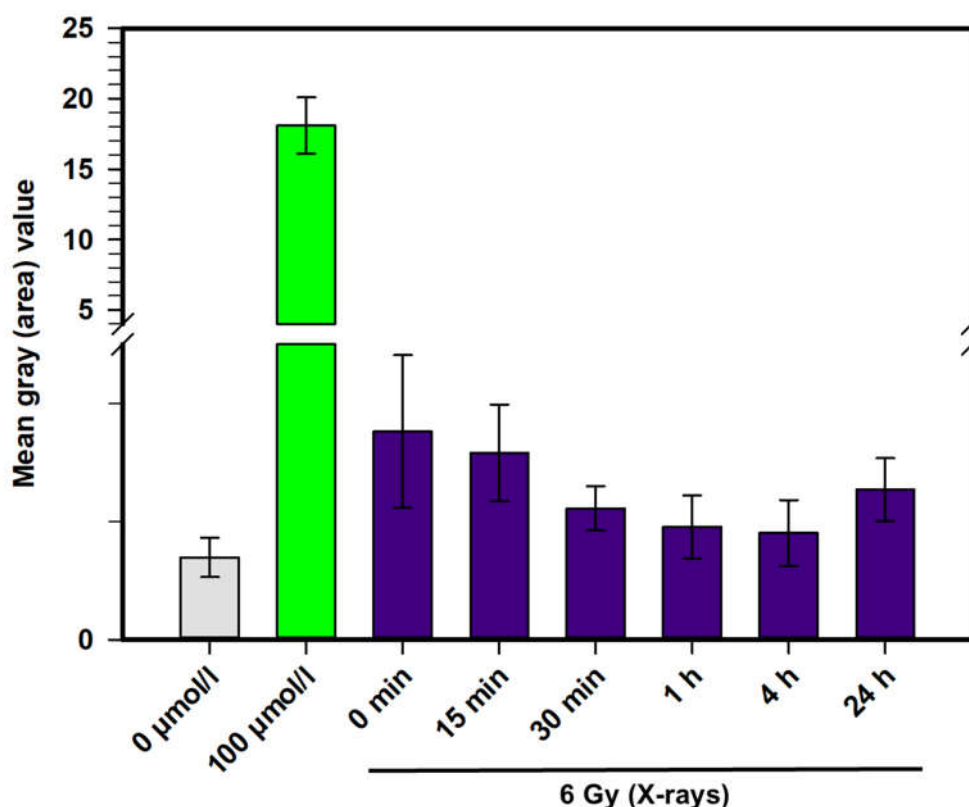


Figure 31: X-ray-induced oxidative stress as a function of time after exposure. pLECs were treated with menadione for an hour or exposed to 6 Gy X-rays (harvesting of cells after 0 min, 15 min, 30 min, 1 h, 4 h and 24 h after irradiation). Samples were stained with 5 $\mu\text{mol/l}$ CellROX[®] Green for 30 min at 37 °C. Images were taken with the AxioCam attached to the fluorescence microscope. The bar graph represents the mean of mean grey value in the monochromatic image of green fluorescence from at least 15 images \pm SEM.

3.4 Radiobiological characterization

The focus of the next set of experiments was the radiobiological characterization of pLECs. Therefore, the plating efficiency and cellular survival after X-irradiation were determined using the colony forming ability assay.

3.4.1 Plating efficiency of pLECs

The plating efficiency is an important parameter for performing the colony forming ability test as it serves as an indicator of cellular survival after radiation exposure. The plating efficiency of pLECs, which was calculated according to Table 14, amounted to 0.095 (9.5 %).

3.4.2 Cellular survival after X-ray exposure

Survival of pLECs after X-rays exposure was performed using colony forming ability test assay. The relative surviving fraction of immediately and late plated pLECs were plotted in order to determine the survival benefit with respect to 24 h incubation time given for possible damage repair. In

Figure 32, both curves were drawn using the single-hit-multi-target model. For immediately plated cells (0 h incubation after radiation exposure before seeding), the parameters D_0 , n and D_q were calculated to be 1.42 Gy, 1.82 and 0.85 Gy respectively. For the late plated cells (24 h incubation before seeding), D_0 , n and D_q were found to be 1.68 Gy, 1.43 and 0.60 Gy, respectively. The comparison of the curves did not show any statistically significant difference in the survival of pLECs with respect to incubation time after X-rays exposure (0 h vs. 24 h of recovery time). The combined D_0 and n was calculated to be 1.54 Gy and 1.61 respectively. For better visualization and comparison of the result, the data are sorted in Table 15.

Table 14: Plating efficiency of pLECs.

| Number of cells seeded | Mean colony count | Plating efficiency (PE) |
|-----------------------------|-------------------|-------------------------|
| 50 | 6.3 ± 1.7 | 0.125 ± 0.034 |
| 100 | 11.5 ± 4.5 | 0.115 ± 0.045 |
| 200 | 19.0 ± 2.4 | 0.095 ± 0.012 |
| 500 | 37.0 ± 2.9 | 0.074 ± 0.006 |
| 1000 | 63.8 ± 4.3 | 0.064 ± 0.004 |
| Mean PE of all measurements | | 0.095 ± 0.020 |

pLECs were seeded on 6 cm petri dishes in different numbers. After 30 days, cells were fixed and stained with crystal violet solution in 3.5 % formaldehyde. Colonies with at least 50 cells were counted.

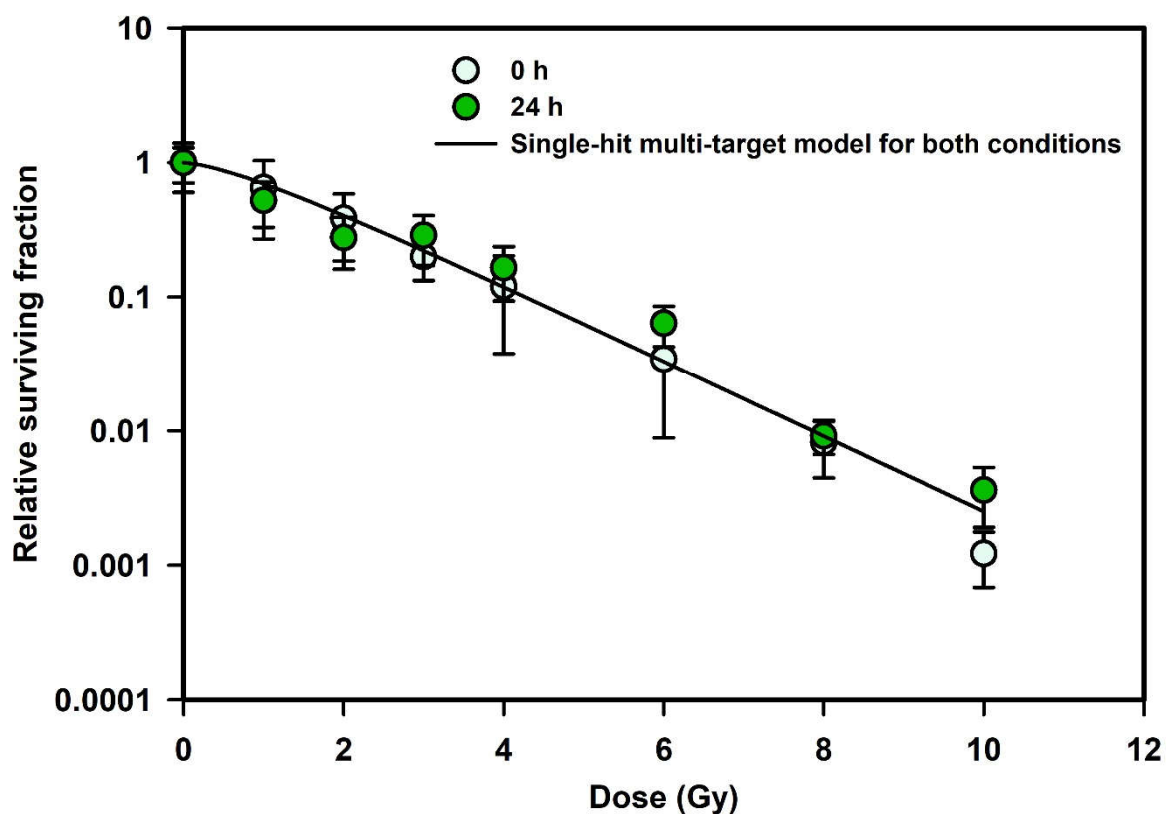


Figure 32: Clonogenic survival of pLECs after exposure to X-rays. Cells were seeded either immediately after irradiation (immediate plating, 0 h) or after incubation for 24 h post irradiation (late plating) and were fixed and stained with crystal violet solution in 3.5 % formaldehyde solution when colonies (at least 50 cells per colony) were visible (~ 30 days incubation). Mean \pm SD were calculated from at least 2 independent experiments.

Table 15: Comparison of survival curve parameters for IP (immediately plated) and LP (lately plated) pLECs.

| Parameters | IP | LP | Combined |
|------------|-----------------|-----------------|-----------------|
| D_0 (Gy) | 1.42 ± 0.07 | 1.68 ± 0.17 | 1.54 ± 0.08 |
| n | 1.82 ± 0.43 | 1.43 ± 0.58 | 1.61 ± 0.53 |
| D_q (Gy) | 0.85 ± 0.36 | 0.60 ± 0.70 | - |

3.5 Cell cycle progression after X-ray exposure

Next, the distribution of pLECs in different phases of cell cycle after X-rays exposure was addressed using the cell cycle assay. Here, the modulation in the cell cycle distribution was determined using propidium iodide and flow cytometry. Exponentially growing cells were irradiated with 0, 1, 2, 4 and 6 Gy and harvested at 4, 24, 48, 72 and 168 h after irradiation. Supplementary figure S1 shows the histograms of propidium iodide fluorescence. As propidium iodide binds stoichiometrically to DNA, the distribution of cells in G1 phase (2n), S-phase (between 2n and 4n) and G2/M phase (4n) of the cell cycle becomes visible. The number of the cells in the different cell cycle phases was determined as mentioned in material and method section 2.2.9.

The percentage of cells in the different cell cycle phases is shown in Figure 33. In the non-irradiated samples (0 Gy), the percentage of cells in G1 phase increased with time (0 h to 168 h) while the percentage of S and G2/M phase cells decreased during the exponential growth of cells. Four hours after exposure to X-rays, there was almost no change in the percentage of cells at G1, S or G2/M phase even with increasing dose. But from 24 h onwards, a clear dose-dependent shift of irradiated cells towards the G2/M phase was observed compared to non-irradiated control cells. The percentage of the G2/M phase cells decreased with time for the non-irradiated sample. This reduction of G2/M phase cells was seen in exponentially growing cells. For lower doses of 1 Gy and 2 Gy, the reduction of the percentage of cells in G2/M phase with increasing time was present but not to the extent as non-irradiated ones. But for higher doses of 4 Gy and 6 Gy, the cells did not return to the normal growth pattern even after a week (168 h). This shift of the cell population to the G2/M phase is denoted as G2/M delay. In this study, the G2/M phase cells did not recover to the exponential growth pattern (i.e. radiation damaged cells did not divide to become G1 phase cells again) instead they remained in G2/M phase (slightly above 40 %) therefore a G2 block was achieved.

In the upcoming results parts only the percentage of cells in the G2/M phase of the cell cycle will be discussed, because radiation exposure of pLECs resulted in a G2/M phase arrest rather than delays in the progression of cells through the G1 or S phase.

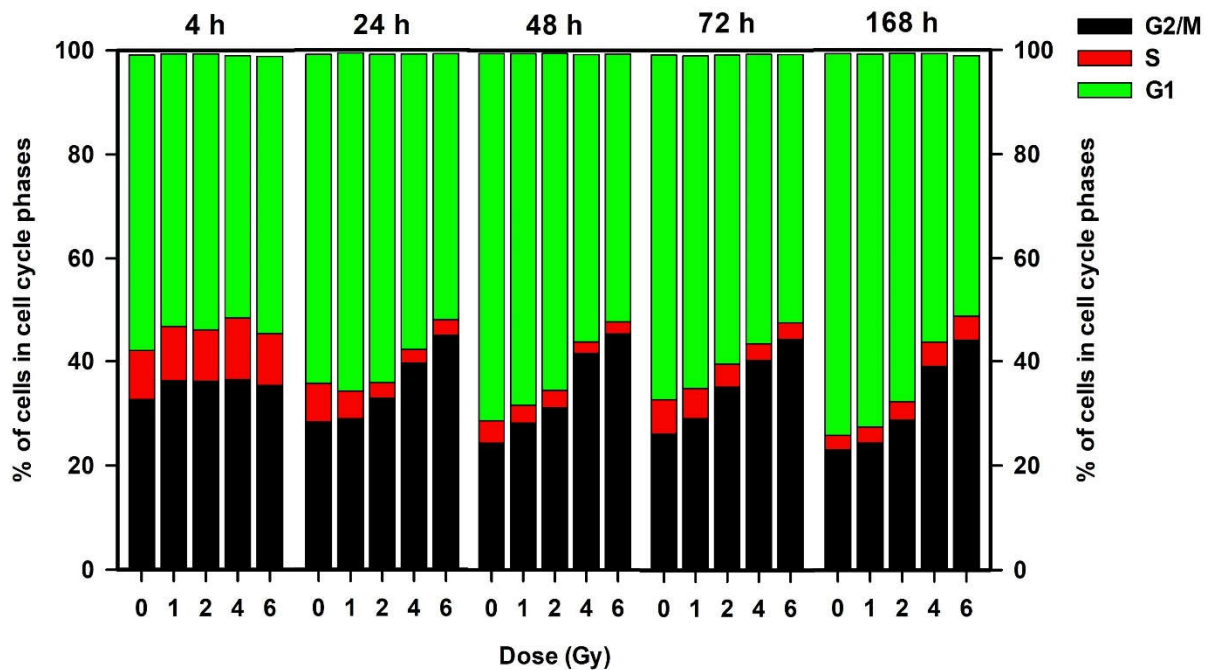


Figure 33: Time-dependent distribution of cells in the different phases of the cell cycle. This exemplary percentage of cells distribution in G1-, S-, and G2/M-phases of the cell cycle was derived from a single experiment (supplementary figure S1).

3.5.1 The effect of passage number on cell cycle progression

The pLECs used for cell cycle analysis are primary cells. Unlike the immortal cell line, the primary cells face the problem of aging with each cell passage. Therefore, by investigating the cell cycle progression of these cells at different passages will help to determine the right limit of passage number, which can be used in further investigations.

Figure 34 shows the behaviour of second passage pLECs after X-ray exposure. Four hours after irradiation, the percentage of cells at G2/M phase of the cell cycle for 1 Gy and 4 Gy samples was significantly higher than in the non-irradiated sample. After 24 h onwards, the G2/M phase percentage of cells for the non-irradiated sample decreased during the exponential growth phase. This reduction of cells in the G2/M phase was true for cell samples exposed to 1 Gy and 2 Gy. A lower G2/M arrest was observed for 1 Gy and 2 Gy although it was not statistically significant compared to 0 Gy at respective time points. For 4 and 6 Gy, there was clear G2/M arrest after 24 h onwards, and the difference compared to the non-irradiated sample was statistically significant. Specifically, the percentage of G2/M phase cells at 4 h and 72 h was 32.8 % and 21.2 % for 0 Gy, respectively, and 36.9 % and 43.1 % for 6 Gy, respectively.

For third passage (P-3) pLECs (Figure 35), the difference in the reduction of G2/M phase cells for 1 Gy and 2 Gy was not significantly different from 0 Gy at all the time points. Also for the P-3 cells, the G2/M phase arrest started 24 h post irradiation for 4 Gy and 6 Gy and continued till 72 h. The difference in the percentage of cells at the G2/M phase of the cell cycle between non-irradiated and 4 and 6 Gy irradiated samples was statistically significant. The percentage of G2/M phase cells at 4 h and 72 h was 27.4 % and 21.7 % for 0 Gy, respectively and 29.9 % and 36.6 % for 6 Gy, respectively.

At passage 4 (Figure 36A), a slight increase in the percentage of G2/M phase cells for 6 Gy irradiated cells compared to 0 Gy cells 24 h onwards post irradiation was observed. At 4 h and 72 h after irradiation, the percentage of G2/M phase cells was 27.2 % and 21.1 % for 0 Gy, respectively and 27.1 % and 27.6 % for 6 Gy.

At passage 5, even the non-irradiated sample failed to show the normal exponential growth of the pLECs (Figure 36B). The percentage of G2/M phase cells for irradiated and non-irradiated cells was almost unchanged at all time points after irradiation. Here, the percentage of G2/M phase cells at 4 h and 72 h after irradiation was 26.7 % and 25.8 % for 0 Gy, respectively, and 26.5 % and 27.0 % for 6 Gy.

It is already known that the number of G1 phase cells increases towards the end of the exponential growth phase whereas the number of cells in G2/M phase decreases (Pollard et al. 2016). At confluency, most of the cells are at G1 phase or even G0 phase. In this part of the study, the exponential growth phase was analysed with reference to a decrease of G2/M phase cells for different passages of non-irradiated pLECs (Figure 37). For the passage 2 pLECs, the decreases in G2/M phase cells after 24 h, 48 h and 72 h were statistically significant compared to the 4 h sample. For passage 3 pLECs, only the 48 h and 72 h samples showed a statistically significant decrease in G2/M phase cells compared to 4 h. Passage 4 pLECs still showed the trend of an exponential growth phase. But at passage 5, the percentage of G2/M phase cells decreased only very slightly with increasing time. Hence the results indicate a decrease in the cellular proliferation potential with increasing passage number, which could be due to aging of the cells.

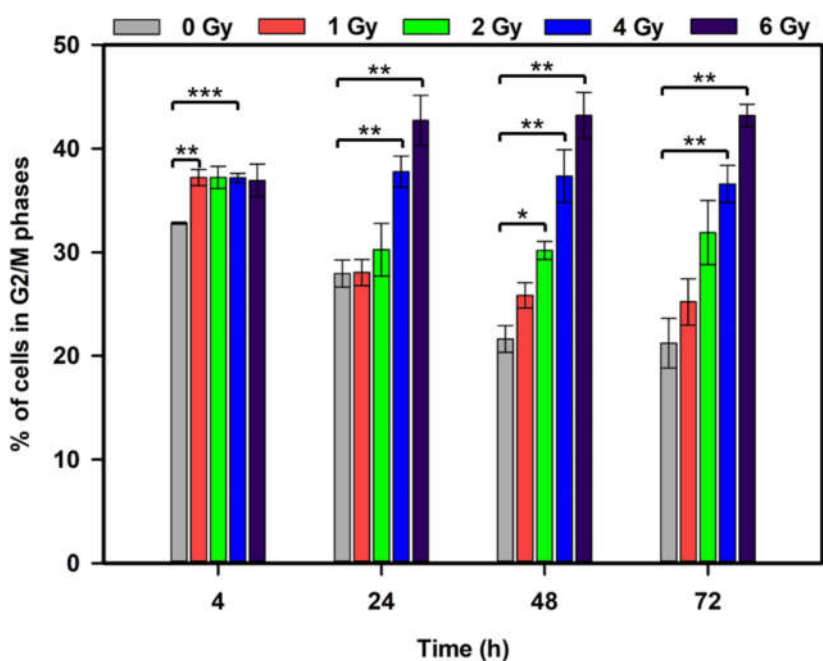


Figure 34: The percentage of cells in G2/M phase for the second passage (P-2) determined by flow cytometry. P-2 pLECs were irradiated with various X-ray doses and were harvested and stained with propidium iodide. The percentages of G2/M phase cells, out of 10,000 events per condition, were plotted against the harvesting time points. The bars indicate mean \pm SEM from three independent experiments. Statistical significance was determined with two-tailed Student's t-tests (*, $p < 0.05$; **, $p < 0.01$; ***, $p < 0.001$).

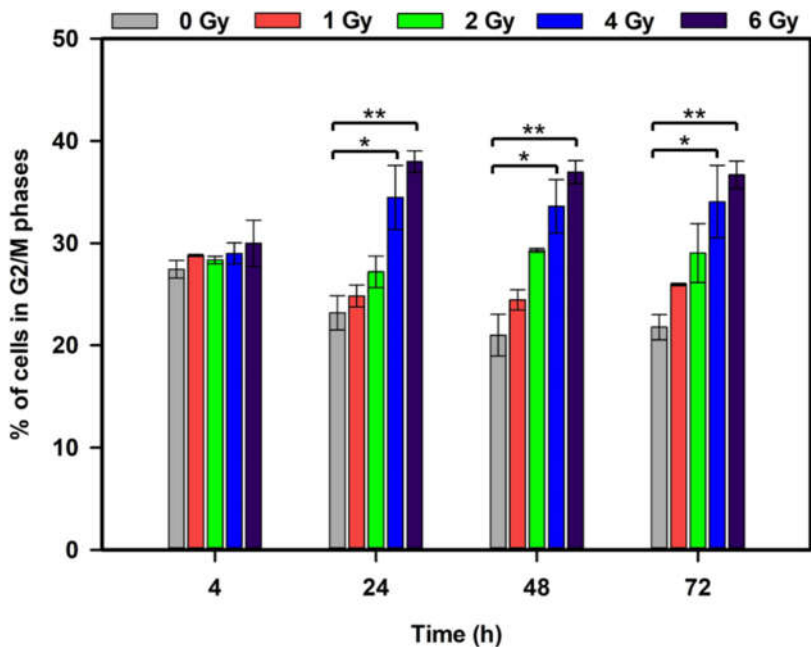


Figure 35: The percentage of cells in G2/M phase for third passage (P-3) determined by flow cytometry. P-3 pLECs were irradiated with various X-ray doses and were harvested and stained with propidium iodide. The percentages of G2/M phase cells, out of 10,000 events per condition, were plotted against the harvesting time points. The bars indicate mean \pm SEM from three independent experiments. Statistical significance was determined with two-tailed Student's t-tests (*, $p < 0.05$; **, $p < 0.01$; ***, $p < 0.001$).

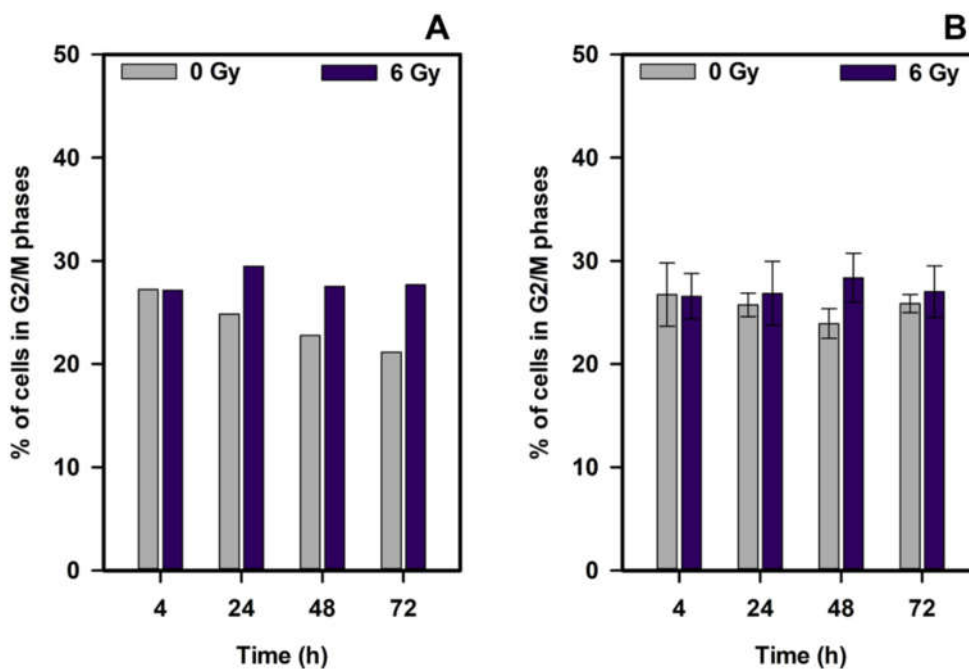


Figure 36: The percentage of cells in G2/M phase for fourth (A) and fifth (B) passage determined by flow cytometry. Cells were irradiated and were harvested to be stained with propidium iodide. The percentages of G2/M phase cells, out of 10,000 events per condition, were plotted against the harvesting time points. The bars indicate mean \pm SEM from two independent experiments for P-5 cells (B). Data for P-4 (A) were from single experiment.

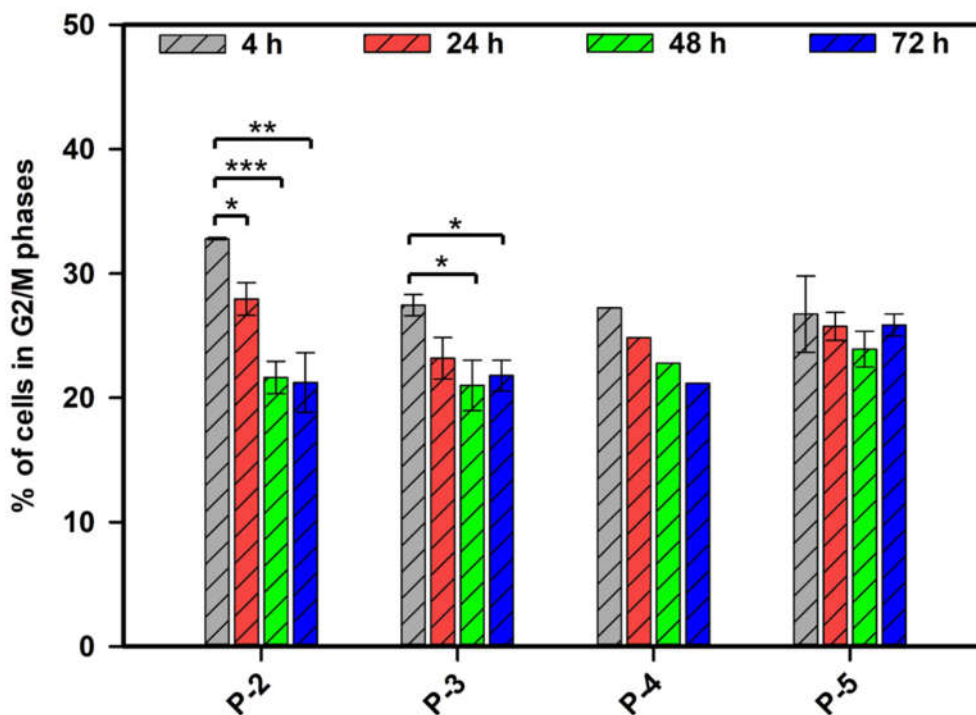


Figure 37: Comparison of the exponential growth of non-irradiated pLECs in passages 2 to 5 (P-2 to P-5). The G2/M percentage cells were out of 10,000 analyzed events. The bars represent mean \pm SEM. For P-2 and p-3, the n-number was three. Data for P-4 were from single experiment, whereas for P-5, it was from two experiments. Statistical significance was determined with two-tailed Student's t-tests (*, $p < 0.05$; **, $p < 0.01$; ***, $p < 0.001$).

3.5.2 The effect of PIKK related kinases on cell cycle progression

From the previous results, it is clear that exposure to ionizing radiation (X-rays) leads to G2/M arrest. In a cell system, these arrests prevent the cells from passing damaged DNA to the daughter cells. Such cell cycle control provides valuable time for repairing the damaged DNA. The next step in this study therefore was to understand the role of key regulator molecules, like ATM, ATR and DNA-PK, which are involved in DNA repair, by adding specific inhibitors to pLECs and analysing the cell cycle progression. These were preliminary experiments and results presented below for all three inhibitors were taken from their respective single experiments.

First of all, the ATM inhibitor KU55933 was used to have a closer look on its effect in modulation of cell cycle phases of pLECs after X-ray exposure. As mentioned in section 1.4.1, ATM activation leads to phosphorylation of molecules required for DNA damage checkpoint as well as cell cycle arrest. The supplementation of the ATM inhibitor to pLECs resulted in a slight increase in the percentage of non-irradiated cells in the G2/M phase at all the time points. After X-ray irradiation, the percentage of G2/M phase cells increased by the ATM inhibitor at 48 h and 72 h (**Figure 38**).

Secondly, ATR was inhibited using VE821. For non-irradiated samples, no change in the percentage of cells in G2/M phase was observed between ATR inhibitor-supplemented and non-supplemented medium. On the contrary, for the irradiated cells, ATR inhibition resulted in comparatively less G2/M arrested cells than cells that were provided with medium that did not contain the ATR inhibitor at all time points (**Figure 39**).

Thirdly, DNA-PK inhibitor NU7441 was tested to have a closer look if it would affect distribution of cell cycle in pLECs. DNA-PK has a crucial role in repairing of DNA DSB by NHEJ (**Figure 6**). DNA-PK supplemented pLECs on the other side did not show any particular trend (**Figure 40**). In the non-irradiated sample, at the 4 h time point, DNA-PK inhibition slightly increased the percentage of cells in G2/M phase. And for the remaining time points, DNA-PK inhibition led to a decrease in G2/M phase cells. For irradiated samples, DNA-PK inhibition had no significant effect on the percentage of cells in G2/M phase.

Since the results for all three inhibitors are derived from single experiments confirmative repeat experiments would be required to prove their effects in pLECs after radiation exposure.

3.6 DNA damage induction and repair

In order to analyse the induction and repair of DNA damage, especially DNA double strand breaks, the γ H2AX assay was performed. X-ray exposure leads to the induction of DNA DSBs and at the break site ATM phosphorylates the histone variant H2AX to become γ H2AX. This γ H2AX then triggers additional molecules that are required for repair of DNA. Using the γ H2AX assay allows to measure γ H2AX as a measured of DNA damage by labelling it with immunofluorescence. The detection of labelled γ H2AX will give information on the DNA damage sites in terms of foci (pink color due to secondary antibody against γ H2AX).

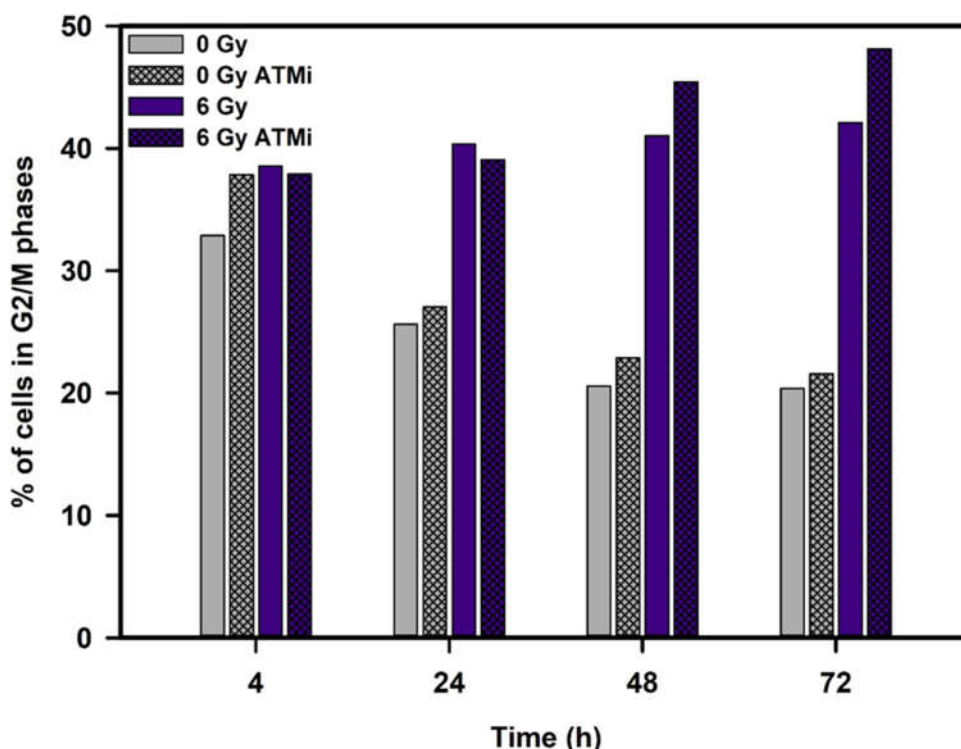


Figure 38: Effect of ATM inhibition on cell cycle progression after exposure to X-rays. Medium change with and without the ATM inhibitor (ATMi) KU55933 (10 μ mol/l) was performed 1 h before irradiation (6 Gy). Cells were harvested at different time points for propidium iodide staining and cell cycle analysis. Bar graph gives the percentage of G2/M phase cells out of 10,000 events from a single experiment.

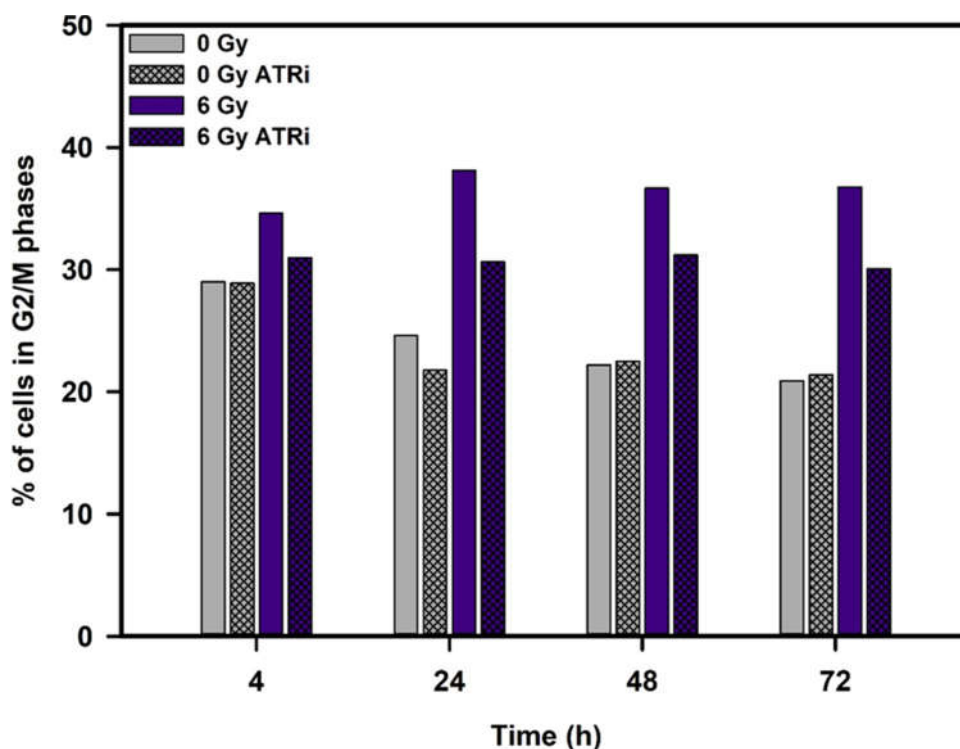


Figure 39: Effect of ATR inhibition on cell cycle progression after X-irradiation. Medium change with and without the ATR inhibitor (ATRi) VE821 (5 $\mu\text{mol/l}$) was performed 1 h before irradiation. Cells were harvested at different time points for propidium iodide staining and cell cycle analysis. Bar graph gives the percentage of G2/M phase cells out of 10,000 events from a single experiment.

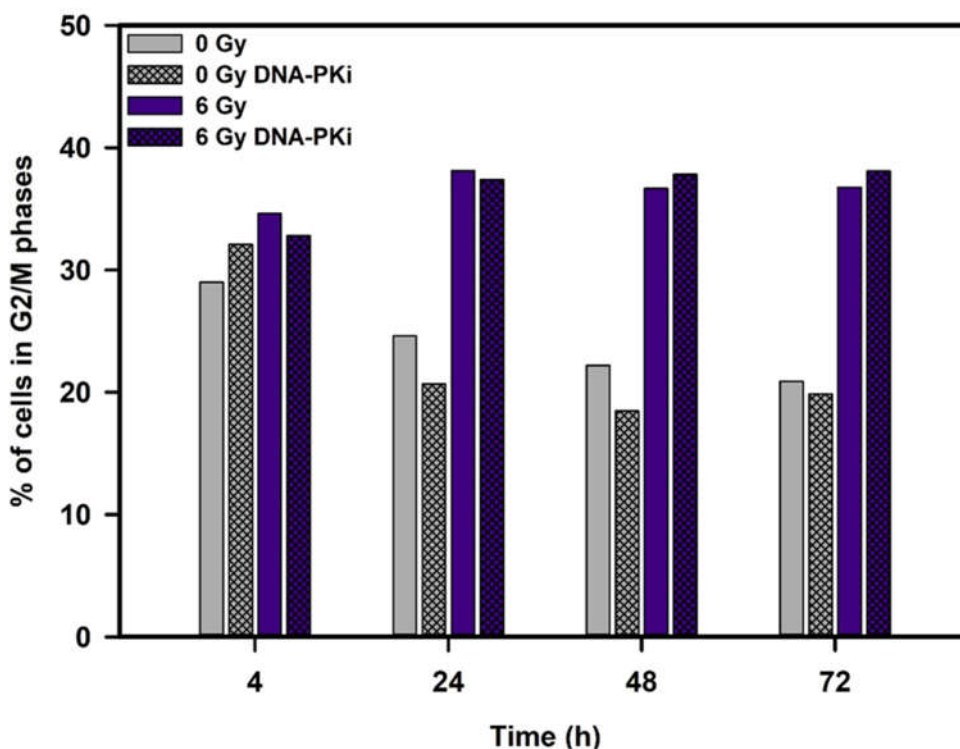


Figure 40: Effect of DNA-PK inhibition on cell cycle progression after X-irradiation. Medium change with and without the DNA-PK inhibitor (DNA-PKi) NU7441 (5 $\mu\text{mol/l}$) was performed 1 h before irradiation. Cells were harvested at different time points for propidium iodide staining and cell cycle analysis. Bar graph gives the percentage of G2/M phase cells out of 10,000 events from a single experiment.

3.6.1 DNA damage induction and repair analysis after X-ray exposure

The number of γ H2AX foci induction after X-irradiation is shown in Figure 41. An ionizing radiation dose-dependent increase in the number of foci was observed 1 h after X-ray exposure. Figure 42 presents a dose-dependent decrease of foci 24 h after X-ray exposure that can be interpreted as successful DNA repair while an increasing number of foci remained at higher doses, pointing towards a hampered repair of DNA damages. It should be noted that the foci at 24 h samples were comparatively larger and more distinct as compared to 1 h samples Figure 42.

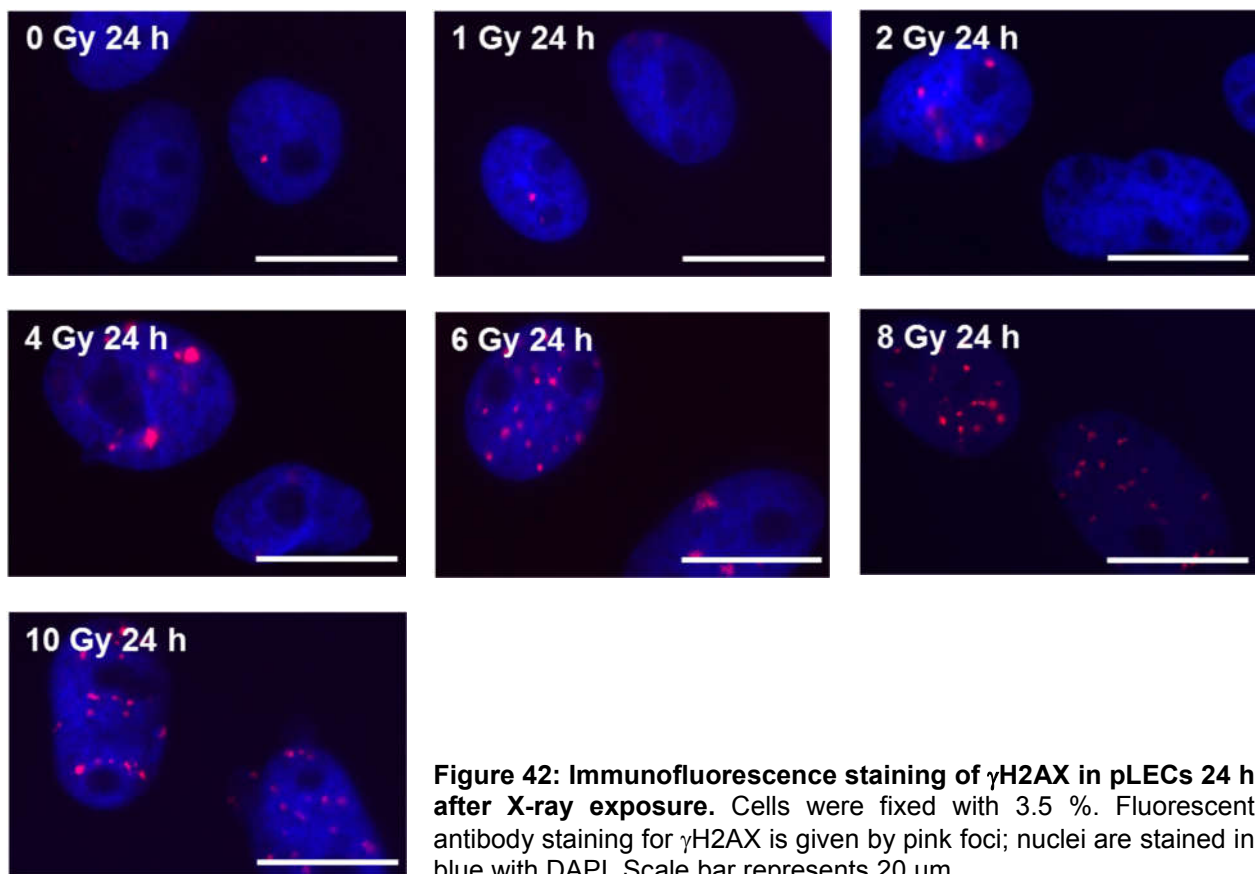
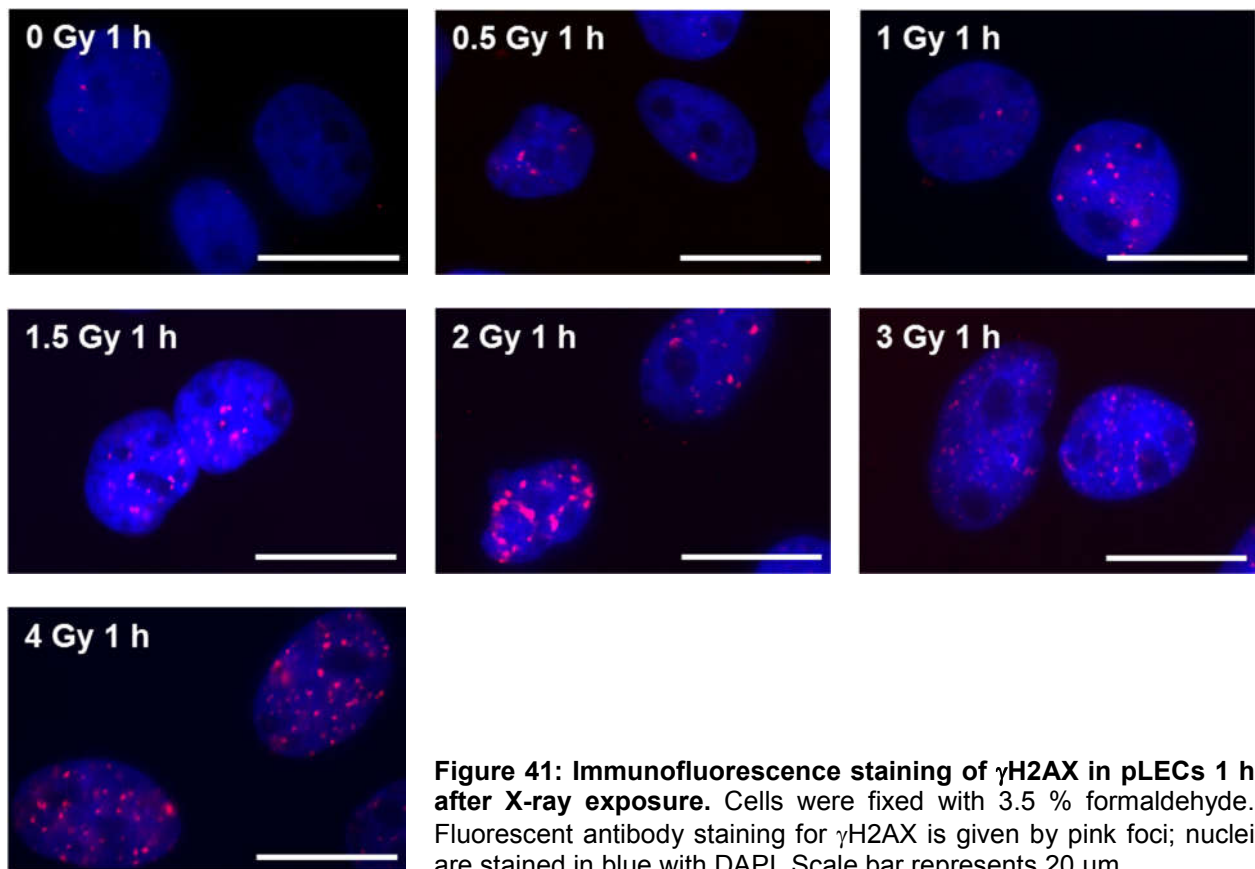
The effect of the ionizing radiation dose on the induction of DNA DSBs 1 h after X-ray exposure and on repair of those breaks 24 h after exposure is provided in Figure 43. The average number of foci per cell nucleus 1 h after irradiation showed a steep, almost linear increase from 0 to 4 Gy. For the repair after 24 h, the steepness of the increase of the average number of foci with increasing X-rays dose was smaller.

It is well-known that the maximal γ H2AX formation occurs between 30 min to an hour after irradiation (Mariotti et al. 2013, Lau et al. 2010). Here, time points of 1 h, 4 h, 24 h and 48 h after X-rays exposure were analysed. The kinetics of γ H2AX formation showed decrease of foci number with respect to time for both 1 Gy and 4 Gy X-ray-exposed samples which persisted even after 48 h (Figure 44).

The average number of foci in pLECs in non-irradiated and irradiated samples is plotted in Figure 45. The non-irradiated samples had an average of 1.2 foci per nucleus. In the 2 Gy-irradiated samples, 20.2 foci per nucleus were detected 1 h after irradiation, which decreased to 3.4 foci 24 h after irradiation. The statistical analysis showed significant changes for 24 h and highly significant differences for 1 h samples in foci formation in X-ray exposed cells as compared to unexposed cells. The reduction in the average number of foci in X-ray exposed sample from 1 h to 24 h was also statistically significant.

3.6.2 γ H2AX formation in pLECs after exposure to low doses of X-rays

In order to confirm the sensitivity and effect of low doses of X-rays, the γ H2AX assay was performed with pLECs. The irradiation of sample was done at a rate of 1 Gy per min. The specific amount of dose was ensured by controlling the time of X-ray exposure over the samples. Results plotted in Figure 46 show that there is also a dose-dependent increase in the number of DNA double strand break sites at doses below 0.5 Gy.



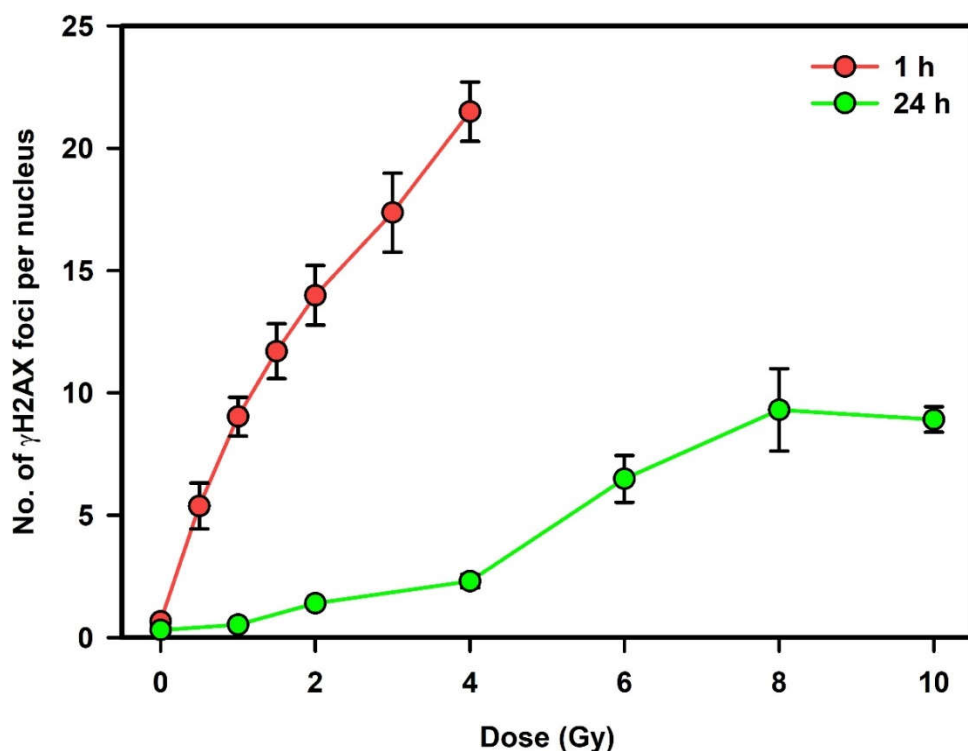


Figure 43: Dose-dependent induction and repair of DNA DSBs in pLECs. Cells irradiated with 0, 0.5, 1, 1.5, 2, 3 and 4 Gy of X-rays and fixed after 1 h. Similarly, cells were irradiated with 0, 1, 2, 4, 6, 8 and 10 Gy and fixed after 24 h to evaluate the repair of DNA DSBs. Bars represent mean foci \pm SEM derived from at least 403 cells.

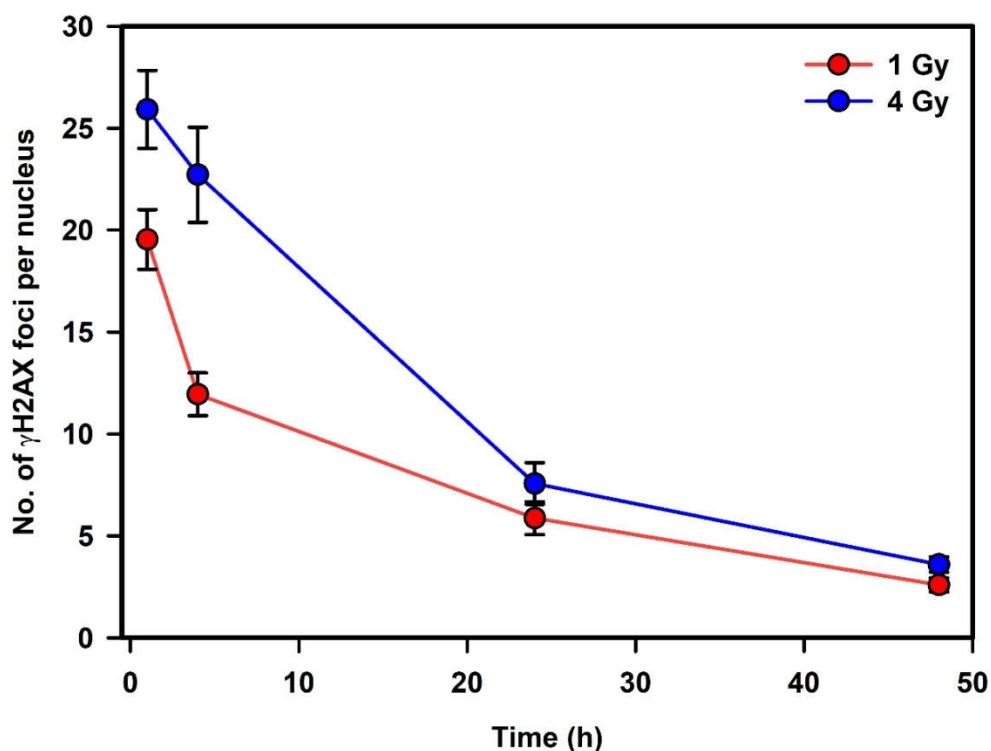


Figure 44: Kinetics of γ H2AX foci disappearance during repair. pLECs irradiated with 1 and 4 Gy were fixed with 3.5 % formaldehyde at different time points. Bars represent mean \pm SEM derived from at least 190 cells.

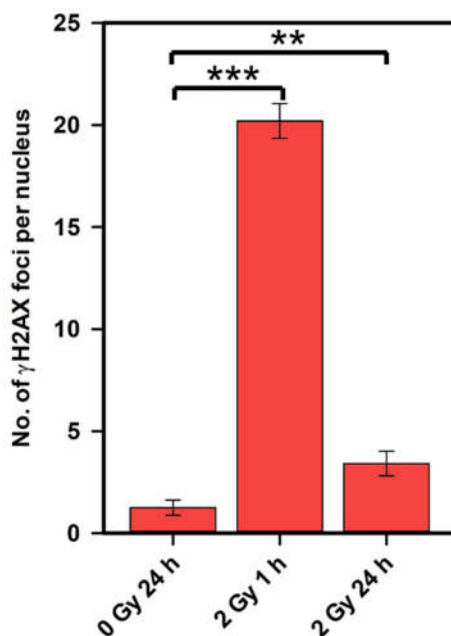


Figure 45: DNA DSBs induction and repair. Cells irradiated with 2 Gy were harvested either at 1 h after X-ray exposure for obtaining a measure of damage induction or after 24 h for obtaining a measure of damage repair. The y-axis gives the average number of foci per nucleus \pm SEM from seven independent experiments and in each experiment at least 173 cells were analyzed. Statistical significance was determined with two-tailed Student's t-tests (*, $p < 0.05$; **, $p < 0.01$; ***, $p < 0.001$).

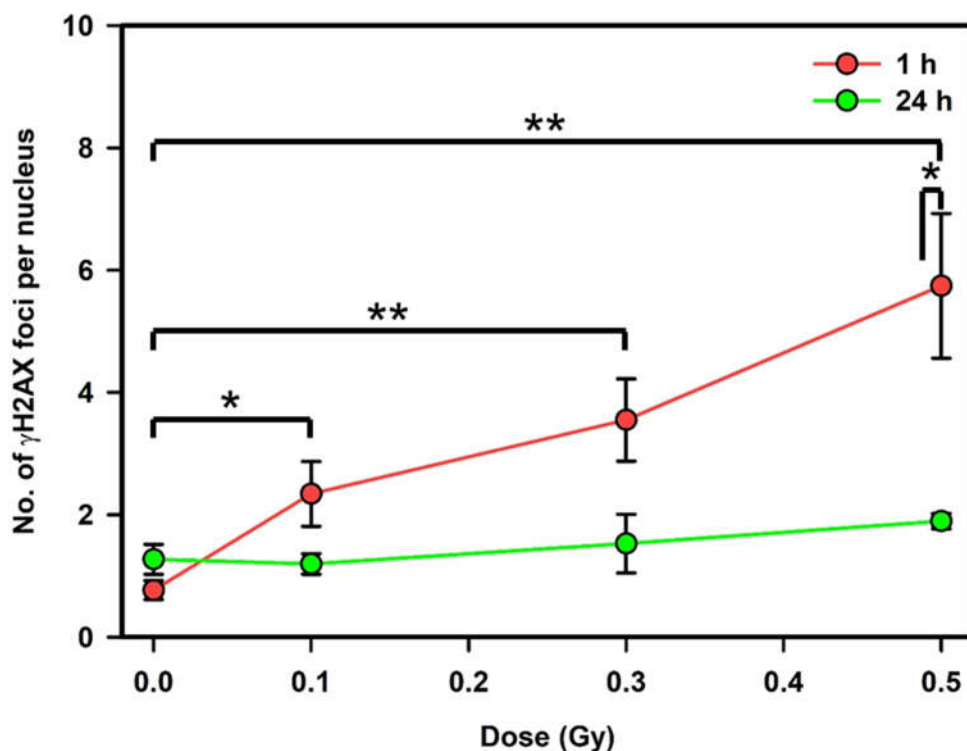


Figure 46: γ H2AX foci formation after exposure to low doses of X-rays. pLECs were irradiated with 0, 0.1, 0.3 and 0.5 Gy and were harvested 1 h after X-ray exposure for damage induction and at 24 h for damage repair. Y-axis gives the average number of foci per nucleus \pm SEM from four independent experiments and in each experiment at least 196 cells were analyzed. Statistical significance was determined with two-tailed Student's t-tests (*, $p < 0.05$; **, $p < 0.01$; ***, $p < 0.001$).

At 0.1 Gy, the average number of foci per nucleus after 1 h was 2.3, which were reduced to 1.2 after 24 h. Similarly, at 0.3 Gy, the average number of foci after 1 h was 3.5, which were later reduced to 1.5 after 24 h. For both 0.1 and 0.3 Gy-exposed samples, the reduction in foci from 1 h to 24 h were not significant. However, the reduction in the average number of foci at 1 h (5.7) to 24 h (1.9) for 0.5 Gy-irradiated samples was statistically significant. Nevertheless, the average numbers of foci for all 0.1, 0.3 and 0.5 Gy-irradiated samples were significantly different compared to the non-irradiated sample at the 1 h time point.

3.6.3 The effect of PIK-related kinases on DNA double strand break repair

DNA DSB induction and repair was also studied under the influence of different inhibitors of key molecules that are involved in the process of DNA damage repair using defined inhibitors (KU55933 is an ATM inhibitor, VE821 is an ATR inhibitor and NU7441 is a DNA-PK inhibitor).

Upon addition of KU55933 (ATM inhibitor), as shown in Figure 47, it was found that the average number of foci per nucleus was comparatively lower than that for controls without inhibitor for irradiated cells. 1 h after exposure to 2 Gy, the average number of foci per nucleus decreased from 21.1 to 12.0, in absence of KU55933 versus presence of KU55933, respectively, and the difference was statistically significant ($p=0.019$). At 24 h, although statistically not significant ($p=0.121$), a noticeable decrease in foci could be seen in cells supplemented with the ATM inhibitor (2.1 foci per nucleus) as compared non-ATM-inhibitors cells (4.6 foci per nucleus).

In contrast to ATM inhibition, ATR inhibition by supplementation of 5 $\mu\text{mol/l}$ VE821 led to slight increase in the number of foci per nucleus as compared to samples not supplemented with the ATR inhibitor (Figure 48). The change in foci number from VE821-absent to -present respectively were 2.2 to 3.9 at 0 Gy after 24 h ($p=0.2$), 21.1 to 23.2 at 2 Gy after 1 h ($p=1$) and 4.6 to 5.3 at 2 Gy after 24 h ($p=0.605$), which were statistically not significant.

Similarly, addition of NU7441 to inhibit DNA-PK also did not show any significant change in foci number compared to NU7441 negative samples (Figure 49). The p -values between NU7441-absent and -present samples at 0 Gy 24 h, 2 Gy 1 h and 2 Gy 24h were 0.390, 0.686 and 0.259 respectively.

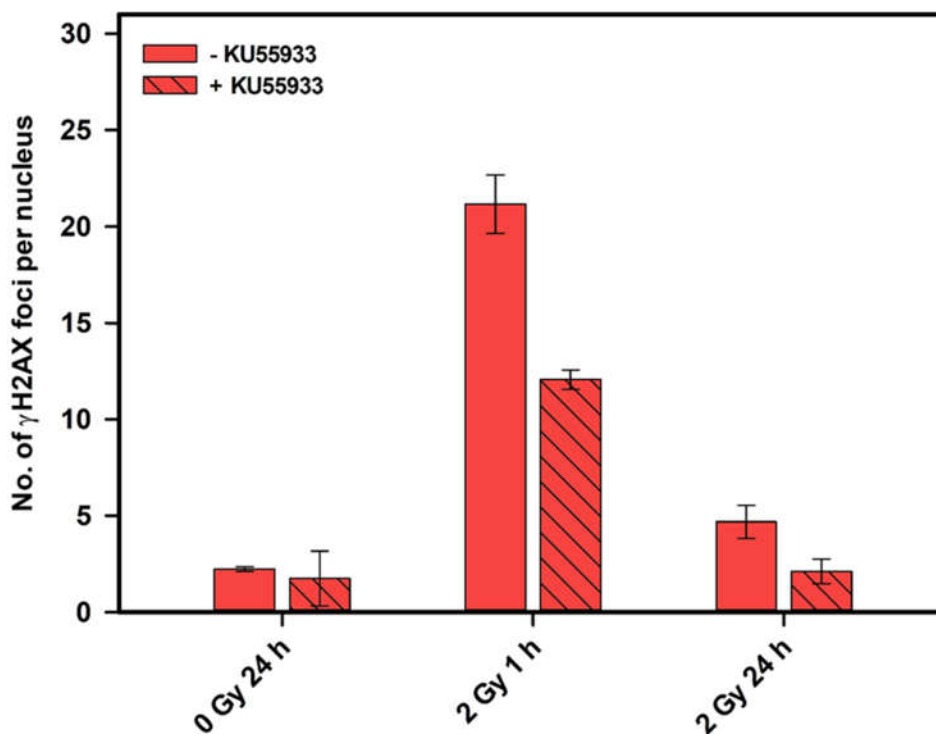


Figure 47: Influence of ATM inhibition on γ H2AX foci formation after X-ray exposure. pLECs irradiated with 2 Gy of X-rays in presence or absence of 10 μ mol/l KU55933 were analysed for γ H2AX 1 h and 24 h after exposure. Y-axis gives the average number of foci per nucleus \pm SEM from 3 independent experiments and in each experiment at least 186 cells were analyzed.

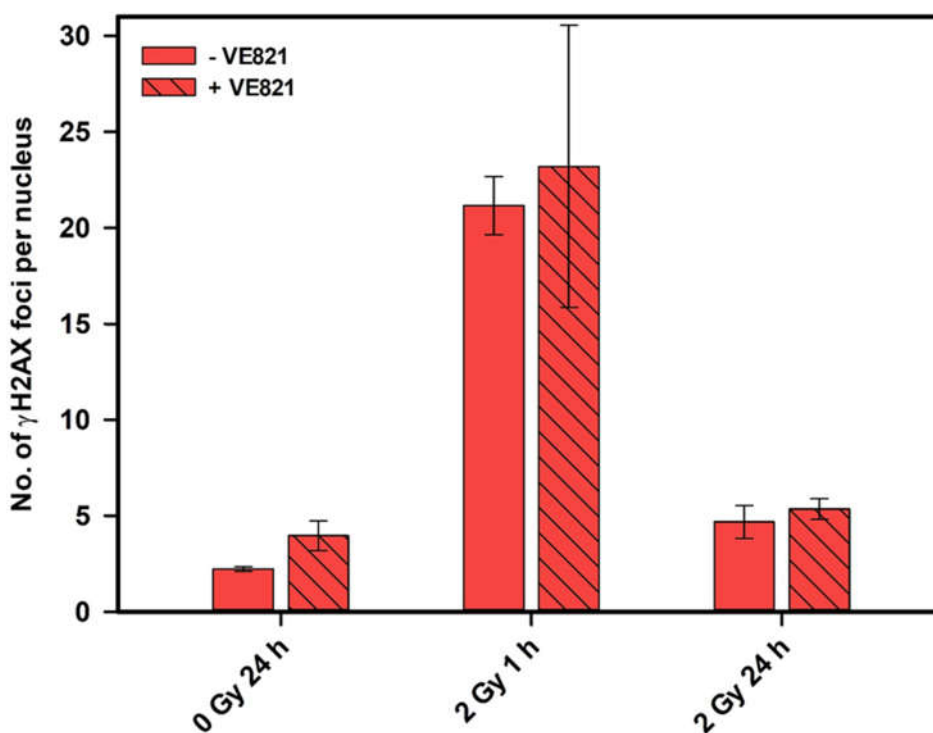


Figure 48: Influence of ATR inhibition on γ H2AX foci formation after X-ray exposure. pLECs irradiated with 2 Gy of X-rays in the presence or absence of 5 μ mol/l VE821 were analysed for γ H2AX 1 h and 24 h after exposure. Y-axis gives the average number of foci per nucleus \pm SEM from 3 independent experiments and in each experiment at least 186 cells were analyzed.

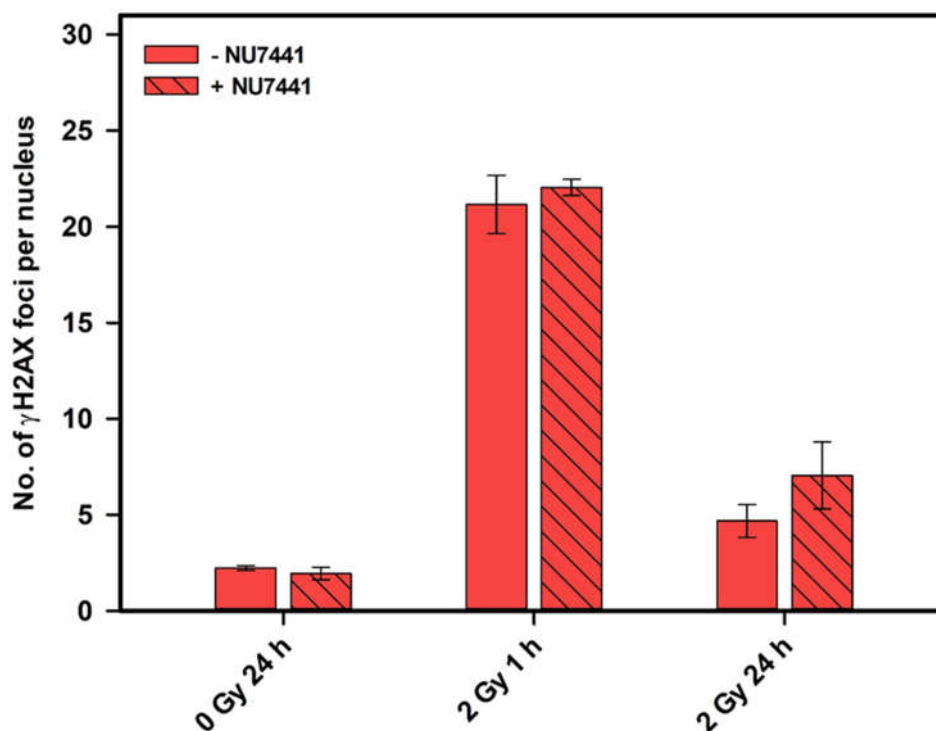


Figure 49: Influence of DNA-PK inhibition on γ H2AX foci formation after X-ray exposure. pLECs irradiated with 2 Gy of X-rays in the presence or absence of 5 μ mol/l NU7441 were analysed for γ H2AX 1 h and 24 h after exposure. Y-axis gives the average number of foci per nucleus \pm SEM from 3 independent experiments and in each experiment at least 186 cells were analyzed.

3.6.4 DNA damage induction and repair after heavy ion exposure

In the cellular system, heavy ions induce complex and higher percentages of damage compared to X-rays and protons due to their higher charge and size. Since such heavy particles are difficult and costly to generate, there are very few studies regarding the role and mechanism of radiation-induced cataract. In this study, two beam times at GANIL with argon and carbon ions were used to study the DNA DSBs induction and repair in pLECs using the gamma H2AX assay.

The exposure of pLECs to argon ions resulted in a dose-dependent increase in the number of foci per cell nucleus (Figure 50). The average numbers of foci were 8.2, 17.1 and 20.9 for 0.5, 1 and 2 Gy, respectively, 1 h after exposure. 24 h after exposure the foci numbers were reduced to 5.3, 7.9 and 5.8, respectively. Statistical analysis with Student's t-tests revealed that the difference in γ H2AX foci induction (1 h samples) between argon ions and X-rays exposed samples were statistically significant for 1 Gy (***, $p < 0.001$) and 2 Gy (**, $p < 0.01$) and statistically insignificant for 0.5 Gy.

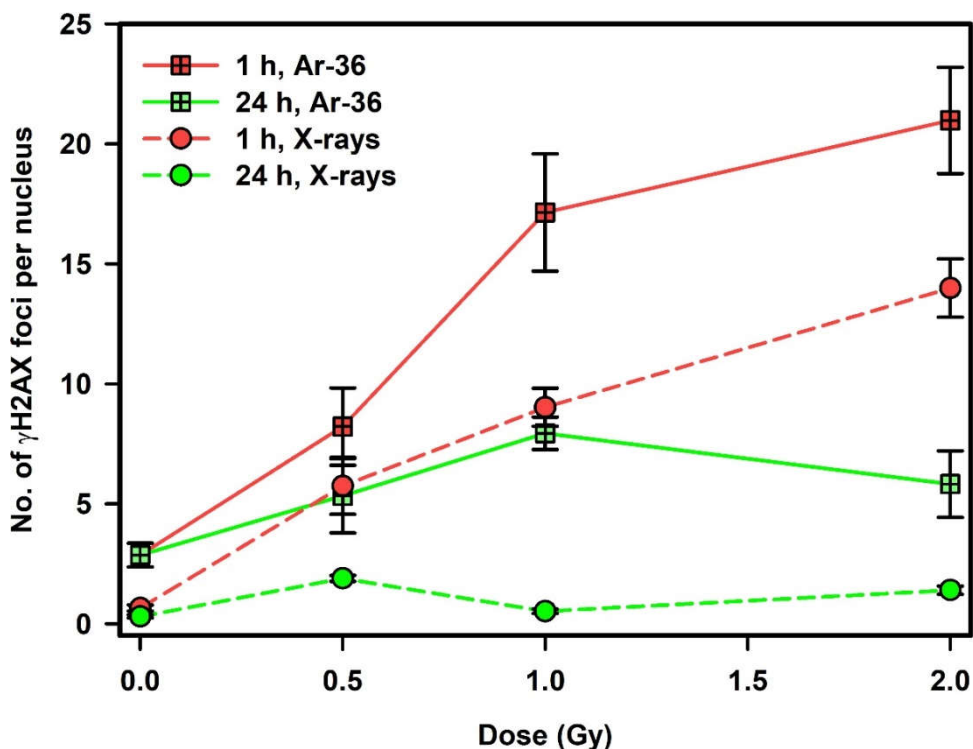


Figure 50: DNA DSBs induction and repair after argon ion (Ar-36, energy on target 84.7 MeV/n, LET 269.4 keV/ μ m) exposure. γ H2AX foci formation was analysed in pLECs exposed to different doses of argon ions. The data are from a single experiment and for each condition at least 255 cells were analysed. Bars represent mean \pm SEM.

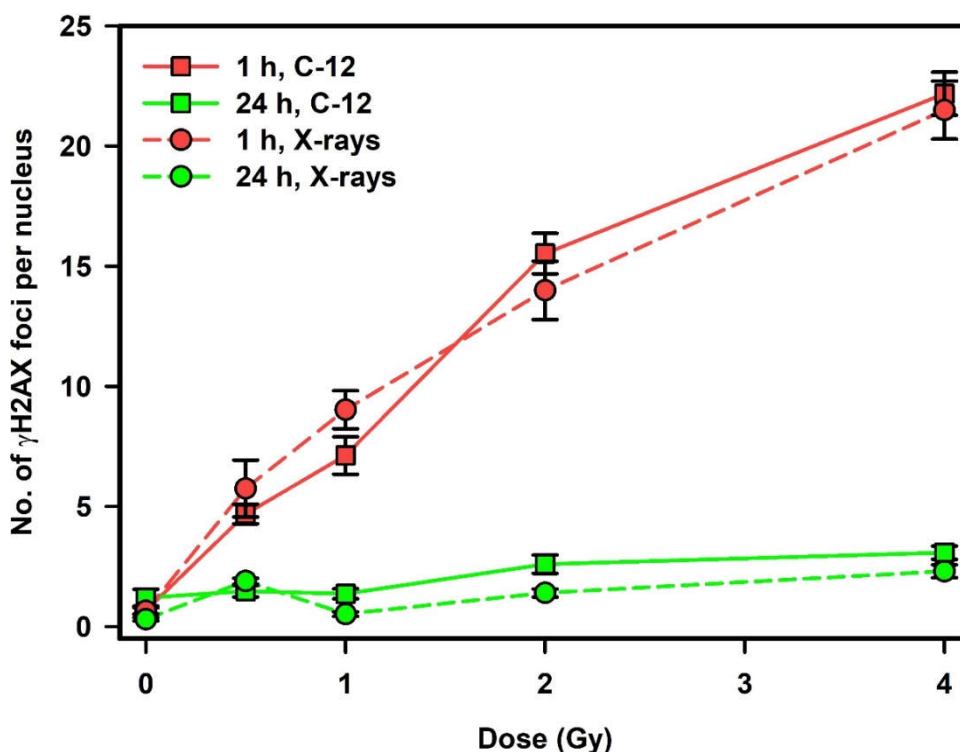


Figure 51: DNA DSBs induction and repair after carbon ion (C-12, energy on target 28.6 MeV/n, LET 71 keV/ μ m) exposure. pLECs exposed to different doses of carbon ions were analysed for γ H2AX foci formation. The data are from a single experiment and for each condition at least 375 cells were analysed. Bar represent mean \pm SEM.

On the other hand, difference in residual γ H2AX foci after 24 h of argon ions and X-rays exposure were statistically significant for all 0.5 Gy (***, $p < 0.001$), 1 Gy (***, $p < 0.001$) and 2 Gy (***, $p < 0.001$).

In carbon ion exposed pLECs (Figure 51), the average number of foci per nucleus was dose-dependent but it was lower in comparison to argon ion-exposed cells. The average number of foci per nucleus for 0.5, 1, 2 and 4 Gy was 4.6, 7.1, 15.5 and 22.1 respectively for 1 h sample and 1.4, 1.3, 2.5 and 3.0, respectively, after 24 h. The difference in γ H2AX foci induction (1 h samples) between carbon ions and X-rays exposed samples were statistically insignificant for all 0.5 Gy, 1 Gy, 2 Gy and 4 Gy.

When comparing the difference in residual γ H2AX foci after 24 h between carbon ions- and X-ray-exposed samples, it was statistically significant for 1 Gy (***, $p < 0.001$) and 2 Gy (**, $p < 0.01$) but for 0.5 Gy and 4 Gy.

To summarize, the average numbers of γ H2AX foci induction (1 h after irradiation) and residual γ H2AX foci (24 h after irradiation) were higher for argon-exposed samples than for carbon-exposed samples. This result hint towards the higher RBE of argon ions compared to carbon ions. The differences in foci number after 1 h of irradiation between argon and carbon were statistically significant for doses 0.5 Gy (*, $p < 0.05$), 1 Gy (***, $p < 0.001$) and 2 Gy (*, $p < 0.05$). Likewise, the differences were statistically significant for samples after 24 h of irradiation for all 0.5 Gy (**, $p < 0.01$), 1 Gy (***, $p < 0.001$) and 2 Gy (**, $p < 0.01$).

3.7 DNA damage response after X-ray exposure in whole organ culture

The analysis on whole lens organ cultures is important as it provides valuable information about DNA DSBs induction and repair at organ level which is more related to the human eye lens. One of the methods to analyse DNA damage was irradiating whole lens to its anterior surface facing upward and then fixing it with formaldehyde. The epithelial layer was isolated to stain for γ H2AX. The images in Figure 52 distinctly show that in the non-irradiated lens, γ H2AX foci are not present. But for lenses that were exposed to 2 Gy of X-rays, DNA DSBs induction was undoubtedly seen 1 h after exposure and the number of those DSBs was reduced after 24 h of repair time. A drawback of this experimental procedure was that the separation and identification of the anterior and the equatorial regions was difficult.

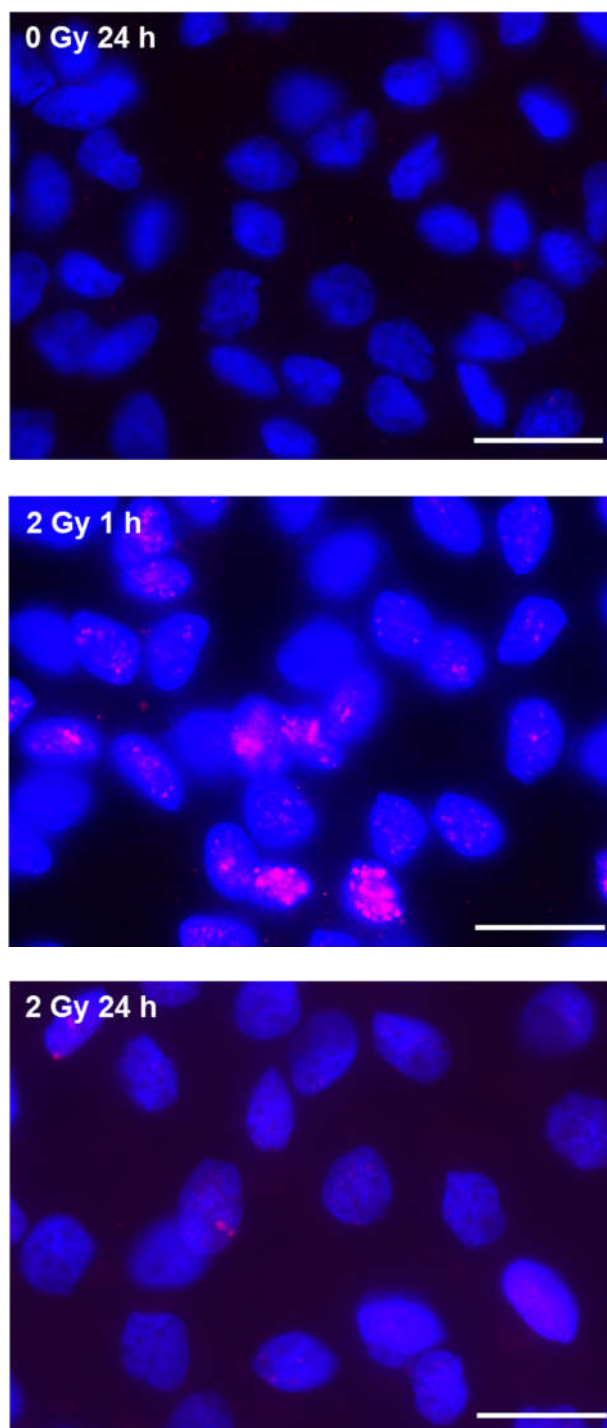


Figure 52: Immunofluorescence staining of γ H2AX in lens epithelial cells in lens epithelial layer after X-ray exposure. Lenses were fixed with 3.5 % formaldehyde 1 h and 24 h after X-ray exposure. The epithelial layers were prepared from the fixed lenses. Fluorescent antibody staining for γ H2AX is given by pink foci; nuclei were stained in blue with DAPI. Scale bar represents 20 μ m.

To enable analysis of different parts of the eye lens, microtome sections of lenses were prepared and stained using the immunofluorescence technique. The advantage of using microtome sections was that both the anterior (containing lens epithelial cells) part and the equatorial part, where differentiation from epithelial cells to fiber cells takes place, could be identified and analyzed. Images in Figure 53 show that in non-irradiated lenses, there were almost no γ H2AX foci in the anterior region whereas cells in the

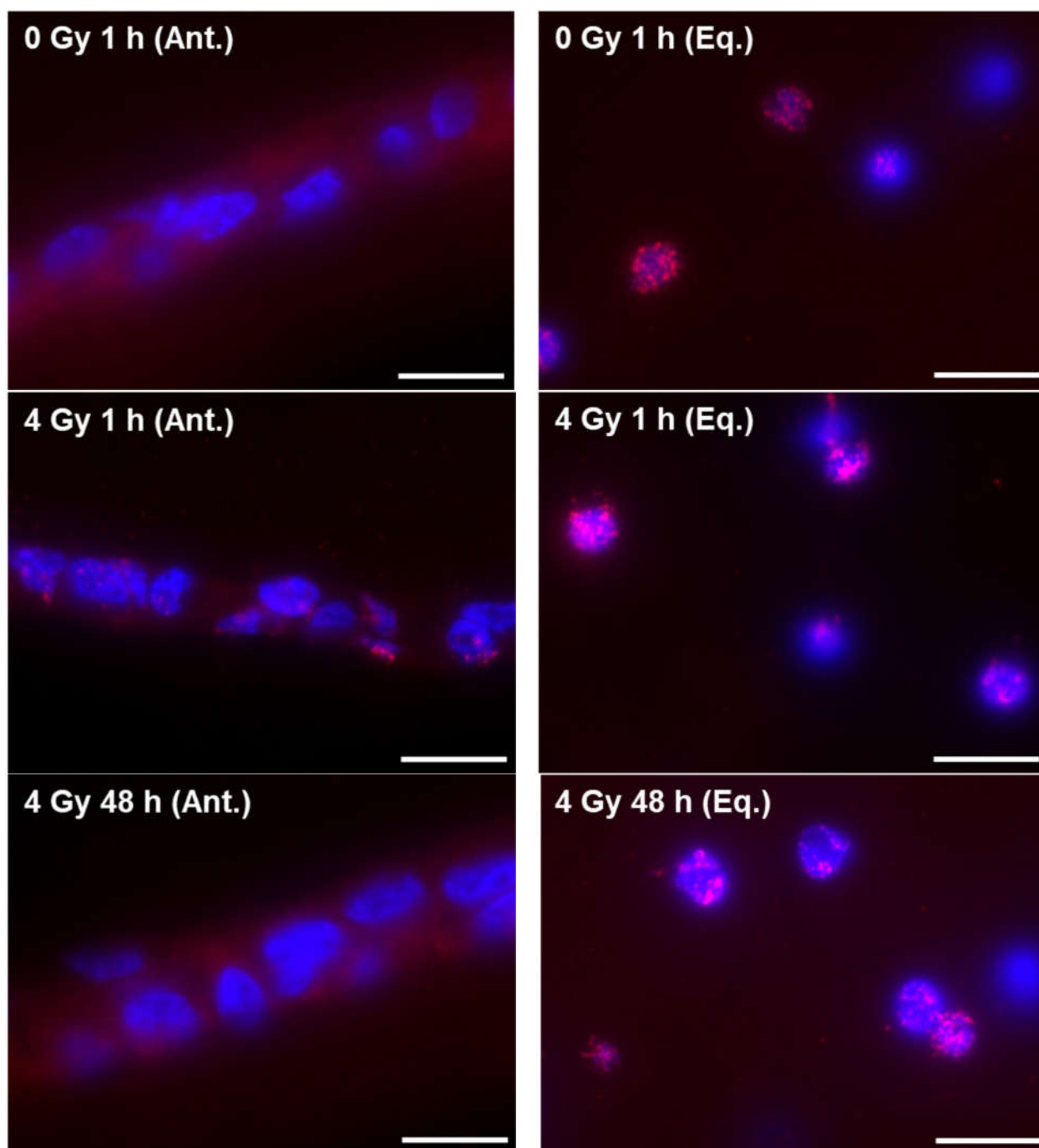


Figure 53: Immunofluorescence staining of γ H2AX in lens epithelial cells in microtome sections of whole porcine lenses after X-ray exposure. Lenses fixed with 3.5 % formaldehyde were used for preparing microtome sections. Fluorescent antibody staining for γ H2AX is given by pink foci; nuclei were stained with DAPI (blue). Scale bar represents 10 μ m.

equatorial region showed γ H2AX foci even without irradiation. After exposure to 4 Gy of X-rays, the cells in the anterior region also presented foci at the 1 h time point which actually were repaired when the lens was incubated for 48 h. For the cells at the equatorial region, the number of γ H2AX foci was slightly increased in the irradiated lenses and appeared unaltered after 48 h incubation.

3.8 Gene expression after exposure of pLECs to different radiation qualities

For survival of pLECs after irradiation, a large number of genes needs to be regulated for survival. In this study, several genes were selected that are involved in DNA repair, cell-cycle progression, cataractogenesis, oxidative stress, growth and survival.

3.8.1 Gene expression after X-ray exposure

Based on their stable expression the three housekeeping genes (HKGs) ACTB, B2M and HPRT were selected as reference genes for assessing the relative expression of the specific chosen genes. The use of multiple HKGs increases the reliability of the results for the chosen genes. However, it has been shown that exposure to ionizing radiation can modulate the expression of even well-established HKGs (Banda et al. 2008, Iyer et al. 2017). In recent years, many experiments have been performed to identify HKGs that are stable after exposure to different doses of ionizing radiation. Only minor fluctuations in the expression of the three selected HKGs were observed, and these changes were not significant (Figure 54). At un-irradiated conditions, the values for n-fold relative expression changes of the genes ACTB, B2M and HPRT are well within the range of -1 to 1. N-fold changes between -2 to 2 were regarded as not significant. The expression of the ACTB gene (n-fold change) decreased dose dependently, but was within $-2/2$. B2M showed some positive regulation with increasing doses of X-rays, but again the values were within $-2/2$. The HPRT gene showed the most stable expression out of three selected HKGs. Next, expression of selected target genes of pLECs were analysed after exposure to different doses of X-radiation.

CDKN1A whose protein product is also known as p21 has an important role in cell cycle regulation (Cazzalini et al. 2010, Bedelbaeva et al. 2010, Karimian et al. 2016). The results show that the expression of the CDKN1A gene depended on both dose and time after X-ray exposure (Figure 55). For all doses, the up-regulation of the gene already started at the 4 h time point with 1.44-fold, 1.49-fold, 1.71-fold and 2.99-fold changes at 1, 4, 8 and 16 Gy, respectively. The up-regulation was lower 12 h after irradiation but again increased at the 24 and 72 h time points for the 4, 8 and 16 Gy-irradiated samples. For 4, 8 and 16 Gy, the up-regulation values were 3.78-fold, 2.10-fold and 3.80-fold at 24 h and 2.32-fold, 2.98-fold and 3.49-fold at 72 h, respectively.

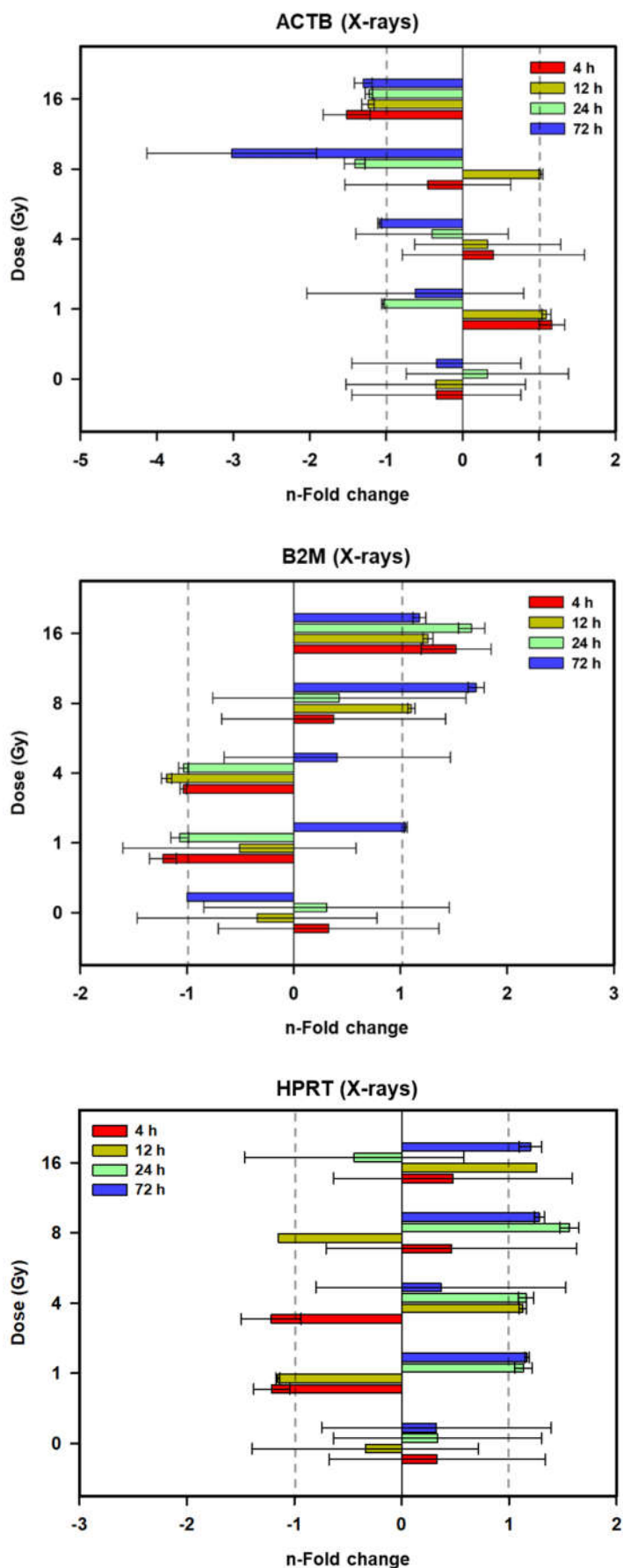


Figure 54: X-ray dependent changes in gene expression of the housekeeping genes ACTB, B2M and HPRT. The housekeepers ACTB, B2M and HPRT are analyzed at 4, 12, 24 and 72 h after exposure to varying dose of X-rays. The data are from three replicates of a single RT-qPCR experiment. The bars represent mean \pm SD.

Growth arrest and DNA damage-inducible gamma (GADD45G) gene transcripts generally increase after growth arrest caused by stress or after treatments with DNA-damaging agents (Ou et al. 2015, Flores and Burnstein 2010, Takekawa and Saito 1998, Ishida et al. 2013). Although the expression changes after X-ray exposure were non-monotonous, a dose dependency was observed at the time point of 4 h after irradiation, reaching a positive 5-fold change at 16 Gy (Figure 56).

CRYAB gene encodes the protein Alpha-crystallin B chain (Jeanpierre et al. 1993), which is a member of the small heat shock protein family and functions as a molecular chaperone (Horwitz 1992, Yamamoto et al. 2014). By binding to beta and gamma crystallins it plays a crucial role in the lens to maintain its transparency and refractive index (Takemoto and Sorensen 2008, Horwitz 2003, Putilina et al. 2003).

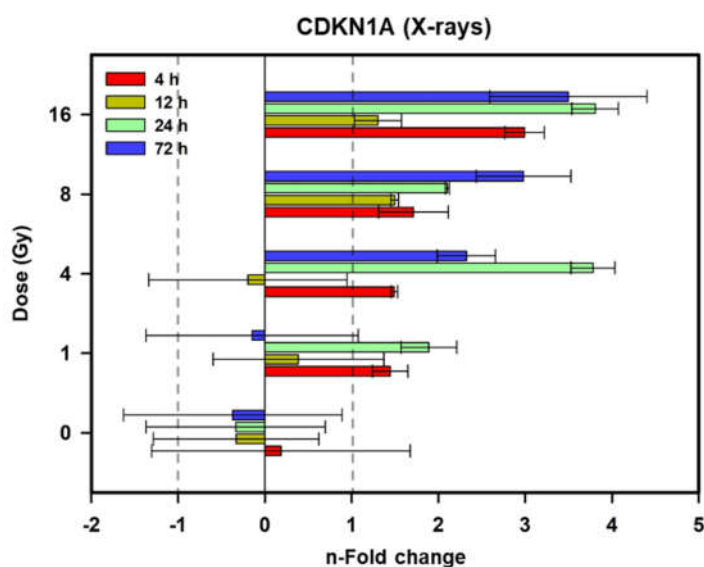


Figure 55: X-ray dependent changes in gene expression of CDKN1A. CDKN1A was analyzed at 4, 12, 24 and 72 h after exposure to varying dose of X-rays. The data are from three replicates of a single RT-qPCR experiment. The bars represent mean \pm SD.

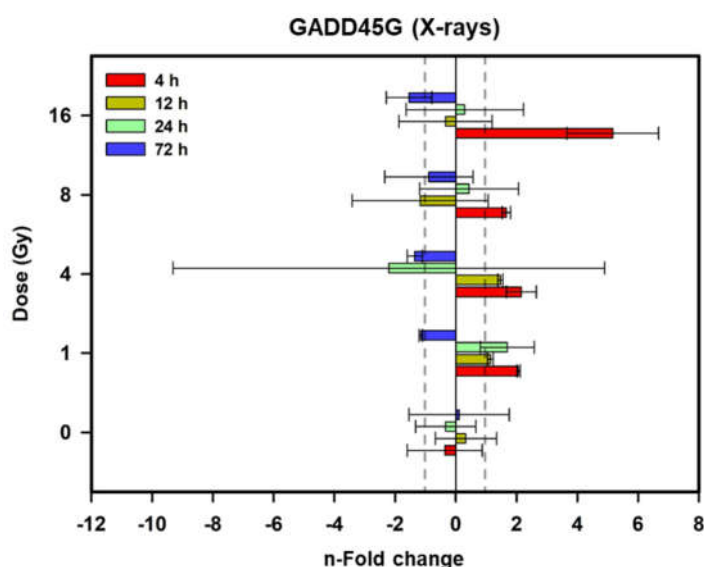


Figure 56: X-ray dependent changes in gene expression of GADD45G. GADD45G was analyzed at 4, 12, 24 and 72 h after exposure to varying dose of X-rays. The data are from three replicates of a single RT-qPCR experiment. The bars represent mean \pm SD.

Exposure to X-rays changed in the gene expression pattern of CRYAB at the later time points of 24 and 72 h after irradiation. The change was below 2-fold for 1 Gy but increased for higher doses (Figure 57) with n-fold changes of 2.11, 2.63 and 2.16 for 4, 8 and 16 Gy, respectively at 24 h time point. Similarly, the up-regulation amounted to 1.23-fold, 2.07-fold and 2.25-fold for 4, 8 and 16 Gy, respectively, 72 h after X-irradiation.

DNASE2 (deoxyribonuclease II) hydrolyses DNA under acidic conditions (Evans and Aguilera 2003). During differentiation from epithelial to fiber cells the cellular organelles along with all DNA content are degraded at the equatorial region of the lens capsule (Nishimoto et al. 2003, Nakahara et al. 2007, Torriglia et al. 1995). This degradation process is crucially required for the transparency of the lens. As depicted in Figure 58, the gene showed similar radiation-induced regulation as the CRYAB gene where the positive up-regulation was dose-dependent and the expression was increased mainly at later time points of 24 and 72 h after irradiation.

Studies have demonstrated that PAX6 is not only required for differentiation of lens epithelial cells to lens fiber cells but also in the development process of the whole eye (Ashery-Padan et al. 2000, Kamachi et al. 2001, Shaham et al. 2009). In pLECs, the gene was up-regulated in a dose- and time-dependent manner after exposure to X-rays compared to un-irradiated samples (Figure 59). In the 1 Gy-exposed sample, there was a 2.59-fold increase at 24 h. In the 4 Gy-irradiated sample, the expression increased 4.33-fold at 72 h. After exposure to 8 and 16 Gy, the expression increased to 2.42-fold and 2.97-fold, respectively, after 24 h. The maximum up-regulation was 6.53-fold and 3.67-fold for 8 and 16 Gy-exposed samples, respectively, at the 72 h time point.

The RELA gene encodes the subunit p65 of the transcription factor NF- κ B. The transcription factor NF- κ B is activated in many biological signal transduction events like cell growth, differentiation, immunity, inflammation, tumorigenesis and apoptosis (Karin 1997, Schreck et al. 1991, Sonenshein 1997, Wu et al. 1996, Chang et al. 1994). Figure 60 shows the RELA gene expression pattern after X-ray exposure of pLECs. Irradiation did not cause coherent changes in the expression pattern of that gene. For all conditions, the n-fold changes were below 2-fold.

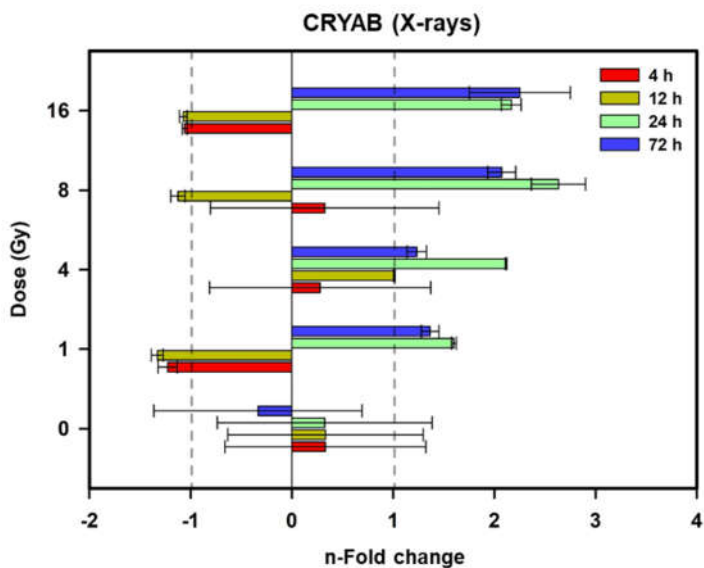


Figure 57: X-ray dependent changes in gene expression of CRYAB. CRYAB was analyzed at 4, 12, 24 and 72 h after exposure to varying dose of X-rays. The data are from three replicates of a single RT-qPCR experiment. The bars represent mean \pm SD.

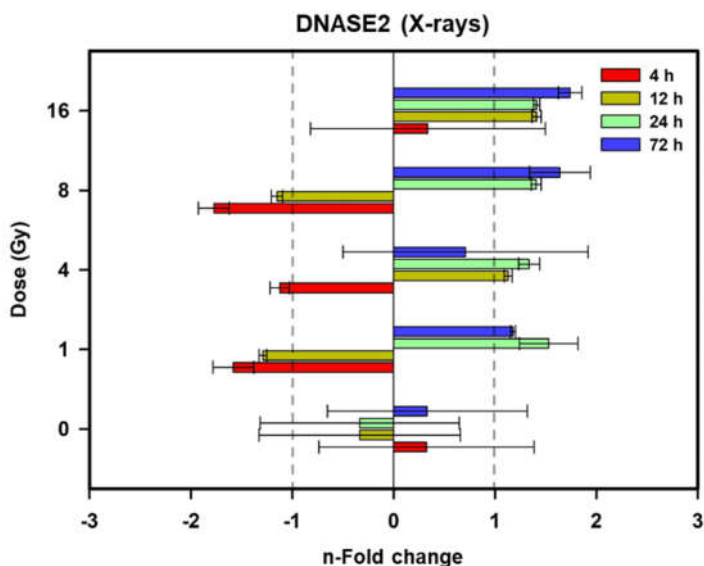


Figure 58: X-ray dependent changes in gene expression of DNASE2. DNASE2 was analyzed at 4, 12, 24 and 72 h after exposure to varying dose of X-rays. The data are from three replicates of a single RT-qPCR experiment. The bars represent mean \pm SD.

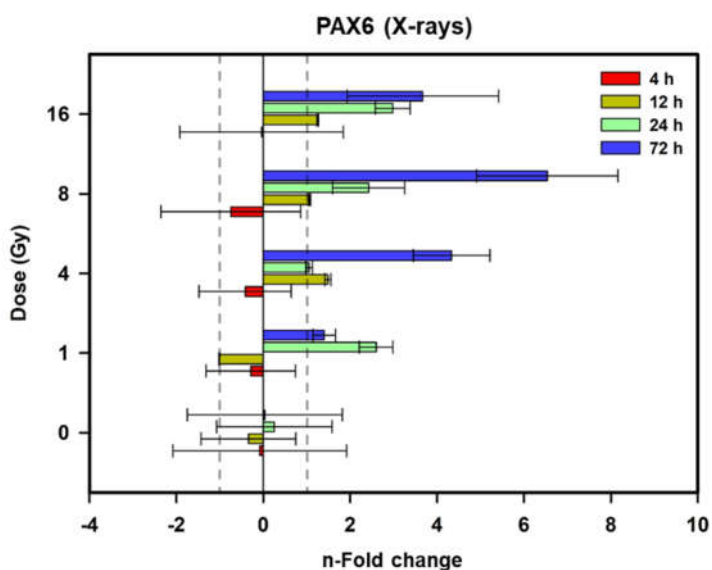


Figure 59: X-ray dependent changes in gene expression of PAX6. PAX6 was analyzed at 4, 12, 24 and 72 h after exposure to varying dose of X-rays. The data are from three replicates of a single RT-qPCR experiment. The bars represent mean \pm SD.

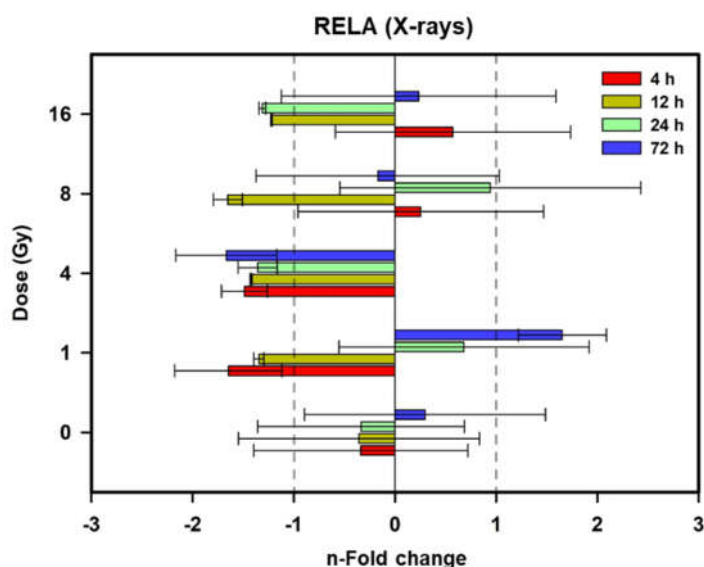


Figure 60: X-ray dependent changes in gene expression of RELA. RelA was analyzed at 4, 12, 24 and 72 h after exposure to varying dose of X-rays. The data are from three replicates of a single RT-qPCR experiment. The bars represent mean \pm SD.

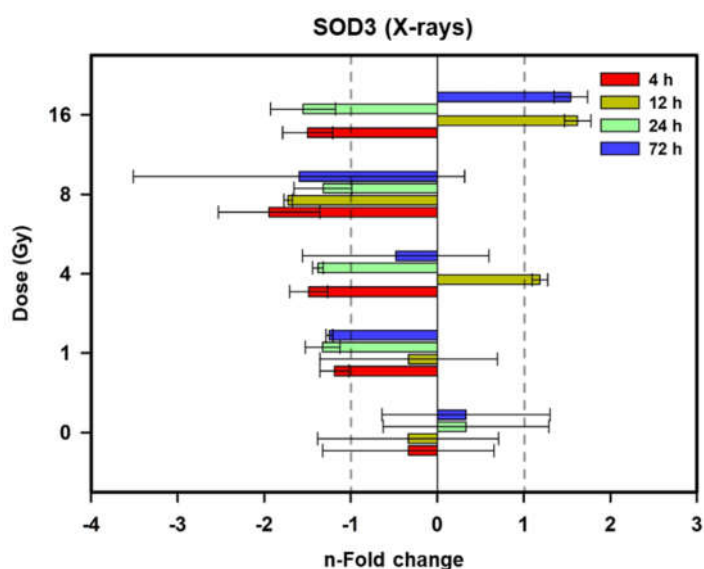


Figure 61: X-ray dependent changes in gene expression of SOD3. SOD3 was analyzed at 4, 12, 24 and 72 h after exposure to varying dose of X-rays. The data are from three replicates of a single RT-qPCR experiment. The bars represent mean \pm SD.

The SOD3 gene encodes a member of the superoxide dismutase protein family (Zelko et al. 2002). This enzyme converts superoxide radicals to oxygen and hydrogen peroxide (Fukai and Ushio-Fukai 2011, Jalilov et al. 2016). In pLECs, the expression of this gene was not significantly affected by X-ray exposure (Figure 61).

3.8.2 Gene expression after heavy ion exposure

To compare the effect of different radiation qualities on gene expression, a parallel experiment with same dose and time points as fore X-ray exposure was performed using heavy ions. Specifically, cells were exposed to carbon ions (C-12) with an energy on target of 28.6 MeV/n, LET 71 keV/ μ m. Again, n-fold expression changes between -2 and 2 was regarded as not significant. First, potential dose-dependent responses of the housekeeping genes ACTB, B2M and HPRT were assessed. Figure 62 shows a more

than 2-fold down-regulation for the ACTB gene after exposure to higher doses of 4, 8 and 16 Gy. On the other hand, B2M and HPRT mostly showed a stable expression within -2 to 2-fold.

CDKN1A gene expression after carbon ion irradiation of pLECs are shown in Figure 63. The up-regulation pattern of the gene was both time- and dose-dependent and was very similar to that after X-irradiation (Figure 55). Here, the up-regulation of the gene started 4 h after irradiation compared to un-irradiated ones. This positive regulation was 2.22-fold, 2.87-fold, 4.23-fold and 3.85-fold for 1, 4, 8 and 16 Gy of C-12, respectively. Thereafter, the up-regulation decreased for the 12 h and 24 h time points and increased again at the later time point of 72 h. The up-regulation of the CDKN1A gene at 72 h was 2.62-fold, 2.76-fold, 3.10-fold and 4.59-fold for 1, 4, 8 and 16 Gy, respectively.

After exposure of pLECs to C-12 ions, the expression of the GADD45G gene was mostly down-regulated (Figure 64). About 13-fold down-regulation was seen at 24 h after 8 Gy of C-12 exposure.

Alpha-crystallin B, which is the product of the CRYAB gene, is required for lens transparency (Takemoto and Sorensen 2008). Unlike in X-ray exposed cells (Figure 57), the expression of the CRYAB gene was mostly unchanged after carbon ion exposure. The up-regulation for most of the irradiation conditions was below 2-fold except for the 4 Gy 24 h sample (4-fold) and for the 8 Gy 12 h sample (more than 2-fold) (Figure 65).

The expression pattern for DNASE2 after C-12 irradiation was non-monotonous and fold changes ranged between -2 and 2 for most conditions. There was more than a 2-fold up-regulation at the 4 h time point at 1 and 4 Gy. On the other hand there was more than 2-fold down-regulation for 16 Gy at 72 h and more than 5-fold down-regulation for 16 Gy at 4 h (Figure 66).

While X-ray exposure resulted in a clear up-regulation of PAX6 gene (Figure 59), the C-12 ion irradiation produced in contrast a down-regulation of this gene (Figure 67). Whereas 1 Gy exposure had no effect, the gene was down-regulated 2.9-fold and 2.3 fold at 4 h and 72 h respectively and 2.2-fold up-regulated at 12 h time point after exposure to 4 Gy. Exposure to 8 Gy caused a down-regulation by 2-fold, 4-fold and 7.8-fold at 4, 12 and 72 h, respectively. Exposure to 16 Gy led to a 4.9-fold up-regulation at the 12 h time point but strikingly to a 23-fold down-regulation at 72 h.

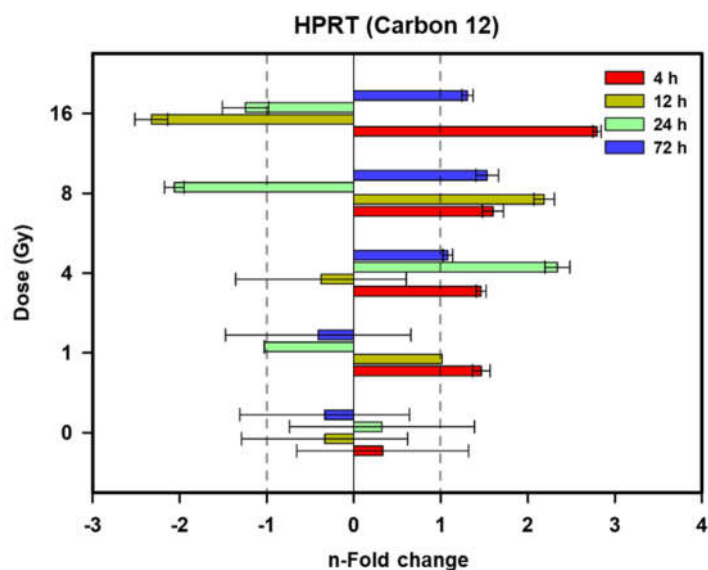
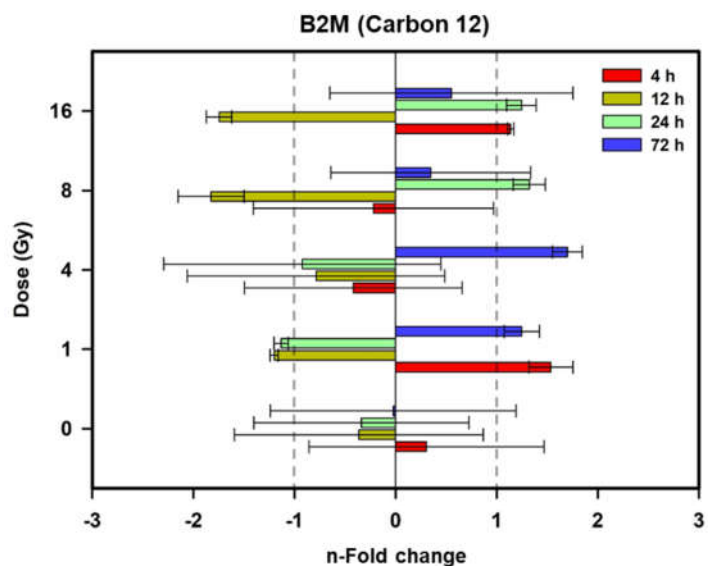
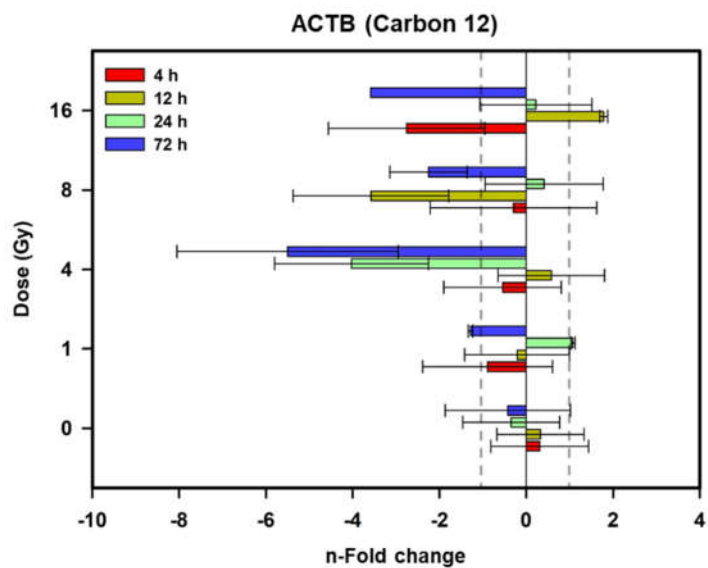


Figure 62: Changes in gene expression of housekeeping genes after exposure to accelerated C ions. ACTB, B2M and HPRT were analyzed at 4, 12, 24 and 72 h after exposure to varying dose of carbon ions. The data are from three replicates of a single RT-qPCR experiment. The bars represent mean \pm SD.

Gene expression of RELA after C-12 ion exposure presented a distinct pattern, which is given in Figure 68. The gene was up-regulated dose-dependently at 4 h after irradiation compared to the un-irradiated one. RELA expression levels were up-regulated 1.79-fold, 2.47-fold, 2-fold and 3.43-fold for 1, 4, 8 and 16 Gy, respectively. At all later time points, expression levels were reduced for all irradiated doses (Figure 68).

The SOD3 gene was down-regulated after exposure to 8 and 16 Gy of C-12 ions (Figure 69). The down-regulation was about 6-fold at 8 Gy and 3-fold at 16 Gy.

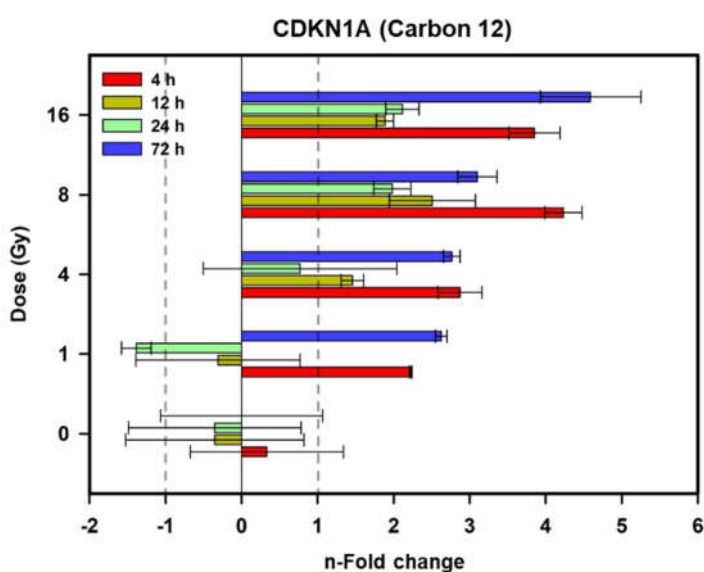


Figure 63: C ion dependent changes in gene expression of CDKN1A. CDKN1A was analyzed at 4, 12, 24 and 72 h after exposure to varying dose of carbon ions. The data are from three replicates of a single RT-qPCR experiment. The bars represent mean \pm SD.

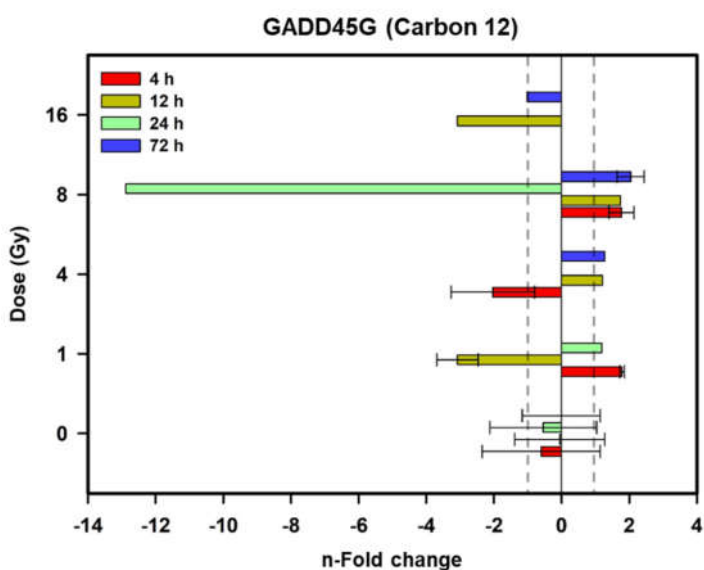


Figure 64: C ion dependent changes in gene expression of GADD45G. GADD45G was analyzed at 4, 12, 24 and 72 h after exposure to varying dose of carbon ions. The data are from three replicates of a single RT-qPCR experiment. The bars represent mean \pm SD.

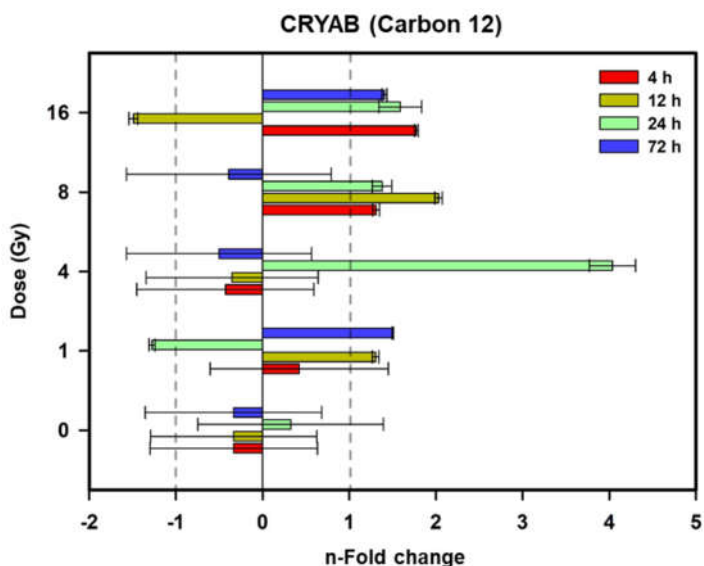


Figure 65: C ion dependent changes in gene expression of CRYAB. CRYAB was analyzed at 4, 12, 24 and 72 h after exposure to varying dose of carbon ions. The data are from three replicates of a single RT-qPCR experiment. The bars represent mean \pm SD.

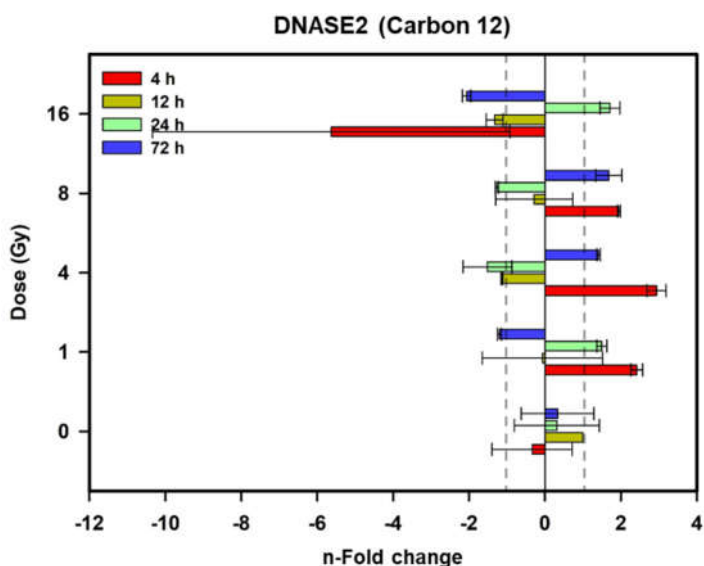


Figure 66: C ion dependent changes in gene expression of DNASE2. DNASE2 was analyzed at 4, 12, 24 and 72 h after exposure to varying dose of carbon ions. The data are from three replicates of a single RT-qPCR experiment. The bars represent mean \pm SD.

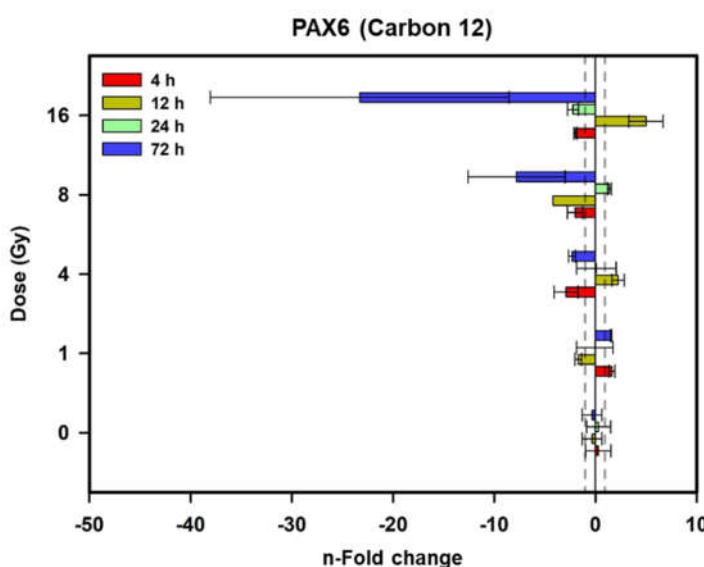


Figure 67: C ion dependent changes in gene expression of PAX6. PAX6 was analyzed at 4, 12, 24 and 72 h after exposure to varying dose of carbon ions. The data are from three replicates of a single RT-qPCR experiment. The bars represent mean \pm SD.

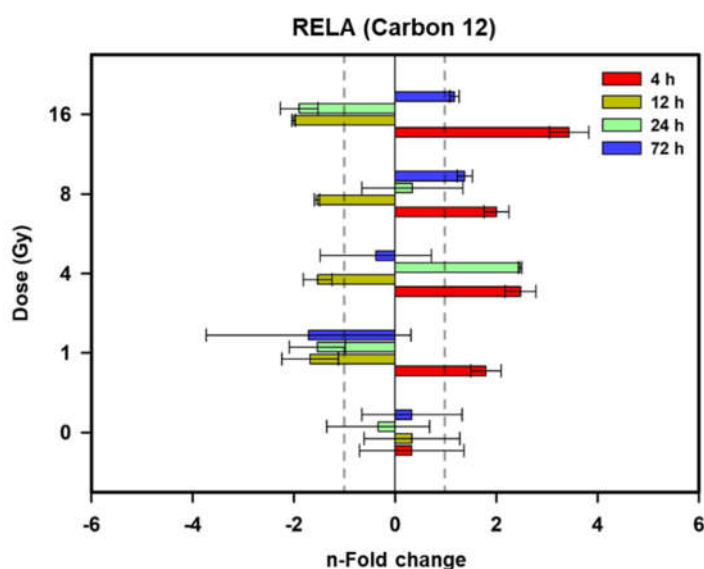


Figure 68: C ion dependent changes in gene expression of RELA. RELA was analyzed at 4, 12, 24 and 72 h after exposure to varying dose of carbon ions. The data are from three replicates of a single RT-qPCR experiment. The bars represent mean \pm SD.

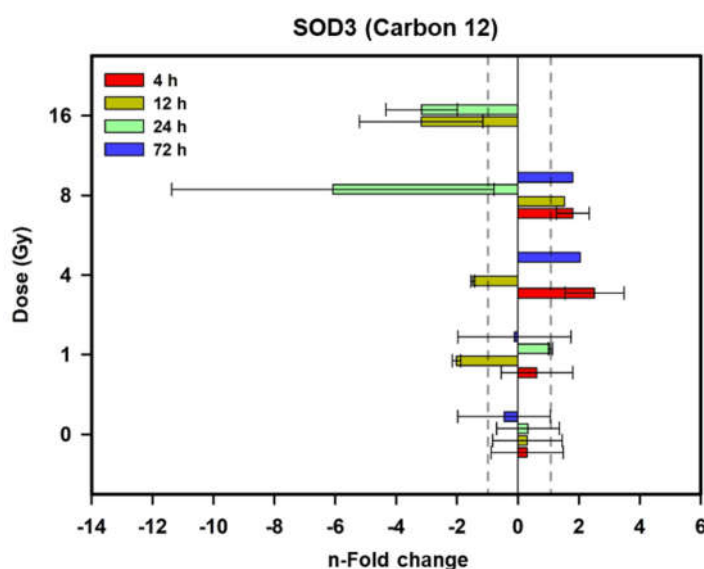


Figure 69: C ion-dependent changes in gene expression of SOD3. SOD3 was analyzed at 4, 12, 24 and 72 h after exposure to varying dose of carbon ions. The data are from three replicates of a single RT-qPCR experiment. The bars represent mean \pm SD.

3.9 Osteogenic differentiation of lens epithelial cells

There are many etiologies of cataract formation. One of the causes of cataract formation is attributed to the calcification of the lens (Werner et al. 2000, Adams 1929, Richardson et al. 1985, Tang et al. 2003, Burge et al. 1937, Balogh et al. 2016). Nonetheless, the exact mechanism for lens calcification has not yet been elucidated. For this reason, it was investigated whether the pLECs also could erroneously differentiate to the osteogenic type by depositing calcium during cell culture. In addition, the expression of selected genes that are involved in osteogenic differentiation was analysed.

3.9.1 Calcium deposition during osteogenic differentiation

Alizarin Red S staining is one of the common and reliable methods to visualize calcium deposition. For this reason, the assay is used to detect osteogenic differentiation. Here, pLECs were incubated with calcification medium (CM) to clarify their differentiation capability, which would allow us to elucidate whether lens calcification contributes to lens opacification (Figure 70).

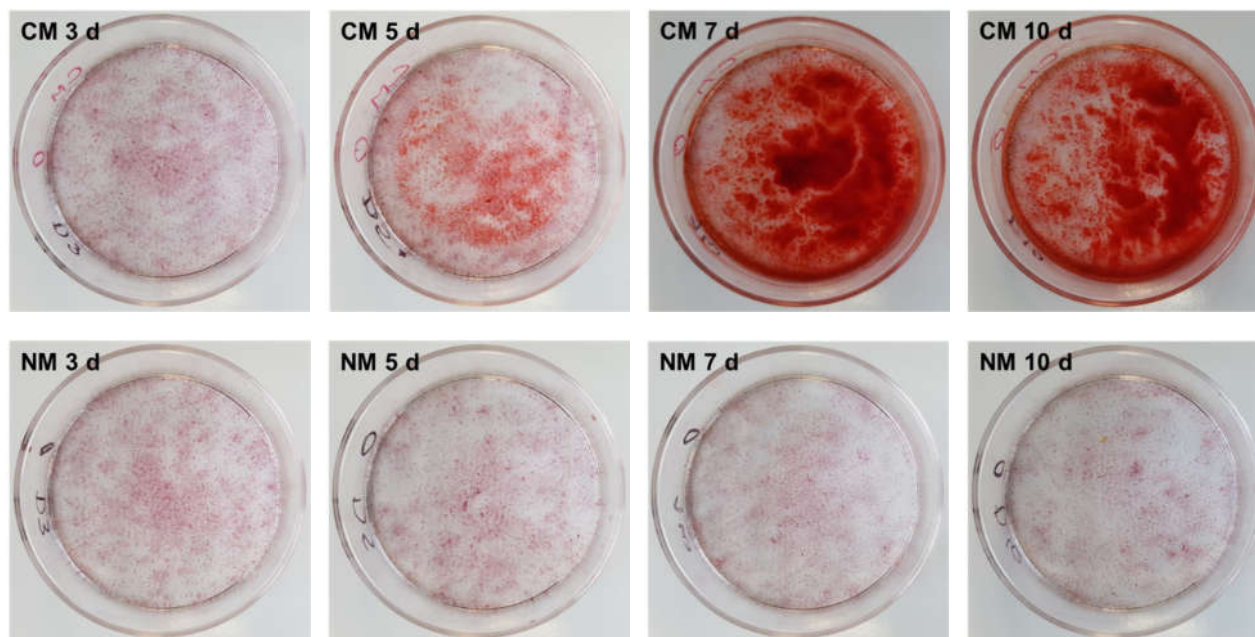


Figure 70: Osteogenic differentiation of pLECs. pLECs were supplied with calcification medium (CM) after a week of growth in normal medium (NM). After 3, 5, 7 and 10 days of CM supplementation, the cells were fixed with 70 % ethanol and stored at -20 °C until all the samples were harvested. Alizarin Red S staining was performed to visualize calcium deposition due to osteogenic differentiation.

The staining showed that no calcium deposition was observed after 3 days of supplementation with CM compared to cells that were incubated with normal medium (NM). From 5 days onwards, however, a red staining became visible in the CM samples. The amount of deposition further increased at days 7 and 10. It should be noted that during the washing step of the staining procedure a lot of deposits were washed away, leading to an under-estimation of the actual amount of deposits. For NM-supplied cells the deposition of calcium was not present at any time points.

3.9.2 Gene expression during differentiation

Differentiation of a cell is characterized by many morphological changes preceded by various genetic up- and down-regulations. Several genes that are related to osteogenic differentiation were selected, which however are not limited to lens epithelial cells only. The two housekeeping genes ACTB and B2M were used as references.

The expression pattern of both housekeeping genes in the presence and absence of calcification medium is given in Figure 71.

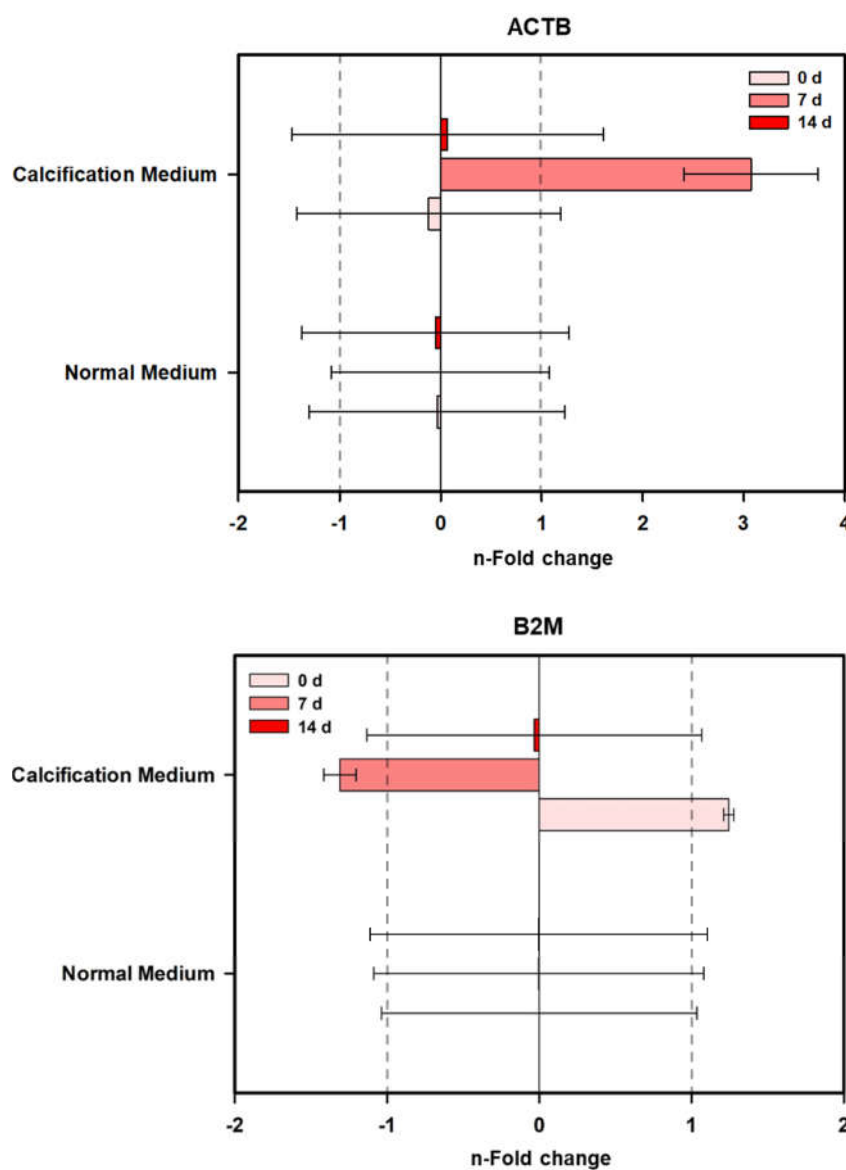


Figure 71: Gene expression changes of the housekeeping genes ACTB and B2M after treatment with calcification medium. Cells were treated with and without calcification medium and analyzed after 0, 7 and 14 d. The data are from two replicates of a single RT-qPCR experiment. The bars represent mean \pm SD.

For both housekeeping genes, no up- or down-regulations were observed with normal medium supplementation at 7 days and 14 days. Supplementation with the calcification medium did not result in many changes in expression of both HKGs. The expression of the ACTB gene was below -1/1 fold except for day 7, where the up-regulation value was 3.07-fold. With regard to B2M, the expression with calcification medium supplementation were well below -2/2 fold at all the time points.

Bone morphogenetic protein 2 (BMP2) has been shown to be required for osteogenic differentiation as well as bone and cartilage development (Liao et al. 2014, Ai et al. 2014, Sun et al. 2015, Rosen 2009, Mukherjee and Rotwein 2009). When the pLECs were compared to own untreated conditions, supplementation of the calcification medium resulted in an overall up-regulation of this gene (Figure 72). Exposure of the cells with CM medium for few minutes only resulted in 1.5-fold up-regulation of the BMP2 gene at day 0. The value of up-regulation further increased with CM supplementation time i.e. to 1.95-fold up-regulation after 7 days and 2.99-fold up-regulation after 14 days.

The Runt-related transcription factor 2 (RUNX2) belongs to a family of transcription factors and plays an essential role in osteoblastic differentiation and skeletal morphogenesis (Komori 2002, Franceschi and Xiao 2003, Yoshida et al. 2002). The gene was up-regulated in CM medium compared to untreated samples (Figure 73). It was 2.10-fold up-regulated on day 0, 1.99-fold at day 7 and 2.62-fold at day 14.

The COL1A2 (Collagen, type 1, alpha 2) gene encodes one of the chains of the type I collagen. These collagens (major component of extracellular matrix) are found mainly in connective tissues and provide an extracellular structure. Upon supplementation of CM, the COL1A2 gene was down-regulated in a time-dependent manner compared to NM (Figure 74). At day 0, the value for n-fold change was 0.7-fold. Over time, the gene was strongly down-regulated with a 6.36-fold change at 1 week and with a 75.36-fold change after 2 weeks.

The n-fold change for the OPN gene with NM amounted to -3.00, -1.17 and -1.51 for 0, 7 and 14 days, respectively. With supplementation of CM these values became -2.88 at 0 days, -33.87 at 7 days and 5.55 at 14 days (Figure 75).

As described earlier, the PAX6 gene is not only required for the differentiation of lens epithelial cells but also for general developmental processes of the eye. With

supplementation of CM, pLECs showed an up-regulation of the PAX6 gene. No up- or down-regulation was observed at day 0. Later, at day 7 and 14, incubation in CM up-regulated PAX6 expression with n-fold changes of 3.69 and 6.65, respectively (Figure 76).

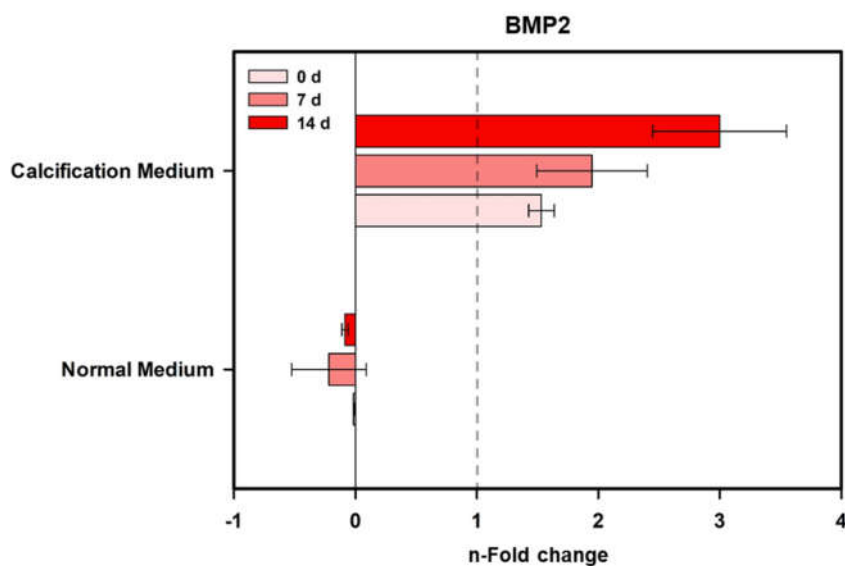


Figure 72: Gene expression changes of BMP2 after treatment with calcification medium. Cells were treated with and without calcification medium and analyzed after 0, 7 and 14 d. The data are from two replicates of two RT-qPCR experiments. The bars represent mean \pm SD.

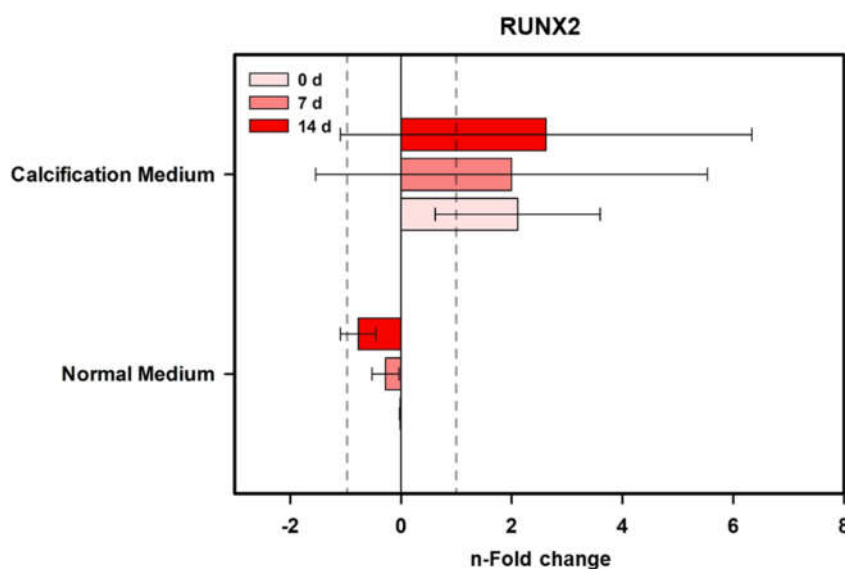


Figure 73: Gene expression changes of RUNX2 after treatment with calcification medium. Cells were treated with and without calcification medium and analyzed after 0, 7 and 14 d. The data are from two replicates of two RT-qPCR experiments. The bars represent mean \pm SD.

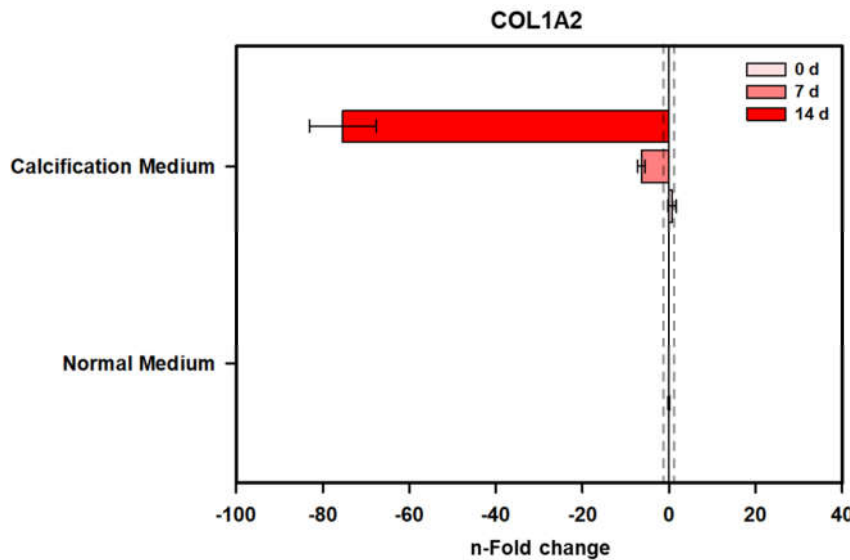


Figure 74: Gene expression changes of COL1A2 after treatment with calcification medium. Cells were treated with and without calcification medium and analyzed after 0, 7 and 14 d. The data are from two replicates of two RT-qPCR experiments. The bars represent mean \pm SD.

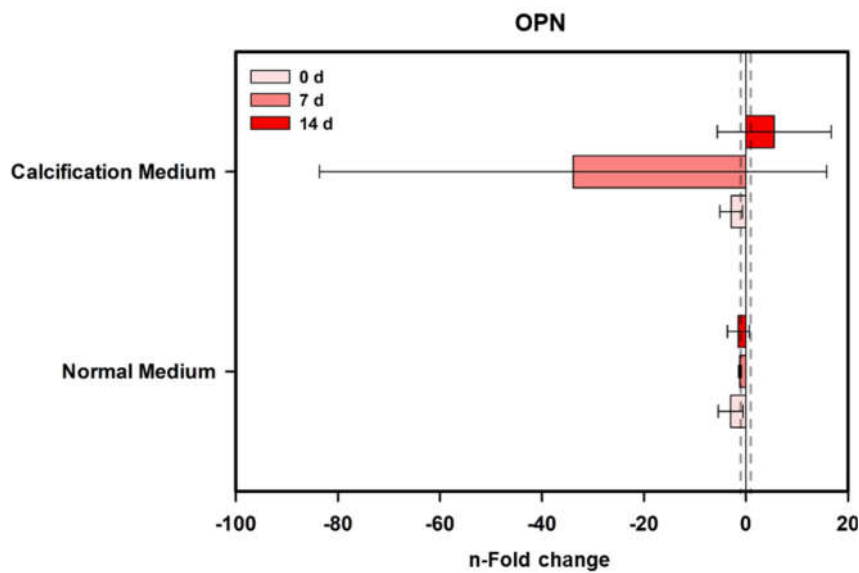


Figure 75: Gene expression changes of OPN after treatment with calcification medium. Cells were treated with and without calcification medium and analyzed after 0, 7 and 14 d. The data are from two replicates of two RT-qPCR experiments. The bars represent mean \pm SD.

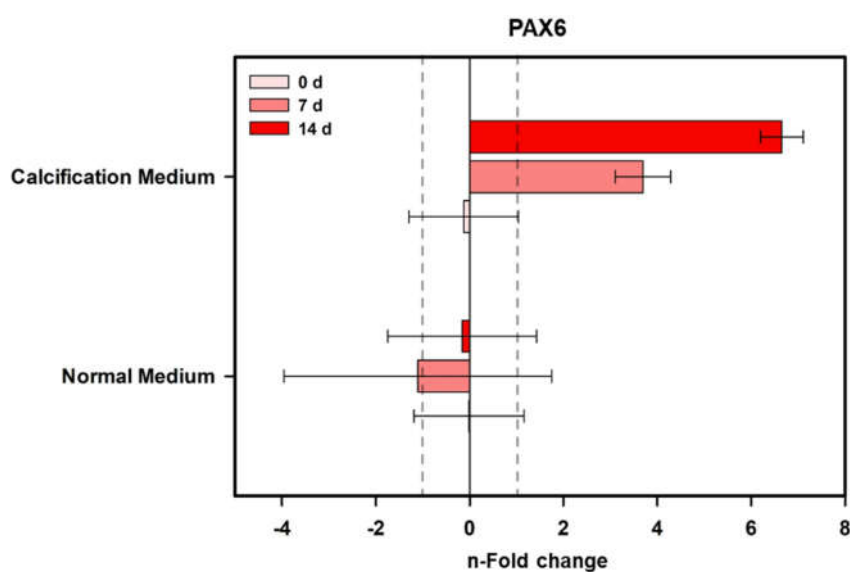


Figure 76: Gene expression changes of PAX6 after treatment with calcification medium. Cells were treated with and without calcification medium and analyzed after 0, 7 and 14 d. The data are from two replicates of two RT-qPCR experiments. The bars represent mean \pm SD.

3.9.3 Influence of X-irradiation on differentiation-related gene expression

The expression patterns of the genes BMP2, COL1A2 and RUNX2 which were analysed in lens osteogenic differentiation, were also analysed after exposure to X-rays. The aim was to investigate if irradiation alone would trigger or affect these genes regarding differentiation process.

The BMP2 gene showed a slight change in expression (Figure 77 **Figure 77: X-ray dependent changes in gene expression of BMP2.**) after exposure to X-rays compared to non-irradiated samples. With the dose of 4 Gy the up-regulation was 1.15-fold and 1.08-fold for 4 and 24 h after irradiation, respectively. Similarly, with 16 Gy, the up-regulation was 1.26-fold at 4 h but at 24 h time this up-regulation increased up to 2.26-fold. The expression of RUNX2 gene was inconclusive in terms of n-fold changes with respect to the doses of X-rays applied as shown in Figure 78. There is an up-regulation of 2.95-fold at 4 h after 4 Gy exposure. Similarly, the gene was 2.43-fold down-regulated at 24 h after 4 Gy exposure and 3.65-fold down-regulated 4 h after 16 Gy exposure. Figure 79 shows the gene expression of the COL1A2 gene after X-irradiation. With 16 Gy of X-rays, there was a slight increase in expression of this gene at both time points but the n-fold change value was below 2. While with 4 Gy of X-rays, the n-fold change value was positive at 4 h and negative at 24 h but surely within $-2/2$.

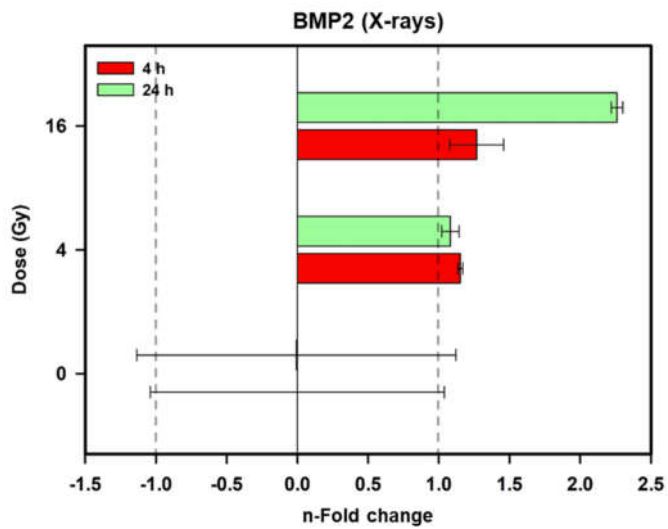


Figure 77: X-ray dependent changes in gene expression of BMP2. The data are from two replicates of a single RT-qPCR experiment. The bars represent mean \pm SD.

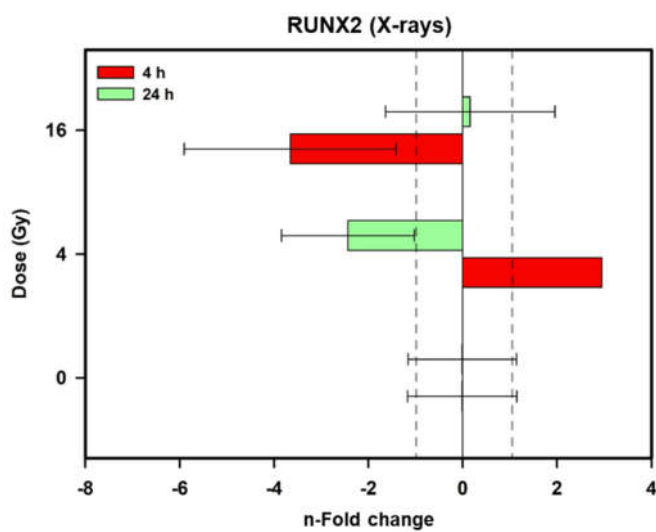


Figure 78: X-ray dependent changes in gene expression of RUNX2 The data are from two replicates of a single RT-qPCR experiment. The bars represent mean \pm SD.

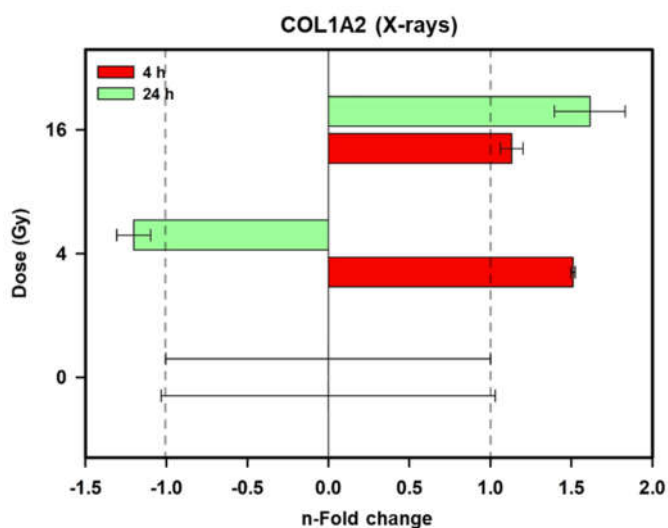


Figure 79: X-ray dependent changes in gene expression of COL1A2. The data are from two replicates of a single RT-qPCR experiment. The bars represent mean \pm SD.

4 DISCUSSION

The eye lens has been recognized as one of the most radiosensitive tissues in the human body. Although numerous epidemiological studies on radiation-induced lens opacifications have been performed (Shore et al. 2010, Cucinotta et al. 2001, Ainsbury et al. 2009, Jacob et al. 2013, Ciraj-Bjelac et al. 2010) the exact mechanism of opacification is still unclear. In long-term space missions, a turbid lens could definitely threaten the mission success, especially, when treatment is not available. Even on earth, the only treatment of lens opacification is surgical removal of lens fibers and lens epithelial cells and implantation of an artificial intraocular lens, which is often followed by reoccurrence of turbidity by proliferation of remaining lens epithelial cells on the surface of the newly implanted lens. Keeping this in mind, it is clear that a non-invasive way to inhibit cataract formation would be an ideal solution to fight against radiation-induced cataract. The focuses of this thesis are the consequences of radiation treatment for lenses and lens epithelial cells, which may contribute to reveal the underlying mechanism of cataract formation. Porcine eye lenses were selected, because unlike human lenses they are easily available. Moreover they provide more similarities to the human lens than lenses of other mammalian animal models, thus resembling an ideal research model.

4.1 Growth properties of porcine lens epithelial cells (pLECs) and whole lens organ culture

Porcine lens epithelial cells were used because they were easily available and provide a non-transformed primary cell model. The use of transformed immortal cell lines accelerates research but such experiments suffer from the genetic instability of the cell systems which may eventually question the reliability of the results. Commonly used human cell lines such as HeLa cells or HEK 293 cells are hypertriploid (76-80 chromosomes) or hypotriploid (64 chromosomes), respectively. A commonly used cell line in lens epithelial cell studies is the human lens epithelial cell line HLE B-3 (Figure 80). It was propagated and immortalized by Andley and colleagues by immortalizing the cells obtained from 5 to 12-month-old patients of retinopathy of prematurity using an adenovirus 12-SV40 virus (Ad12-SV40) (Andley et al. 1994). This cell line was shown to be aneuploid with most of the chromosomes in the tetraploid range. To check whether porcine epithelial cells also show aneuploidies, the chromosome number of porcine lens

epithelial cells was determined. pLECs had exactly 38 chromosomes, meaning 18 pairs of autosomal chromosomes and a pair of allosome (sex) chromosomes (Figure 19) providing thus a genetically stable model for research.

Figure 20 shows the propagation capability of the lens epithelial cells after isolation of cells from the lens capsule. Within the epithelial layer (Figure 20A), the cells were tightly packed with polygonal epithelial appearance. Once the cells start to proliferate on the plastic surface of the culture dish, the cells maintain their polygonal structure mainly when they are close to each other. In other cases, if they have more space to grow they show a slightly longer fibroblastic appearance (Figure 20B). During further passages, the cellular morphology deviated from polygonal to flat and fibroblastic-like (Figure 21). Such change in cell shape could be mostly due to the two-dimensional culture surface, which is completely different from being within the lens. In a petri dish, the cells could grow without contact inhibition and chemical influence. It is well-known that lens epithelial cells proliferate during the whole life and start to differentiate to fiber cells at the equatorial region of the lens (Kuwabara 1975, Remington and Goodwin 2011). These fiber cells are then pushed towards the inner central region of the lens by newly formed fiber cells. During this differentiation process, the fiber cells lose their nucleus and other cell organelles, which is one of main reason for lens transparency. With such a property of the lens, one may predict that lens epithelial cells would tend towards a fibrous shape with increasing number of passaging.

In the proliferation experiment of Blakely and colleagues, the exponential growth phase for the cell line was steep and showed a doubling time of about 24 h for both non-transformed human lens epithelial (HLE) cells and immortalized HLE B-3 cells, where the initial seeding density was 3000 to 4000 cells per cm^2 (Figure 80). Here, pLECs were seeded at a density of 5000 cells per cm^2 , and the exponential growth phase was less steep compared to the HLE cells, in accordance to their slow growth (Figure 80). A reason for differences in growth might be the concentration of serum used in the experiments. In Blakely's experiment, HLE and HLE B-3 were supplemented with 15 % and 20 % FBS (Blakely et al. 2000) while in the experiments of this study only 10 % FBS was used.

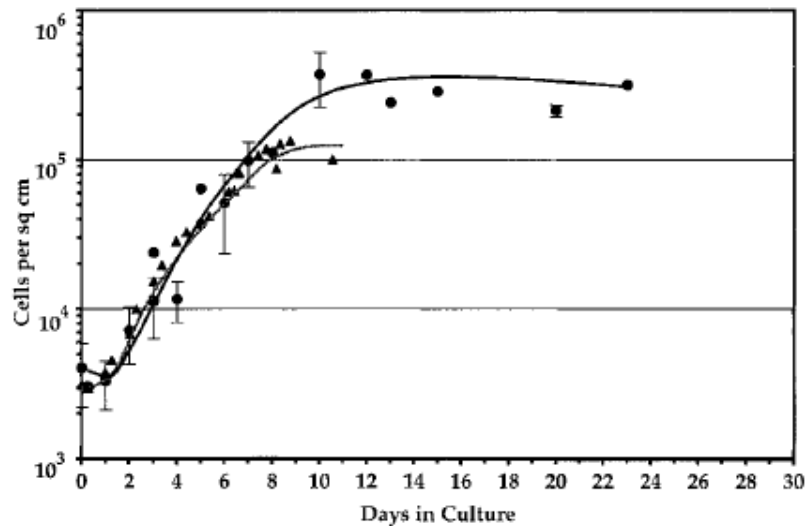


Figure 80: Growth of human epithelial cells in vitro. The growth curves of non-transformed HLE cells (●) and virally transformed HLE B-3 cells (▲). In the exponential phase of both growth curves, a doubling time of approximately 24 h was determined for both cell types. (Adapted from (Blakely et al. 2000))

Many researches have already proven the capability of most of mammalian eye lenses to be cultivated as a whole organ *ex vivo* over a longer period of time (Kleiman et al. 2007, Shirai et al. 2001, Worgul et al. 2002, Tumminia et al. 1994). In this study, it was observed that lenses stayed intact and clear for more than 2 weeks. Nevertheless, it is also evident that the transparency decreased with increasing incubation time in the culture medium (Figure 23). The viability of the lens epithelial cells during organ culture was shown by nuclear staining of live cells with Hoechst solution (Figure 24). To get the reliable results, the experiments with whole lenses were performed within the first week along with visual inspection of lens transparency.

Because it was intended to study pLEC in monolayer culture as well as in organ culture, next to the survival of these cells, it was important to verify that these cells also could divide and proliferate in the different environments. The Click-iT EdU Assay was used to determine pLECs ability of DNA synthesis (section 2.2.13). For the pLECs in epithelial layer cut-offs and in monolayer culture, incubation for 24 h after supplementation of EdU for 2 h revealed more DNA synthesis activity compared to cells which were exposed only to a 2 h pulse of EdU and directly fixed for staining. The longer time of incubation provided the cells with more time for incorporation of EdU, some cells that had incorporated EdU got time into divide to daughter cells with comparatively lower fluorescence (Figure 26 and Figure 27). Interestingly, the EdU incorporation process

was less efficient in pLECs within the lens capsule compared with the monolayer culture. The lower fluorescence of lens epithelial cells might be due to physical unavailability of EdU for the pLECs that were enclosed inside the lens capsule.

4.2 Oxidative stress determination in pLEC monolayer culture

When interacting with biological systems, ionizing radiation can either directly ionize a molecule or indirectly interact with water to produce free radical and other ROS. To cope with such hazards, cells have evolved many defence mechanisms like compartmentalization of vital molecules e.g. DNA, antioxidant enzymes to remove ROS, free radical scavengers like glutathione, repair mechanisms and even self-destruction by apoptosis. In lens epithelial cells, glutathione is the main free radical scavenger and the etiology of the frequently occurring age-related cataract is mainly caused by reduction of glutathione in the lens (Reddy 1990, Truscott 2000, Truscott 2005, Sweeney and Truscott 1998). Oxidative damage in a cell occurs very quickly but may have deleterious effects. This short-lived nature of ROS makes it difficult to study their involvement in cataractogenesis. In an attempt to determine this type of stress in pLECs, the amount of ROS production was quantified by the CellROX[®] Green assay (section 2.2.12). ROS generated by menadione were quantified as a positive control for ROS production after X-ray treatment of pLECs. Treatment of pLECs with increasing concentrations of menadione (generates ROS) resulted in a concentration-dependent increase in ROS indicated by green fluorescence (Figure 30).

As shown in **Figure 31**, the amount of ROS production after X-ray exposure detected by this method was not significantly different compared to the mock-irradiated controls. ROS, which are generated within very short time, quickly oxidises CellROX[®] green reagent in less than a second. Live imaging of ROS generation during irradiation would allow detecting very short-lived ROS. On the other hand, detecting delayed ROS production (Yamashita et al. 2004, Busija et al. 2008) could be performed for cells with longer incubation times. Here, one needs to carefully take into account background fluorescence of non-irradiated and irradiated samples.

4.3 pLEC survival after X-ray exposure

The survival assay is a basic experiment in radiation biology to determine the dose-effect relationship of radiation-induced reproductive cell death. Although many experiments have been carried out on the effects of ionizing radiation on lens epithelial

cells, not many dose-effect curves for these cells were established. Here, two dose-effect curves were produced: 1) when pLECs were irradiated and seeded directly after irradiation i.e. immediate plating, IP; and 2) the cells were incubated for 24 h after irradiation before seeding i.e. late plating, LP. Normally, when radiation-exposed cells are incubated before seeding the width of shoulder, i.e. the n-value, tends to increase showing their ability to repair in the time provided (Frankenberg and Frankenberg-Schwager 1981, Baumstark-Khan et al. 1991).

For pLECs, the D_0 and n-values for IP were 1.42 Gy and 1.82, respectively, and for LP 1.68 Gy and 1.42, respectively (Figure 32). No statistically significant differences of the IP and LP survival curves of pLECs were found. The average D_0 and n were 1.54 Gy and 1.61. This value of D_0 is comparable to the D_0 of human diploid fibroblasts which is 1.28–1.64 Gy (Weichselbaum et al. 1980). Studies of the Cellular Biodiagnostics group at DLR, revealed D_0 and n values of 1.83 Gy and 2.35 for the immortalized cell line OCT-1 (murine osteoblastic cell line) (Lau et al. 2010) and 0.96 Gy and 2.87 for SAOS-2 (human osteosarcoma cell line) (Konda 2013). Primary adipose tissue-derived stem cell (LW24) showed D_0 and n of 0.75 Gy and 1.26 (Konda 2013). These studies show that immortalized cell lines show more recovery potential from the damage and hence better survival apparent from their wider shoulders (higher n-value). On the contrary, the survival curve of the primary cell line LW24 had a smaller shoulder (lower n-value). Thus, the results of the current experiments on pLECs (n = 1.61) showed a recovery potential or shoulder width close to primary human cells but not to immortalized ones indicating that pLECs were more radiosensitive.

Interestingly, in a study on radiation sensitivity of bovine lens epithelial cells, the D_{37} (or D_0) value was found to be 1.38 Gy when the cells were irradiated in the exponential growth phase (Baumstark-Khan et al. 1991). The D_0 -value of 1.54 Gy for pLECs of this study is quite similar to the value from bovine lens epithelial cells. In addition to that, the D_0 -value of pLECs well matches the D_0 -value of primary human lens epithelial cells as well as of primary human lung fibroblast cells with values of 1.55 Gy and 1.40 Gy, respectively (Fujimichi and Hamada 2014).

Table 16: Comparison of radiobiological parameters for different cell types.

| Cell type | Radiobiological parameters | | References |
|------------------------------|----------------------------|------|-----------------------------|
| | D ₀ (Gy) | n | |
| pLECs (primary cells) | | | |
| IP | 1.46 | 1.59 | this study |
| LP | 1.76 | 1.20 | this study |
| Average | 1.54 | 1.61 | this study |
| Immortalized cells | | | |
| OCT-1 | 1.83 | 2.35 | Lau et al., 2010 |
| SAOS-2 | 0.96 | 2.87 | Konda, 2013 |
| Primary cells | | | |
| Human diploid fibroblasts | 1.28-1.64 | - | Weichselbaum et al., 1980 |
| Human lung fibroblasts | 1.40 | - | Fujimichi & Hamada, 2014 |
| Human lens epithelial cells | 1.55 | - | Fujimichi & Hamada, 2014 |
| LW24 | 0.75 | 1.26 | Konda, 2013 |
| Bovine lens epithelial cells | 1.38 | - | Baumstark-Khan et al., 1991 |

4.4 Cell cycle progression after X-ray exposure

It is widely known that many intrinsic and extrinsic factors can cause genetic damage in the cell. Along with the damage, the cells have also evolved different kinds of repair mechanisms. Nevertheless, such cellular repair mechanisms are time-consuming, which is caused by various checkpoints at different phases of the cell cycle. Particularly the G2/M checkpoint plays a central role in dealing with radiation-induced DNA damage. G2/M arrest is attained by phosphorylation of Chk1 by ATM, which in turn phosphorylates Cdc25C the latter inhibiting Cyclin B-Cdk1 activity (Figure 7).

So far, data on cell cycle progression after radiation treatment of lens epithelial cells is scarce. During the exponential growth phase of non-irradiated pLECs, the amount of G1 phase cells increased and the amount of G2/M phase cells decreased with increasing confluency (Figure 33). After X-ray exposure, however, the amount of cells in the G2/M phase increased dose-dependently. Only the cells exposed to lower doses could re-enter the cell cycle whereas the cells exposed to high doses remained arrested in G2/M phase. Similar results were seen with OCT-1 cells. Lau and colleagues showed that in OCT-1 cells almost the total cell population was arrested in G2/M phase at 8 h after irradiation with 7 Gy. There was a reduction of arrested cells after 48 h but not to the same amount as in the non-irradiated control (Lau et al. 2010). Similarly, Hu et al. showed that the amount of cells in the G2/M phase after 10 Gy of X-rays was 62% at 8

h after irradiation, which was reduced after 24 h later but still remained elevated compared to non-irradiated controls (Hu et al. 2014). This immortalized murine cell line either showed a substantial capability to repair, given the repair time by G2/M checkpoint, or the cells entered the cell cycle still carrying damaged DNA. On the contrary, pLECs were not that efficient in repairing damages especially at doses of 4 Gy and 6 Gy and got arrested at G2/M rather than re-entering the cell cycle.

Up to 80 % of the previously mentioned SAOS-2 cells accumulated in the G2/M phase 24 h after exposure to 6 Gy X-rays. This arrest was reduced to around 50 % at 72 h after irradiation (Konda 2013). Similarly, 6 Gy of X-ray exposed LW24 cells resulted in almost 50 % of cells in G2/M phase after 24 h, which did not decrease as it did in cells exposed to lower doses of ionizing radiation. These results suggest that pLECs behave very similar to LW24 primary cells.

The G2/M checkpoint provides cells with critical time for damage repair, which is essential for cellular survival as well as passing healthy genetic material to daughter cells. Extensive studies have been performed to elucidate this G2/M checkpoint pathway and revealed multiple pathways ensuring the G2/M checkpoint for a healthier cellular fate (Carson et al. 2003, Kastan et al. 1992, Yarden et al. 2002, Xu et al. 2002). In general, these pathways are either p53-dependent or p53-independent. Despite the evidence of the involvement of p53 in G2/M arrest, studies have shown that the arrest could also be achieved when p53 was not functional or even absent (Concin et al. 2003). The p53-independent pathway (Figure 7) is activated by phosphorylation of Chk1 and Chk2 by protein kinases ATM and ATR where Chk1 and Chk2 inhibit cdc2 (also called CDK1) by inactivating cdc25 (Taylor and Stark 2001). In the other pathway, p53-dependent G2/M arrest is achieved by inhibiting cdc2, eventually cyclin B1, through transcriptional targets of p53 i.e. Gadd45, p21 and 14-3-3_σ (Taylor and Stark 2001). p53 is well established as a tumor suppressor gene which regulates the cellular response mainly via apoptosis, cell cycle arrest and DNA repair pathway activation. Interestingly, it has been shown that p53 is important in prolonging the duration of G2/M arrest (Hirose et al. 2001). The consistent blockage of our pLECs at G2/M - like LW24 and unlike SAOS-2 (Konda 2013) - could be possibly due to the presence of wild-type p53 in such primary pLEC culture. SAOS-2 actually is a p53-deficient cell line (Masuda et al. 1987, Marcellus et al. 1996). A study performed in α B crystallin knockout mice showed the relation of hyperproliferation of lens epithelial cells due to expression of functionally

impaired p53, which could be a factor promoting immortalization of lens epithelial cells (Bai et al. 2003).

Passaging of primary cells has both advantages as well as disadvantages. Primary cells exhibit a limited lifespan usually due to aging (passaging). Studies show that with increasing passage number of primary cells their behavior and function change (Chennazhy and Krishnan 2005, Wall et al. 2007). Changes in structure and function of cells are continuously going on in living organisms with aging e.g. in stem cells, lens epithelial cells, etc. Immortal cells, which can be used for longer passages with constant morphology, however in many cases have a deregulated cell cycle and DNA repair pathways unlike the primary cells. In addition to that, many studies have shown that even in immortal cell lines the health and proliferation potential declines with increasing passage number (Clynes 2012, Peterson et al. 2004, Kwist et al. 2016) and should not be used after a certain number of passages (von Zglinicki et al. 1995). Passaging experiments on pLECs (**Figure 37**) clearly showed that with increasing passage number their proliferation potential decreased. For this reason, only pLECs in passage 2, 3 or 4 were used in all experiments. Likewise, Wall et al. showed similar results for primary adipose-derived human mesenchymal stem cells where the growth rate of the cells decreased after the 5th passage (Wall et al. 2007). The result obtained in this study is supported by the study made with non-immortalized HLE cells which showed a significantly decreased proliferation potential after passage 10 (Blakely et al. 2000).

Since the results showed a blockade of the G2/M phase of the cell cycle after X-ray exposure, key proteins that are required for DNA damage repair and cell cycle control (ATM, ATR and DNA-PK) were chemically inhibited in a next set of experiments. Unregulated proliferation of lens epithelial cells is hypothesized to be a crucial reason for lens opacification, and cell cycle modulation under the influence of ATM, ATR and DNA-PK inhibition has not yet been performed. Such experiments might open new possibilities for mechanistic investigations of cataractogenesis. The results obtained with pLECs showed an increased G2/M percentage upon ATM inhibition (**Figure 38**) with and without X-rays exposure and a decreased G2/M percentage upon ATR inhibition (**Figure 39**) after X-rays exposure. The results obtained in this study were very closely comparable to the results from the work of Dueva for inhibition of ATM and ATR (Dueva 2016). As for DNA-PK, X-ray-induced inhibition of DNA-PK resulted in a drastic increase of cells in G2 phase which was not the case for pLECs (Dueva 2016). In

pLECs, DNA-PK inhibition had little effect on the X-ray-induced cell cycle arrest (Figure 40). According to previous studies, ATM is the initial kinase that is activated by damage in the G2 phase and causes a downstream activation of Chk2. In spite of its prompt action, ATM is unable to prolong the G2 arrest alone. For the longer suppression of crossing the G2 phase, activation of ATR and subsequent activation of Chk1 (ATR-Chk1) is required (Jazayeri et al. 2006). This downstream activation of ATR is actually a consequence of ATM-Chk2 signalling in response to DSB (Smith et al. 2010). The results also comply with the requirement of ATM for initiation of G2/M block such that repair can take place with further downstream activation of ATR prolonging the arrest. Hence, failure of ATM resulted in the accumulation of cells in the G2/M phase as repair was hindered after X-rays exposure. On the other hand, decrease of G2/M percentage due to ATR inhibition may be due to failure of ATR to block cells at G2/M damage, although the damage was recognized by ATM. Such inability to block cells for repair might follow division and proliferation of cells with unrepaired genetic material and hence be the cause for cataract and cancer. DNA-PK is mainly known for its role in NHEJ and V(D)J recombination in mammalian cells (Burma and Chen 2004, Moshous et al. 2001). In terms of G2 phase checkpoint and HR, DNA-PK is proposed to enable crosstalk between ATM and ATR in the dissociation step of p53-RPA complex by phosphorylation of p53 by ATM and ATR and phosphorylation of RPA32 by DNA-PK (Serrano et al. 2013).

4.5 DNA damage induction and repair after exposure to X-rays

Radiation-induced DNA DSBs are the most relevant lesions leading to genetic instability as well as cell death (Rothkamm and Lobrich 2002, Morgan et al. 1996, Olive 1998). Overcoming of such lethal damage in mammalian cell is well regulated and initiated through phosphorylation of a histone variant, H2AX (Rogakou et al. 1998) at serine 139 within its conserved C-terminal region at the site of a DSB. The phosphorylated form is then called γ H2AX which can be visualized as foci by immunofluorescence using specific antibodies (Rogakou et al. 1998, Paull et al. 2000). The number of γ H2AX foci correlates with the number of DSBs (Sedelnikova et al. 2002). ATM, ATR and DNA-PK, which have a crucial role in cell cycle control, are the main kinases that phosphorylate H2AX (Redon et al. 2002, Stiff et al. 2004, Ward and Chen 2001).

4.5.1 Comparison to foci formation in other cell types

Many studies have been performed to investigate the DNA DSB induction and repair by using the γ H2AX assay in different cell types. Only few results are available for lens epithelial cells. In a well-reproducible experiment (Figure 45), it has been shown that 2 Gy of X-rays induced about 20 γ H2AX foci per cell nucleus within an hour. Those damages were repaired afterwards resulting in \sim 3 foci per cell nucleus at 24 h. The presence of foci in the non-irradiated controls (\sim 1 focus) can be explained by H2AX phosphorylation required for repairing naturally occurring DNA damage. Comparing these results with similar studies, about 36 foci per cell nucleus were counted in murine osteoblasts (transformed cell line) 1 h after exposure to 1 Gy of X-rays and 24 h of incubation resulted in 3 foci per cell nucleus (Lau et al. 2010). In human primary AG01522 fibroblasts, the number of foci 1 h after exposure to 1 Gy and 2 Gy X-rays were 21 and 37, respectively, which then decreased to about 5 foci after 24 h (Mariotti et al. 2013). In both studies, more foci were detected compared with the foci number in pLECs. This variation may be explained by different phosphorylation potentials of selected cell types, organs or tissues (Bannik et al. 2013, Koike et al. 2008). The difference may also slightly vary due to counting criteria of foci used in such experiments. Surprisingly, Rothkamm and Löbrich detected 71 and 7.2 foci in the primary fibroblast cell line MCR-5 after 2 and 0.2 Gy of X-rays, respectively, 3 min post-irradiation, resulting in an average of 35 DSBs per Gy (Rothkamm and Löbrich 2003).

In conclusion, one has to be cautious when comparing foci formation between different cell types may. Similarly, counting foci at different times post irradiation also affects the number of foci formed. Therefore both factors need to be taken into account while performing the γ H2AX assay.

4.5.2 Comparison to foci formation in lens epithelial cells from other species

Considering the studies on induction and repair of DSBs using the γ H2AX assay in lens epithelial cells, lens epithelial cells from C57BL/6J mice showed a dose-dependent induction of DSB foci 1 h after γ -irradiation with ^{137}Cs -source at a dose rate of 0.5 Gy/min (Bannik et al. 2013). The number of foci were about 4, 7 and 17 for doses of 0.25, 0.5 and 1 Gy, respectively. The foci number decreased 24 h after irradiation. In that study, the sensitivity of lens epithelial cells was actually 3 times higher compared to lymphocytes for low doses of <0.5 Gy. In the present study, pLECs also showed dose-

dependent increase in DSBs formation as expected. The foci numbers were similar to those found by Bannik and colleagues (Bannik et al. 2013). The foci numbers were 5.3 and 11.7 per cell nucleus at 0.5 and 1 Gy, respectively, 1 h after X-ray exposure (Figure 43). The number of foci per cell nucleus increased up to 20 at 4 Gy. With 24 h time provided to pLECs after X-rays exposure, the DNA DSBs repair reduced the number of γ H2AX foci. Higher doses of X-rays resulted in more breaks that remained unrepaired which were displayed by dose-dependent remaining foci after 24 h (Figure 43, Figure 44).

4.5.3 Obstacles in foci quantification

One of the important aspects that should be noticed during γ H2AX foci analysis is the size of the foci. The remaining foci after 24 h post-irradiation (Figure 42) were larger than the foci observed 1 h after irradiation (Figure 41). Studies have shown that foci that form after radiation exposure fully develop after 1 h and only few unrepaired damage sites remain as larger foci even after 24 h of incubation (Lau et al. 2010). One concerning factor in γ H2AX foci analysis has always been the size and intensity of the foci. Researchers have developed particular software for foci counting (Böcker and Iliakis 2006, Ivashkevich et al. 2011) but setting the size limit to eliminate the background is still subjective and the discrimination of overlapping of foci especially at earlier time points following damage induction remains difficult. The challenge of correctly counting overlapping foci is also complicated in this study. With higher doses, the number of overlapping foci increased. Elimination of background was performed by the investigator using the non-irradiated sample as control. One should also keep in mind that depending on the cell type and proliferative state of cells, the number of spontaneous foci in a non-irradiated sample varies. One good way of overcoming the problem of background foci was defining background foci number from different cell types of several passage levels (Rothkamm and Löbrich 2003). Nevertheless, foci from irradiated or non-irradiated samples were counted only in one plane. The foci above and below the plane have very high probability to be missed as they are completely outside of the plane or their size is below the threshold. This is one of big hurdles for both manual foci counters as well as for the software. The solution is definitely 3D imaging and foci counting-system.

4.5.4 Relevance for the threshold dose of radiation-induced cataractogenesis

In ICRP publication 118, the acute dose threshold for lens opacities or cataract was set to 0.5 Sv (Clement 2012) which was concluded from several studies. Based on studies from atomic bomb survivors (Nakashima et al. 2006, Neriishi et al. 2007) the acute threshold dose for cataract was estimated to be 0.1-0.7 Gy with 90-95 % confidence interval (CI) including 0 Gy. Similarly, the threshold for protracted exposure was estimated between 0.34 and 0.50 Gy with CI 95 % at 0.17-0.69 Gy (Worgul et al. 2007). In another study, a dose-threshold estimation of 0.4 Gy was reported with 95 % CI at 0-0.8 Gy (Blakely et al. 2010). Although ICRP-118 classifies cataracts as a deterministic effect of radiation with a dose threshold, recent studies suggest that it is a stochastic late effect that lacks a threshold. The hypothetical zero threshold for cataract formation is supported by the study performed by Di Paola and colleagues where lens opacities were studied after exposure to X-rays (0-3 Gy) and neutrons (0-0.38 Gy) (Di Paola et al. 1978). Similarly, early development of cataract in ATM, RAD9 and/or BRCA1 heterozygous mice compared to wild-type also backs the suggested stochastic nature of cataract formation (Worgul et al. 2002, Kleiman et al. 2007). There is also the possibility that such cataract formation may be an outcome of low dose radiation exposure (< 0.5 Gy). Only few researches have explored the effects of low dose radiation on lens epithelial cells; therefore in this study the formation of DSBs corresponding to γ H2AX foci with exposure of 0.1, 0.3 and 0.5 Gy was evaluated. A significant increase in the foci number after X-rays exposure was seen compared to non-irradiated controls (Figure 46). The formation of foci after 0.3 Gy X-irradiation in pLECs in this thesis is similar to the number of ~4 foci/nucleus in lens epithelial cells of C57BL/6J mice 1 h after 0.25 Gy γ -rays exposure (Bannik et al. 2013). Because of the specific sensitivity of lens epithelial cells towards low dose, the risk of radiation-induced cataractogenesis should be kept in mind both, for space travel or terrestrial radiation exposures.

4.5.5 DNA damage and repair in the porcine eye lens

It is evident that when examining the damage of ionizing radiation, the use of whole porcine lenses would give more relevant results compared to the monolayer culture of pLECs in cell culture dishes. While irradiating whole lenses with 2 Gy of X-rays, the number of distinct foci after 1 h was reduced due to repair after 24 h (Figure 52) just like in monolayer culture (Figure 45). Although γ H2AX foci were present, it was difficult to quantify them due to their blurred appearance that might have been due to the presence

of some fiber cells that could not be completely removed while preparing epithelial layers from the formaldehyde-fixed lens. At this point, one might also argue about the mixing of fiber cells during generation of pLEC from the lens. However, there is not much of concern because fiber cells do not contain a nucleus and other organelles that could interfere with the γ H2AX assay.

Lens epithelial cells divide and differentiate into fiber cells at the equatorial region (Remington and Goodwin 2011). Therefore, this region would be more vulnerable to DNA damage induced by ionizing radiation, which could lead to radiation cataractogenesis. The analysis of γ H2AX foci in microtome sections of the porcine eye lens (Figure 53) revealed that epithelial cells at the anterior region are less sensitive than the cells at the equatorial region. The increased incidence of foci indicating the site of damaged DNA at the equatorial region even 48 h after irradiation supports the higher radiation sensitivity of lens epithelial cells in this region. Markiewicz and colleagues obtained similar results by demonstrating formation of γ H2AX foci at peripheral (equatorial) and central (anterior) regions of the lens after exposure of mice to 20 and 100 mGy of X-rays (Markiewicz et al. 2015). Interestingly, their result showed the repair of damage after 3 and 24 h in the central region. On the other hand, the damage in the equatorial region (where lens epithelial cells differentiate to fiber cells) was not resolved after 3 h but only after 24 h. This indicates increased radio-sensitivity of the lens at the equatorial region.

4.5.6 Involvement of kinases in γ H2AX phosphorylation

In the study by (Stiff et al. 2004) it was shown that both ATM and DNA-PK redundantly and non-competitively phosphorylate H2AX. The foci formation in ATM-deficient MEFs was lower compared to control and DNA-PK-deficient MEFs. Addition of a DNA-PK inhibitor to ATM deficient MEFs led to ablation of γ H2AX foci formation showing the requirement of both kinases for phosphorylation of H2AX. In addition, the dominant role of ATM in H2AX phosphorylation was verified by slower kinetics of γ H2AX induction in ATM-deficient human and mouse cells. In another study, it has been shown that phosphorylation of H2AX by ATR is due to its response to DNA replication block rather than DSB recognition and/or repair (Ward and Chen 2001). The above-mentioned studies are in good agreement with the results obtained in this thesis. The decreased amount of γ H2AX foci in Figure 47 due to ATM inhibition could be explained by the

dominating role of ATM in H2AX phosphorylation due to radiation-induced DSB recognition. Not surprisingly, the number of foci in irradiated pLECs was slightly increased when ATR and DNA-PK were inhibited (Figure 48 and Figure 49) compared to control as well as ATM inhibition alone. Plausible reasons for such an increase are the formation of foci due to phosphorylation by ATM and that some foci did not disappear because of the impairment in repair by ATR and DNA-PK inhibition.

4.5.7 Relevance for space missions

During long-term space missions, cataract-free eyes are critical for the astronauts and mission success. It has been suggested that even relatively low doses of space radiation cause increased and early appearance of cataract in astronauts (Cucinotta et al. 2001). Space radiation differs in quality and quantity from the radiation field on Earth and consists also of heavy, charged particles that have higher biological effectiveness. Hall and colleagues showed that after exposure to space-relevant high-LET heavy ions (^{56}Fe) ATM-haploinsufficient mice developed stronger cataract compared to low-LET X-rays (Hall et al. 2006). Nevertheless, experiments using space-relevant heavy ions either with human or animal lens epithelial cells are still low in number to result in concrete conclusions regarding lens opacification. Here, pLECs were irradiated with ^{36}Ar and ^{12}C ions to investigate DSBs induction and repair. Table 17 summarizes the results from Figure 43, Figure 50 and Figure 51, and shows the comparison of foci formation after exposure to X-rays and ^{36}Ar and ^{12}C ions. With increasing atomic number, the foci number increased for carbon and argon ions after 1 h of irradiation. Similarly, the incapability of repairing DSBs was proportional to the size or atomic number of atoms as well as LET of radiation.

Table 17: Comparison of γ H2AX foci with respect to different qualities of radiation

| Dose (Gy) | Number of foci per nucleus after 1 h | | | Number of foci per nucleus after 24 h | | |
|-----------|--------------------------------------|--|--|---------------------------------------|--|--|
| | X-rays 3 keV/ μm | ^{12}C 71 keV/ μm | ^{36}Ar 269 keV/ μm | X-rays 3 keV/ μm | ^{12}C 71 keV/ μm | ^{36}Ar 269 keV/ μm |
| 0.5 | 5.7 | 4.6 | 8.2 | 1.8 | 1.4 | 5.3 |
| 1 | 9.0 | 7.1 | 17.1 | 0.5 | 1.3 | 7.9 |
| 2 | 13.9 | 15.5 | 20.9 | 1.4 | 2.5 | 5.8 |

Similar induction and repair of DNA damage as a consequence of exposure to X-rays and heavy ions were also seen in previous studies that support the present results (Aufderheide et al. 1987, Baumstark-Khan et al. 2003). Those studies showed three main differences in DNA strand break repair in diploid bovine lens epithelial cells. Firstly, repair after heavy ions was slower than after X-irradiation. Secondly, the rate and extent of repair decreased with increasing dose or particle fluence. And finally, the amount of non-rejoined breaks in heavy ions exposed samples was higher, despite of long incubation time.

Concerning the proposed hypothesis of radiation-induced cataractogenesis implying proliferation and differentiation of genetically damaged lens epithelial cells, the results of this study also demonstrate a larger genetic damage caused by heavy charged particles. Therefore, protection of the lens from radiation exposure should be taken seriously to prevent radiation-induced lens opacification during long-term space missions as well as in occupational and therapeutic exposures.

4.6 Gene expression after exposure of pLECs to different radiation quantities and qualities

All the above-mentioned vital cellular processes like DNA repair, cell-cycle progression, oxidative stress, growth, and survival require a well-regulated expression of corresponding genes that initiate phenotypic changes. In this study, changes in expression of selected genes were analyzed after exposure to X-rays as well as carbon ions.

The selection of housekeeping genes (HKGs) is a very important step in order to determine relative expression levels of target genes. Studies have shown that some commonly used HKGs may be regulated in response to ionizing radiation (Banda et al. 2008, Iyer et al. 2017). Banda et al. showed that B2M was one of most stable HKG and can be used as internal control after exposure to ionizing radiation. Since the n-fold expression changes of genes between -2 to 2 were regarded as not being significant, the expression of B2M and HPRT were quite stable at all doses and timepoints both after X-rays (Figure 54) as well as carbon ion exposure (Figure 62). ACTB, the expression of which was very stable at 0 and 1 Gy, was slightly down-regulated after high doses of carbon ion exposure. Nevertheless, the use of three HKGs makes the results more reliable for the expression analysis of target gene.

CDKN1A (p21) and GADD45G genes are known to be involved in cell-cycle arrest (Bedelbaeva et al. 2010, Cazzalini et al. 2010, Karimian et al. 2016) and DNA repair after cellular injury (Ou et al. 2015, Ishida et al. 2013), respectively. Both genes have been shown to be consistently up-regulated after exposure to ionizing radiation (Snyder and Morgan 2004, Daino et al. 2002). The dose- and time-dependent increase of CDKN1A (Figure 55 and Figure 63) after radiation exposure is well supported by many other studies (Paul and Amundson 2008, Budworth et al. 2012) which actually reflect the activation of DNA repair pathways governed by cell-cycle arrest. Not surprisingly, the C-12 ion exposure resulted in higher expression of the CDKN1A gene, which might be explained by the higher amount and complexity of DNA damage after heavy ion exposure. This result is supported by a similar higher up-regulation CDKN1A gene in human lens epithelial cells after exposure to iron ions and protons (high-LET) compared to X-irradiation (low-LET) (Chang et al. 2005). Similarly, a study from the dog's cataractous lens also demonstrated up-regulation of the CDKN1A gene (Bras et al. 2007). Such findings suggest cell-cycle and proliferation of lens epithelial cells are dysregulated in cataractogenesis and that its severity is greatly affected by the radiation quality.

With regard to the CRYAB gene, neither X-rays nor C-12 exposure resulted in distinguished changes of the expression pattern (Figure 57 and Figure 65). α B-crystallins, which are a product of CRYAB genes, are basically structural proteins. They belong to the heat-shock protein family, which have molecular chaperone activity and bind β - and γ -crystallins in cooperation with α A-crystallins to maintain lens transparency. A number of studies has shown that mutations in the CRYAB gene lead to formation of congenital cataracts (Chen et al. 2009, Berry et al. 2001, Liu et al. 2006, Jiaox et al. 2015). Interestingly, Li et al. concluded that the Pro20Ser mutation in α B-crystallin is a functional mutation that reduces the chaperon activity of α A-crystallin, resulting in increased nuclear transport of α B-crystallin and increased apoptosis of human lens epithelial cells (Li et al. 2008a). Furthermore, Andley proposed a model where cataract formation is the consequence of production of conformationally altered proteins due to mutation in α -crystallin genes (Andley 2009). In this study, neither X-rays nor carbon ion irradiation affected the gene expression pattern. It might be possible that these radiation qualities induce genetic alterations, which lead to non-functional crystallins during protein translation.

The transparency of a crystalline lens depends on the tight arrangement of fiber cells, which are devoid of cell organelles as well as the nucleus. The involvement of DNase II for nuclear degradation in chicken lenses have been shown in studies performed by Torriglia et al. and also Bassnett and Mataic (Bassnett and Mataic 1997, Torriglia et al. 1995). Two acid DNases, DNase II and DNase II β (DNase II-like acid DNase (DLAD)), have been found in mammalian lenses. However, for the porcine lens, only DNase II has been reported and so far the presence of DNase II β has not been investigated. Here, the expression of DNASE2 (DNase II) gene was not significantly altered after X-ray and C-12 ion exposure (Figure 58 and Figure 66). Nevertheless, the importance of DLAD can be seen in the study of Nishimoto et al. where DLAD^{-/-} mice developed cataracts indicating the requirement of DLAD in degradation of nuclear DNA during lens cell differentiation (Nishimoto et al. 2003). Interestingly, Nakahara and colleagues reported that DLAD was more abundant in fiber cells than in epithelial cells of mice lenses. The abundance of DLAD protein in fiber cells, located a few layers adjacent to the organelle-free zone, indicated that DLAD expression was deeply connected to lens fiber differentiation (Nakahara et al. 2007). The role of DNase II β or DLAD is further supported by Maria and Bassnett who showed its necessity in fiber cell denucleation (De Maria and Bassnett 2007).

As mentioned in the results section, the critical importance of PAX6 in differentiation and development of the lens and the iris because mutation in the gene cause conditions like aniridia and cataracts (Shiels and Hejtmancik 2013, Brémond-Gignac et al. 2010, Cai et al. 2010). In addition to that, PAX6 is also known to play a crucial role in lens fiber differentiation (Lovicu et al. 2004, Shaham et al. 2009). The current study is one of the first investigations on the effects of different doses and qualities of ionizing radiation on PAX6 gene expression. The dose-dependent increase in expression of the PAX6 gene mainly 24 and 72 h after X-ray exposure (Figure 59) would certainly have some effect on lens epithelial and fiber cells. Notably, transgenic mice with overexpression of human PAX6(5a) developed cataract as well as abnormalities in the fiber cells' shape (Duncan et al. 2000). In contrast to exposure to X-rays, C-12 ion exposure resulted in dose-dependent down-regulation of PAX6 gene expression. The reason for these contradicting results for two different radiation qualities is unclear. Nevertheless, a reduced level of the Pax6 transcription factor was found in TGF- β -induced sub-capsular plaques (Lovicu et al. 2004). It seems that both up- and down-regulation of PAX6 is a

threat to the health of the lens and a balanced expression is required for lens transparency.

The NF- κ B /Rel family consists of five different related monomers: RelA (p65), RelB, c-Rel, p50/p105 (NF- κ B1) and p52/p100 (NF- κ B2) that form homo- and hetero-dimers. NF- κ B are transcription factors that are present in cells in an inactive form yet respond rapidly upon detection of harmful cellular stimuli such as stress, cytokines, bacterial and viral antigens, ionizing radiation etc. to promote cellular survival e.g. by suppressing apoptosis. Notably, NF- κ B is activated in different types of cancers (Notarbartolo et al. 2005, Suh et al. 2002, Dolcet et al. 2005). Under normal conditions, RelA is not regulated on the gene expression level. The activation and translocation of RelA is a good indicator of NF- κ B activation by radiation. On the gene expression level, NF- κ B activation can be observed by measuring the upregulation of NF- κ B target genes such as NFKB1A or TNF. Expectedly, the exposure of lens epithelial cells to X-rays did not significantly change the expression of RelA (Figure 60). In contrast, C-12 ion exposure (Figure 68) led to slight up-regulation at earlier time points which decreased with time for all doses for unclear reasons. Hellweg et al. could show an increase of nuclear p65 content in HEK/293 cells, which indicates nuclear translocation of NF- κ B after radiation exposure (Hellweg et al. 2018). From experiments with rat eye lenses Shao and colleagues concluded that Akt and NF- κ B signaling pathways were likely related to the occurrence and development of posterior capsule opacification (Shao et al. 2017). It could be possible that survival of radiation injured lens epithelial cells direct the lens towards opacification.

One of the major and initial events known in cataract development is oxidative stress induced by various agents (Matsuda et al. 1981, Worgul and Merriam Jr 1981, Babizhayev et al. 1988, Padgaonkar et al. 1989, Spector et al. 1995). Such stress leads to metabolic and cellular changes in the lens organ and in cell culture comparable to the observation in human cataracts (Giblin et al. 1995, Kleiman et al. 1990, Kleiman and Spector 1993, Spector et al. 1998, Zigler Jr et al. 1989). Superoxide dismutase (SOD) is one of first defense mechanism against oxidative stress that catalyzes conversion of highly dangerous superoxide anion (O_2^-) to less reactive hydrogen peroxide (H_2O_2) and molecular oxygen. At present, three isoforms of SOD are known: CuZn-SOD (SOD1), Mn-SOD (SOD2) and SOD3. SOD3 is also dependent on copper and zinc as SOD1 and all these isoforms are expressed in human lens epithelium (Rajkumar et al. 2008).

Shankarnarayanan and colleagues showed that the activity and expression of SOD1 plays important role to prevent cataract and is reduced in the cataractous lens (Rajkumar et al. 2013). Despite lower amounts of SOD3 activity (Skiljic 2014) compared to SOD1, the activity of SOD3 cannot be neglected. The gene expression level of SOD3 in this study was not significantly affected by different doses of X-rays (Figure 61). On the other hand, SOD3 expression followed an inconsistent pattern after C-12 ion exposure (Figure 69). In other studies the activity or expression of SOD3 was compared between normal and cataractous lenses. However, a direct comparison of these results with pLECs in culture is not meaningful. Here, it was tested if radiation exposure led to similar results as in cataractous lenses. In addition to that, the cells used in this study were from porcine lenses, which might add some inter-species variations in the overall SOD content as well.

4.7 Role of epithelial to mesenchymal transition in cataractogenesis

It is well established that lens epithelial cells develop via epithelial to mesenchymal transition (EMT) to lens fiber cells. Radiation-induced cataract is known to occur as the result of EMT whereby genetically damaged lens epithelial cells proliferate to fiber cells (Rothstein et al. 1982, Worgul and Merriam Jr 1980, Worgul and Merriam Jr 1981). Many studies have demonstrated the presence of high amounts of calcium and phosphate forming bone-like hydroxyapatite crystals in senile or age-related cataract (Chen et al. 2005, Chiang et al. 2004, Lin et al. 2010). Such deposition of calcium is seen in osteogenic differentiation of vascular smooth muscle cells as well (Liu and Shanahan 2011, Steitz et al. 2001, Giachelli 2001). For this reason the assumption was made that cell-mediated osteogenic differentiation of lens epithelial cells could result in deposition of calcium in the crystalline lens. Another theory relies on the ionizing effect of radiation, which generates negative phosphate ions that combine with positive calcium ions to form an insoluble calcium phosphate precipitate. A very recent study conducted by Balogh et al. showed that the osteogenic induction of human lens epithelial cells resulted in osteogenic differentiation which was demonstrated by up-regulation of the osteo-/chondrogenic transcription factors Runx2 and Sox9 at mRNA and protein level (Balogh et al. 2016). Nevertheless, the exact mechanism of such a differentiation is still unclear.

In this study, the differentiation potential of pLECs under osteogenic induction and the expression of some genes of interest were analysed.

4.7.1 Osteogenic differentiation of lens epithelial cells

The deposition of calcium that is stained by Alizarin Red S staining was expectedly seen in pLECs which were supplied with osteogenic induction medium, in contrast to normal medium, after 5 days of incubation. With this evidence, the gene expression analysis of pLECs with and without induction medium was conducted.

4.7.2 Gene expression during differentiation

The two housekeeping genes used as reference to analyze the osteogenic differentiation of lens epithelial cells are ACTB and B2M shown in Figure 71. The expression of B2M under both normal and calcification medium (or osteogenic induction medium) was quite stable. An approximately 3-fold up-regulation of the beta actin gene (ACTB) was observed after 7 days of incubation with osteogenic induction medium. The reason for such up-regulation is most probably associated with the structural changes that accompany osteogenic differentiation. In the study performed by Quiroz et al. to investigate the expression stability of housekeeping genes, during osteogenic differentiation of human bone marrow mesenchymal stem cells, beta actin was 4.38 fold up-regulated (Quiroz et al. 2010). Many studies have concluded that actin quantity and its polymerizing activity play a decisive role in differentiation of various stem cells towards osteogenic fate (Sonowal et al. 2013, Chen et al. 2015, Sen et al. 2015, Rubin and Sen 2017). Despite expression levels of B2M had been shown to be rather instable (Ragni et al. 2013) and varying with particular differentiation stages of the cells (Evans et al. 2012), the result from this study showed stable expression of B2M.

Bone morphogenetic protein 2 (BMP2) belongs to the transforming growth factor- β (TGF- β) super-family and its importance in osteogenic differentiation in various cell types has been proven by experiments where BMP2 was supplemented (Ai et al. 2014, Marupanthorn et al. 2017) or the BMP2 gene was transfected (Sun et al. 2015, Zhou et al. 2016) into the test cell system which resulted in upregulation of osteogenic differentiation marker genes like RUNX2 (Runt-related transcription factor 2), SOX9 (Transcription factor SOX-9), OCN (Osteocalcin), OPN (Osteopontin), COL1 (Collagen type I) and ALP (Alkaline phosphatase). Considering at the necessity of BMP2, an up-regulation of the BMP2 gene (Figure 72) was indeed anticipated. This result suggests that BMP2 expression in lens epithelium is involved in the osteogenic differentiation process. Similarly, a study indicated that BMP2 expression in chicken lens epithelial

cells participates in the differentiation towards lens fiber cells (Belecky-Adams et al. 2002). Further, the importance of BMP signaling in fibroblast growth factor (FGF)-induced secondary lens fiber differentiation has been shown by Boswell et al. (Boswell et al. 2008). From this one can predict that depending on the expression level of BMP2 there is the possibility of differentiation of lens epithelial cells towards the osteogenic fate instead of fiber cells. This BMP2 expression probably depends on osteogenic induction medium or calcification medium (i.e. concentration of inorganic phosphate and calcium), which might be similar to serum/blood in an organism. As the result illustrates, the time-dependent expression rate of BMP2 due to osteogenic induction could be a positive feedback loop established by continuous deposition of calcium and phosphate.

One essential early transcription factor that is required for osteoblast differentiation as well as for the differentiation of mesenchymal stem cells towards the osteoblastic lineage is Runx2 (Yoshida et al. 2002, Franceschi and Xiao 2003, Komori 2002, Shakibaei et al. 2012). Runx2 is also known as a master transcription factor of osteogenesis. During osteogenic differentiation, Runx2 induces the mesenchymal stem cells to become immature osteoblasts, but it inhibits formation of mature osteoblasts (Bruderer et al. 2014). The target genes of Runx2, which are involved in osteogenic differentiation, are Col I, BSP, OPN and OCN. In this thesis, the expression level of Runx2 under osteogenic condition was about 2-fold up-regulated (Figure 73) regardless of the time of incubation with the osteogenic induction medium which lasted up to day 14. Osteogenic induction of rat bone marrow-derived mesenchymal stem cells also resulted in a 2-fold relative expression of Runx2 up to day 14 which then decreased to normal values at day 21 and 28 (Sun et al. 2017). Interestingly, in a similar experiment performed on human bone marrow-derived mesenchymal stromal cells (BM-MSCs), treatment with osteogenic differentiation medium increased the relative expression of RUNX2 to about 2-fold at day 3 which peaked at day 14 (~8-fold) and was reduced again to about 2-fold at day 28 (Marupanthorn et al. 2017). Surprisingly, in the same study, in umbilical cord-derived mesenchymal stromal cells (UC-MSCs), the expression of RUNX2 was about 2-fold only at day 14. It was however reduced at day 3 and 7; and the expression increased to about 6-fold and 10-fold at day 21 and 28, respectively. The results for Runx2 expression in UC-MSCs (Marupanthorn et al. 2017) coincide with results from this thesis for the time points used (day 7 and 14). Although the authors did not discuss the late expression of RUNX2 in UC-MSC than BM-MSC, the most probable

reason could be the type or location of cells from where they were isolated. As the name suggests, bone marrow cells are more prone to readily differentiate to the bone lineage than the umbilical cord cells. This is likely similar for lens epithelial cells, which show an expression pattern more like UC-MSCs rather than BM-MSCs. May be longer incubation with osteogenic induction medium could change the RUNX2 expression level. In support of the results of pLECs, osteogenic differentiation of human lens epithelial cells where osteogenic medium was supplied for 24 h demonstrated a doubling of mRNA of RUNX2 compared to control (Balogh et al. 2016).

Collagen type I, which is made up of two alpha-1 type I collagen and one alpha-2 type I collagen, is an important component of bone extracellular matrix. It is well accepted as an early marker of osteogenic differentiation (Rodan and Noda 1991). In addition to that, many studies have observed the up-regulation of collagen I gene during induction of osteogenic differentiation (Sun et al. 2015, Sun et al. 2017). Enhancement of osteogenic differentiation on a collagen I gel (Kang et al. 2013) or with supplementation of soluble collagen I (Kihara et al. 2006) have additionally supported its importance. Because all these studies were supporting the up-regulation of the collagen I gene, the drastic down-regulation of COL1A2 (alpha-2 type I collagen) under osteogenic induction conditions (Figure 74) was noteworthy. Not any of the studies have specifically examined the two different genes COL1A1 and COL1A2. There could be difference in regulation for these two genes especially when the cell type is completely different from that of osteogenic lineage. On top of that, comparison with other studies of collagen gene expression for lens epithelial cells is limited because of their very low number. While looking at the collagen content of human lens epithelial cells isolated from cataract lenses, the most abundant was collagen IV and a lower amount of collagen I and III was observed (Nishi et al. 1995). In a study using bovine lens epithelial cells, it was suggested that lens cells produce collagen IV at the initial passage and this collagen phenotype may alter during passaging to collagen I (after 14th passage) (Laurent et al. 1981). Such findings put forward a lot of questions before drawing conclusions for collagen gene expression in porcine lens epithelial cells as well.

Osteopontin (OPN) is the member of Small Integrin-Binding Ligand N-Linked Glycoprotein (SIBLING) family. SIBLING proteins are known to be key regulators in biomineralization of the tissues. Involvement of OPN in osteogenic cell differentiation is not yet clearly understood. Interestingly, in a recent study on *Opn*^{-/-} osteoblasts, Holm et al.

showed that OPN could play role in regulating bio-mineralization but not necessarily in osteogenic cell differentiation (Holm et al. 2014). The gene expression analysis in this thesis showed down-regulation at day 7 followed by up-regulation at day 14 of osteogenic induction of the pLECs (Figure 75). Despite initial down-regulation at day 7, the eventual up-regulation after day 14 is supported by the fact that OPN is one of late osteogenic markers when mineralization of bone starts. Many studies with osteogenic induction of different cell types have shown up-regulation of the OPN gene like human endometrium-derived stem cells (Ai et al. 2014) around 3-fold at day 21, rat bone mesenchymal stem cells (Sun et al. 2015) and human amniotic fluid-derived mesenchymal stem cells (Glemžaitė and Navakauskienė 2016) 3-fold at day 15. These data also support the results obtained with pLECs.

Although the role of the PAX6 gene is important in differentiation and developmental processes of the lens, no studies exist that investigate its expression pattern under osteogenic induction conditions. In this study, the clear time-dependent up-regulation of PAX6 gene expression with supplementation of osteogenic induction medium to pLECs (Figure 76) hints towards its involvement in osteogenic differentiation of lens epithelial cells as well. Further investigations are required to test the detailed engagement of this gene in this process.

BMP2, RUNX2 and COL1A2 genes were additionally investigated to test if radiation alone would affect their expression pattern, which could finally lead to osteogenic differentiation. The radiation effects on these osteogenic differentiation marker genes are limited to very few experiments. The 2-fold up-regulation of BMP2 gene was pronounced mainly at the high dose of 16 Gy of X-rays at the 24 h time point after irradiation (Figure 77). Arnold et al. showed a decrease of BMP2 mRNA by 75 % in a highly metastatic breast cancer cell line 2 days after irradiation with 5 Gy of X-rays (Arnold et al. 1999). In contrast, isolated human aortic valve interstitial cells displayed up-regulation of osteogenic markers 24 h after exposure to 10 Gy γ -rays (cesium-137 irradiator) (Nadlonek et al. 2012). The values for increases of expression of BMP2 2-fold, OPN 7-fold, ALP 3-fold and RUNX2 2-fold reveals the osteogenic inductive capacity of ionizing radiation. While the study by Nadlonek et al. gave a mechanistic insight into radiation-induced pathogenesis of aortic valve-related heart disease due to triggering of osteogenic induction, radiation-induced osteogenic differentiation of lens epithelial cells could also be a side effect of BMP2 expression. On the other hand, the

COL1A2 gene was minimally affected by X-rays at least at the earlier time point of the experiment (Figure 79). Likewise, the expression of RUNX2 (Figure 78) was ambiguous for the pLECs after radiation exposure.

4.8 Conclusion and Outlook

The aim of this work was to establish a cellular and an organ system that can be used for understanding the underlying mechanisms of radiation-induced cataract formation by radio-biological characterization of the porcine lens and lens epithelial cells. The need of an animal cell system rises, as it is almost impossible to obtain lenses from a healthy human donor.

Although pLECs have a slow proliferation rate, the easy isolation and culture of the cells compensate this problem. This study also suggests using pLECs at lower passage number (up to 4th passage). Colony forming assays did not show a significant difference in survival of immediately and late plated pLECs, which would have indicated an impairment in damage recovery. Prolonging the incubation time would be an interesting future experiment.

Determination of ROS after radiation exposure did not reveal a significant increase for the time points and doses used in this thesis. Since the ROS are short-lived in nature, novel protocols to harvest the cells at much shorter time points after exposure or even an assay that could detect live ROS generation would provide significant new insights.

Cell cycle analysis after X-irradiation imposed a dose-dependent increase in G2/M phase cells, which was demonstrated by a persistent cell cycle block up to 168 h. In this thesis, effects of ATM, ATR and DNA-PK inhibition on cell-cycle regulation of pLECs have been shown for the first time. Despite the fact that the experiments were not repeated, the results obtained for ATM (increased G2/M phase cells) and ATR inhibition (decreased G2/M phase cells) clearly justify a role of these molecules. Repeating those experiments would help to establish statistical significance. Studying the effect of p53, a key downstream molecule of ATM and ATR, would help to complete the picture of cell-cycle regulation in pLECs after radiation exposure. Those studies would be of great importance because radiation-induced cataractogenesis is hypothesized to depend on post-proliferative activity of lens epithelial cells.

The analysis of DNA DSB repair via γ H2AX assay points out the impairment in DSB repair in pLECs as well as whole lenses. The study also hints towards the possibility of

damage induction even at lower doses of irradiation with X-rays or heavy ions like argon- and carbon ions. The amount of damage induction and impairment of repair processes increased with increasing LET of radiation. These harmful effects make space travel unsafe with regard to damage to lens epithelial cells of the astronauts. Interestingly, such damage in lens epithelial cells residing in whole lenses was not uniformly distributed in different regions of the lens after X-irradiation. More damage persisted at the equatorial region (differentiation zone), which could possibly be the initial step in lens opacification.

Gene expression analysis revealed upregulation of the cell-cycle control gene CDKN1A, where high-LET carbon ions triggered greater fold-changes than low-LET X-rays.

Osteogenic induction of pLECs led to deposition of calcium on the cell culture plate, which was supported by upregulation of osteogenic induction genes. This possibility of differentiation of lens epithelial cells put forward a novel hypothesis of lens opacification due to calcium deposition. This preliminary experiment should be further investigated taking into consideration that astronauts in space suffer bone loss (calcium and phosphorus) due to microgravity. An early study claimed that radiation-induced production of negative phosphate ions interact with calcium ions in the lens to result in calcium phosphate precipitation leading to lens opacification (Burge et al. 1937).

The main concern of this study is how to prevent the induction of radiation-induced cataractogenesis and what countermeasures could be taken, which is possible only when the exact mechanisms are elucidated. Such studies would require a lot of samples. Due to rarity of human lenses, the possibility of using porcine lens and lens epithelial cells was investigated by testing them with numerous radio-biological experiments. Since most of the experiments in this thesis were performed with X-irradiation, repeating the experiments with space-relevant heavy charged particles irradiation would help in drawing much stronger conclusions. Finally, using the whole lens culture system will make it possible to investigate specific molecules involved in radiation cataractogenesis mechanisms and to side by side compare it with the monolayer culture as it was done for γ H2AX in this thesis.

5 ABSTRACT

The eye lens is known to be a radiosensitive mammalian organ, and ionizing radiation is considered to be a widely known risk factor inducing lens opacities. During space missions, astronauts are constantly exposed to galactic cosmic radiation, which contains energetic heavy ions of high linear energy transfer (LET). Due to higher dose and different patterns of cellular energy deposition from the high-LET ions, astronauts have higher risk for developing cataract compared to low-LET radiation exposure on earth. Although the exact mechanism of opacification is not known in detail, it is hypothesized that it initiates from the post-irradiation proliferative activity of genetically damaged lens epithelial cells.

As the porcine eye lens resembles the human eye lens in anatomy, size and crystalline content, the DNA damage reaction was investigated in lens organ culture (*ex-vivo*), in *in-vitro* cultivated lens epithelial layer and in monolayer culture (porcine lens epithelial cells (pLEC)). Colony forming ability assay demonstrated no significant difference in survival of pLECs with or without a recovery period of 24 h after X-irradiation. Induction of DNA double strand breaks and their repair verified using the molecular marker γ H2AX was dependent on dose and LET of radiation. In whole lenses, the DSB repair at the central epithelial region seemed to be similar to *in-vitro* cultivated pLECs whereas more damage persisted at the equatorial region even after a recovery time of 48 h. Investigation of cell cycle progression revealed a dose-dependent G2/M phase arrest in pLECs. Analysis of gene expression by reverse transcriptase quantitative real-time polymerase chain reaction (RT-qPCR) demonstrated dose-dependent up-regulation of the CDKN1A gene after both X-rays and carbon-ion exposure, where carbon ions (high-LET) resulted in higher n-fold changes.

Osteogenic induction of pLECs with supplementation of inorganic phosphate was verified with Alizarin Red S staining which was visible after 5 days of induction. RT-qPCR analysis showed up-regulation of BMP2, RUNX2 and PAX6 genes whereas down-regulation of COL1A2 gene due to supplementation of osteogenic induction medium.

Findings like persistence of DNA-DSB in pLECs and whole lens and cell-cycle disturbances indicate the vulnerability and sensitivity of lens epithelial cells towards ionizing radiation and support the hypothesis of radiation-induced cataract.

ABSTRACT

Misdifferentiation of pLECs to osteogenic type might also be a reason for calcium deposition that leads to lens opacification. Finally, the successful performance of experiments with pLECs and whole lens culture allows porcine lenses to be used as a new cell system for mechanistic and countermeasure studies of lens opacification.

6 ZUSAMMENFASSUNG

Die Augenlinse ist als strahlungsempfindliches Säugetierorgan bekannt und ionisierende Strahlung gilt als allgemein bekannter Risikofaktor, der eine Linsentrübung verursachen kann. Bei Weltraummissionen sind Astronauten kontinuierlich der galaktischen kosmischen Strahlung ausgesetzt, welche energiereiche schwere Ionen mit hohem linearem Energietransfer (LET) enthält. Aufgrund der höheren Dosis und der unterschiedlichen Muster der Energiedeposition durch die hoch-LET Ionen haben Astronauten ein höheres Risiko, einen Katarakt zu entwickeln, verglichen mit einer Exposition mit Niedrig-LET-Strahlung auf der Erde. Obwohl der genaue Mechanismus der Trübung nicht im Detail bekannt ist, wird angenommen, dass die Trübung durch die Proliferationsaktivität genetisch geschädigter Linsenepithelzellen nach Bestrahlung ausgelöst wird.

Da die Schweine-Linse in ihrer Anatomie, Größe und ihrem Kristallingehalt der menschlichen Linse ähnlich ist, wurde die Reaktionen auf DNA-Schäden in der Linsenorgankultur (*ex-vivo*), in der *in-vitro* kultivierten Linsenepithelschicht und in Monolayer-Kulturen von Linsenepithelzellen des Schweins (pLEC) untersucht. Der Kolonie-Bildungs-Test (Colony Forming Ability (CFA)-Assay) zeigte, dass es keinen signifikanten Unterschied im Überleben von pLECs nach Röntgenbestrahlung mit 24 h Erholungszeit oder ohne diese gibt. Die Induktion von DNA-Doppelstrangbrüchen (DSB) und deren Reparatur wurde mit dem molekularen Marker γ H2AX nachgewiesen und war abhängig von der Dosis und dem LET der Strahlung.

In ganzen Linsen schien die DSB-Reparatur in der zentralen Epithelregion mit *in-vitro* kultivierten pLECs ähnlich zu sein, während im äquatorialen Bereich auch nach einer Regenerationszeit von 48 h mehr Schäden persistierten. Die Untersuchung der Zellzyklusprogression zeigte einen dosisabhängigen Stopp der pLECs in der G2/M-Phase.

Die Analyse der Genexpression durch Reverse Transkriptase quantitative Echtzeit-Polymerase-Kettenreaktion (RT-qPCR) zeigte eine dosisabhängige Hoch-Regulierung des CDKN1A-Gens nach Röntgen- und Kohlenstoffionen-Exposition, wobei Kohlenstoffionen (hoch-LET) stärkere Hoch-Regulierungen auslösten.

Die osteogene Induktion von pLECs durch Supplementierung von anorganischem Phosphat wurde mit Hilfe der Alizarin Red S Färbung verifiziert, die nach fünf Tagen

Induktion sichtbar war. Die RT-qPCR-Analyse ergab eine Hoch-Regulierung der Gene BMP2, RUNX2 und PAX6, während das COL1A2-Gen durch Supplementierung des osteogenen Induktionsmediums herunter reguliert wurde.

Die Ergebnisse, insbesondere die Persistenz von DNA DSB in pLECs und in der gesamten Linse sowie Störungen im Zellzyklusverlauf, deuten auf die Anfälligkeit und Empfindlichkeit von Linsenepithelzellen gegenüber Exposition mit ionisierender Strahlung hin, welche die Hypothese der strahlungsinduzierten Kataraktbildung unterstützen. Fehldifferenzierung von pLECs zum osteogenen Typ könnte auch ein Grund für Kalziumablagerung sein, die ebenfalls zu einer Linsentrübung führt. Schließlich zeigt die erfolgreiche Durchführung von Experimenten mit pLECs und Ganzlinsenkulturen die Möglichkeit, dass Schweine-Linsen als neues Zellsystem für die mechanistische Untersuchung der Linsentrübung und die Entwicklung von Gegenmaßnahmen verwendet werden können.

7 REFERENCES

- ABDELKAWI S. 2012. Lens crystallin response to whole body irradiation with single and fractionated doses of gamma radiation. *International journal of radiation biology* 88: 600-606.
- ABRAHAM RT. 2001. Cell cycle checkpoint signaling through the ATM and ATR kinases. *Genes & development* 15: 2177-2196.
- ADAMS DR. 1929. The role of calcium in senile cataract. *Biochemical Journal* 23: 902.
- AI J, AZIZI E, SHAMSIAN A, ESLAMI A, KHOSHZABAN A, EBRAHIMI-BAROUGH S, AI A AND ALIZADEH A. 2014. BMP-2 can promote the osteogenic differentiation of human endometrial stem cells. *Asian Biomedicine* 8: 21-29.
- AINSBURY E, BOUFFLER S, DÖRR W, GRAW J, MUIRHEAD C, EDWARDS A AND COOPER J. 2009. Radiation cataractogenesis: a review of recent studies. *Radiation research* 172: 1-9.
- ANDLEY UP. 2009. Effects of α -crystallin on lens cell function and cataract pathology. *Current molecular medicine* 9: 887-892.
- ANDLEY UP, RHIM JS, CHYLACK L AND FLEMING TP. 1994. Propagation and immortalization of human lens epithelial cells in culture. *Investigative ophthalmology & visual science* 35: 3094-3102.
- ARNOLD S, TIMS E AND MCGRATH B. 1999. Identification of bone morphogenetic proteins and their receptors in human breast cancer cell lines: importance of BMP2. *Cytokine* 11: 1031-1037.
- ASHERY-PADAN R, MARQUARDT T, ZHOU X AND GRUSS P. 2000. Pax6 activity in the lens primordium is required for lens formation and for correct placement of a single retina in the eye. *Genes & development* 14: 2701-2711.
- AUFDERHEIDE E, RINK H, HIEBER L AND KRAFT G. 1987. Heavy ion effects on cellular DNA: strand break induction and repair in cultured diploid lens epithelial cells. *International Journal of Radiation Biology and Related Studies in Physics, Chemistry and Medicine* 51: 779-790.
- AVDEEV S, BIDOLI V, CASOLINO M, DE GRANDIS E, FURANO G, MORSELLI A, NARICI L, DE PASCALE M, PICOZZA P AND REALI E. 2002. Eye light flashes on the Mir space station. *Acta Astronautica* 50: 511-525.
- BABIZHAYEV MA, DEYEV AI AND LINBERG LF. 1988. Lipid peroxidation as a possible cause of cataract. *Mechanisms of ageing and development* 44: 69-89.
- BADHWAR G AND O'NEILL P. 1994. Long-term modulation of galactic cosmic radiation and its model for space exploration. *Advances in Space Research* 14: 749-757.
- BADHWAR GD. 1997. Deep space radiation sources, models, and environmental uncertainty. *Shielding Strategies for Human Space Exploration* 3360: 17-28.
- BAI F, XI JH, WAWROUSEK EF, FLEMING TP AND ANDLEY UP. 2003. Hyperproliferation and p53 status of lens epithelial cells derived from α B-crystallin knockout mice. *Journal of Biological Chemistry* 278: 36876-36886.
- BALOGH E, TÓTH A, TOLNAI E, BODÓ T, BÁNYAI E, SZABÓ DJ, PETROVSKI G AND JENEY V. 2016. Osteogenic differentiation of human lens epithelial cells might

- contribute to lens calcification. *Biochimica et Biophysica Acta (BBA)-Molecular Basis of Disease* 1862: 1724-1731.
- BANDA M, BOMMINENI A, THOMAS RA, LUCKINBILL LS AND TUCKER JD. 2008. Evaluation and validation of housekeeping genes in response to ionizing radiation and chemical exposure for normalizing RNA expression in real-time PCR. *Mutation Research/Genetic Toxicology and Environmental Mutagenesis* 649: 126-134.
- BANNIK K, RÖSSLER U, FAUS-KESSLER T, GOMOLKA M, HORNHARDT S, DALKE C, KLYMENKO O, ROSEMANN M, TROTT K-R AND ATKINSON M. 2013. Are mouse lens epithelial cells more sensitive to γ -irradiation than lymphocytes? *Radiation and environmental biophysics* 52: 279-286.
- BARANOV D, DERGACHEV V, GAGARIN YF, LYAGUSHIN V, NYMMIK R, PANASYUK M, SOLOV'EV A AND YAKUBOVSKII E. 2002. The high-energy heavy-particle fluences in the orbits of manned space stations. *Radiation measurements* 35: 423-431.
- BASSNETT S AND MATAIC D. 1997. Chromatin degradation in differentiating fiber cells of the eye lens. *The Journal of cell biology* 137: 37-49.
- BAUMSTARK-KHAN C. 1993. X-ray-induced DNA double-strand breaks as lethal lesions in diploid human fibroblasts compared to Chinese hamster ovary cells. *International journal of radiation biology* 63: 305-311.
- BAUMSTARK-KHAN C, HALBE E AND RINK H. 1998. X-Ray Sensitivity and Dna Damage in Bovine Lens Epithelial Cells in Vitro. *Ocular Radiation Risk Assessment in Populations Exposed to Environmental Radiation Contamination*: 153-162.
- BAUMSTARK-KHAN C, HEILMANN J AND RINK H. 2003. Induction and repair of DNA strand breaks in bovine lens epithelial cells after high LET irradiation. *Advances in Space Research* 31: 1583-1591.
- BAUMSTARK-KHAN C, SCHNEIDER J AND RINK H. 1991. Radiation sensitivity of cultured bovine lens epithelial cells. *Ophthalmic research* 23: 235-239.
- BAZILEVSKAYA G, KRAINEV M, STOZHKOVA YI, SVIRZHEVSKAYA A AND SVIRZHEVSKY N. 1994. Stratospheric measurements of cosmic rays in the 19th–22nd solar activity cycles. *Advances in Space Research* 14: 779-782.
- BEAUJEAN R, KOPP J, BURMEISTER S, PETERSEN F AND REITZ G. 2002. Dosimetry inside MIR station using a silicon detector telescope (DOSTEL). *Radiation measurements* 35: 433-438.
- BECK GR AND KNECHT N. 2003. Osteopontin regulation by inorganic phosphate is ERK1/2, PKC and proteasome dependent. *Journal of Biological Chemistry*.
- BECK JR GR. 2003. Inorganic phosphate as a signaling molecule in osteoblast differentiation. *Journal of cellular biochemistry* 90: 234-243.
- BECK JR GR, MORAN E AND KNECHT N. 2003. Inorganic phosphate regulates multiple genes during osteoblast differentiation, including Nrf2. *Experimental cell research* 288: 288-300.
- BEDELBAEVA K, SNYDER A, GOUREVITCH D, CLARK L, ZHANG X-M, LEFEROVICH J, CHEVERUD JM, LIEBERMAN P AND HEBER-KATZ E. 2010. Lack of p21 expression links cell cycle control and appendage regeneration in mice. *Proceedings of the National Academy of Sciences* 107: 5845-5850.

- BELECKY-ADAMS TL, ADLER R AND BEEBE DC. 2002. Bone morphogenetic protein signaling and the initiation of lens fiber cell differentiation. *Development* 129: 3795-3802.
- BENTZEN SM. 2006. Preventing or reducing late side effects of radiation therapy: radiobiology meets molecular pathology. *Nature Reviews Cancer* 6: 702.
- BERRY V, FRANCIS P, REDDY MA, COLLYER D, VITHANA E, MACKAY I, DAWSON G, CAREY AH, MOORE A AND BHATTACHARYA SS. 2001. Alpha-B crystallin gene (CRYAB) mutation causes dominant congenital posterior polar cataract in humans. *The American Journal of Human Genetics* 69: 1141-1145.
- BIDOLI V, CASOLINO M, DE PASCALE MP, FURANO G, MINORI M, MORSELLI A, NARICI L, PICOZZA P, REALI E AND SPARVOLI R. 2002. The Sileye-3/Alteino experiment for the study of light flashes, radiation environment and astronaut brain activity on board the International Space Station. *Journal of radiation research* 43: S47-S52.
- BLAKELY E, KLEIMAN NJ, NERIISHI K, CHODICK G, CHYLACK L, CUCINOTTA F, MINAMOTO A, NAKASHIMA E, KUMAGAMI T AND KITAOKA T. 2010. Radiation cataractogenesis: epidemiology and biology. *Radiation research* 173: 709-717.
- BLAKELY EA, BJORNSTAD KA, CHANG PY, MCNAMARA MP, CHANG E, ARAGON G, LIN SP, LUI G AND POLANSKY JR. 2000. Growth and differentiation of human lens epithelial cells in vitro on matrix. *Investigative ophthalmology & visual science* 41: 3898-3907.
- BÖCKER W AND ILIAKIS G. 2006. Computational methods for analysis of foci: Validation for radiation-induced γ -H2AX foci in human cells. *Radiation research* 165: 113-124.
- BOSWELL BA, OVERBEEK PA AND MUSIL LS. 2008. Essential role of BMPs in FGF-induced secondary lens fiber differentiation. *Developmental biology* 324: 202-212.
- BOUTROS G, KOCH H, JANSEN R, JACOB T AND DUNCAN G. 1984. Effect of 8-methoxypsoralen on rat lens cations, membrane potential and protein levels. *Experimental eye research* 38: 509-513.
- BRAS ID, COLITZ CM, KUSEWITT DF, CHANDLER H, LU P, GEMENSKY-METZLER AJ AND WILKIE DA. 2007. Evaluation of advanced glycation end-products in diabetic and inherited canine cataracts. *Graefe's Archive for Clinical and Experimental Ophthalmology* 245: 249-257.
- BRÉMOND-GIGNAC D, BITOUN P, REIS LM, COPIN H, MURRAY JC AND SEMINA EV. 2010. Identification of dominant FOXE3 and PAX6 mutations in patients with congenital cataract and aniridia. *Molecular vision* 16: 1705.
- International Congress Series, 2003. Elsevier, 287-295 p.
- BRUDERER M, RICHARDS R, ALINI M AND STODDART MJ. 2014. Role and regulation of RUNX2 in osteogenesis. *Eur Cell Mater* 28: 269-286.
- Seminars in radiation oncology, 2007. Elsevier, 121-130 p.
- BUDWORTH H, SNIJDERS AM, MARCHETTI F, MANNION B, BHATNAGAR S, KWONG E, TAN Y, WANG SX, BLAKELY WF AND COLEMAN M. 2012. DNA repair and cell cycle biomarkers of radiation exposure and inflammation stress in human blood. *PLoS one* 7: e48619.

- BUNTING SF, CALLÉN E, WONG N, CHEN H-T, POLATO F, GUNN A, BOTHMER A, FELDHahn N, FERNANDEZ-CAPETILLO O AND CAO L. 2010. 53BP1 inhibits homologous recombination in Brca1-deficient cells by blocking resection of DNA breaks. *Cell* 141: 243-254.
- BURGE W, WICKWIRE G AND SCHAMP H. 1937. CAUSE OF CALCIFICATION OF THE CRYSTALLINE LENS: WITH ADVANCE IN AGE AND IN CATARACT. *Archives of Ophthalmology* 17: 234-240.
- BURMA S, CHEN BP, MURPHY M, KURIMASA A AND CHEN DJ. 2001. ATM phosphorylates histone H2AX in response to DNA double-strand breaks. *Journal of Biological Chemistry* 276: 42462-42467.
- BURMA S AND CHEN DJ. 2004. Role of DNA-PK in the cellular response to DNA double-strand breaks. *DNA repair* 3: 909-918.
- BUSIJA DW, GASPAR T, DOMOKI F, KATAKAM PV AND BARI F. 2008. Mitochondrial-mediated suppression of ROS production upon exposure of neurons to lethal stress: mitochondrial targeted preconditioning. *Advanced drug delivery reviews* 60: 1471-1477.
- CAI F, ZHU J, CHEN W, KE T, WANG F, TU X, ZHANG Y, JIN R AND WU X. 2010. A novel PAX6 mutation in a large Chinese family with aniridia and congenital cataract. *Molecular vision* 16: 1141.
- CALDECOTT KW. 2008. Single-strand break repair and genetic disease. *Nature Reviews Genetics* 9: 619.
- CANCER IAFRO. 1994. Direct estimates of cancer mortality due to low doses of ionising radiation: an international study. *Lancet (British Edition)* 344: 1039-1043.
- CARPER DA, SUN JK, IWATA T, ZIGLER JS, IBARAKI N, LIN L-R AND REDDY V. 1999. Oxidative stress induces differential gene expression in a human lens epithelial cell line. *Investigative ophthalmology & visual science* 40: 400-406.
- CARSON CT, SCHWARTZ RA, STRACKER TH, LILLEY CE, LEE DV AND WEITZMAN MD. 2003. The Mre11 complex is required for ATM activation and the G2/M checkpoint. *The EMBO journal* 22: 6610-6620.
- CASOLINO M. 2006. Observations of the Light Flash phenomenon in space. *Advances in Space Research* 38: 1177-1181.
- CAZZALINI O, SCOVASSI AI, SAVIO M, STIVALA LA AND PROSPERI E. 2010. Multiple roles of the cell cycle inhibitor p21 CDKN1A in the DNA damage response. *Mutation Research/Reviews in Mutation Research* 704: 12-20.
- CELESTE A, FERNANDEZ-CAPETILLO O, KRUHLAK MJ, PILCH DR, STAUDT DW, LEE A, BONNER RF, BONNER WM AND NUSSENZWEIG A. 2003. Histone H2AX phosphorylation is dispensable for the initial recognition of DNA breaks. *Nature cell biology* 5: 675.
- CHANG C-C, ZHANG J, LOMBARDI L, NERI A AND DALLA-FAVERA R. 1994. Mechanism of expression and role in transcriptional control of the proto-oncogene NFKB-2/LYT-10. *Oncogene* 9: 923-933.
- CHANG P, BJORNSTAD K, CHANG E, MCNAMARA M, BARCELLOS-HOFF M, LIN S, ARAGON G, POLANSKY J, LUI G AND BLAKELY E. 2000. Particle irradiation induces FGF2 expression in normal human lens cells. *Radiation research* 154: 477-484.

- CHANG P, BJORNSTAD K, ROSEN C, LIN S AND BLAKELY E. 2007. Particle radiation alters expression of matrix metalloproteases resulting in ECM remodeling in human lens cells. *Radiation and environmental biophysics* 46: 187-194.
- CHANG P, BJORNSTAD K, ROSEN C, MCNAMARA M, MANCINI R, GOLDSTEIN L, CHYLACK L AND BLAKELY E. 2005. Effects of iron ions, protons and X rays on human lens cell differentiation. *Radiation research* 164: 531-539.
- CHEN KH, CHENG WT, LI MJ, YANG DM AND LIN SY. 2005. Calcification of senile cataractous lens determined by Fourier transform infrared (FTIR) and Raman microspectroscopies. *Journal of microscopy* 219: 36-41.
- CHEN L, SHI K, FRARY CE, DITZEL N, HU H, QIU W AND KASSEM M. 2015. Inhibiting actin depolymerization enhances osteoblast differentiation and bone formation in human stromal stem cells. *Stem cell research* 15: 281-289.
- CHEN Q, MA J, YAN M, MOTHABI ME, LIU Y AND ZHENG F. 2009. A novel mutation in CRYAB associated with autosomal dominant congenital nuclear cataract in a Chinese family. *Molecular vision* 15: 1359.
- CHENNAZHY KP AND KRISHNAN LK. 2005. Effect of passage number and matrix characteristics on differentiation of endothelial cells cultured for tissue engineering. *Biomaterials* 26: 5658-5667.
- CHIANG S-Y, HORNG C-T, LEE W-H AND CHANG C-J. 2004. Calcified cataractous lens. *Journal of Cataract & Refractive Surgery* 30: 1586-1589.
- CHYLACK JR LT, PETERSON LE, FEIVESON AH, WEAR ML, MANUEL FK, TUNG WH, HARDY DS, MARAK LJ AND CUCINOTTA FA. 2009. NASA study of cataract in astronauts (NASCA). Report 1: Cross-sectional study of the relationship of exposure to space radiation and risk of lens opacity. *Radiation research* 172: 10-20.
- CIMPRICH KA AND CORTEZ D. 2008. ATR: an essential regulator of genome integrity. *Nature reviews Molecular cell biology* 9: 616.
- CIRAJ-BJELAC O, REHANI MM, SIM KH, LIEW HB, VANO E AND KLEIMAN NJ. 2010. Risk for radiation-induced cataract for staff in interventional cardiology: Is there reason for concern? *Catheterization and Cardiovascular Interventions* 76: 826-834.
- CLEMENT CH 2012. ICRP statement on tissue reactions and early and late effects of radiation in normal tissues and organs: threshold doses for tissue reactions in a radiation protection context. Elsevier.
- CLYNES M 2012. Animal cell culture techniques. Springer Science & Business Media.
- COGAN DG AND DONALDSON DD. 1951. Experimental radiation cataracts: I. Cataracts in the rabbit following single x-ray exposure. *AMA archives of ophthalmology* 45: 508-522.
- CONCIN N, STIMPFL M, ZEILLINGER C, WOLFF U, HEFLER L, SEDLAK J, LEODOLTER S AND ZEILLINGER R. 2003. Role of p53 in G2/M cell cycle arrest and apoptosis in response to γ -irradiation in ovarian carcinoma cell lines. *International journal of oncology* 22: 51-57.
- COUSINS C, MILLER D, BERNARDI G, REHANI M, SCHOFIELD P, VAÑÓ E, EINSTEIN A, GEIGER B, HEINTZ P AND PADOVANI R. 2011. International Commission on Radiological Protection. ICRP publication 120: 1-125.

- COVAS D, SIUFI J, SILVA A AND ORELLANA M. 2003. Isolation and culture of umbilical vein mesenchymal stem cells. *Brazilian journal of medical and biological research* 36: 1179-1183.
- CUCINOTTA F, MANUEL F, JONES J, ISZARD G, MURREY J, DJOJONEGRO B AND WEAR M. 2001. Space radiation and cataracts in astronauts. *Radiation research* 156: 460-466.
- CUCINOTTA FA AND DURANTE M. 2006. Cancer risk from exposure to galactic cosmic rays: implications for space exploration by human beings. *The lancet oncology* 7: 431-435.
- CUDE K, WANG Y, CHOI H-J, HSUAN S-L, ZHANG H, WANG C-Y AND XIA Z. 2007. Regulation of the G2-M cell cycle progression by the ERK5-NFkB signaling pathway. *The Journal of cell biology* 177: 253-264.
- DAINO K, ICHIMURA S AND NENOI M. 2002. Early induction of CDKN1A (p21) and GADD45 mRNA by a low dose of ionizing radiation is due to their dose-dependent post-transcriptional regulation. *Radiation research* 157: 478-482.
- DALINKA M AND MAZZEO JV. 1985. Complications of radiation therapy. *Critical reviews in diagnostic imaging* 23: 235-267.
- DANYSH BP AND DUNCAN MK. 2009. The lens capsule. *Experimental eye research* 88: 151-164.
- DE MARIA A AND BASSNETT S. 2007. DNase II β distribution and activity in the mouse lens. *Investigative ophthalmology & visual science* 48: 5638-5646.
- DELAMERE NA AND TAMIYA S 2008. Lens Na⁺, K⁺-ATPase. *Ocular Transporters In Ophthalmic Diseases And Drug Delivery*: Springer, p. 111-123.
- DELAMERE NA AND TAMIYA S. 2009. Lens ion transport: from basic concepts to regulation of Na, K-ATPase activity. *Experimental eye research* 88: 140-143.
- DENG C-X. 2006. BRCA1: cell cycle checkpoint, genetic instability, DNA damage response and cancer evolution. *Nucleic acids research* 34: 1416-1426.
- DENHAM JW. 2001. Is it time for a new formalism to categorise normal tissue radiation injury? *Int J Radiat Oncol Biol Phys* 50: 1105-1106.
- DEOKAR SA, RAI PS, RAI AB, SUNDHARAN S AND BAKSHI AA. 2018. Serum calcium and phosphorus levels: a marker of disease activity in senile cataract patients. *International Journal of Advances in Medicine* 5: 371-374.
- DHOLAKIA SA AND VASAVADA AR. 2004. Intraoperative performance and longterm outcome of phacoemulsification in age-related cataract. *Indian journal of ophthalmology* 52: 311.
- DI PAOLA M, BIANCHI M AND BAARLI J. 1978. Lens opacification in mice exposed to 14-MeV neutrons. *Radiation research* 73: 340-350.
- DOHERTY TM, ASOTRA K, FITZPATRICK LA, QIAO J-H, WILKIN DJ, DETRANO RC, DUNSTAN CR, SHAH PK AND RAJAVASHISTH TB. 2003. Calcification in atherosclerosis: bone biology and chronic inflammation at the arterial crossroads. *Proceedings of the National Academy of Sciences* 100: 11201-11206.
- DOLCET X, LLOBET D, PALLARES J AND MATIAS-GUIU X. 2005. NF-kB in development and progression of human cancer. *Virchows archiv* 446: 475-482.

- DUEVA R. 2016. A Role for DNA-PKcs in G2 Checkpoint Response and DNA End Resection After Exposure to Ionizing Radiation. Universitätsbibliothek Duisburg-Essen.
- DUNCAN MK, KOZMIK Z, CVEKLOVA K, PIATIGORSKY J AND CVEKL A. 2000. Overexpression of PAX6 (5a) in lens fiber cells results in cataract and upregulation of (alpha) 5 (beta) 1 integrin expression. *Journal of Cell Science* 113: 3173-3185.
- DURANTE F, BALANZAT E, CASSIMI A, CHEVALIER F, NGONO-RAVACHE Y, MADI T, POULLY J-C, RAMILLON J-M, ROTHARD H AND ROPARS F. 2016. Dosimetry for radiobiology experiments at GANIL. *Nuclear Instruments and Methods in Physics Research Section A: Accelerators, Spectrometers, Detectors and Associated Equipment* 816: 70-77.
- DYNLACHT JR. 2013. The role of age, sex and steroid sex hormones in radiation cataractogenesis. *Radiation research* 180: 559-566.
- DYNLACHT JR, VALLURI S, GARRETT J, MENDONCA MS, LOPEZ JT, CAPERELL-GRANT A AND BIGSBY RM. 2010. Age and hormonal status as determinants of cataractogenesis induced by ionizing radiation. I. Densely ionizing (high-LET) radiation. *Radiation research* 175: 37-43.
- ECCLES LJ, O'NEILL P AND LOMAX ME. 2011. Delayed repair of radiation induced clustered DNA damage: friend or foe? *Mutation Research/Fundamental and Molecular Mechanisms of Mutagenesis* 711: 134-141.
- ECSS. 2008. Space Environment Standard ECSS-E-ST-10-04C. ESA Requirements and Standards Division (Retrieved 2018-10-10).
- EVANS CJ AND AGUILERA RJ. 2003. DNase II: genes, enzymes and function. *Gene* 322: 1-15.
- EVANS ND, SWAIN RJ, GENTLEMAN E, GENTLEMAN MM AND STEVENS MM. 2012. Embryonic stem cells undergoing osteogenic differentiation produce mineral non-specifically compared to marrow stromal cells or calvarial osteoblasts. *European cells & materials* 24: 211.
- FAGERHOLM P, LUNDEVALL E, TROCMÉ S AND WROBLEWSKI R. 1986. Human and experimental lens repair and calcification. *Experimental eye research* 43: 965-972.
- FAKIR H, SACHS RK, STENERLÖW B AND HOFMANN W. 2006. Clusters of DNA double-strand breaks induced by different doses of nitrogen ions for various LETs: experimental measurements and theoretical analyses. *Radiation research* 166: 917-927.
- FLORES O AND BURNSTEIN KL. 2010. GADD45γ: a new vitamin D-regulated gene that is antiproliferative in prostate cancer cells. *Endocrinology* 151: 4654-4664.
- FORD HL, KABINGU EN, BUMP EA, MUTTER GL AND PARDEE AB. 1998. Abrogation of the G2 cell cycle checkpoint associated with overexpression of HSIX1: a possible mechanism of breast carcinogenesis. *Proceedings of the National Academy of Sciences* 95: 12608-12613.
- FRANCESCHI RT AND XIAO G. 2003. Regulation of the osteoblast-specific transcription factor, Runx2: Responsiveness to multiple signal transduction pathways. *Journal of cellular biochemistry* 88: 446-454.
- FRANKENBERG D AND FRANKENBERG-SCHWAGER M. 1981. Interpretation of the Shoulder of Dose—response Curves with Immediate Plating in Terms of Repair of

- Potentially Lethal Lesions During a Restricted time Period. *International Journal of Radiation Biology and Related Studies in Physics, Chemistry and Medicine* 39: 617-631.
- FUGLESANG C. 2007. Using the human eye to image space radiation or the history and status of the light flash phenomena. *Nuclear Instruments and Methods in Physics Research Section A: Accelerators, Spectrometers, Detectors and Associated Equipment* 580: 861-865.
- FUJIMICHI Y AND HAMADA N. 2014. Ionizing irradiation not only inactivates clonogenic potential in primary normal human diploid lens epithelial cells but also stimulates cell proliferation in a subset of this population. *PLoS One* 9: e98154.
- FUJITA T, IZUMO N, FUKUYAMA R, MEGURO T, NAKAMUTA H, KOHNO T AND KOIDA M. 2001. Phosphate provides an extracellular signal that drives nuclear export of Runx2/Cbfa1 in bone cells. *Biochemical and biophysical research communications* 280: 348-352.
- FUKAI T AND USHIO-FUKAI M. 2011. Superoxide dismutases: role in redox signaling, vascular function, and diseases. *Antioxidants & redox signaling* 15: 1583-1606.
- GANUSHKINA NY, DANDOURAS I, SHPRITS Y AND CAO J. 2011. Locations of boundaries of outer and inner radiation belts as observed by Cluster and Double Star. *Journal of Geophysical Research: Space Physics* 116.
- GIACHELLI CM. 2001. Ectopic calcification: new concepts in cellular regulation. *Zeitschrift für Kardiologie* 90: 31-37.
- GIACHELLI CM. 2003. Vascular calcification: in vitro evidence for the role of inorganic phosphate. *Journal of the American Society of Nephrology* 14: S300-S304.
- GIACHELLI CM, JONO S, SHIOI A, NISHIZAWA Y, MORI K AND MORII H. 2001. Vascular calcification and inorganic phosphate. *American journal of kidney diseases* 38: S34-S37.
- GIACHELLI CM, SPEER MY, LI X, RAJACHAR RM AND YANG H. 2005. Regulation of vascular calcification: roles of phosphate and osteopontin. *Circulation research* 96: 717-722.
- GIBLIN FJ, PADGAONKAR VA, LEVERENZ VR, LIN L-R, LOU MF, UNAKAR NJ, DANG L, DICKERSON JR JE AND REDDY VN. 1995. Nuclear light scattering, disulfide formation and membrane damage in lenses of older guinea pigs treated with hyperbaric oxygen. *Experimental eye research* 60: 219-235.
- GLEMŽAITĖ M AND NAVAKAUSKIENĖ R. 2016. Osteogenic differentiation of human amniotic fluid mesenchymal stem cells is determined by epigenetic changes. *Stem cells international* 2016.
- GOGINENI VR, NALLA AK, GUPTA R, DINH DH, KLOPFENSTEIN JD AND RAO JS. 2011. Chk2-mediated G2/M cell cycle arrest maintains radiation resistance in malignant meningioma cells. *Cancer letters* 313: 64-75.
- GOODARZI AA, BLOCK WD AND LEES-MILLER SP. 2003. The role of ATM and ATR in DNA damage-induced cell cycle control. *Progress in cell cycle research* 5: 393-411.
- GRIGORIEV A, SVETAYLO E AND EGOROV A. 1998. Manned interplanetary missions: prospective medical problems. *Environmental medicine: annual report of the Research Institute of Environmental Medicine, Nagoya University* 42: 83-94.

- HADA M AND SUTHERLAND BM. 2006. Spectrum of complex DNA damages depends on the incident radiation. *Radiation research* 165: 223-230.
- HALL EJ 2008. Individual Genetic Susceptibility. Center for Radiological Research.
- HALL EJ, AND GIACCIA, A.J. 2012. Radiobiology for the radiologist. 7th Edition, Lippincott Williams and Wilkins, Philadelphia.
- HALL EJ, WORGUL BV, SMILENOV L, ELLISTON CD AND BRENNER DJ. 2006. The relative biological effectiveness of densely ionizing heavy-ion radiation for inducing ocular cataracts in wild type versus mice heterozygous for the ATM gene. *Radiation and environmental biophysics* 45: 99-104.
- HARTWELL L. 1992. Defects in a cell cycle checkpoint may be responsible for the genomic instability of cancer cells. *Cell* 71: 543-546.
- HEER M, KAMPS N, BIENER C, KORR C, BOERGER A, ZITTERMANN A, STEHLE P AND DRUMMER C. 1999. Calcium metabolism in microgravity. *Eur J Med Res* 4.
- HEIRTZLER J. 2002. The future of the South Atlantic anomaly and implications for radiation damage in space. *Journal of Atmospheric and Solar-Terrestrial Physics* 64: 1701-1708.
- HELLWEG C, SPITTA L, KOCH K, CHISHTI A, HENSCHENMACHER B, DIEGELER S, KONDA B, FELES S, SCHMITZ C AND BERGER T. 2018. The Role of the Nuclear Factor κ B Pathway in the Cellular Response to Low and High Linear Energy Transfer Radiation. *International journal of molecular sciences* 19: 2220.
- HELLWEG CE AND BAUMSTARK-KHAN C. 2007. Getting ready for the manned mission to Mars: the astronauts' risk from space radiation. *Naturwissenschaften* 94: 517-526.
- HIROSE Y, BERGER MS AND PIEPER RO. 2001. p53 effects both the duration of G2/M arrest and the fate of temozolomide-treated human glioblastoma cells. *Cancer research* 61: 1957-1963.
- HODGE WG, WHITCHER JP AND SATARIANO W. 1995. Risk factors for age-related cataracts. *Epidemiologic reviews* 17: 336-346.
- HOLM E, GLEBERZON JS, LIAO Y, SØRENSEN ES, BEIER F, HUNTER GK AND GOLDBERG HA. 2014. Osteopontin mediates mineralization and not osteogenic cell development in vitro. *Biochemical Journal* 464: 355-364.
- HORNECK G, FACIUS R, REICHERT M, RETTBERG P, SEBOLDT W, MANZEY D, COMET B, MAILLET A, PREISS H AND SCHAUER L. 2006. HUMEX, a study on the survivability and adaptation of humans to long-duration exploratory missions, part II: missions to Mars. *Advances in Space Research* 38: 752-759.
- HORWITZ J. 1992. Alpha-crystallin can function as a molecular chaperone. *Proceedings of the National Academy of Sciences* 89: 10449-10453.
- HORWITZ J. 2003. Alpha-crystallin. *Experimental eye research* 76: 145-153.
- HRUSKA KA, MATHEW S AND SAAB G. 2005. Bone morphogenetic proteins in vascular calcification. *Circulation research* 97: 105-114.
- HU Y. 2014. Effects of space-relevant radiation on pre-osteoblasts. Rheinischen Friedrich-Wilhelms-Universität Bonn.

- HU Y, HELLWEG CE, BAUMSTARK-KHAN C, REITZ G AND LAU P. 2014. Cell cycle delay in murine pre-osteoblasts is more pronounced after exposure to high-LET compared to low-LET radiation. *Radiation and environmental biophysics* 53: 73-81.
- HU Y, LAU P, BAUMSTARK-KHAN C, HELLWEG CE AND REITZ G. 2012. X-ray induced alterations in the differentiation and mineralization potential of murine preosteoblastic cells. *Advances in Space Research* 49: 1422-1431.
- IMAI F, YOSHIZAWA A, FUJIMORI-TONOU N, KAWAKAMI K AND MASAI I. 2010. The ubiquitin proteasome system is required for cell proliferation of the lens epithelium and for differentiation of lens fiber cells in zebrafish. *Development: dev.* 053124.
- ISHIDA K, YUGE Y, HANAOKA M, YASUKAWA M, MINAMI Y, OGAWA M, MASUMOTO KH, SHIGEYOSHI Y, SAITO M AND TSUJI T. 2013. Gadd45g regulates dental epithelial cell proliferation through p38 MAPK-mediated p21 expression. *Genes to Cells* 18: 660-671.
- IVASHKEVICH AN, MARTIN OA, SMITH AJ, REDON CE, BONNER WM, MARTIN RF AND LOBACHEVSKY PN. 2011. γ H2AX foci as a measure of DNA damage: a computational approach to automatic analysis. *Mutation Research/Fundamental and Molecular Mechanisms of Mutagenesis* 711: 49-60.
- IYAMA T AND WILSON DM. 2013. DNA repair mechanisms in dividing and non-dividing cells. *DNA repair* 12: 620-636.
- IYER G, WANG AR, BRENNAN SR, BOURGEOIS S, ARMSTRONG E, SHAH P AND HARARI PM. 2017. Identification of stable housekeeping genes in response to ionizing radiation in cancer research. *Scientific reports* 7: 43763.
- JACOB S, BOVEDA S, BAR O, BRÉZIN A, MACCIA C, LAURIER D AND BERNIER M-O. 2013. Interventional cardiologists and risk of radiation-induced cataract: results of a French multicenter observational study. *International journal of cardiology* 167: 1843-1847.
- JALILOV AS, ZHANG C, SAMUEL EL, SIKKEMA WK, WU G, BERKA V, KENT TA, TSAI A-L AND TOUR JM. 2016. Mechanistic study of the conversion of superoxide to oxygen and hydrogen peroxide in carbon nanoparticles. *ACS applied materials & interfaces* 8: 15086-15092.
- JAZAYERI A, FALCK J, LUKAS C, BARTEK J, SMITH GC, LUKAS J AND JACKSON SP. 2006. ATM-and cell cycle-dependent regulation of ATR in response to DNA double-strand breaks. *Nature cell biology* 8: 37.
- JEANPIERRE C, AUSTRUY E, DELATTRE O, JONES C AND JUNIEN C. 1993. Subregional physical mapping of an α B-crystallin sequence and of a new expressed sequence D11S877E to human 11q. *Mammalian Genome* 4: 104-108.
- JIAOX X, KHAN SY, IRUM B, KHAN AO, WANG Q, KABIR F, KHAN AA, HUSNAIN T, AKRAM J AND RIAZUDDIN S. 2015. Missense mutations in CRYAB are liable for recessive congenital cataracts. *PloS one* 10: e0137973.
- JOHNSON RC, LEOPOLD JA AND LOSCALZO J. 2006. Vascular calcification: pathobiological mechanisms and clinical implications. *Circulation research* 99: 1044-1059.
- JONES JA, MCCARTEN M, MANUEL K, DJOJONEGORO B, MURRAY J, FEIVERSEN A AND WEAR M. 2007. Cataract formation mechanisms and risk in aviation and space crews. *Aviation, space, and environmental medicine* 78: A56-A66.

- JONO S, MCKEE MD, MURRY CE, SHIOI A, NISHIZAWA Y, MORI K, MORII H AND GIACHELLI CM. 2000. Phosphate regulation of vascular smooth muscle cell calcification. *Circulation research* 87: e10-e17.
- KAMACHI Y, UCHIKAWA M, TANOUCI A, SEKIDO R AND KONDOH H. 2001. Pax6 and SOX2 form a co-DNA-binding partner complex that regulates initiation of lens development. *Genes & development* 15: 1272-1286.
- KANG B-J, KIM Y, LEE SH, KIM WH, WOO H-M AND KWEON O-K. 2013. Collagen I gel promotes homogenous osteogenic differentiation of adipose tissue-derived mesenchymal stem cells in serum-derived albumin scaffold. *Journal of Biomaterials Science, Polymer Edition* 24: 1233-1243.
- KARIMIAN A, AHMADI Y AND YOUSEFI B. 2016. Multiple functions of p21 in cell cycle, apoptosis and transcriptional regulation after DNA damage. *DNA repair* 42: 63-71.
- KARIN M. 1997. Nuclear factor-kappaB: a pivotal transcription factor in chronic inflammatory diseases. *N Engl J Med* 336: 1066-1071.
- KASTAN MB, ZHAN Q, EL-DEIRY WS, CARRIER F, JACKS T, WALSH WV, PLUNKETT BS, VOGELSTEIN B AND FORNACE JR AJ. 1992. A mammalian cell cycle checkpoint pathway utilizing p53 and GADD45 is defective in ataxia-telangiectasia. *Cell* 71: 587-597.
- KEENAN J, ORR D AND PIERSCIONEK B. 2008. Patterns of crystallin distribution in porcine eye lenses. *Molecular vision* 14: 1245.
- KENDRICK J AND CHONCHOL M. 2011. The role of phosphorus in the development and progression of vascular calcification. *American Journal of Kidney Diseases* 58: 826-834.
- KERN S, EICHLER H, STOEVE J, KLÜTER H AND BIEBACK K. 2006. Comparative analysis of mesenchymal stem cells from bone marrow, umbilical cord blood, or adipose tissue. *Stem cells* 24: 1294-1301.
- KIEFER J. 1971. Target theory and survival curves. *Journal of theoretical biology* 30: 307-317.
- KIHARA T, HIROSE M, OSHIMA A AND OHGUSHI H. 2006. Exogenous type I collagen facilitates osteogenic differentiation and acts as a substrate for mineralization of rat marrow mesenchymal stem cells in vitro. *Biochemical and biophysical research communications* 341: 1029-1035.
- KLEIMAN NJ, DAVID J, ELLISTON CD, HOPKINS KM, SMILENOV LB, BRENNER DJ, WORGUL BV, HALL EJ AND LIEBERMAN HB. 2007. Mrad9 and atm haploinsufficiency enhance spontaneous and X-ray-induced cataractogenesis in mice. *Radiation research* 168: 567-573.
- KLEIMAN NJ AND SPECTOR A. 1993. DNA single strand breaks in human lens epithelial cells from patients with cataract. *Current eye research* 12: 423-431.
- KLEIMAN NJ, WANG R-R AND SPECTOR A. 1990. Hydrogen peroxide-induced DNA damage in bovine lens epithelial cells. *Mutation Research/Genetic Toxicology* 240: 35-45.
- KOIKE M, SUGASAWA J, YASUDA M AND KOIKE A. 2008. Tissue-specific DNA-PK-dependent H2AX phosphorylation and γ -H2AX elimination after X-irradiation in vivo. *Biochemical and biophysical research communications* 376: 52-55.

- KOMORI T. 2002. Runx2, a multifunctional transcription factor in skeletal development. *Journal of cellular biochemistry* 87: 1-8.
- KONDA B. 2013. Effects of Ionizing Radiation on Human Adipose Derived Mesenchymal Stem Cells and their Differentiation towards the Osteoblastic Lineage. *Bibliothek Hochschule Bonn-Rhein-Sieg*.
- KORLIMBINIS A, BERRY Y, THIBAUT D, SCHEY KL AND TRUSCOTT RJ. 2009. Protein aging: truncation of aquaporin 0 in human lens regions is a continuous age-dependent process. *Experimental eye research* 88: 966-973.
- KOZUBEK S AND KRASAVIN E. 1984. Cell sensitivity to irradiation and DNA repair processes. II. The cell sensitivity to ionizing radiation of different LETs. *Neoplasma* 31: 685-695.
- KURNOSOVA L, KOLOBYANINA T, LOGACHEV V, RAZORENOV L, SIROTKIN I AND FRADKIN M. 1962. Discovery of radiation anomalies above the South Atlantic at heights of 310-340 km. *Planetary and Space Sci* 9.
- KUWABARA T. 1975. The maturation of the lens cell: a morphologic study. *Experimental eye research* 20: 427-443.
- KWIST K, BRIDGES W AND BURG K. 2016. The effect of cell passage number on osteogenic and adipogenic characteristics of D1 cells. *Cytotechnology* 68: 1661-1667.
- LAU P, BAUMSTARK-KHAN C, HELLWEG CE AND REITZ G. 2010. X-irradiation-induced cell cycle delay and DNA double-strand breaks in the murine osteoblastic cell line OCT-1. *Radiation and environmental biophysics* 49: 271-280.
- LAURENT M, KERN P, COURTOIS Y AND REGNAULT F. 1981. Synthesis of types I, III and IV collagen by bovine lens epithelial cells in long-term culture. *Experimental cell research* 134: 23-31.
- LEBLANC A, SCHNEIDER V, SHACKELFORD L, WEST S, OGANOV V, BAKULIN A AND VORONIN L. 2000. Bone mineral and lean tissue loss after long duration space flight. *J Musculoskelet Neuronal Interact* 1: 157-160.
- LETT J, COX A AND LEE A. 1985. Some perspectives on cataractogenesis from heavy charged particles. *Radiation Research* 104: S201-S207.
- LI H, LI C, LU Q, SU T, KE T, LI DW-C, YUAN M, LIU J, REN X AND ZHANG Z. 2008a. Cataract mutation P20S of α B-crystallin impairs chaperone activity of α A-crystallin and induces apoptosis of human lens epithelial cells. *Biochimica et Biophysica Acta (BBA)-Molecular Basis of Disease* 1782: 303-309.
- LI Z, HASSAN MQ, VOLINIA S, VAN WIJNEN AJ, STEIN JL, CROCE CM, LIAN JB AND STEIN GS. 2008b. A microRNA signature for a BMP2-induced osteoblast lineage commitment program. *Proceedings of the National Academy of Sciences* 105: 13906-13911.
- LIAO J, HU N, ZHOU N, LIN L, ZHAO C, YI S, FAN T, BAO W, LIANG X AND CHEN H. 2014. Sox9 potentiates BMP2-induced chondrogenic differentiation and inhibits BMP2-induced osteogenic differentiation. *PloS one* 9: e89025.
- LIN S-Y, CHEN K-H, LIN C-C, CHENG W-T AND LI M-J. 2010. Spectral analysis and comparison of mineral deposits forming in opacified intraocular lens and senile cataractous lens. *Spectrochimica Acta Part A: Molecular and Biomolecular Spectroscopy* 77: 703-708.

- LIU M, KE T, WANG Z, YANG Q, CHANG W, JIANG F, TANG Z, LI H, REN X AND WANG X. 2006. Identification of a CRYAB mutation associated with autosomal dominant posterior polar cataract in a Chinese family. *Investigative ophthalmology & visual science* 47: 3461-3466.
- LIU Y AND SHANAHAN CM. 2011. Signalling pathways and vascular calcification. *Front Biosci* 16: 1302-1314.
- LOVICU FJ, STEVEN P, SAIKA S AND MCAVOY JW. 2004. Aberrant lens fiber differentiation in anterior subcapsular cataract formation: a process dependent on reduced levels of Pax6. *Investigative ophthalmology & visual science* 45: 1946-1953.
- MAIDMENT JM, DUNCAN G, TAMIYA S, COLLISON DJ, WANG L AND WORMSTONE IM. 2004. Regional differences in tyrosine kinase receptor signaling components determine differential growth patterns in the human lens. *Investigative ophthalmology & visual science* 45: 1427-1435.
- MARCANTONIO JM, DUNCAN G AND RINK H. 1986. Calcium-induced opacification and loss of protein in the organ-cultured bovine lens. *Experimental eye research* 42: 617-630.
- MARCELLUS RC, TEODORO JG, CHARBONNEAU R, SHORE GC AND BRANTON PE. 1996. Expression of p53 in Saos-2 osteosarcoma cells induces apoptosis which can be inhibited by Bcl-2 or the adenovirus E1B-55 kDa protein. *Cell growth & differentiation: the molecular biology journal of the American Association for Cancer Research* 7: 1643-1650.
- MARIOTTI LG, PIROVANO G, SAVAGE KI, GHITA M, OTTOLENGHI A, PRISE KM AND SCHETTINO G. 2013. Use of the γ -H2AX assay to investigate DNA repair dynamics following multiple radiation exposures. *PloS one* 8: e79541.
- MARKIEWICZ E, BARNARD S, HAINES J, COSTER M, VAN GEEL O, WU W, RICHARDS S, AINSBURY E, ROTHKAMM K AND BOUFFLER S. 2015. Nonlinear ionizing radiation-induced changes in eye lens cell proliferation, cyclin D1 expression and lens shape. *Open biology* 5: 150011.
- MARUPANTHORN K, TANTRAWATPAN C, KHEOLAMAI P, TANTIKANLAYAPORN D AND MANOCHANTR S. 2017. Bone morphogenetic protein-2 enhances the osteogenic differentiation capacity of mesenchymal stromal cells derived from human bone marrow and umbilical cord. *International journal of molecular medicine* 39: 654-662.
- MASUDA H, MILLER C, KOEFFLER H, BATTIFORA H AND CLINE M. 1987. Rearrangement of the p53 gene in human osteogenic sarcomas. *Proceedings of the National Academy of Sciences* 84: 7716-7719.
- MATSUDA H, GIBLIN FJ AND REDDY VN. 1981. The effect of X-irradiation on cation transport in rabbit lens. *Experimental eye research* 33: 253-265.
- MERRIAM JR GR AND SZECHTER A. 1973. The effect of age on the radiosensitivity of rat lenses. *Transactions of the American Ophthalmological Society* 71: 88.
- MIZOBUCHI M, TOWLER D AND SLATOPOLSKY E. 2009. Vascular calcification: the killer of patients with chronic kidney disease. *Journal of the American Society of Nephrology* 20: 1453-1464.
- MOFFAT B, LANDMAN K, TRUSCOTT R, SWEENEY M AND POPE J. 1999. Age-related changes in the kinetics of water transport in normal human lenses. *Experimental eye research* 69: 663-669.

- MORGAN WF, DAY JP, KAPLAN MI, MCGHEE EM AND LIMOLI CL. 1996. Genomic instability induced by ionizing radiation. *Radiation research* 146: 247-258.
- MORRISON C, SONODA E, TAKAO N, SHINOHARA A, YAMAMOTO KI AND TAKEDA S. 2000. The controlling role of ATM in homologous recombinational repair of DNA damage. *The EMBO journal* 19: 463-471.
- MOSHOUS D, CALLEBAUT I, DE CHASSEVAL R, CORNEO B, CAVAZZANA-CALVO M, LE DEIST F, TEZCAN I, SANAL O, BERTRAND Y AND PHILIPPE N. 2001. Artemis, a novel DNA double-strand break repair/V (D) J recombination protein, is mutated in human severe combined immune deficiency. *Cell* 105: 177-186.
- MUKHERJEE A AND ROTWEIN P. 2009. Akt promotes BMP2-mediated osteoblast differentiation and bone development. *J Cell Sci* 122: 716-726.
- NADLONEK NA, WEYANT MJ, JESSICA AY, CLEVELAND JR JC, REECE TB, MENG X AND FULLERTON DA. 2012. Radiation induces osteogenesis in human aortic valve interstitial cells. *The Journal of thoracic and cardiovascular surgery* 144: 1466-1470.
- NAKAHARA M, NAGASAKA A, KOIKE M, UCHIDA K, KAWANE K, UCHIYAMA Y AND NAGATA S. 2007. Degradation of nuclear DNA by DNase II-like acid DNase in cortical fiber cells of mouse eye lens. *The FEBS journal* 274: 3055-3064.
- NAKASHIMA E, NERIISHI K AND MINAMOTO A. 2006. A reanalysis of atomic-bomb cataract data, 2000–2002: a threshold analysis. *Health physics* 90: 154-160.
- NERIISHI K, NAKASHIMA E, MINAMOTO A, FUJIWARA S, AKAHOSHI M, MISHIMA HK, KITAOKA T AND SHORE RE. 2007. Postoperative cataract cases among atomic bomb survivors: radiation dose response and threshold. *Radiation research* 168: 404-408.
- NISHI O, NISHI K, FUJIWARA T AND SHIRASAWA E. 1995. Types of collagen synthesised by the lens epithelial cells of human cataracts. *British journal of ophthalmology* 79: 939-943.
- NISHIMOTO S, KAWANE K, WATANABE-FUKUNAGA R, FUKUYAMA H, OHSAWA Y, UCHIYAMA Y, HASHIDA N, OHGURO N, TANO Y AND MORIMOTO T. 2003. Nuclear cataract caused by a lack of DNA degradation in the mouse eye lens. *Nature* 424: 1071.
- NOTARBARTOLO M, POMA P, PERRI D, DUSONCHET L, CERVELLO M AND D'ALESSANDRO N. 2005. Antitumor effects of curcumin, alone or in combination with cisplatin or doxorubicin, on human hepatic cancer cells. Analysis of their possible relationship to changes in NF-kB activation levels and in IAP gene expression. *Cancer letters* 224: 53-65.
- OLIVE PL. 1998. The role of DNA single- and double-strand breaks in cell killing by ionizing radiation. *Radiation research* 150: S42-S51.
- OU D-L, SHYUE S-K, LIN L-I, FENG Z-R, LIOU J-Y, FAN H-H, LEE B-S, HSU C AND CHENG A-L. 2015. Growth arrest DNA damage-inducible gene 45 gamma expression as a prognostic and predictive biomarker in hepatocellular carcinoma. *Oncotarget* 6: 27953.
- PADGAONKAR V, GIBLIN FJ AND REDDY V. 1989. Disulfide cross-linking of urea-insoluble proteins in rabbit lenses treated with hyperbaric oxygen. *Experimental eye research* 49: 887-899.

- PAUL S AND AMUNDSON SA. 2008. Development of gene expression signatures for practical radiation biodosimetry. *International Journal of Radiation Oncology* Biology* Physics* 71: 1236-1244. e1276.
- PAULL TT, ROGAKOU EP, YAMAZAKI V, KIRCHGESSNER CU, GELLERT M AND BONNER WM. 2000. A critical role for histone H2AX in recruitment of repair factors to nuclear foci after DNA damage. *Current Biology* 10: 886-895.
- PETERSON LE, PEPPER LJ, HAMM PB AND GILBERT SL. 1993. Longitudinal study of astronaut health: mortality in the years 1959-1991. *Radiation research* 133: 257-264.
- PETERSON W, TACHIKI K AND YAMAGUCHI D. 2004. Serial passage of MC3T3-E1 cells down-regulates proliferation during osteogenesis in vitro. *Cell proliferation* 37: 325-336.
- PIERCE DA, SHIMIZU Y, PRESTON DL, VAETH M AND MABUCHI K. 1996. Studies of the mortality of atomic bomb survivors. Report 12, Part I. Cancer: 1950-1990. *Radiation research* 146: 1-27.
- PISSARENKO N. 1994. Radiation environment due to galactic and solar cosmic rays during manned mission to Mars in the periods between maximum and minimum solar activity cycles. *Advances in Space Research* 14: 771-778.
- POLLARD TD, EARNSHAW WC, LIPPINCOTT-SCHWARTZ J AND JOHNSON G 2016. *Cell Biology E-Book*. Elsevier Health Sciences.
- PUCK TT AND MARCUS PI. 1956. Action of x-rays on mammalian cells. *Journal of Experimental Medicine* 103: 653-666.
- PUTILINA T, SKOURI-PANET F, PRAT K, LUBSEN NH AND TARDIEU A. 2003. Subunit exchange demonstrates a differential chaperone activity of calf alpha-crystallin towards beta low-and individual gamma-crystallins. *Journal of Biological Chemistry*.
- QUIROZ FG, POSADA OM, GALLEGO-PEREZ D, HIGUITA-CASTRO N, SARASSA C, HANSFORD DJ, AGUDELO-FLOREZ P AND LÓPEZ LE. 2010. Housekeeping gene stability influences the quantification of osteogenic markers during stem cell differentiation to the osteogenic lineage. *Cytotechnology* 62: 109-120.
- RAGNI E, VIGANO M, REBULLA P, GIORDANO R AND LAZZARI L. 2013. What is beyond aq RT-PCR study on mesenchymal stem cell differentiation properties: how to choose the most reliable housekeeping genes. *Journal of cellular and molecular medicine* 17: 168-180.
- RAJ SM, VASAVADA AR, JOHAR SK, VASAVADA VA AND VASAVADA VA. 2007. Post-operative capsular opacification: a review. *International journal of biomedical science: IJBS* 3: 237.
- RAJKUMAR S, PRAVEEN MR, GAJJAR D, VASAVADA AR, ALAPURE B, PATEL D AND KAPUR S. 2008. Activity of superoxide dismutase isoenzymes in lens epithelial cells derived from different types of age-related cataract. *Journal of Cataract & Refractive Surgery* 34: 470-474.
- RAJKUMAR S, VASAVADA AR, PRAVEEN MR, ANANTHAN R, REDDY GB, TRIPATHI H, GANATRA DA, ARORA AI AND PATEL AR. 2013. Exploration of molecular factors impairing superoxide dismutase isoforms activity in human senile cataractous lenses. *Investigative ophthalmology & visual science* 54: 6224-6233.

- RASTEGAR Z, ECKART P AND MERTZ M. 2002. Radiation-induced cataract in astronauts and cosmonauts. *Graefe's Archive for Clinical and Experimental Ophthalmology* 240: 543-547.
- REDDY VN. 1990. Glutathione and its function in the lens—an overview. *Experimental eye research* 50: 771-778.
- REDON C, PILCH D, ROGAKOU E, SEDELNIKOVA O, NEWROCK K AND BONNER W. 2002. Histone H2a variants H2AX and H2AZ. *Current opinion in genetics & development* 12: 162-169.
- REITZ G, BEAUJEAN R, BENTON E, BURMEISTER S, DACHEV T, DEME S, LUSZIK-BHADRA M AND OLKO P. 2005. Space radiation measurements on-board ISS—the DOSMAP experiment. *Radiation Protection Dosimetry* 116: 374-379.
- REITZ G AND BERGER T. 2006. The MATROSHKA facility—Dose determination during an EVA. *Radiation protection dosimetry* 120: 442-445.
- REMINGTON LA AND GOODWIN D 2011. *Clinical anatomy of the visual system E-Book*. Elsevier Health Sciences.
- REYNOLDS JL, JOANNIDES AJ, SKEPPER JN, MCNAIR R, SCHURGERS LJ, PROUDFOOT D, JAHNEN-DECHENT W, WEISSBERG PL AND SHANAHAN CM. 2004. Human vascular smooth muscle cells undergo vesicle-mediated calcification in response to changes in extracellular calcium and phosphate concentrations: a potential mechanism for accelerated vascular calcification in ESRD. *Journal of the American Society of Nephrology* 15: 2857-2867.
- RIBALLO E, KÜHNE M, RIEF N, DOHERTY A, SMITH GC, RECIO MA-J, REIS C, DAHM K, FRICKE A AND KREMPLER A. 2004. A pathway of double-strand break rejoining dependent upon ATM, Artemis, and proteins locating to γ -H2AX foci. *Molecular cell* 16: 715-724.
- RICHARDSON NL, HIGGS DA, BEAMES RM AND MCBRIDE JR. 1985. Influence of dietary calcium, phosphorus, zinc and sodium phytate level on cataract incidence, growth and histopathology in juvenile chinook salmon (*Oncorhynchus tshawytscha*). *The Journal of nutrition* 115: 553-567.
- RODAN G AND NODA M. 1991. Gene expression in osteoblastic cells. *Critical reviews in eukaryotic gene expression* 1: 85-98.
- ROGAKOU EP, PILCH DR, ORR AH, IVANOVA VS AND BONNER WM. 1998. DNA double-stranded breaks induce histone H2AX phosphorylation on serine 139. *Journal of biological chemistry* 273: 5858-5868.
- ROODHOOFT JMJ. 2002. Leading causes of blindness worldwide. *Bull Soc Belge Ophtalmol* 283: 19-25.
- ROSEN V. 2009. BMP2 signaling in bone development and repair. *Cytokine & growth factor reviews* 20: 475-480.
- ROTHKAMM K AND LOBRICH M. 2002. Misrepair of radiation-induced DNA double-strand breaks and its relevance for tumorigenesis and cancer treatment. *International journal of oncology* 21: 433-440.
- ROTHKAMM K AND LÖBRICH M. 2003. Evidence for a lack of DNA double-strand break repair in human cells exposed to very low x-ray doses. *Proceedings of the National Academy of Sciences* 100: 5057-5062.

- ROTHSTEIN H, WORGUL B, MEDVEDOVSKY JR C AND MERRIAM GR. 1982. G₀/G₁ Arrest of Cell Proliferation in the Ocular Lens Prevents Development of Radiation Cataract. *Ophthalmic research* 14: 215-220.
- RUBIN J AND SEN B. 2017. Actin up in the Nucleus: Regulation of Actin Structures Modulates Mesenchymal Stem Cell Differentiation. *Transactions of the American Clinical and Climatological Association* 128: 180.
- RYOO H-M, LEE M-H AND KIM Y-J. 2006. Critical molecular switches involved in BMP-2-induced osteogenic differentiation of mesenchymal cells. *Gene* 366: 51-57.
- SAGE AP, LU J, TINTUT Y AND DEMER LL. 2011. Hyperphosphatemia-induced nanocrystals upregulate the expression of bone morphogenetic protein-2 and osteopontin genes in mouse smooth muscle cells in vitro. *Kidney international* 79: 414-422.
- SANCHEZ I, MARTIN R, USSA F AND FERNANDEZ-BUENO I. 2011. The parameters of the porcine eyeball. *Graefe's Archive for Clinical and Experimental Ophthalmology* 249: 475-482.
- SANNITA WG, NARICI L AND PICOZZA P. 2006. Positive visual phenomena in space: A scientific case and a safety issue in space travel. *Vision research* 46: 2159-2165.
- SCATENA M, LIAW L AND GIACHELLI CM. 2007. Osteopontin: a multifunctional molecule regulating chronic inflammation and vascular disease. *Arteriosclerosis, thrombosis, and vascular biology* 27: 2302-2309.
- SCHAFHEIMER N AND KING J. 2013. Tryptophan Cluster Protects Human γ D-Crystallin from Ultraviolet Radiation-Induced Photoaggregation In Vitro. *Photochemistry and photobiology* 89: 1106-1115.
- SCHMIDBAUER JM, VARGAS LG, APPLE DJ, ESCOBAR-GOMEZ M, IZAK A, ARTHUR SN, GOLESCU A AND PENG Q. 2002. Evaluation of neodymium: yttrium-aluminum-garnet capsulotomies in eyes implanted with AcrySof intraocular lenses1. *Ophthalmology* 109: 1421-1426.
- SCHRECK R, RIEBER P AND BAEUERLE PA. 1991. Reactive oxygen intermediates as apparently widely used messengers in the activation of the NF-kappa B transcription factor and HIV-1. *The EMBO journal* 10: 2247-2258.
- SCHROEDER A, MUELLER O, STOCKER S, SALOWSKY R, LEIBER M, GASSMANN M, LIGHTFOOT S, MENZEL W, GRANZOW M AND RAGG T. 2006. The RIN: an RNA integrity number for assigning integrity values to RNA measurements. *BMC molecular biology* 7: 3.
- SCUTT A AND BERTRAM P. 1999. Basic fibroblast growth factor in the presence of dexamethasone stimulates colony formation, expansion, and osteoblastic differentiation by rat bone marrow stromal cells. *Calcified tissue international* 64: 69-77.
- SEDELNIKOVA OA, ROGAKOU EP, PANYUTIN IG AND BONNER WM. 2002. Quantitative detection of ¹²⁵I-dU-induced DNA double-strand breaks with γ -H2AX antibody. *Radiation research* 158: 486-492.
- SEN B, XIE Z, UZER G, THOMPSON WR, STYNER M, WU X AND RUBIN J. 2015. Intranuclear actin regulates osteogenesis. *Stem Cells* 33: 3065-3076.
- SERRANO MA, LI Z, DANGETI M, MUSICH PR, PATRICK S, ROGINSKAYA M, CARTWRIGHT B AND ZOU Y. 2013. DNA-PK, ATM and ATR collaboratively regulate

- p53–RPA interaction to facilitate homologous recombination DNA repair. *Oncogene* 32: 2452.
- SHAHAM O, SMITH AN, ROBINSON ML, TAKETO MM, LANG RA AND ASHERY-PADAN R. 2009. Pax6 is essential for lens fiber cell differentiation. *Development* 136: 2567-2578.
- SHAKIBAEI M, SHAYAN P, BUSCH F, ALDINGER C, BUHRMANN C, LUEDERS C AND MOBASHERI A. 2012. Resveratrol mediated modulation of Sirt-1/Runx2 promotes osteogenic differentiation of mesenchymal stem cells: potential role of Runx2 deacetylation. *PLoS One* 7: e35712.
- SHAO D, ZHU X, HUO L, SUN W, PAN P, CHEN W, WANG H AND LIU B. 2017. The significance of Akt/NF- κ b signaling pathway in the posterior cataract animal model. *Bratislavske lekarske listy* 118: 423-426.
- SHAO J-S, CAI J AND TOWLER DA. 2006. Molecular mechanisms of vascular calcification: lessons learned from the aorta. *Arteriosclerosis, thrombosis, and vascular biology* 26: 1423-1430.
- SHEA M AND SMART D. 1998. Space weather: The effects on operations in space. *Advances in Space Research* 22: 29-38.
- SHIELS A AND HEJTMANCIK J. 2013. Genetics of human cataract. *Clinical genetics* 84: 120-127.
- SHIRAI K, OKADA Y, SAIKA S, SENBA E AND OHNISHI Y. 2001. Expression of transcription factor AP-1 in rat lens epithelial cells during wound repair. *Experimental eye research* 73: 461-468.
- SHORE RE, NERIISHI K AND NAKASHIMA E. 2010. Epidemiological studies of cataract risk at low to moderate radiation doses:(not) seeing is believing. *Radiation research* 174: 889-894.
- SHRIVASTAV M, DE HARO LP AND NICKOLOFF JA. 2008. Regulation of DNA double-strand break repair pathway choice. *Cell research* 18: 134.
- SIBONGA JD, CAVANAGH PR, LANG TF, LEBLANC AD, SCHNEIDER VS, SHACKELFORD LC, SMITH SM AND VICO L. 2007. Adaptation of the skeletal system during long-duration spaceflight. *Clinical Reviews in Bone and Mineral Metabolism* 5: 249-261.
- SIVAK JM, WEST-MAYS JA, YEE A, WILLIAMS T AND FINI ME. 2004. Transcription factors Pax6 and AP-2 α interact to coordinate corneal epithelial repair by controlling expression of matrix metalloproteinase gelatinase B. *Molecular and cellular biology* 24: 245-257.
- SKILJIC D 2014. The role of estrogen and superoxide dismutase in cataractogenesis. University of Gothenburg.
- SMART D AND SHEA M 2003. The local time dependence of the anisotropic solar cosmic ray flux. AIR FORCE RESEARCH LAB HANSCOM AFB MA.
- SMITH J, THO LM, XU N AND GILLESPIE DA 2010. The ATM–Chk2 and ATR–Chk1 pathways in DNA damage signaling and cancer. *Advances in cancer research*: Elsevier, p. 73-112.
- SMITH SM, DAVIS-STREET JE, FESPERMAN JV, CALKINS D, BAWA M, MACIAS BR, MEYER RS AND HARGENS AR. 2003. Evaluation of treadmill exercise in a lower

- body negative pressure chamber as a countermeasure for weightlessness-induced bone loss: a bed rest study with identical twins. *Journal of Bone and Mineral Research* 18: 2223-2230.
- SMITH SM, MCCOY T, GAZDA D, MORGAN JL, HEER M AND ZWART SR. 2012. Space flight calcium: implications for astronaut health, spacecraft operations, and Earth. *Nutrients* 4: 2047-2068.
- SMITH SM, ZWART SR, HEER M, LEE SM, BAECKER N, MEUCHE S, MACIAS BR, SHACKELFORD LC, SCHNEIDER S AND HARGENS AR. 2008. WISE-2005: supine treadmill exercise within lower body negative pressure and flywheel resistive exercise as a countermeasure to bed rest-induced bone loss in women during 60-day simulated microgravity. *Bone* 42: 572-581.
- SNYDER AR AND MORGAN WF. 2004. Gene expression profiling after irradiation: clues to understanding acute and persistent responses? *Cancer and Metastasis Reviews* 23: 259-268.
- Seminars in cancer biology, 1997. Elsevier, 113-119 p.
- SONNEVELD P, PEPPERKAMP E AND VAN BEKKUM DW. 1979. Incidence of cataracts in rhesus monkeys treated with whole-body irradiation. *Radiology* 133: 227-229.
- SONOWAL H, KUMAR A, BHATTACHARYYA J, GOGOI PK AND JAGANATHAN BG. 2013. Inhibition of actin polymerization decreases osteogenic differentiation of mesenchymal stem cells through p38 MAPK pathway. *Journal of biomedical science* 20: 71.
- SPECTOR A, KUSZAK JR, MA W, WANG R-R, HO Y-S AND YANG Y. 1998. The effect of photochemical stress upon the lenses of normal and glutathione peroxidase-1 knockout mice. *Experimental eye research* 67: 457-471.
- SPECTOR A, WANG G-M, WANG R-R, LI W-C AND KLEIMAN NJ. 1995. A brief photochemically induced oxidative insult causes irreversible lens damage and cataract II. Mechanism of action. *Experimental eye research* 60: 483-493.
- STEITZ SA, SPEER MY, CURINGA G, YANG H-Y, HAYNES P, AEBERSOLD R, SCHINKE T, KARSENTY G AND GIACHELLI CM. 2001. Smooth muscle cell phenotypic transition associated with calcification: upregulation of Cbfa1 and downregulation of smooth muscle lineage markers. *Circulation research* 89: 1147-1154.
- STIFF T, O'DRISCOLL M, RIEF N, IWABUCHI K, LÖBRICH M AND JEGGO PA. 2004. ATM and DNA-PK function redundantly to phosphorylate H2AX after exposure to ionizing radiation. *Cancer research* 64: 2390-2396.
- SUH J, PAYVANDI F, EDELSTEIN LC, AMENTA PS, ZONG WX, GÉLINAS C AND RABSON AB. 2002. Mechanisms of constitutive NF- κ B activation in human prostate cancer cells. *The Prostate* 52: 183-200.
- SUN J, LI J, LI C AND YU Y. 2015. Role of bone morphogenetic protein-2 in osteogenic differentiation of mesenchymal stem cells. *Molecular medicine reports* 12: 4230-4237.
- SUN X, SU W, MA X, ZHANG H, SUN Z AND LI X. 2017. Comparison of the osteogenic capability of rat bone mesenchymal stem cells on collagen, collagen/hydroxyapatite, hydroxyapatite and biphasic calcium phosphate. *Regenerative biomaterials* 5: 93-103.

- SWEENEY MH AND TRUSCOTT RJ. 1998. An impediment to glutathione diffusion in older normal human lenses: a possible precondition for nuclear cataract. *Experimental eye research* 67: 587-595.
- TAKEKAWA M AND SAITO H. 1998. A family of stress-inducible GADD45-like proteins mediate activation of the stress-responsive MTK1/MEKK4 MAPKKK. *Cell* 95: 521-530.
- TAKEMOTO L AND SORENSEN CM. 2008. Protein–protein interactions and lens transparency. *Experimental eye research* 87: 496-501.
- TANG D, BORCHMAN D, YAPPERT MC, VRENSSEN GF AND RASI V. 2003. Influence of age, diabetes, and cataract on calcium, lipid-calcium, and protein-calcium relationships in human lenses. *Investigative ophthalmology & visual science* 44: 2059-2066.
- TAYLOR WR AND STARK GR. 2001. Regulation of the G2/M transition by p53. *Oncogene* 20: 1803.
- THOMAS DM, CARTY SA, PISCOPO DM, LEE J-S, WANG W-F, FORRESTER WC AND HINDS PW. 2001. The retinoblastoma protein acts as a transcriptional coactivator required for osteogenic differentiation. *Molecular cell* 8: 303-316.
- THOMPSON A, SACHDEV N, WONG T, RILEY A, GRUPCHEVA C AND MCGHEE C. 2004. The Auckland Cataract Study: 2 year postoperative assessment of aspects of clinical, visual, corneal topographic and satisfaction outcomes. *British journal of ophthalmology* 88: 1042-1048.
- TICHÝ A, VÁVROVÁ J, PEJCHAL J AND REZÁCOVÁ M. 2010. Ataxia-telangiectasia mutated kinase (ATM) as a central regulator of radiation-induced DNA damage response. *Acta Medica (Hradec Kralove)* 53: 13-17.
- TORRIGLIA A, CHAUDUN E, CHANY-FOURNIER F, JEANNY J-C, COURTOIS Y AND COUNIS M-F. 1995. Involvement of DNase II in nuclear degeneration during lens cell differentiation. *Journal of Biological Chemistry* 270: 28579-28585.
- TROKEL S. 1962. The physical basis for transparency of the crystalline lens. *Investigative Ophthalmology & Visual Science* 1: 493-501.
- TRUSCOTT RJ. 2000. Age-related nuclear cataract: a lens transport problem. *Ophthalmic research* 32: 185-194.
- TRUSCOTT RJ. 2005. Age-related nuclear cataract—oxidation is the key. *Experimental eye research* 80: 709-725.
- TUMMINIA SJ, QIN C, ZIGLER JR JS AND RUSSELL P. 1994. The integrity of mammalian lenses in organ culture. *Experimental eye research* 58: 367-374.
- VALENTIN J 2007. The 2007 recommendations of the international commission on radiological protection. Elsevier Oxford.
- VON ZGLINICKI T, SARETZKI G, DÖCKE W AND LOTZE C. 1995. Mild hyperoxia shortens telomeres and inhibits proliferation of fibroblasts: a model for senescence? *Experimental cell research* 220: 186-193.
- WALL ME, BERNACKI SH AND LOBOA EG. 2007. Effects of serial passaging on the adipogenic and osteogenic differentiation potential of adipose-derived human mesenchymal stem cells. *Tissue engineering* 13: 1291-1298.

REFERENCES

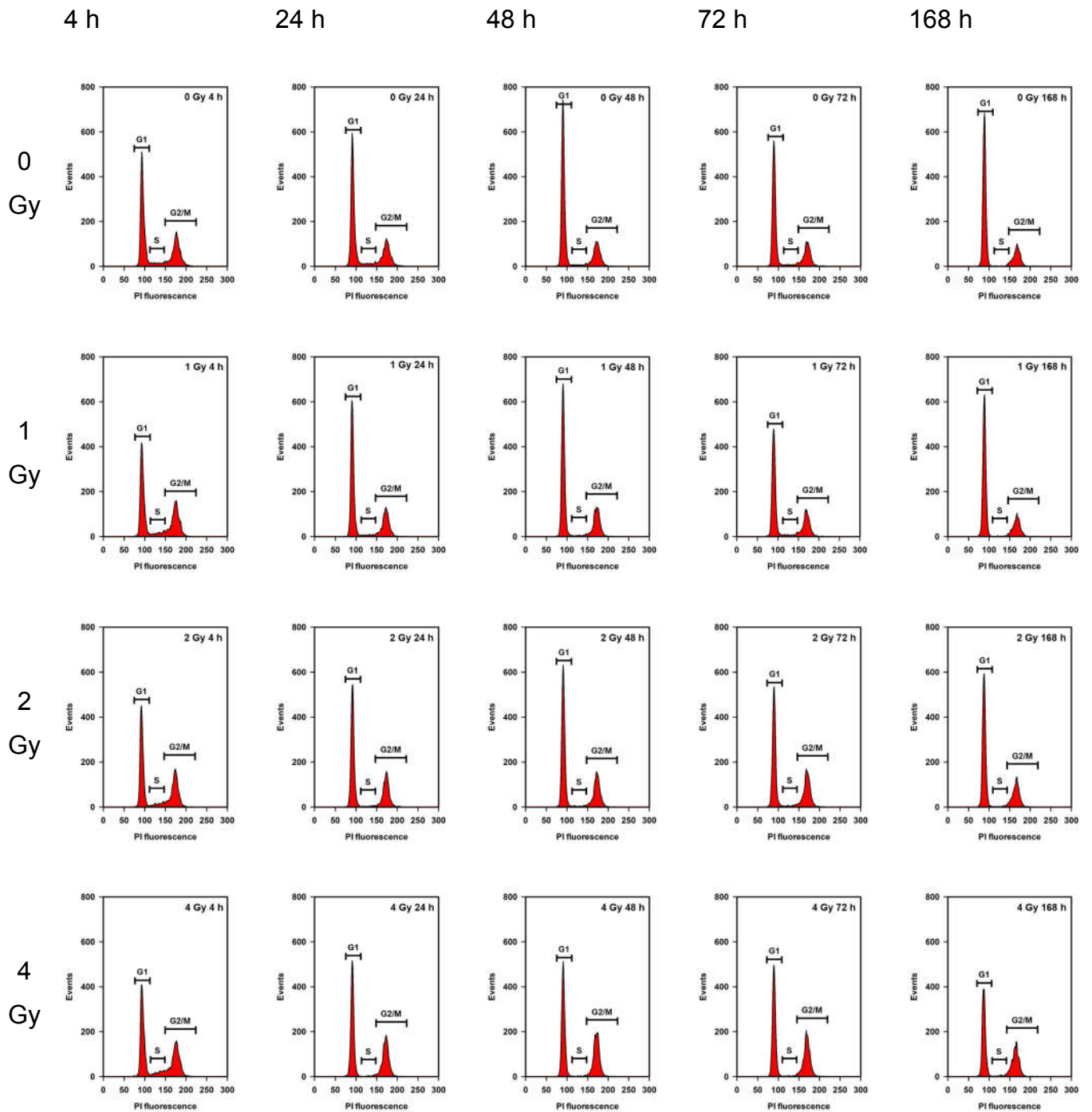
- WANG YH, LIU Y, MAYE P AND ROWE DW. 2006. Examination of mineralized nodule formation in living osteoblastic cultures using fluorescent dyes. *Biotechnology progress* 22: 1697-1701.
- WARD IM AND CHEN J. 2001. Histone H2AX is phosphorylated in an ATR-dependent manner in response to replicational stress. *Journal of Biological Chemistry* 276: 47759-47762.
- WARD J. 1994. The complexity of DNA damage: relevance to biological consequences. *International journal of radiation biology* 66: 427-432.
- WARMERDAM DO AND KANAAR R. 2010. Dealing with DNA damage: relationships between checkpoint and repair pathways. *Mutation Research/Reviews in Mutation Research* 704: 2-11.
- WEATHERALL M, JENNIFER C, JAMES K, PERRIN K, SHIRTCLIFFE P AND BEASLEY R. 2009. Dose-response relationship of inhaled corticosteroids and cataracts: A systematic review and meta-analysis. *Respirology* 14: 983-990.
- WEICHSELBAUM RR, NOVE J AND LITTLE JB. 1980. X-ray sensitivity of fifty-three human diploid fibroblast cell strains from patients with characterized genetic disorders. *Cancer Research* 40: 920-925.
- WERNER L, APPLE DJ, ESCOBAR-GOMEZ M, ÖHRSTRÖM A, CRAYFORD BB, BIANCHI R AND PANDEY SK. 2000. Postoperative deposition of calcium on the surfaces of a hydrogel intraocular lens¹. *Ophthalmology* 107: 2179-2185.
- WILSON GD. 2004. Radiation and the cell cycle, revisited. *Cancer and Metastasis Reviews* 23: 209-225.
- WILSON JW, CUCINOTTA F, SHINN J, SIMONSEN L, DUBEY R, JORDAN W, JONES T, CHANG C AND KIM M. 1999. Shielding from solar particle event exposures in deep space. *Radiation measurements* 30: 361-382.
- WILSON JW, TOWNSEND LW, NEALY JE, CHUN SY, HONG B, BUCK WW, LAMKIN S, GANAPOL BD, KHAN F AND CUCINOTTA FA. 1989. BRYNTRN: A baryon transport model.
- WORGUL B, KUNDIYEV Y, SERGIYENKO N, CHUMAK V, VITTE P, MEDVEDOVSKY C, BAKHANOVA E, JUNK A, KYRYCHENKO O AND MUSIJACHENKO N. 2007. Cataracts among Chernobyl clean-up workers: implications regarding permissible eye exposures. *Radiation research* 167: 233-243.
- INVESTIGATIVE OPHTHALMOLOGY & VISUAL SCIENCE, 1979. LIPPINCOTT-RAVEN PUBL 227 EAST WASHINGTON SQ, PHILADELPHIA, PA 19106, 128-128 p.
- WORGUL B, SMILENOV L, BRENNER D, VAZQUEZ M AND HALL E. 2005. Mice heterozygous for the ATM gene are more sensitive to both X-ray and heavy ion exposure than are wildtypes. *Advances in Space Research* 35: 254-259.
- WORGUL BV AND MERRIAM JR GR. 1980. The lens epithelium and radiation cataracts: II. Interphase death in the meridional rows? *Radiation research* 84: 115-121.
- WORGUL BV AND MERRIAM JR GR. 1981. The role of inflammation in radiation cataractogenesis. *Experimental eye research* 33: 167-173.
- WORGUL BV, SMILENOV L, BRENNER DJ, JUNK A, ZHOU W AND HALL EJ. 2002. Atm heterozygous mice are more sensitive to radiation-induced cataracts than are their

- wild-type counterparts. *Proceedings of the National Academy of Sciences* 99: 9836-9839.
- WU M, BIAN Q, LIU Y, FERNANDES AF, TAYLOR A, PEREIRA P AND SHANG F. 2009. Sustained oxidative stress inhibits NF- κ B activation partially via inactivating the proteasome. *Free Radical Biology and Medicine* 46: 62-69.
- WU M, LEE H, BELLAS RE, SCHAUER SL, ARSURA M, KATZ D, FITZGERALD MJ, ROTHSTEIN TL, SHERR DH AND SONENSHEIN GE. 1996. Inhibition of NF-kappaB/Rel induces apoptosis of murine B cells. *The EMBO Journal* 15: 4682-4690.
- WU X, RANGANATHAN V, WEISMAN DS, HEINE WF, CICCONE DN, O'NEILL TB, CRICK KE, PIERCE KA, LANE WS AND RATHBUN G. 2000. ATM phosphorylation of Nijmegen breakage syndrome protein is required in a DNA damage response. *Nature* 405: 477.
- WULF H, KRAFT-WEYRATHER W, MILTENBURGER H, BLAKELY E, TOBIAS C AND KRAFT G. 1985. Heavy-ion effects on mammalian cells: inactivation measurements with different cell lines. *Radiation Research* 104: S122-S134.
- XIA Z, YANG Z, HUYNH T, KING JA AND ZHOU R. 2013. UV-radiation Induced Disruption of Dry-Cavities in Human cD-crystallin Results in Decreased Stability and Faster Unfolding. *Sci Rep* 3.
- XU B AND KASTAN MB 2004. Analyzing cell cycle checkpoints after ionizing radiation. *Checkpoint Controls and Cancer: Springer*, p. 283-292.
- XU B, KIM S-T, LIM D-S AND KASTAN MB. 2002. Two molecularly distinct G2/M checkpoints are induced by ionizing irradiation. *Molecular and cellular biology* 22: 1049-1059.
- YAMAMOTO S, YAMASHITA A, ARAKAKI N, NEMOTO H AND YAMAZAKI T. 2014. Prevention of aberrant protein aggregation by anchoring the molecular chaperone α B-crystallin to the endoplasmic reticulum. *Biochemical and biophysical research communications* 455: 241-245.
- YAMASHITA D, JIANG H-Y, SCHACHT J AND MILLER JM. 2004. Delayed production of free radicals following noise exposure. *Brain research* 1019: 201-209.
- YANG H, CURINGA G AND GIACHELLI CM. 2004. Elevated extracellular calcium levels induce smooth muscle cell matrix mineralization in vitro¹¹. *Kidney international* 66: 2293-2299.
- YARDEN RI, PARDO-REOYO S, SGAGIAS M, COWAN KH AND BRODY LC. 2002. BRCA1 regulates the G2/M checkpoint by activating Chk1 kinase upon DNA damage. *Nature genetics* 30: 285.
- YOSHIDA CA, FURUICHI T, FUJITA T, FUKUYAMA R, KANATANI N, KOBAYASHI S, SATAKE M, TAKADA K AND KOMORI T. 2002. Core-binding factor β interacts with Runx2 and is required for skeletal development. *Nature genetics* 32: 633.
- ZACONTE V, BELLI F, BIDOLI V, CASOLINO M, DI FINO L, NARICI L, PICOZZA P, RINALDI A, RUGGIERI D AND CAROZZO S. 2006. ALTEA: flight model calibration at GSI. *Advances in Space Research* 37: 1704-1709.
- ZAIDER M. 2001. The risk of leukemia from low doses of low-LET radiation. *Mathematical and computer modelling* 33: 1307-1313.

- ZARJOU A, JENEY V, AROSIO P, POLI M, ANTAL-SZALMÁS P, AGARWAL A, BALLA G AND BALLA J. 2009. Ferritin prevents calcification and osteoblastic differentiation of vascular smooth muscle cells. *Journal of the American Society of Nephrology* 20: 1254-1263.
- ZELKO IN, MARIANI TJ AND FOLZ RJ. 2002. Superoxide dismutase multigene family: a comparison of the CuZn-SOD (SOD1), Mn-SOD (SOD2), and EC-SOD (SOD3) gene structures, evolution, and expression. *Free Radical Biology and Medicine* 33: 337-349.
- ZHANG J, YAN H, LÖFGREN S, TIAN X AND LOU MF. 2012. Ultraviolet Radiation-Induced Cataract in Mice: The Effect of Age and the Potential Biochemical Mechanism. *Investigative ophthalmology & visual science* 53: 7276-7285.
- ZHANG Y, OUYANG S, ZHANG L, TANG X, SONG Z AND LIU P. 2010. Oxygen-induced changes in mitochondrial DNA and DNA repair enzymes in aging rat lens. *Mechanisms of ageing and development* 131: 666-673.
- ZHAO S, WENG Y-C, YUAN S-SF, LIN Y-T, HSU H-C, LIN S-CJ, GERBINO E, SONG M-H, ZDZIENICKA MZ AND GATTI RA. 2000. Functional link between ataxia-telangiectasia and Nijmegen breakage syndrome gene products. *Nature* 405: 473.
- ZHOU N, LI Q, LIN X, HU N, LIAO J-Y, LIN L-B, ZHAO C, HU Z-M, LIANG X AND XU W. 2016. BMP2 induces chondrogenic differentiation, osteogenic differentiation and endochondral ossification in stem cells. *Cell and tissue research* 366: 101-111.
- ZIGLER JR JS, HUANG Q-L AND DU X-Y. 1989. Oxidative modification of lens crystallins by H₂O₂ and chelated iron. *Free Radical Biology and Medicine* 7: 499-505.

8 APPENDIX

8.1 Supplementary results



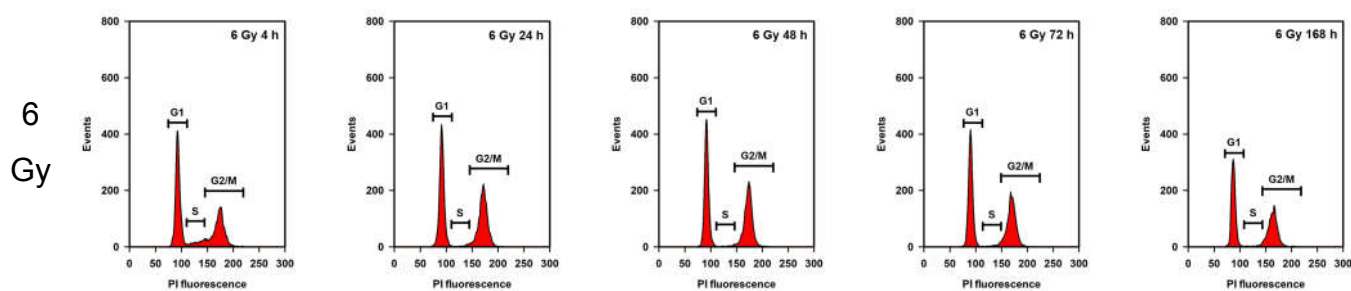


Figure S1: Cell cycle distribution histogram after exposure to X-rays. pLECs were harvested and fixed with 70 % ethanol at different time points and stained with propidium iodide (PI). In the above histograms, x-axis gives the cell count and y-axis gives the PI fluorescence.

Table 18: Quantity and integrity of RNA isolated from X-ray exposed pLECs.

| # | Conditions | RNA conc ⁿ (ng/μl) | RIN |
|----|------------|-------------------------------|-----|
| 1 | 4 h 0 Gy | 207.8 | 8.9 |
| 2 | 4 h 1 Gy | 259.3 | 8.7 |
| 3 | 4 h 4 Gy | 309.6 | 8.7 |
| 4 | 4 h 8 Gy | 258.5 | 8.6 |
| 5 | 4 h 16 Gy | 245.7 | 9 |
| 6 | 12 h 0 Gy | 328.4 | 9 |
| 7 | 12 h 1 Gy | 332.9 | 9.1 |
| 8 | 12 h 4 Gy | 312.9 | 9 |
| 9 | 12 h 8 Gy | 320.5 | 8.8 |
| 10 | 12 h 16 Gy | 337.4 | 8.9 |
| 11 | 24 h 0 Gy | 431.2 | 9 |
| 12 | 24 h 1 Gy | 436.7 | 8.8 |
| 13 | 24 h 4 Gy | 370.6 | 9 |
| 14 | 24 h 8 Gy | 195.1 | 8.8 |
| 15 | 24 h 16 Gy | 357.9 | 9.3 |
| 16 | 48 h 0 Gy | 311.5 | 9.5 |
| 17 | 48 h 1 Gy | 239.0 | 9.4 |
| 18 | 48 h 4 Gy | 363.3 | 8.8 |
| 19 | 48 h 8 Gy | 319.5 | 8.8 |
| 20 | 48 h 16 Gy | 273.4 | 8.9 |
| 21 | 72 h 0 Gy | 446.5 | 8.7 |
| 22 | 72 h 1 Gy | 454.5 | 8.9 |
| 23 | 72 h 4 Gy | 272.7 | 8.7 |
| 24 | 72 h 8 Gy | 339.9 | 8.8 |
| 25 | 72 h 16 Gy | 289.4 | 8.3 |

Table 19: Quantity and integrity of RNA isolated from Carbon-12 exposed pLECs.

| # | Conditions | RNA conc ⁿ (ng/μl) | RIN |
|----|------------|-------------------------------|-----|
| 1 | 4 h 0 Gy | 79.2 | 6.4 |
| 2 | 4 h 1 Gy | 136.7 | 7.1 |
| 3 | 4 h 4 Gy | 172.6 | 7.4 |
| 4 | 4 h 8 Gy | 105.3 | 7.8 |
| 5 | 4 h 16 Gy | 50.2 | 7.6 |
| 6 | 12 h 0 Gy | 196.6 | 7.6 |
| 7 | 12 h 1 Gy | 105.3 | 6.4 |
| 8 | 12 h 4 Gy | 83.7 | 6.8 |
| 9 | 12 h 8 Gy | 87.9 | 7.5 |
| 10 | 12 h 16 Gy | 173.1 | 7.2 |
| 11 | 24 h 0 Gy | 123.1 | 7.2 |
| 12 | 24 h 1 Gy | 241.6 | 7.5 |
| 13 | 24 h 4 Gy | 62.6 | 8.4 |
| 14 | 24 h 8 Gy | 137.8 | 7.4 |
| 15 | 24 h 16 Gy | 160.6 | 7.3 |
| 16 | 72 h 0 Gy | 175.4 | 8 |
| 17 | 72 h 1 Gy | 146.8 | 7.1 |
| 18 | 72 h 4 Gy | 123.5 | 7.3 |
| 19 | 72 h 8 Gy | 124.2 | 6.8 |
| 20 | 72 h 16 Gy | 64.1 | 7.7 |

Table 20: Quantity and integrity of RNA isolated from pLECs with or without calcification medium.

| # | Conditions | RNA conc ⁿ (ng/μl) | RIN |
|---|------------|-------------------------------|-----|
| 1 | NM day 0 | 391.0 | 10 |
| 2 | NM day 7 | 40.8 | 7.2 |
| 3 | NM day 14 | 83.1 | 9.6 |
| 4 | CM day 0 | 226.3 | 9.8 |
| 5 | CM day 7 | 107.6 | 9.9 |
| 6 | CM day 14 | 138.6 | 9.7 |

8.2 Abbreviations

| Abbreviation | Description |
|---------------|--|
| α -MEM | Alpha minimum essential medium eagle |
| γ H2AX | H2A histone family member X (phosphorylated at Serine-139) |
| $^{\circ}$ C | Degree Centigrade |
| μ g | Microgram |
| μ l | Microliter |
| μ m | Micrometer |
| μ M | Micro-molar |
| 53BP1 | p53 binding protein 1 |
| Å | Ångström (1×10^{-10} m) |
| A | Adenine |
| ACTB | Beta-actin |
| ADP | Adenosine diphosphate |
| ALP | Alkaline phosphatase |
| Ar | Argon |
| ATM | Ataxia telangiectasia mutant protein |
| ATR | Ataxia telangiectasia and Rad3-related protein |
| B2M | Beta-2 microglobulin |
| BER | Base excision repair |
| BLAST | Basic Local Alignment Search Tool |
| BMP2 | Bone morphogenetic protein 2 |
| bp | Basepair |
| BRCA1/2 | Breast cancer gene 1/2 |
| BSA | Bovine serum albumin |
| BSP | Bone sialoprotein |
| C | Carbon |
| C | Cytosine |
| Ca | Calcium |
| CAT | Catalase |
| Cdc | Cell division cycle |
| Cdk | Cyclin-dependent kinase |
| CDKN1A | Cyclin-dependent kinase inhibitor 1 |
| cDNA | Complementary DNA |
| CFA | Colony forming ability |
| Chk1, Chk2 | Checkpoint kinase 1, 2 |
| CM | Calcification medium |
| COL1 | Collagen type I |
| COL1A2 | Collagen type I alpha 2 chain |
| CRYAB | Crystallin Alpha B |
| C_t | Threshold cycle |
| CtIP | CtBP-interacting protein |
| D | Dose |
| DAPI | 4',6-diamidino-2-phenylindole |
| DLAD | DNase II-like acid DNase |
| DLR | Deutsches Zentrum für Luft- und Raumfahrt |
| DMSO | Dimethyl sulfoxide |
| DNA | Deoxyribonucleic acid |

| Abbreviation | Description |
|----------------|--|
| DNA-PK | DNA protein kinase |
| DNASE2 | Deoxyribonuclease II |
| DN-PKcs | DNA protein kinase catalytic subunit |
| DSB | Double strand break |
| DSBR | Double strand break repair |
| e ⁻ | Electron |
| EDTA | Ethylenediaminetetraacetic acid |
| EdU | 5-Ethynyl-2'-deoxyuridine |
| EMT | Epithelial to mesenchymal transition |
| ESA | European Space Agency |
| EXO1 | Exonuclease 1 |
| F | Fluence |
| FACS | Fluorescence-activated cell scanner |
| FBS | Fetal bovine serum |
| Fe | Iron |
| FGF | Fibroblast growth factor |
| FSC | Forward scatter |
| g | Gram |
| G | Guanine |
| GADD45G | Growth Arrest And DNA Damage Inducible Gamma |
| GANIL | Grand Accélérateur National d'Ions Lourds |
| GCR | Galactic cosmic radiation |
| G1 phase | Gap phase between M- and S-phase |
| G2 phase | Gap phase between S- and M-phase |
| Gy | Gray |
| H• | Hydrogen radical |
| He | Helium |
| HeLa | Cervical cancer derived cells (from patient Henrietta Lacks) |
| HEK | Human embryonic kidney cells |
| HKGs | Housekeeping genes |
| HLE | Human lens epithelial cells |
| HPRT | Hypoxanthine-guanine phosphoribosyltransferase |
| HR | Homologous recombination |
| H _T | Equivalent dose |
| HZE | High (H) atomic number (Z) and energy (E) |
| IARC | International Agency for Research on Cancer |
| ICRP | International Commission on Radiological Protection |
| IL6 | Interleukin 6 |
| IOL | Intra-ocular lens |
| IP | Immediate plating |
| ISS | International Space Station |
| IU | International units |
| J | Joule |
| K | Potassium |
| kb | Kilobases |
| keV | Kilo electron volt |
| kV | Kilo volt |
| l | Liter |

| Abbreviation | Description |
|----------------|---|
| LEO | Low Earth orbit |
| LET | Linear energy transfer |
| LIG4 | Ligase 4 |
| LP | Late plating |
| LW24 | Primary adipose derived stem cell |
| M | Molar |
| M | Mitosis phase of the cell cycle |
| mA | Milliampere |
| Mdm2 | Mouse double minute 2 homolog |
| MeV/n | Mega electron volt per nucleon |
| MEF | Mouse embryonic fibroblast |
| ml | Milliliter |
| mm | Millimeter |
| mM | Milli-molar |
| MMLV | Moloney Murine Leukemia Virus |
| MMP | Matrix metalloproteinase |
| mol | Mole |
| MRE11 | MRE11 homolog, double strand break repair nuclease |
| MRN | Complex of MRE11, RAD50 and NBS1 |
| mSv | Milli-Sievert |
| Na | Sodium |
| NBS1 | Nijmegen breakage syndrome 1 protein |
| NCBI | National Center for Biotechnology Information |
| NFKBIA | NF-κB inhibitor alpha |
| NF-κB | Nuclear Factor κB |
| ng | Nanogram |
| NHEJ | Non-homologous end joining |
| nm | Nanometer (1×10^{-9} m) |
| nM | Nano-molar |
| NM | Normal medium |
| OCN | Osteocalcin |
| OCT-1 | Murine osteoblastic cell line |
| OH• | Hydroxyl radical |
| OPN | Osteopontin |
| P | Particles |
| P ⁺ | Proton |
| p21 | Protein 21 CDK2-interacting protein 1 |
| p53 | Tumor protein p53 |
| PARP1 | Poly(ADP-ribose) polymerase 1 |
| PAX6 | Paired Box 6 |
| PBS | Phosphate buffered saline |
| PE | Plating efficiency |
| pH | Pondus Hydrogenii (-log [H ⁺]) |
| PI | Propidium iodide (C ₂₇ H ₃₄ I ₂ N ₄) |
| Pi | Inorganic phosphate |
| PIKK | Phosphatidylinositol-3-kinase-related kinase |
| pLEC | Porcine lens epithelial cell |
| PS3 | Petri dish, Ø 30 mm |

| Abbreviation | Description |
|----------------|--|
| PS6 | Petri dish, Ø 60 mm |
| PSC | Posterior sub-capsular cataract |
| qPCR | Quantitative polymerase chain reaction |
| RT-qPCR | Reverse Transcriptase Quantitative real-time polymerase chain reaction |
| RAD9 | DNA repair protein RAD9 |
| RAD50 | Recombinant DNA Repair Protein RAD50 |
| RAD51 | RAD51 recombinase |
| RAD52 | RAD52 homolog, DNA repair protein |
| RBE | Relative biological effectiveness |
| RELA | Transcription factor p65 |
| RIN | RNA integrity number |
| RNA | Ribonucleic acid |
| ROS | Reaction oxygen species |
| RPA | Replication protein A |
| rRNA | Ribosomal RNA |
| RT | Room temperature |
| RUNX2 | Runt-related transcription factor 2 |
| S-phase | DNA synthesis phase of the cell cycle |
| S | Relative survival |
| SAA | South atlantic anomaly |
| SAOS-2 | Human osteosarcoma cell line |
| SCR | Solar cosmic radiation |
| SD | Standard deviation |
| SE | Standard error |
| SIBLING | Small Integrin-Binding LIgand N-Linked Glycoprotein |
| SM | Standard medium |
| SMC | Structural maintenance of chromosomes |
| SOD | Superoxide dismutase |
| Sox9 | SRY-box 9 (Transcription factor) |
| SPE | Solar particle events |
| SSB | Single strand break |
| SSC | Side scatter |
| S _v | Sievert |
| T _a | Annealing temperature |
| TBST | Tris-buffered saline with tween 20 |
| T _d | Doubling time |
| TGF-β | Transforming growth factor beta |
| T _m | Melting temperature |
| TNF | Tumor necrosis factor |
| VSMC | Vascular smooth muscle cells |
| v/v | Volume per volume |
| W _R | Radiation weighting factor |
| w/v | Weight per volume |
| ×g | Relative centrifugal force |
| XLF | XRCC4 like Factor |
| XRCC1 | X-ray cross complementing protein 1 |
| XRCC4 | X-ray cross complementing protein 4 |

8.3 List of figures

| | |
|--|----|
| Figure 1: International Space Station (ISS). | 1 |
| Figure 2: RBE and LET relationship. | 4 |
| Figure 3: Space radiation..... | 5 |
| Figure 4: Direct and indirect radiation damage. | 9 |
| Figure 5: Consequences of ionizing radiation exposure of a biological system. | 9 |
| Figure 6: DNA double strand break repair pathways. | 12 |
| Figure 7: Role of ATM and its downstream effectors in the regulation of the cell cycle. | 13 |
| Figure 8: A cross-section diagram of the human eye lens. | 14 |
| Figure 9 : Isolation of lens from the porcine eye. | 29 |
| Figure 10: Isolation of lens epithelial layer from the porcine lens for lens epithelial cells | 30 |
| Figure 11: Packing of lenses into the plastic cassette for paraffin infiltration | 31 |
| Figure 12: Paraffin dispenser and embedded lens | 32 |
| Figure 13: Sectioning of the lens. | 33 |
| Figure 14: Heavy ion irradiation at the GANIL accelerator..... | 34 |
| Figure 15: Parameters of dose-effect curves..... | 38 |
| Figure 16: Analysis of cell cycle distribution by flow cytometry of PI-stained cells | 39 |
| Figure 17: Electropherogram of separated RNA..... | 44 |
| Figure 18: Amplification curves and melting curves from qPCR of B2M gene..... | 48 |
| Figure 19: Chromosome preparation | 51 |
| Figure 20: Cultivation of porcine lens epithelial cells (pLEC). | 52 |
| Figure 21: Morphology of pLECs during a growth period of 7 days. | 53 |
| Figure 22: Growth behavior of pLECs..... | 53 |
| Figure 23: Lens organ culture..... | 54 |
| Figure 24: Live staining of lens epithelial cells in lens organ culture..... | 55 |
| Figure 25: Hematoxylin-Eosin staining of lens..... | 55 |
| Figure 26: DNA synthesis in the epithelial layer. | 56 |
| Figure 27: DNA synthesis in epithelial cell monolayer culture. | 57 |

| | |
|--|----|
| Figure 28: Flow-cytometric analysis of DNA synthesis, determined by EdU incorporation into the DNA of pLECs..... | 57 |
| Figure 29: DNA synthesis in the whole lens. | 58 |
| Figure 30: Oxidative Stress measurement by CellROX® Green | 59 |
| Figure 31: X-ray-induced oxidative stress as a function of time after exposure..... | 60 |
| Figure 32: Clonogenic survival of pLECs after exposure to X-rays..... | 62 |
| Figure 33: Time-dependent distribution of cells in the different phases of the cell cycle..... | 64 |
| Figure 34: The percentage of cells in G2/M phase for the second passage (P-2) determined by flow cytometry..... | 66 |
| Figure 35: The percentage of cells in G2/M phase for third passage (P-3) determined by flow cytometry..... | 66 |
| Figure 36: The percentage of cells in G2/M phase for fourth (A) and fifth (B) passage determined by flow cytometry. | 67 |
| Figure 37: Comparison of the exponential growth of non-irradiated pLECs in passages 2 to 5 (P-2 to P-5)..... | 67 |
| Figure 38: Effect of ATM inhibition on cell cycle progression after exposure to X-rays..... | 69 |
| Figure 39: Effect of ATR inhibition on cell cycle progression after X-irradiation..... | 70 |
| Figure 40: Effect of DNA-PK inhibition on cell cycle progression after X-irradiation..... | 70 |
| Figure 41: Immunofluorescence staining of γ H2AX in pLECs 1 h after X-ray exposure..... | 72 |
| Figure 42: Immunofluorescence staining of γ H2AX in pLECs 24 h after X-ray exposure..... | 72 |
| Figure 43: Dose-dependent induction and repair of DNA DSBs in pLECs..... | 73 |
| Figure 44: Kinetics of γ H2AX foci disappearance during repair..... | 73 |
| Figure 45: DNA DSBs induction and repair..... | 74 |
| Figure 46: γ H2AX foci formation after exposure to low doses of X-rays | 74 |
| Figure 47: Influence of ATM inhibition on γ H2AX foci formation after X-ray exposure..... | 76 |
| Figure 48: Influence of ATR inhibition on γ H2AX foci formation after X-ray exposure..... | 76 |

| | |
|--|----|
| Figure 49: Influence of DNA-PK inhibition on γ H2AX foci formation after X-ray exposure..... | 77 |
| Figure 50: DNA DSBs induction and repair after argon ion (Ar-36, energy on target 84.7 MeV/n, LET 269.4 keV/ μ m) exposure..... | 78 |
| Figure 51: DNA DSBs induction and repair after carbon ion (C-12, energy on target 28.6 MeV/n, LET 71 keV/ μ m) exposure. | 78 |
| Figure 52: Immunofluorescence staining of γ H2AX in lens epithelial cells in lens epithelial layer | 80 |
| Figure 53: Immunofluorescence staining of γ H2AX in lens epithelial cells in microtome sections of whole porcine lenses | 81 |
| Figure 54: X-ray dependent changes in gene expression of the housekeeping genes ACTB, B2M and HPRT. | 83 |
| Figure 55: X-ray dependent changes in gene expression of CDKN1A. | 84 |
| Figure 56: X-ray dependent changes in gene expression of GADD45G..... | 84 |
| Figure 57: X-ray dependent changes in gene expression of CRYAB. | 86 |
| Figure 58: X-ray dependent changes in gene expression of DNASE2. | 86 |
| Figure 59: X-ray dependent changes in gene expression of PAX6. | 86 |
| Figure 60: X-ray dependent changes in gene expression of RELA. | 87 |
| Figure 61: X-ray dependent changes in gene expression of SOD3..... | 87 |
| Figure 62: Changes in gene expression of housekeeping genes after exposure to accelerated C ions..... | 89 |
| Figure 63: C ion dependent changes in gene expression of CDKN1A. | 90 |
| Figure 64: C ion dependent changes in gene expression of GADD45G..... | 90 |
| Figure 65: C ion dependent changes in gene expression of CRYAB. | 91 |
| Figure 66: C ion dependent changes in gene expression of DNASE2. | 91 |
| Figure 67: C ion dependent changes in gene expression of PAX6..... | 91 |
| Figure 68: C ion dependent changes in gene expression of RELA. | 92 |
| Figure 69: C ion-dependent changes in gene expression of SOD3..... | 92 |
| Figure 70: Osteogenic differentiation of pLECs. | 93 |
| Figure 71: Gene expression changes of the housekeeping genes ACTB and B2M after treatment with calcification medium. | 94 |
| Figure 72: Gene expression changes of BMP2 after treatment with calcification medium..... | 96 |

| | |
|--|-----|
| Figure 73: Gene expression changes of RUNX2 after treatment with calcification medium. | 96 |
| Figure 74: Gene expression changes of COL1A2 after treatment with calcification medium. | 97 |
| Figure 75: Gene expression changes of OPN after treatment with calcification medium..... | 97 |
| Figure 76: Gene expression changes of PAX6 after treatment with calcification medium..... | 97 |
| Figure 77: X-ray dependent changes in gene expression of BMP2..... | 99 |
| Figure 78: X-ray dependent changes in gene expression of RUNX2 | 99 |
| Figure 79: X-ray dependent changes in gene expression of COL1A2..... | 99 |
| Figure 80: Growth of human epithelial cells in vitro. | 102 |
| Figure S1: Cell cycle distribution histogram after exposure to X-rays. | 153 |

8.4 List of tables

| | | |
|-----------|--|-----|
| Table 1: | Radiation effects in humans after whole body irradiation (adapted from (Hellweg and Baumstark-Khan 2007))..... | 7 |
| Table 2: | Equipment | 23 |
| Table 3: | Consumables..... | 24 |
| Table 4: | Reagents and Kits | 24 |
| Table 5 : | Medium for cell culture | 26 |
| Table 6: | Buffers and solutions | 26 |
| Table 7: | Antibodies and antibody diluent..... | 27 |
| Table 8: | Software | 27 |
| Table 9: | Click-iT reaction mixture. | 42 |
| Table 10: | The cDNA synthesis reaction mixture..... | 45 |
| Table 11: | Primers used for gene expression analysis with their gene name, product size and NCBI database codes. | 46 |
| Table 12: | Reaction mix for qPCR per well..... | 47 |
| Table 13: | qPCR amplification protocol | 47 |
| Table 14: | Plating efficiency of pLECs..... | 61 |
| Table 15: | Comparison of survival curve parameters for IP (immediately plated) and LP (lately plated) pLECs. | 62 |
| Table 16: | Comparison of radiobiological parameters for different cell types. | 105 |
| Table 17: | Comparison of γ H2AX foci with respect to different qualities of radiation..... | 113 |
| Table 18: | Quantity and integrity of RNA isolated from X-ray exposed pLECs. | 153 |
| Table 19: | Quantity and integrity of RNA isolated from Carbon-12 exposed pLECs..... | 154 |
| Table 20: | Quantity and integrity of RNA isolated from pLECs with or without calcification medium. | 154 |

9 ACKNOWLEDGMENTS

First and foremost, I would like to express my sincere gratitude to my Supervisor Hon. Prof. Dr. Christa Baumstark for continuous support, motivation and immense knowledge. She has been a good guardian as well as a friend whose guidance helped me in all the time of research and writing of this thesis. Equally, I would like to appreciate PD Dr. Christine Hellweg for her constant support, supervision, suggestions and encouragement. I could not imagine having a better supervisor for my Ph.D. study. I would also like to convey my thanks to Prof. Dr. Jutta Engel and PD Dr. Yvonne Dzierma for timely support and accepting me as one of their doctoral students.

I would like to thank the Helmholtz Space Life Sciences Research School (SpaceLife) and the director of Institute of Aerospace Medicine for the scholarship and providing an interesting field in research. Similarly, I would like to thank the whole Radiation Biology Department for the great working environment.

My sincere thanks also go to PD. Dr. Alfred Wegener and his group members from the University Eye Hospital Bonn where I learnt to prepare and work with porcine eye lenses. I am grateful to Dr. Ralf Moeller for being my mentor whose positive attitude and encouragement kept my motivation always high.

The time I spent in Cellular Biodiagnostics group has become a beautiful unforgettable chapter of my life. The wonderful working atmosphere, friendly scientific discussions, supporting one another in labs, especially in night shifts during beam times, and cheerful celebrations are the memories linked to this group. For these pretty moments I would like to thank dear colleges Luis, Claudia, Sebastian, Bernd, Luna, Arif, Tina, Sebastian (Diegeler) and others who were part of this group.

Finally I would like to thank my parents Mr. and Mrs. Ganesh Bhakta and Neer Shova Konda and sister Neelam whose love and support are with me on all of my pursuits. Most importantly, I thank my wife Tammy for her faith, care and support which provides me unending inspiration.